HAL
open science

Origin and evolution of two distinct Cretaceous oceanic plateaus accreted in Western Ecuador (South America) : Petrological, geochemical and isotopic evidence

Marc Mamberti

To cite this version:

Marc Mamberti. Origin and evolution of two distinct Cretaceous oceanic plateaus accreted in Western Ecuador (South America) : Petrological, geochemical and isotopic evidence. Geochemistry. Université Joseph-Fourier - Grenoble I, 2001. English. NNT : . tel-00688387

HAL Id: tel-00688387

https://theses.hal.science/tel-00688387v1

Submitted on 17 Apr 2012

HAL is a multi-disciplinary open access archive for the deposit and dissemination of scientific research documents, whether they are published or not. The documents may come from teaching and research institutions in France or abroad, or from public or private research centers.

L'archive ouverte pluridisciplinaire **HAL**, est destinée au dépôt et à la diffusion de documents scientifiques de niveau recherche, publiés ou non, émanant des établissements d'enseignement et de recherche français ou étrangers, des laboratoires publics ou privés.

M.GEOSCIENCES.GRENOBLE UJF
D 050 036624 3

UNIVERSITE JOSEPH FOURIER
SCIENCES. TECHNOLOGIE. MEDECINE

Laboratoire de Géodynamique des Chaînes Alpines

Thèse de doctorat

présentée à la

Faculté des Sciences de l'Université de Lausanne
en cotutelle avec l'Université Joseph Fourier (Grenoble)

par

Marc Mamberti

Pour obtenir le titre de
DOCTEUR
DE L'UNIVERSITÉ JOSEPH FOURIER – GRENOBLE 1
(spécialité: Sciences de la Terre)

06 MARS 2006

Origin and evolution of two distinct Cretaceous oceanic plateaus accreted in Western Ecuador (South America) : Petrological, geochemical and isotopic evidence.

Univ. J. Fourier - OSUG
MAISON DES SCIENCES DE L'ORGANISATION
DOCUMENTATION
BP 53
F. 38041 GRENOBLE CEDEX
Tél. 04 76 63 54 27 - Fax 04 76 51 40 58
Mail : ptalour@ujf-grenoble.fr

Jury

Prof. Raymond ROULET, Président
Prof. Richard ARCULUS, Expert
Prof. René C. MAURY, Expert
Dr. Etienne JAILLARD, Expert
Prof. Peter O. BAUMGARTNER, Expert
Prof. Henriette LAPIERRE, Co-directeur de thèse
Prof. Jean HERNANDEZ, Co-directeur de thèse

GRENOBLE
2001

UNIVERSITE JOSEPH FOURIER
SCIENCES. TECHNOLOGIE. MEDECINE

Laboratoire de Géodynamique des Chaînes Alpines

Thèse de doctorat

présentée à la

Faculté des Sciences de l'Université de Lausanne
en cotutelle avec l'Université Joseph Fourier (Grenoble)

par

Marc Mamberti

Pour obtenir le titre de
DOCTEUR
DE L'UNIVERSITÉ JOSEPH FOURIER – GRENOBLE 1
(spécialité: Sciences de la Terre)

Origin and evolution of two distinct Cretaceous oceanic plateaus accreted in Western Ecuador (South America) : Petrological, geochemical and isotopic evidence.

Univ. J. Fourier - O.S.U.G.
MAISON DES GEOSCIENCES
DOCUMENTATION
B.P. 53
F. 38041 GRENOBLE CEDEX
Tél. 04 76 63 54 27 - Fax 04 76 51 40 58
Mail : ptalour@ujf-grenoble.fr

08 MARS 2006

Jury

Prof. Raymond ROULET, Président
Prof. Richard ARCULUS, Expert
Prof. René C. MAURY, Expert
Dr. Etienne JAILLARD, Expert
Prof. Peter O. BAUMGARTNER, Expert
Prof. Henriette LAPIERRE, Co-directeur de thèse
Prof. Jean HERNANDEZ, Co-directeur de thèse

GRENOBLE
2001

UNIVERSITE DE LAUSANNE

Faculté des sciences

Univ. J. Fourier - O.S.U.G.
MAISON DES GEOSCIENCES
DOCUMENTATION
B.P. 53
F. 38041 GRENOBLE CEDEX
Tél. 04 76 63 54 27 - Fax 04 76 51 40 58
Mail : ptalour@ujf-grenoble.fr

Imprimatur

Vu le rapport présenté par le jury d'examen, composé de

Président	Monsieur Prof. Raymond **Roulet**
Co-Directeur de thèse	Monsieur Prof. Jean **Hernandez**
Co-Directeur de thèse	Madame Prof. Henriette **Lapierre**
Rapporteur	Monsieur Prof. Richard **Arculus**
Experts	Monsieur Prof. Peter O. **Baumgartner**
	Monsieur Prof. René C. **Maury**
	Monsieur Dr Etienne **Jaillard**

le Conseil de Faculté autorise l'impression de la thèse de

Monsieur Marc Mamberti

Titulaire d'un DEA matériaux/minéraux , Université des Sciences d'Orléans, France

intitulée

Origin and evolution of two distinct Cretaceous oceanic plateaus accreted in Western Ecuador (South america) evidenced by petrology, geochemistry and isotopic chemistry

Lausanne, le 4 avril 2001

pour Le Doyen de la Faculté des Sciences

Prof. Raymond Roulet

Remerciements

Comment arriver à remercier toutes les personnes qui ont croisé ma route lors de ces trois années de thèse? Difficile tâche et surtout périlleuse, car la liste est longue et il ne faudrait oublier personne... C'est pour cela qui j'irai au plus court et que je ne listerai pas (trop) ces remerciements.

Commençons par remercier le FNRS (projets n°20.50812197 et 20.51954.999) ainsi que le programme Intérieur de la Terre qui m'ont permis de réaliser cette thèse dans les meilleures conditions possibles.

Henriette Lapierre est LE géologue la plus dynamique, la plus enthousiaste et la plus exigeante (si si) qu'il m'ait été donné de rencontrer durant ma courte carrière de géologue. Si j'écris ces quelques phrases aujourd'hui, c'est en grande partie grâce à elle. Elle m'a « bousté » dés le début, en maîtrise, et ne m'a pas oublié pour faire cette thèse. Bref, un grand merci. Je tiens aussi à remercier Jean Hernandez qui m'a permis de vadrouiller en toute liberté entre les deux Universités et dont les conseils « minéralogiques » se sont révélés très utiles. Je n'oublie pas Etienne Jaillard pour ses discussions scientifiques toujours claires et ses idées « à la pelle ». Merci d'avoir toujours laissé la porte de ton bureau ouverte pour moi et mes questions foireuses ...

J'associe à ces remerciements Nick Arndt pour ses implications dans ma thèse et Catherine Chauvel pour ses discussions enrichissantes.

Merci à Richard Arculus, René Maury et Peter Baumgartner de faire partie de mon jury.

Une thèse en cotutelle et des travaux en multiples collaborations impliquent de nombreuses rencontres dans les Universités. Certaines sont rapides, mais apportent toujours autant sur le plan relationnel que sur le plan scientifique. D'autres se renouvellent plus souvent et donnent lieu à des amitiés naissantes. C'est dans cette seconde catégorie que se situe Delphine Bosch qui a énormément contribué à mes connaissances de laboratoire et d'isotopie. Merci pour ses longs moments passés à me montrer ces manips d'isotopies dans cette salle blanche bien climatisée...

Je ne vais pas faire une liste des personnes que je tiens à remercier dans chacun des laboratoires où je suis passé, je suis sûr d'en oublier. Mais je pense leur avoir traduit mes remerciements lors de nos diverses rencontres. En tous les cas, à vous qui vous reconnaissez, MERCI ! !

Je termine avec une pensée très forte à ma famille et belle famille, ainsi qu'à Adam et Eve et Fleurice...

Et merci à ma R25 d'avoir tenu le choc...

Résumé

La géologie de l'Equateur se distingue de celle du reste des Cordillères andines par la présence de terrains océaniques qui s'accrètent successivement à la marge depuis la fin du Crétacé jusqu'au Paléocène. Ces terrains exotiques sont constitués de fragments de deux plateaux océaniques du Crétacé inférieur (123 Ma) et supérieur (90 Ma) et de plusieurs arcs insulaires (100 à 40 Ma). Dans la Cordillère occidentale, le plateau crétacé inférieur et les terrains océaniques du crétacé supérieur (plateau et arcs insulaires) s'accrètent respectivement à 85-80 Ma et 70-65 Ma.

Le plateau océanique daté à 123 Ma est constitué: (i) de cumulats basiques et ultrabasiques (série de San Juan) et (ii) de basaltes en coussins et de dolérites massives recoupés par des petites intrusions de gabbro sub-doléritique. Les cumulats forment une série continue depuis des dunites et wehrlites jusqu'à des gabbros à clinopyroxène. Basaltes, dolérites et gabbros présentent tous les caractères de basalte de plateau océanique (OPB; MgO = 7%; spectres de terres rares plats, pas d'anomalie négative en Nb et Ta). Les compositions isotopiques (Nd et Pb) des cumulats et de l'ensemble basalte-dolérite sont identiques et démontrent que toutes ces roches dérivent d'une source mantellique enrichie.

Les picrites et les basaltes enrichis ou non en MgO, associés à des dolérites et des gabbros, représentent des témoins accrétés du plateau océanique crétacé supérieur caraïbe. Les picrites (MgO ~20 %) sont appauvries en terres rares légères, peu radiogéniques en Pb et caractérisées par des εNd élevés (+8 à +10). Les basaltes riches en MgO (9-10%) sont enrichis en terres rares légères. La géochimie en éléments traces des basaltes pauvres en MgO est identique à celle d'OPB. Par contre, les rapports isotopiques du Pb des basaltes, riches en MgO ou non, sont très élevés indiquant que toutes ces laves dérivent d'une source enrichie de type HIMU, caractère commun à tous les basaltes du plateau caraïbe.

Abstract

The geology of Ecuador is very different from that of the Cordillera Andes because of the presence of accreted oceanic terranes. These terranes consist of Early (123 Ma) and Late Cretaceous (90 Ma) crustal fragments of oceanic plateau affinity overlain by several island-arcs, the ages of which range between 100 to 40 Ma. In the Western Cordillera, the ages of accretion of the Early Cretaceous and Late Cretaceous crustal fragments (plateau and arcs) are 85-80 Ma and 70-65 Ma, respectively.

The Early Cretaceous oceanic plateau is composed of: (i) ultramafic to mafic cumulates (San Juan section), and (ii) pillow basalts and dolerites intruded by shallow level gabbroic plugs (Merced-Multitud section). The cumulates consist of a complete sequence, which range from dunites and wehrlites to clinopyroxene gabbros. Basalts, dolerites and gabbros display geochemical features of oceanic plateau basalts (OPB; MgO = 7 %, flat rare earth element (REE) patterns, negative Nb and Ta anomalies). The Nd and Pb isotopic compositions of the cumulates and basalts, dolerites and gabbros are similar and suggest that all these rocks were derived from a mildly enriched mantle source.

The Late Cretaceous lithologies include picrites (MgO = ~ 20 %), the MgO-rich (MgO ~ 9-10 %) basalts, and MgO-poor (MgO ~ 6-7 %) basalts associated with dolerites and shallow level gabbros, and represent accreted remnants of the Caribbean oceanic plateau. The picrites are Light (L)REE-depleted and characterized by low Pb isotopic ratios and high εNd (+8 to +10). The MgO-rich basalts are LREE-enriched. The Pb isotopic ratios of the MgO-rich and MgO-poor basalts are very high, suggesting that these volcanic rocks were derived from the melting of an enriched source with a HIMU component. These high Pb isotopic ratios are a common feature to all the basalts related to the Late Cretaceous magmatic event of the Caribbean oceanic plateau.

Figure caption

Fig. 1: General map of the Large Igneous Provinces (Coffin & Heldholm, 1993).

Fig. 2: Schematic map showing the location of the Mesozoic plateau crustal fragments exposed in Costa Rica, Greater Antilles, Curaçao, Colombia, and western Ecuador.

Fig. 3: Schematic geological map of Western Ecuador showing the main geological and tectonic units.

Fig. 1.1. (A) Schematic geological map of Ecuadorshowing the main geological and tectonic units and the location of the studied area. (B) Geological sketch of southern coastal Ecuador showing the distribution of the studied magmatic units and the location of the samples analyzed.

Fig. 1.2. Stratigraphic nomenclature and geodynamic setting of the Cretaceous-Tertiary rocks of western Ecuador.

Fig. 1.3. Zr (ppm), Nb (ppm), TiO_2 (wt%) and Y (ppm) vs. MgO (wt%) correlation diagrams of the basalts and dolerites of the Piñón Formation.

Fig. 1.4. Chondrite-normalized (Sun & McDonough, 1989) rare earth elements patterns of the basalts (A) and dolerites (B) of the Piñón Formation.

Fig. 1.5. N-MORB (Sun & McDonough, 1989) spidergrams of the basalts (A) and dolerites (B) of the Piñón Formation.

Fig. 1.6. Ta-Nb, Hf-Zr, U-Th, Nb/U-U correlation diagrams of the basalts and dolerites of the Piñón Formation. Altered samples have been omitted in the U-Th and Nb/U-U diagrams.

Fig. 1.7. εNdi-Zr/Nb (A), εNdi-(La/Yb)N (B) and εNdi-($^{87}Sr/^{86}Sr$)i (C) correlation diagrams for the basalts and dolerites of the Piñón Formation (data from Aitken & Echeverria (1984) and Castillo et al. (1986),among others).

Fig. 1.8. ($^{208}Pb/^{204}Pb$)i vs ($^{206}Pb/^{204}Pb$)i and ($^{207}Pb/^{204}Pb$)i vs ($^{206}Pb/^{204}Pb$)i correlation diagrams for the basalts and dolerites of the Piñón Formation. data from Nicoya and Heradura (90 MA) igneous complexes (Costa Rica) after Hauff et al. (1997) and Sinton et al. (1997, 1998). Fields of the Gorgona picrites, komatiites, tholeiites and K-tholeiites are after Dupré & Echeverria (1984). The field of the Dumisseau basalts from Haiti is fron Sen et al. (1988). East Pacific MORB and Galápagos Island are from White et al. (1987, 1993). NHRL = North Hemisphere Line after Hart (1984).

Fig. 1.9. Trace-element geochemical similarities of the basalts and dolerites of the Piñón Formation with Late Cretaceous oceanic plateau basalts from Hispaniola and western Colombia and oceanic floor basalts of the Nauru Plateau.

Fig. 1.10. Chondrite normalized (Sun & McDonough, 1989) rare earth elements patterns (A) and N-MORB-normalized (Sun & McDonough, 1989) spidegrams (B) of the igneous rocks of the Las Orquideas Member ans San Lorenzo Formation.

Fig. 1.11. Schematic geological map of the western Colombia and western Ecuador. Numbers indicate the age of the oceanic pateaus (bold) and island arcs (standard).

Fig. 2.1: Schematic map showing the location of the Mesozoic plateau crustal fragments exposed in western central Mexico, Costa Rica, Greater Antilles, Curaçao, Aruba, Colombia, and wextern Ecuador.

Fig. 2.3. Schematic map of Ecuador showing the location of the analyzed samples discussed in the text.

Fig. 2.4: Schematic map of the Arperos basin and the Guerrero terrane showing the location of the samples quoted in the text. A, Acapulco; Al, Alisitos; Ar, Arcelia; C, Colima; D, Durango; G, Guadalajara; GTO, Guanajuato; H, Hermosillo; L, Leon; M, Mexico city; T, Taxco; Te, Teloloapan; Z, Zacatecas; Zi, Zijuatanejo.

Fig. 2.5: Chondrite-normalized (*N*) rare earth element patterns of the minerals and host rocks which show oceanic plateau affinities. San Juan cumulates and Piñón diabases are from Ecuador. Cumulus-enriched picrites and ankaramites belong to the Duarte Complex from Dominican Republic. Chondrite values are from Sun and McDonough (1989).

Fig. 2.6: NMORB-normalized trace element patterns for the minerals and host rocks from Dominican Republic and Ecuador. NMORB values are from Sun and McDonough (1989).

Fig. 2.7: U-Th, Hf-Zr, Ta-Nb, Nb/U-U, and Pb/Ce-Ce plots for the igneous rocks from Dominican Republic, Ecuador, and western Mexico.

Fig. 2.8: Chondrite-normalized *(N)* rare earth and NMORB normalized trace element patterns of the basalts of the Arperos Formation (westerncentral Mexico) which show oceanic plateau affinities. Chondrite and NMORB values are from Sun and McDonough (1989).

Fig. 2.9: Rare earth*N* patterns of calculated melts in equilibrium with the Duarte (Dominican Republic) and Piñón (Ecuador) clinopyroxenes. Chondrite values are from Sun and McDonough (1989).

Fig. 2.10: The εNd -εSr and εNd -($^{87}Sr/^{86}Sr$)*i* plots for the minerals and host rocks from Dominican Republic, Ecuador, and westerncentral Mexico.

Fig. 2.11: The ^{208}Pb-^{204}Pb versus ^{206}Pb-^{204}Pb and ^{207}Pb-^{204}Pb versus ^{206}Pb-^{204}Pb correlation diagrams for the minerals and host rocks. Recalculated initial ratios have been reported for minerals and whole rocks from cumulates and clinopyroxene-rich basalts from Dominican Republic (86 Ma), gabbros and diabases from Ecuador (123 Ma), and pillow basalts from Arperos from Mexico (110 Ma). Typical analytical uncertainties are indicated by the size of the symbols. Various analytical points and data fields have been reported from the literature. Data from the Nicoya Complex, Jaco rocks and Herradura, Costa Rica (90 Ma), are after Hauff et al. (1997), and Sinton et al. (1997 and 1998). The Gorgona picrites, komatiites; tholeiites; and K-tholeiites fields are after Dupré and Echeverria (1984). The field of the Dumisseau basalts from Haiti field is from Sen et al. (1988). The Galápagos lavas field is reported byWhite et al. (1993). East Pacific MORB data and Galápagos Islands field are from White et al. (1987, 1993).

Fig. 2.12: Sm/Nd isochron plot for minerals and whole-rock from the Ecuadorian SJ13 Gabbro. The regression analysis (Ludwig, 1987) yields T = 123 ± 13 Ma, (143Nd/144Nd)o = 0.512875 ± 37, εNdo = +7.76, and MSWD = 2.05 for plagioclase, whole rock and Amphibole.

Fig. 3.1. Schematic geological map of Ecuador showing the main geological and tectonic units.

Fig. 3.2a: Schematic cross section of the Merced-Multitud sequence showing the different components of the uppermost levels of the Early Cretaceous Ecuadorian oceanic plateau.

Fig. 3.2b: Schematic cross section of the San Juan plutonic sequence showing the different components of the deep levels of the Early Cretaceous Ecuadorian oceanic plateau.

Fig. 3.3: Chondrite- and primitive mantle-normalized (Sun & McDonough, 1989) rare earth element patterns and multi-element diagrams for basalts, dolerite and isotropic gabbro of the Merced-Multitud sequences. Samples 82119, 82126 and 82106 are basalts from Lebrat et al. (1987).

Fig. 3.4: Rb (ppm), Ba (ppm) and Sr (ppm) vs Ce (ppm) correlation diagrams of the San Juan peridotites and gabbros.

Fig. 3.5: Al_2O_3 (wt%), CaO (wt%), SiO_2 (wt%) and FeO (wt%) vs MgO (wt%) correlation diagrams of the San Juan peridotites and gabbros.

Fig. 3.6: TiO_2 (wt%) vs MgO (wt%) correlation diagram of the San Juan peridotites and gabbros.

Fig. 3.7: Cr (ppm) and Ni (ppm) vs Ce (ppm) correlation diagrams of the San Juan peridotites and gabbros. Diamond represents an evolved gabbroic liquid derived from the parental magma after removal of olivine and plagioclase.

Fig. 3.8: Chondrite- and primitive mantle-normalized (Sun & McDonough, 1989) rare earth element patterns and multi-element plots for peridotites, gabbros and mineral separates of the San Juan sequence.

Fig. 3.9: Chondrite- and primitive mantle-normalized (Sun & McDonough, 1989) rare earth element patterns and multi-element diagrams for amphibole and plagioclase of the 97SJ13 isotropic gabbro.

Fig. 3.10: Chondrite- and primitive mantle-normanlized (Sun & McDonough, 1989) rare earth element patterns and multi-element diagram for the San Juan ultramafic dyke.

Fig. 3.11: εNd(i) - εSr(t) correlation diagram of the San Juan plutonic rocks.

Fig. 3.12: εNd(i) vs ($^{87}Sr/^{86}Sr$)i diagram of the San Juan plutonic rocks. Fields of volcanic rocks from Gorgona (Aitken & Echeverria, 1984), Galápagos (White et al., 1993), Ontong Java (Mahoney et al., 1993) and Nauru (Castillo et al., 1986) are given for comparison.

Fig. 3.13: $^{208}Pb/^{204}Pb$ vs $^{206}Pb/^{204}Pb$ and $^{207}Pb/^{204}Pb$ vs $^{206}Pb/^{204}Pb$ diagrams for peridotites, gabbros and mineral separates from the San Juan sequence. Basalts and dolerites from the Piñón Formation are reported after Reynaud et al., 1999 and Lapierre et al., 2000. The "Northern Hemisphere Reference Line" (NHRL) and the field from some mantle reservoirs are reported after Zindler & Hart (1986). East Pacific Rise (EPR) MORB and Mid Atlantic Ridge (MAR) MORB data and Galápagos Islands field are from White et al. (1987). The Gorgona field is reported after White et al. (1993).

Fig. 3.14: Chondrite-normalized REE patterns of calculated melts from the cpx of San Juan wehrlite and olivine-gabbro. These calculated melts are compared to dolerites (97MA18 and 97M5).

Fig. 3.15: Primitive mantle-normalized (Sun & McDonough, 1989) multi-element plots showing the compositional range of isotropic and layered gabbros, and dunites and wehrlites from Ecuador (this study) compared to the gabbros from Gorgona (Révillon, 1999; Révillon et al., 2000), and Bolivar (Kerr et al. 1998).

Fig. 4.1: Schematic map showing the location of the Mesozoic plateau crustal fragments exposed in Costa Rica, Greater Antilles, Curaçao, Colombia, and western Ecuador.

Fig. 4.2: Schematic geological map of Western Ecuador showing the main geological and tectonic units.

Fig. 4.3: Schematic Guaranda cross section showing structural location of the Guaranda unit, and studied samples.

Fig. 4.4: Al_2O_3 (wt%), SiO_2 (wt%), TiO_2 (wt%), CaO (wt%), FeO (wt%), Zr (ppm), Ni (ppm), and Cr (ppm) vs MgO (wt%) correlation diagrams of dolerites, ankaramites, basalts and picrites.

Fig. 4.5: La (ppm) vs Nb (ppm) correlation diagram of dolerites, ankaramites, basalts and picrites.

Fig. 4.6: Chondrite- and primitive mantle-normalized (Sun & McDonough, 1989) rare earth element patterns and multi-element plots for dolerites (A), basalts (B), ankaramites (C) and picrites (D).

Fig. 4.7: Chondrite-normalized (Sun & McDonough, 1989) rare earth element patterns for cplinopyroxene of picrites and ankaramites from Guaranda cross section.

Fig. 4.8: εNd-($^{87}Sr/^{86}Sr$)*i* plots for ankaramites, picrites and basalts from the Guaranda cross section.

Fig. 4.9: ($^{208}Pb/^{204}Pb$)i vs ($^{206}Pb/^{204}Pb$)i and ($^{207}Pb/^{204}Pb$)i vs ($^{206}Pb/^{204}Pb$)i diagrams for dolerites, ankaramites, basalts and picrites.

The "Northern Hemisphere Reference Line" (NHRL) and the field from some mantle reservoirs are reported after Zindler and Hart (1986). East Pacific Rise (EPR) MORB and Mid Atlantic Ridge (MAR) MORB data and Galápagos Islands field are from White et al. (1987). The Duarte field is reported after Lapierre et al. (1997).

Fig. 4.10: εNd vs MgO (wt%), ($^{206}Pb/^{204}Pb$)i, and (La/Yb)n correlation diagrams for ankaramites,

Fig. 4.11: Chondrite-normalized REE patterns of calculated melts from the cpx of Guaranda picrites (A) and ankaramites (B).

The melts are calculated using partition coefficients for picrite and ankaramite (Shimizu, 1982; Ulmer, 1989; Hart & Dunn, 1993).

Fig. 4.12: Comparisons of the Pb isotopic ratio from the Early Cretaceous rocks (Lapierre et al., 2000; Mamberti et al., submitted) and the studied rocks. The "Northern Hemisphere

Reference Line" (NHRL) and the field from some mantle reservoirs are reported after Zindler and Hart (1986). East Pacific Rise (EPR) MORB and Mid Atlantic Ridge (MAR) MORB data and Galápagos Islands field are from White et al. (1987). The Duarte field is reported after Lapierre et al. (1997).

Fig. 4.13: Spatial and temporal relationships between the picritic, ankaramitic and basaltic magmas.

Fig. 4.14: Chronostratigraphic sketch of some accreted oceanic terranes of western Ecuador. Shaded area: oceanic plateaus; dotted areas: quartz-rich deposits; heavy lines: inferred accretion episodes.

Fig. 5.1: Cr/(Cr+Al) versus Mg/(Mg+Fe) correlation g Osdiagram for the magnesiochromite from Ecuador. The Gorgona field is reported after Echeverria (1980).

Fig. 5.2: Chondrite- and primitive mantle-normanlized (Sun & McDonough, 1989) rare earth element patterns and multi-element diagram for the glass and the whole rock.

Fig. 5.3: εNd versus Sm/Nd of various basalts and picrites. Compositions of endmembers are from Anderson, 1982, 1983, 1985. Gorgona field (picrite and komatiite) from Révillon et al., 2000.

Fig. 5.4: γ Osversus εNd and $^{206}Pb/^{204}Pb$ for the Ecuadorian picrite. Gorgona picrites and komatiites are reported after Walker et al. (2000).

Fig. 5.5: Chondrite- and primitive mantle-normanlized (Sun & McDonough, 1989) rare earth element patterns and multi-element diagram for the Pedernales and Gorgona picrites. Gorgona picrite data are reported after Révillon et al. (2000).

Fig. 6.1. Schematic geological map of Ecuador showing the main geological and tectonic units.

Fig. 6.2: Schematic cross section of the Selva Alegre sequence showing the different components of the island arc.

Fig. 6.3: Chemical variations from core to rim in clinopyroxene from Otavalo.

Fig. 6.4: Chondrite- and primitive mantle-normalized (Sun & McDonough, 1989) rare earth element patterns and multi-element diagrams for basalts of the San Juan section.

Fig. 6.5: Chondrite- and primitive mantle-normalized (Sun & McDonough, 1989) rare earth element patterns and multi-element diagrams for basalts and andesites of the Selva Alegre section.

Fig. 6..6: Chondrite- and primitive mantle-normalized (Sun & McDonough, 1989) rare earth element patterns and multi-element diagrams for clinopyroxene of some lavas from Selva Alegre section.

Fig. 6.7: Nd and Sr isotopic composition of the island arc rocks from Ecuador. Data from Dominican republic are reported after Dupuis (1999). Puerto Rico after Lebron and Perfit (1994). Data of basalts from Las Orquideas Member and San Lorenzo Formation after Reynaud et al. (1999).

Fig. 6.8: $^{208}Pb/^{204}Pb$ vs $^{206}Pb/^{204}Pb$ and $^{207}Pb/^{204}Pb$ vs $^{206}Pb/^{204}Pb$ diagrams of some lavas from the Selva Alegre sequence. The "Northern Hemisphere Reference Line" (NHRL) and the field from some mantle reservoirs are reported after Zindler & Hart (1986). East Pacific Rise (EPR) MORB and Mid Atlantic Ridge (MAR) MORB data and Galápagos Islands field are from White et al. (1987). The pelagic sediment field is reported after Sun, 1980; White et Dupré, 1986; Ben Othman et al., 1989).

Fig. 6.9: Comparison of the chondrite- and primitive mantle-normalized (Sun & McDonough, 1989) rare earth element patterns and multi-element diagrams for island-arc basalts of Western Cordillera and Coast of Ecuador. Data of basalts from Las Orquideas Member and San Lorenzo Formation after Reynaud et al. (1999).

Fig. 6.10: Chondrite-normalized (Sun & McDonough, 1989) rare earth element diagrams for island-arc basalts from the Western Cordillera of Ecuador and Colombia. Data of basalts from the Colombia after Spadea & Espinosa (1996).

Fig. 6.11: Comparison of the chondrite-normalized (Sun & McDonough, 1989) rare earth element diagrams for island-arc basalts of Western Cordillera of Ecuador and peri-Caribbean area. Data of basalts from Dominican Republic and Puerto Rico after Dupuis (1999) and Freydier (1995) respectively.

Fig. 7.1: Hypothetical cross section through the Early Cretaceous oceanic plateau.

Fig. 7.2: Spatial and temporal relationships between the picritic, ankaramitic and basaltic magmas.

Fig. 7.3: Accretion sequences of oceanic terranes in Ecuador.

Fig. 7.4: Paleotectonic sketch of accretions in Ecuador.

Fig. 7.5: Position and motion of one point on the Nazca plate, between anomalies 30-31 (69-70 Ma) and Present, with respect to south America (After Pardo-Casas & Molnar, 1987 (below); and Pilger, 1984 (above)).

Table 1.1. Location and Petrographic characteristics for the Cretaceous-Paleocene igneous rocks from western Ecuador.

Table 1.2. Major and trace-element concentrations of igneous oceanic rocks from western Ecuador.

Table 1.3. 87Sr/86Sr and 143Nd/144Nd isotope ratios of the igneous oceanic rocks from western Ecuador.

Tab. 2.1. Location and Descriptions of Duarte Complex (Dominican Republic), Piñón Formation (Ecuador), and Arperos Formation (Mexico) Samples

Tab 2.2. Major and Trace Element Analyses for the Duarte Complex and Ecuadorian Minerals and Host rocks, and Arperos Basalts

Tab. 2.3: Nd, Sr and Pb isotopic Analyses for the Duarte complex, Ecuadorian, and Mexican Minerals and Host Rocks.

Tab. 2.4: Sm and Nd Contents and $^{143}Nd/^{144}Nd$ Ratios From SJ13 Whole Rock, Amphibole, and Plagioclase Concentrates

Table 3.1: Petrographic descriptions of the San Juan cumulate rocks.

Table 3.2: Major (wt%) and trace element (ppm) analyses for the San Juan and Merced-Multitud samples. Nd: not detected, -: not analysed, * samples analysed in ANU (Canberra).

Table 3.4: Nd, Sr and Pb isotopic compositions for the San Juan rocks and mineral separates. (m): ratios measured; (i): recalculated initial ratios based on the U, Th and Pb contents determinated by ICP-MS (refer Table 2); (*): initial ratios recalculated using the Pb and U abundances determinated on the basis of the measured Nb/U and Ce/Pb ratios and assuming that Nb and Ce have not been mobilized (Hofmann et al., 1986).

Table 3.3: Major (wt%) and trace element (ppm) analyses for the San Juan and Merced-Multitud mineral separates.

Table 5.1: Major (wt%) and trace element (ppm) analyses for the Guaranda, Galán and Pedernales samples. -: not analysed.

Table 5.2: Major (wt%), trace element (ppm), and isotopic analyses for the Guaranda mineral separates.

Table 5.3: Nd, Sr and Pb isotopic compositions for the Guaranda, Pallatanga, Pedernales and Esmeraldas rocks and mineral separates. (m): ratios measured; (i): initial recalculated ratios (90Ma) based on the U, Th and Pb contents determinated by ICP-MS (refer Table 5.1).

Table 6.1: Major (wt%) and trace element (ppm) analyses for the Selva Alegre and San Juan samples. -: not analysed.

Table 6.2: Nd, Sr and Pb isotopic compositions for the Selva Alegre rocks and mineral separates. (i): recalculated initial ratios based on the Sm, Nd, U, Th and Pb contents determinated by ICP-MS (refer Table 6.1).

Table 6.3: trace element (ppm) analyses for

Fig. 7.1: Hypothetical cross section through the Early Cretaceous oceanic plateau.

Fig. 7.2: Accretion sequences of oceanic terranes in Ecuador.

Fig. 7.3: Paleotectonic sketch of accretions in Ecuador.

Fig. 7.4: Position and motion of one point on the Nazca plate, between anomalies 30-31 (69-70 Ma) and Present, with respect to south America (After Pardo-Casas & Molnar, 1987 (below); and Pilger, 1984 (above)).

Fig. 7.5: Geodynamic evolution of northwestern South America and the peri-Caribbean area.

Table 7.1: Characterisation of oceanic terranes accreted in Ecuador.

INTRODUCTION **7**

LARGE IGNEOUS PROVINCES (LIPS). 9

OCEANIC PLATEAUS 11

THE CARIBBEAN-COLOMBIAN OCEANIC PLATEAU (CCOP) 11

GEOLOGICAL BACKGROUND OF ECUADOR. 14

THESIS OUTLINE 16

OBJECTIVES AND TOOLS 17

CHAPTER 1: OCEANIC PLATEAU AND ISLAND ARCS OF SOUTHWESTERN ECUADOR: THEIR PLACE IN THE GEODYNAMIC EVOLUTION OF THE NORTHWESTERN SOUTH AMERICA. **19**

OCEANIC PLATEAU AND ISLAND ARCS OF SOUTHWESTERN ECUADOR: THEIR PLACE IN THE GEODYNAMIC EVOLUTION OF THE NORTHWESTERN SOUTH AMERICA **20**

ABSTRACT 20

INTRODUCTION 21

GEOLOGICAL FRAMEWORK 23

ANALYTICAL PROCEDURES AND LOW GRADE METAMORPHISM OF THE IGNEOUS ROCKS OF WESTERN ECUADOR 25

Analytical procedures *28*

Metamorphism and alteration of the igneous rocks of western Ecuador *29*

BASEMENT OF SOUTHERN COASTAL ECUADOR (PIÑÓN FORMATION) 29

Petrology and mineral chemistry *29*

Geochemistry *30*

Nd and Sr and Pb isotopic composition *33*

Summary and comparisons *37*

UPPER CRETACEOUS (-LOWER PALEOCENE ?) LAVAS (LAS ORQUÍDEAS MEMBER, CAYO AND SAN LORENZO FORMATIONS) 37

Petrology and mineral chemistry of the lavas and volcaniclastic sediments *37*

Geochemistry *38*

Isotopic chemistry *40*

COMPARISONS WITH THE NEIGHBOURING AREAS AND ORIGIN OF THE "PIÑÓN TERRANE" 40

Comparison between the Coast and the Western Cordillera of Ecuador *40*

Comparison between Western Ecuador and Western Colombia *42*

A southeastern Pacific origin for the Early Cretaceous terrane of Ecuador *44*

SUMMARY AND CONCLUSIONS 45

CHAPTER 2: MULTIPLE PLUME EVENTS IN THE GENESIS OF THE PERI-CARIBBEAN CRETACEOUS OCEANIC PLATEAU PROVINCE **47**

MULTIPLE PLUME EVENTS IN THE GENESIS OF THE PERI-CARIBBEAN CRETACEOUS OCEANIC PLATEAU PROVINCE **48**

INTRODUCTION 49
GEOLOGICAL INFORMATION 52
Dominican Republic. *52*
Ecuador. *53*
Western Central Mexico. *55*
ANALYTICAL PROCEDURES 57
TRACE ELEMENT CHEMISTRY ON MINERAL SEPARATES AND THEIR HOST ROCKS 60
Dominican Republic *60*
Ecuador *62*
Western Mexico *64*
Characteristics of Calculated Melts in Equilibrium with clinopyroxene *65*
ISOTOPIC CHEMISTRY OF THE MINERAL SEPARATES AND HOST ROCKS 66
The cpx-rich basalts of the Duarte Complex *66*
Basalts, Diabases, and Cumulate Gabbro from Ecuador and Mexico *70*
DISCUSSION: PRESENCE OF THREE DISTINCT MAGMATIC SUITES IN THE CCOP 73
GEODYNAMIC IMPLICATIONS 74
CONCLUSIONS 76

CHAPTER 3: THE EARLY CRETACEOUS SAN JUAN PLUTONIC SUITE, ECUADOR: A MAGMA CHAMBER IN AN OCEANIC PLATEAU 79

THE EARLY CRETACEOUS SAN JUAN PLUTONIC SUITE, ECUADOR: A MAGMA CHAMBER IN AN OCEANIC PLATEAU 80

INTRODUCTION 81
GEOLOGICAL SETTING 82
PETROLOGY AND MINERAL CHEMISTRY OF THE MERCED-MULTITUD AND SAN JUAN SECTIONS 86
Merced-Multitud section (Type 1) *86*
San Juan section (Type 2) *86*
Peridotite 87
Layered gabbro 87
Amphibole bearing gabbro (97SJ13) 88
ANALYTICAL METHODS 90
RESULTS 93
Merced-Multitud sequence (Type 1) *93*
San Juan sequence (Type 2) *94*
Mobility of major and trace elements 94
Magmatic aspects 94
Nd, Sr, Pb isotopic chemistry 100
DISCUSSION 104
Compositions of magmatic liquids *104*
Criteria that discriminate between intrusions in oceanic plateaus, normal oceanic crust and island arcs *107*

Geodynamic setting and lithological associations. 107
Magma compositions and crystallization sequences. 107
Trace elements and isotopes. 108
Test cases 109
Intrusions at mid-ocean ridges 109
Ophiolites 109
Intrusions in oceanic islands 110
Intrusion in an oceanic island arc: the Chilas complex of Kohistan 111
Conclusion 111
Plutonic rocks from the Caribbean and Ontong Java plateaus 112
Criteria that demonstrate that the San Juan sequence belongs to an oceanic plateau *115*
Geodynamic setting and broad lithological associations. 115
Mineral assemblages and crystallization sequences: 115
Trace element and isotopic compositions: 115
What is the relationship between the two sequences and the structure of the oceanic plateau *116*
CONCLUSION 117
ACKNOLEDGEMENTS 117

CHAPTER 4: ACCRETED FRAGMENTS OF THE LATE CRETACEOUS CARIBBEAN-COLOMBIAN PLATEAU IN ECUADOR 119

ACCRETED FRAGMENTS OF THE LATE CRETACEOUS CARIBBEAN-COLOMBIAN PLATEAU IN ECUADOR 120

ABSTRACT 120
INTRODUCTION 120
GEOLOGICAL SETTING 123
PETROLOGY AND MINERALOGY 127
Igneous rocks from the Western Cordillera *127*
Mg-rich basalts, ankaramites and dolerites 127
Picrites 128
Igneous rocks from northwestern coastal Ecuador *129*
ANALYTICAL METHODS 130
GEOCHEMISTRY 133
Major and trace elements *133*
REE compositions of the igneous rocks and their host minerals *136*
Nd, Sr and Pb isotopic chemistry *139*
Calculated melts in equilibrium with the clinopyroxenes *144*
DISCUSSION 146
Comparison with the nearby Early Cretaceous and Late Cretaceous oceanic plateau sequences *146*
Spatial and temporal relationships between picrites, ankaramites, dolerites and basalts *148*
Multi-stage model for the emplacement of the Ecuadorian picrites, ankaramites and basalts *149*
Age and tectonic history of the two oceanic plateau sequences *151*
CONCLUSIONS 154

ACKNOWLEDGEMENTS 155

CHAPTER 5: ULTRA-DEPLETED PICRITE IN ECUADOR: REMNANT OF THE CCOP PLUME HEAD. 157

ULTRA-DEPLETED PICRITE IN ECUADOR: REMNANT OF THE CCOP PLUME HEAD 158

INTRODUCTION 158
PETROGRAPHY 159
GEOCHEMISTRY 162
TEMPERATURE AND PRESSURE OF THE PICRITIC MELT 167
Olivine Morphology. 167
MGO CONTENT OF THE PARENTAL MELT 168
LIQUIDUS TEMPERATURE 168
COMPARISON WITH GORGONA PICRITES AND KOMATIITES 169
Petrography 169
Major, trace element and isotopic chemistry 169
DISCUSSION 171

CHAPTER 6 175

PETROLOGY AND GEOCHEMISTRY OF A LATE CRETACEOUS ISLAND ARC IN THE WESTERN CORDILLERA OF ECUADOR 175

INTRODUCTION 175
GEOLOGICAL NOTES 175
THE LATEST CRETACEOUS RÍO CALA ISLAND ARC 178
Petrology 178
Geochemistry 180
COMPARISON WITH THE CONTEMPORANEOUS ARC-ROCKS FROM COASTAL ECUADOR AND THE GREATER ANTILLES 188
Coastal Ecuador 188
Western Cordillera of Colombia 190
Central America 191
The proto-Caribbean arc in the Greater Antilles 191
CONCLUSIONS AND GEODYNAMIC IMPLICATIONS 193

CHAPTER 7: PALINSPASTIC RECONSTITUTION OF THE GEODYNAMIC EVOLUTION OF WESTERN ECUADOR 195

INTRODUCTION 195
CROSS SECTION THROUGH THE EARLY CRETACEOUS OCEANIC PLATEAU 196
TIMING OF ACCRETION OF THE TWO OCEANIC PLATEAUS AND INTRA-OCEANIC ISLAND ARCS 199
RECONSTITUTION OF THE GEODYNAMIC EVOLUTION OF THE NORTHWESTERN SOUTH AMERICA AND NEIGHBOURING AREAS 205
Location of the hotspots linked to the Early and Late Cretaceous (CCOP) oceanic plateaus 205

Preliminary remarks 205
Geodynamic evolution of northwestern South America and the peri-Caribbean area. 207
GENERAL CONCLUSIONS 220

REFERENCES 223

INTRODUCTION

INTRODUCTION

It is widely admitted that the building up of mountain ranges is related to global plate tectonics, and derives from subduction processes. Within this framework, orogenic belts are related to two major processes.

- (1) Subduction of oceanic lithosphere beneath continental lithosphere gives rise to linear mountain belts located on the overthrusting plate margin, parallel to the subduction zone. Such mountain belts are generally termed Andean-type mountain ranges.

- (2) Collisional mountain ranges develop when subduction bring to the trench lithospheric material, the density of which is sufficiently low that its buoyancy prevents its descent. This anomalous material is commonly a continent, but may be also lithosphere carrying the thickened crust of an island arc or an oceanic plateau, or a microcontinent making up an integral part of the subducting oceanic lithosphere. The resulting collision of buoyant crust causes the creation of a collisional range by the stacking of thrust slices of crust material. Lateral movements in the welded continents may continue, however, for a considerable time interval after collision. These collisional-type mountains are found in the North American Cordillera, the Alps, and the Himalayas. Detailed geological studies in western North America during the 1970's provided evidence that the continental back-trench region of the North American Cordillera is made up of a collage of exotic, suspect or mosaic tectonic units ("suspect terranes" of Coney et al., 1980). The evidence from the North American Cordillera and other areas (Pigram and Davies, 1987) strongly suggests that the arrival of exotic terranes at a subduction zone leads to the subsequent thrusting of the material onto the continental plate. Suspect terranes may be of continental, oceanic, and island arc origin.

Ben-Avraham et al. (1981) suggested that modern analogues of the material giving rise to suspect terranes could be the abundant ridges, rises and plateaus which make up about 10 % of the area of the present ocean basins. For example, the Ontong Java Plateau partly obducted onto the Solomon islands when the margin of this plateau collided with the Vitiaz intra-oceanic arc 10 My ago (Tejada et al., 1996; Neal et al., 1997). Thus, suspect terranes could be formed of various oceanic material already amalgamated by collisional events, which then accreted to an upper plate by means of large transcurrent faults.

The Andes are related to the subduction of oceanic lithosphere under the South American plate since the Early Jurassic. The Cordilleras from Ecuador and Colombia, located

in northwestern South America, differ from the Central Andes in that their development is linked to the accretion of exotic oceanic material in the Mesozoic and Early Tertiary (Gansser, 1973; Feininger and Bristow, 1980; Bourgois et al., 1987). These oceanic crustal fragments exposed in western and coastal Ecuador offer a unique opportunity to study different components of oceanic plateaus and island arcs.

The main goals of this study are firstly, to characterize the magmatic affinities of the accreted oceanic fragments exposed in the Western Cordillera and the Coast of Ecuador, and secondly, to propose a geodynamic evolution of this part of the northern Andes during the Cretaceous and Early Tertiary.

Petrological and geochemical investigations will help to characterize the geodynamic setting of the accreted oceanic fragments. Do they belong to normal oceanic crust, to oceanic plateaus, to oceanic island arcs, or to intra-oceanic islands ? Ages of these exotic terranes and the dates of their accretion will help to specify the main stages of development of the Western Cordillera and Coast of Ecuador. Finally, these data will also allow study of the geodynamic links of the Ecuadorian and Colombian Cordilleras with the neighbouring areas, *i.e.*, the Caribbean and central American ranges.

Previous and recent work in the Caribbean Sea and peri-Caribbean areas have shown that remnants of the Late Cretaceous (90-86 Ma) oceanic plateau are exposed in Costa Rica, Venezuela, Dominican Republic and Colombia. In Ecuador, preliminary studies (Goossens and Rose, 1973; Juteau et al., 1977; Lebrat et al., 1987; Wallrabe-Adams, 1990; Desmet, 1994) have shown that the magmatic rocks exposed in the Western Cordillera and along the coast are of oceanic affinity. More recent studies based on trace element and isotopic chemistry demonstrated that these accreted fragments display oceanic plateau or island arc affinities (Cosma et al., 1998; McCourt et al., 1998; Reynaud et al., 1999; Boland et al., 2000). Thus, several questions are raised. Do the accreted fragments of oceanic plateau affinity belong to the Late Cretaceous Caribbean plateau or to a distinct older plateau ? Are these oceanic plateau fragments remnants of a single or more than one oceanic plateau ?

In order to answer to these questions, we have based our study on the petrology, major-, trace- element and isotopic (Nd, Sr and Pb) geochemistry of the igneous rocks and their preserved minerals. In order to constrain the age of the accreted fragments, we have tried to date the rocks using Sm and Nd internal isochrons.

Before presenting the geological setting of Ecuador, and because most of this thesis is devoted to the petrology and geochemistry of oceanic plateau fragments nowadays exposed in Ecuador, we will briefly present the main characteristics of Large Igneous Provinces (LIPs)

and of Oceanic Plateaus, their distribution, ages and their development (classically considered to be related to large scale mantle plumes). Finally, the last section will be devoted to the Caribbean Cretaceous oceanic plateau, since Upper Cretaceous picrites and basalts accreted in Ecuador exhibit many similarities with basaltic rocks of the Late Cretaceous Caribbean oceanic plateau.

LARGE IGNEOUS PROVINCES (LIPS).

A world-wide distribution of the LIPs is reported by Coffin and Eldhlom (1993). The LIPs include oceanic plateaus and their continental analogous, the "traps". The LIPs derive from the melting of a mantle plume and correspond to the outpouring of voluminous lava flows, generally > 1 million km^3. They are added to the oceanic or continental crust. In the case of oceanic plateaus, seismic and gravimetric analyses indicate that the thickness of the crust ranges between 10 to 40 km. The largest oceanic plateau is Ontong Java in the western Pacific where the thickness of crust reaches 39 km (Mahoney et al., 1993). Some characteristics, like huge fluid lava flows and few sediments between two flows, indicate the rapid development of the Ontong Java Plateau. The development of the Deccan traps lasted less than 1 Ma (White & McKenzie, 1989).

The main difference between oceanic plateau and traps is the geological environment. The presence of continental crust below the traps creates the problem of contamination of mantle-derived magmas by continental lithosphere during ascent. Traps are the best material to understand the processes of contamination, fractionation and differentiation of mantle plume magmas. In contrast, investigations of oceanic plateau magmas, and more precisely of picritic primitive magmas, represent the best way to have a direct access to the mantle plume-derived melts devoid of any contamination or assimilation. Thus, picrites and high-Mg basalts associated with the oceanic plateau basalts represent the best opportunity to study melting processes occurring during the ascent of large, hot and heterogeneous plumes. A chapter of this thesis will address the origin of Mg-rich basalts related to the Caribbean Plateau.

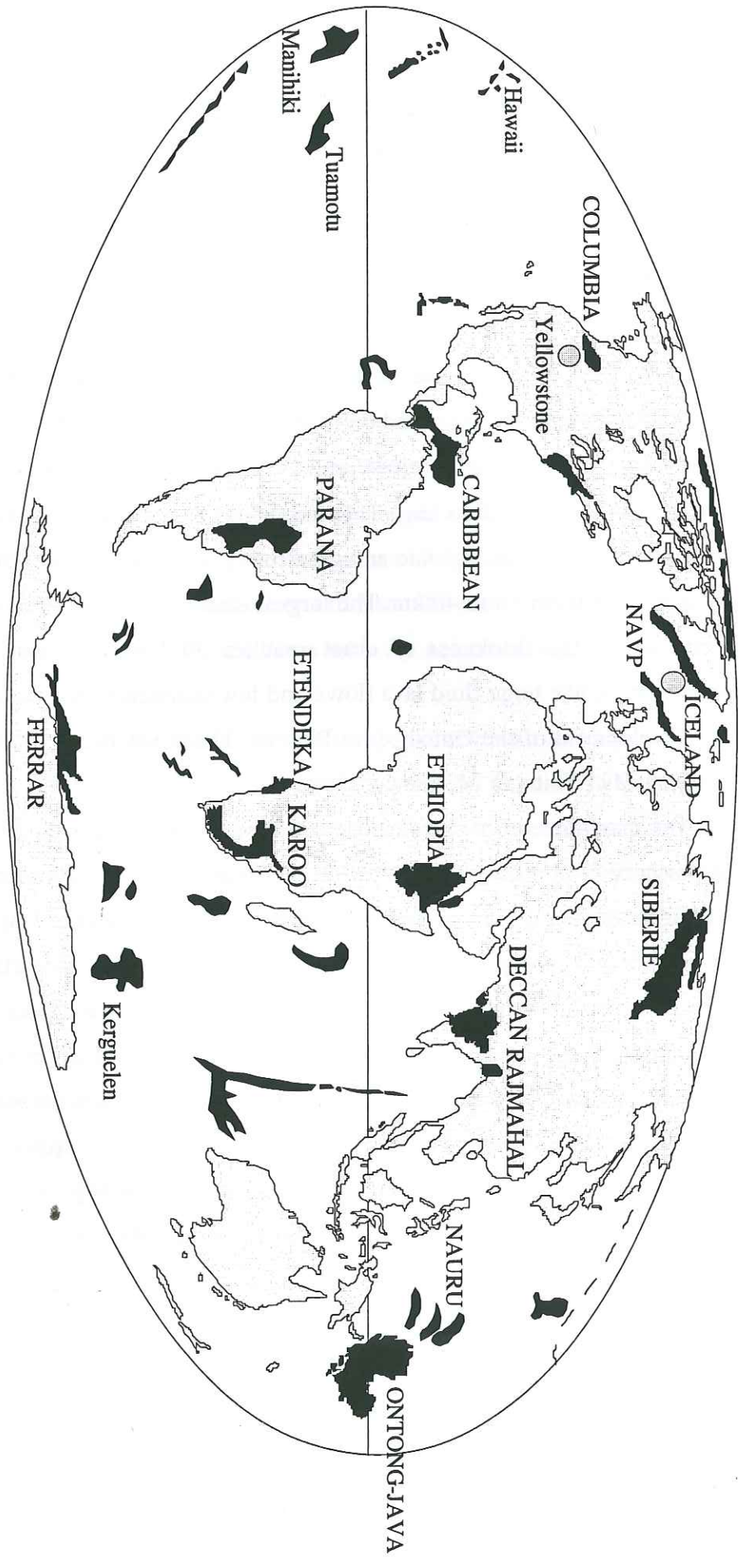

Fig. 1.1: General map of the Large Igenous Provinces (Coffin & Heldholm, 1993).

OCEANIC PLATEAUS

Oceanic plateaus are, together with oceanic island basalts (OIB) and traps, the expression of intraplate volcanism. Oceanic plateaus originate through eruption of large volumes of mafic magmas with cogenetic plutonic intrusions trapped within the oceanic lithosphere. The emplacement of these mafic magmas increases the thickness of the oceanic crust, and these over-thickened areas tend to be more buoyant than normal oceanic crust due to both thermal and density differences (Cloos, 1993). Thus, oceanic plateaus are not so easily subducted and have the potential to be obducted onto continental margins, thus increasing both the possiblity of their preservation and accessibility for detailed study. According to the literature, the source of an oceanic plateau is a mantle plume. Oceanic plateau basalts are generally similar to Mid Oceanic Ridge Basalts (MORB) but also differ by enrichments in Light Rare Earth Element (LREE), Sr and Nd isotopic compositions, and often by the presence of highly magnesian basalts (Anderson, 1994; Kerr et al., 1994; Arndt et al., 1997) while the REE compositions of oceanic plateau basalts from different occurrences are relatively similar, they exhibit a large range of isotopic compositions which reflectinvolvement of heterogeneous sources. This large range of isotopic compositions of basaltic melts produced by the same plume reflects the complexity of the mantle sources and processes required to produce such different melts.

Oceanic plateau basalts are the most studied and the best known component of oceanic plateaus because of the difficulties of access to the deeper plutonic roots. The accretion and sometimes the obduction of an oceanic plateau onto the margin of a continent represents the only way to study plutonic rocks of an oceanic plateau. The presence in the Western Cordillera of Ecuador of plutonic rocks inferred to belong to an oceanic plateau offered us the opportunity to investigate the petrology and geochemistry of these rocks. A chapter of this thesis is devoted to this plutonic association.

THE CARIBBEAN-COLOMBIAN OCEANIC PLATEAU (CCOP)

Cretaceous oceanic plateau rocks are exposed at different locations in the Caribbean and Central America: Aruba and Curaçao islands, Hispaniola (Dumisseau formation), Dominican Republic (Duarte complex), Jamaica, Costa Rica (Nicoya, Santa Helena), Gorgona Island, Colombia, and Ecuador. They represent remnants of an oceanic plateau which has been added to a Late Jurassic oceanic crust, forming the present-day Caribbean Plate, part of which is

accreted to South America (Venezuela, Colombia and Ecuador, Donelly et al., 1990; Kerr et al., 1996).

Three different ages of magmatism are found in the CCOP. The most volumetrically important is the 90-85 Ma event (Sinton et al., 1998). Most exposures of volcanic rocks from the Greater Antilles, Central America and South America are related to this event. This is the case for the basalts, picrites associated locally with komatiites from Gorgona and Curaçao Islands, Hispaniola and Haiti. The second event is dated at 76 Ma. This age is reported in Colombia and in the Beata ridge (Révillon et al., 2000). The third and youngest event (55 Ma) is reported in the Beata ridge and Costa Rica (Quepos Formation). These three events attest to the long period of magmatic activity in the Caribbean, but raise the questions of the location, and presence of one or more mantle plumes related to these igneous events.

Two models for the genesis of the CCOP have been proposed. In the first model, the Caribbean plateau was formed in the Pacific, accreted to the Greater Antilles arc and to the margin of South America because of the eastward displacement of the Farallón Plate. In this interpretation, the Caribbean oceanic plateau is linked either to the Galápagos (Duncan & Hargraves, 1984) or to the Sala y Gómez hotspots (at least for the 90 Ma event; Révillon et al., 2000).

In the second model, the CCOP was formed close to the North and South American Plates and remained more or less stationary, while the westward drift of the North and South American Plates eventually sandwiched the CCOP. In this interpretation, the plume related to the development of this plateau was located somewhere in the eastern equatorial Pacific, close to the present-day location of the Caribbean Plate (Winsemann et al., 1994; Meschede et al., 1998; Dupuis, 1999).

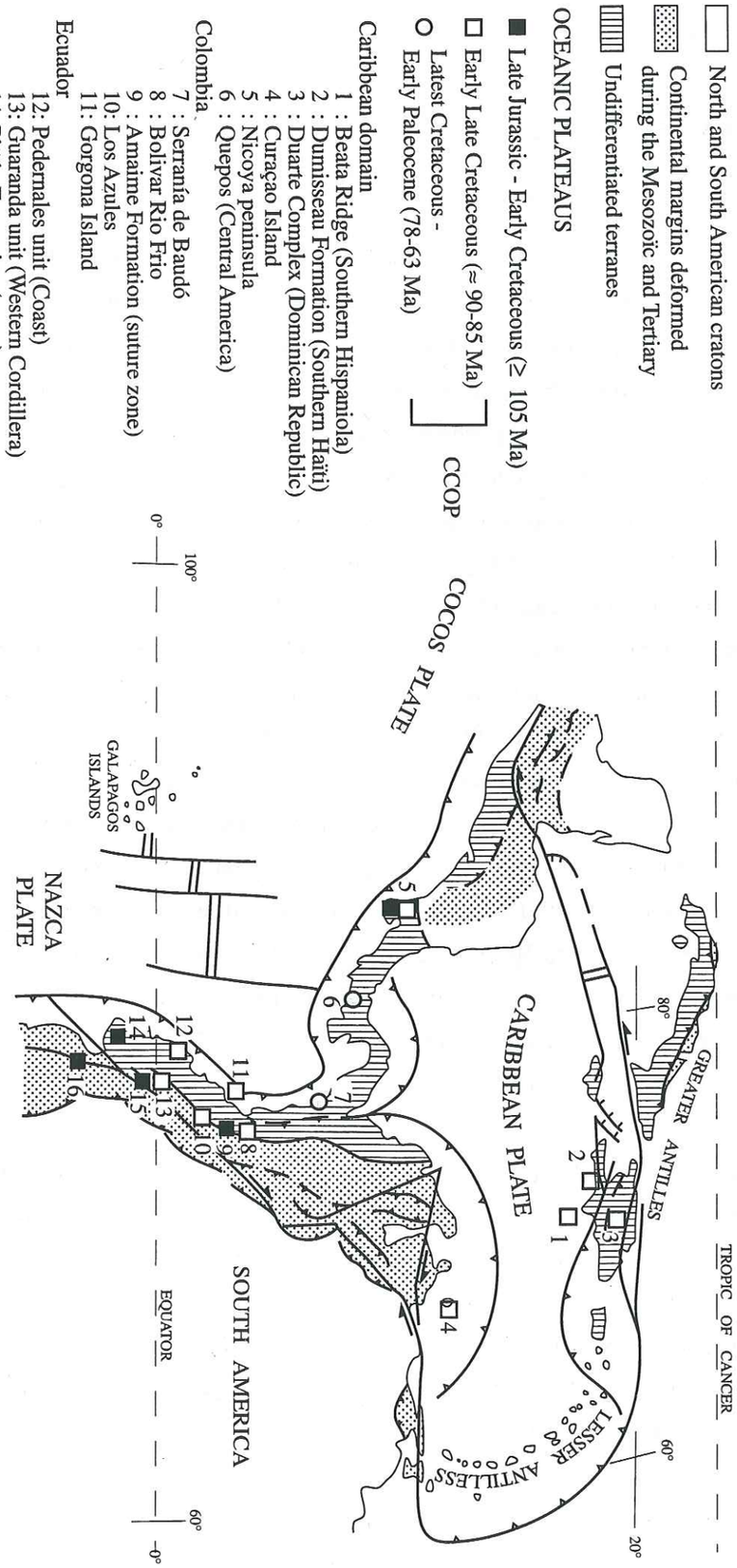

Fig. 1.2: Schematic map showing the location of the Mesozoic plateau crustal fragments exposed in Costa Rica, Greater Antilles, Curaçao, Colombia, and western Ecuador.

GEOLOGICAL BACKGROUND OF ECUADOR.

Ecuador is located along the northwestern margin of South America and comprises, from east to west, three main geological domains: the Oriente Basin, the Andean Cordillera and the coastal zone.

The Oriente basin represents the foreland basin of the Andean orogeny (Baldock, 1982; Jaillard, 1997; Christophoul et al., in press). The Andean cordillera is crosscut and overlain by the products of Tertiary to Recent magmatic arcs (Aspden et al., 1992; Lavenu et al., 1992). It consists of two cordillera separated by the inter-Andean valley. The geology of the two cordilleras is described in detail in chapter 3, devoted to the San Juan section. The coastal area, as well as the Western Cordillera, are made of oceanic exotic terranes.

Some authors (Goossens & Rose, 1973; Goossens et al., 1977; Juteau et al., 1977; Lebrat et al., 1987; Wallrabe-Adams, 1990) have shown that the basement of the Late Cretaceous-Paleogene island arcs of the western part of Ecuador exhibits N-MORB affinity. Recent works (Desmet, 1994; Cosma et al., 1998; Reynaud et al., 1999; Lapierre et al., 2000) demonstrate that this basement (formerly undifferentiated and named the Piñón Formation) exhibits oceanic plateau affinities. The so-called Piñón Formation consists of pillow basalts and dolerites, which are overlain unconformably, in the Guayaquil area, by Cenomanian-Maastrichtian island arc successions (Jaillard et al., 1995; Benítez, 1995). Thus, at least part of the oceanic basement of Western Ecuador is pre-Upper Cretaceous in age (pre-95 Ma).

During the Jurassic (≈ 190-140 Ma), as a result of southeast-ward oceanic convergence, an Andean-type magmatism developed along the Ecuadorian margin leading to the emplacement of subduction-related volcanic and plutonic rocks exposed now along the Subandean zone, east of the Eastern Cordillera (Litherland et al. 1994; Jaillard, 1997). In the latest Jurassic, subduction ceased beneath the Colombian-Ecuadorian segment of the margin, due to a drastic change in the convergence direction, which turned northeast-ward (Aspden et al., 1987; Jaillard et al., 1990). From latest Jurassic to Eocene times (≈ 140-50 Ma), the motion of the paleo-Pacific Plate was too oblique with respect to the Colombian-Ecuadorian margin, and no magmatic arc developed in that area (Jaillard et al., 1995). Between Late Cretaceous and Eocene times, exotic crustal fragments of Cretaceous to Early Tertiary age, with oceanic plateau and intra-oceanic arc affinities accreted successively to the Ecuadorian margin (Feininger and Bristow, 1980; Lebrat et al., 1987; Daly, 1989). They are now exposed in the Western Cordillera and along the coast.

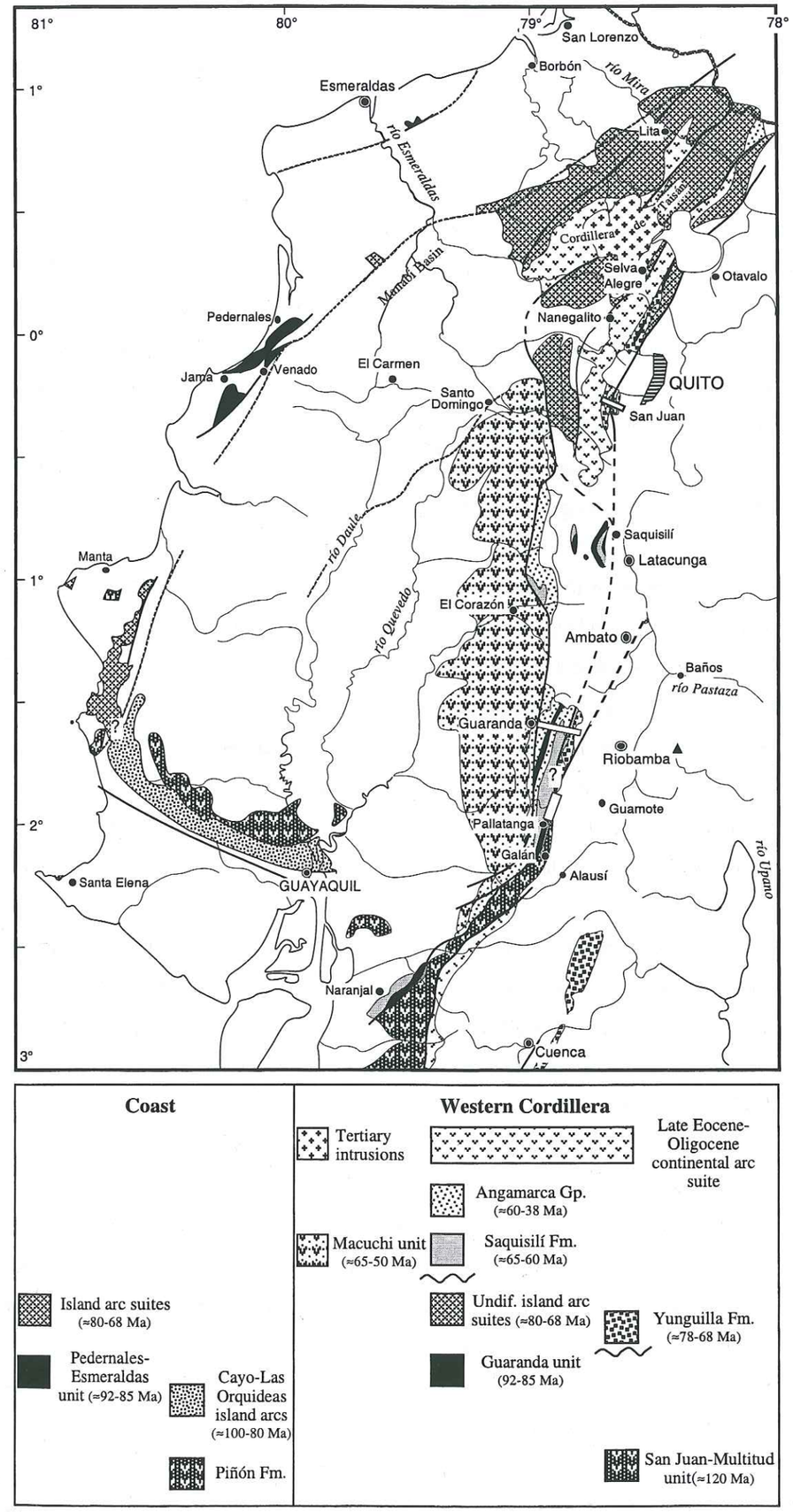

Fig. 1.3: Schematic geological map of Western Ecuador showing the main geological and tectonic units.

THESIS OUTLINE

In this work, we have studied the geology, petrology and geochemistry of several cross sections of oceanic rocks exposed in the Western Cordillera and along the coast in order to provide information about the structure of oceanic plateaus, and to better constrain the geodynamic environment and evolution of western Ecuador and the north-western margin of South America from Cretaceous to Early Tertiary times. We have focussed our investigations on the rocks (basalts, dolerites, ankaramites, picrites, isotropic gabbros and cumulates) which displayed oceanic plateau affinities. The geological setting of the major units of Ecuador is described in detail in the beginning of each chapter.

The first two chapters of this thesis consist of two publications of which I was a co-author, show the state of knowledge on the petrology and geochemistry of the Ecuadorian oceanic accreted terrranes when I started this research. In the first paper, Reynaud et al. (1999) show on the basis of petrological and geochemical data that the basalts and dolerites exposed in the Coast of southern Ecuador display features of oceanic plateau basalts, and that locally, these rocks are overlain by Upper Cretaceous intra-oceanic island arc lavas. In the second publication, Lapierre et al. (2000) point out the age, petrological, and geochemical differences between the oceanic plateau fragments exposed in parts of Ecuador and in the Caribbean.

The next three chapters present detailed petrological and geochemical data on the accreted fragments of oceanic plateau exposed in Ecuador. In two of these papers, submitted for publication, we present the petrological and geochemical characteristics of the different igneous components (cumulates, shallow level gabbros and extrusive rocks) of the Early Cretaceous and Late Cretaceous oceanic plateaus, respectively. A detailed geochemical study including Nd, Sr, Pb, and Os/Re data is dedicated to aa especially well preserved picrite which likely represents, together with the Gorgona komatiites and picrites, the products of the 90-86 Ma plume head of the Cretaceous Caribbean Oceanic Plateau (CCOP). To conclude on the oceanic plateaus accreted in Ecuador, and on the basis of the specific characteristics of the different exhumed parts of the Early Cretaceous plateau, we present a hypothetical cross section through the oceanic crust of an oceanic plateau including its plutonic roots.

Chapter six deals with the petrology and geochemistry of the Late Cretaceous intra-oceanic arcs from the Western Cordillera at 0°15'N .

Finally, in the last and seventh chapter, on the basis of the data acquired during this work, we discuss the models already proposed for the geodynamic evolution of north-western South America, and we bring some constraints on the geodynamic model proposed by Mercier de Lépinay (in Dupuis, 1999) for the north-western margin of South America and the Caribbean domain from the Early Cretaceous up to the Tertiary.

OBJECTIVES AND TOOLS

The main targets of this work are to describe and analyze the magmatic rocks of the Ecuadorian oceanic plateaus in order to :

(1) show the specific characteristics of the plutonic roots of an oceanic plateau;

(2) identify and constrain the mantle plume sources which generated the two oceanic plateaus (which allowed us to demonstrate the presence of two oceanic plateau sequences which differ in age and composition);

(3) propose a hypothetical cross-section through the crust of an oceanic plateau on the basis of the petrological and geochemical characteristics of the cumulates and volcanic rocks;

(4) determine the southernmost extension of the CCOP;

(5) propose a plate tectonic model for the geodynamic evolution of Ecuador and Eastern Pacific since the Early Cretaceous.

This study is based on the petrological, mineralogical and whole rock chemical analysis, including major, trace and Nd, Sr and Pb isotopic compositions. The equipments used for these investigations are electron microprobe (University of Lausanne), X-ray fluorescence (University of Lausanne, ANU, Canberra), Inductively Coupled Plasma Mass Spectrometry (ICP-MS, OSUG, Grenoble), multicollector mass spectrometer (Finnigan MAT261, CNRS, Toulouse) and VGP54 magnetic sector ICPMS (ENS, Lyon). All the analytical data presented in this work were done by the author, in collaboration with Delphine Bosch (Université de Montpellier II),

Chapitre 1

Desmet (1994) a présenté en détail les différents faciès pétrographiques de plusieurs associations de roches magmatiques en Equateur. Il a été le premier à montrer que certaines roches océaniques accrétées en Equateur présentaient des affinités de plateau océanique. Les premières études géochimiques et isotopiques portent sur des roches de formations de plateau océanique provenant du Sud-Ouest Equateur. Les résultats sont présentés dans ce chapitre et ont fait l'objet d'un papier (Raynaud et al., 1999). Les études pétrologiques et géochimiques des tholéiites de la formation Piñón de cette région indiquent qu'elles représentent le témoin d'un fragment de plateau océanique qui se serait accrété à la marge Andine pendant le Paléocène supérieur. Localement, ces roches sont surmontées par des sédiments du Crétacé inférieur à supérieur. Les roches de la Formation Piñón ne peuvent donc pas appartenir au plateau océanique Caraïbe-Colombien Crétacé Supérieur. Le plateau océanique Crétacé Inférieur peut être relié à un point chaud localisé plus au Sud-Ouest par rapport au point chaud des Galápagos.

Chapter 1

OCEANIC PLATEAU AND ISLAND ARCS OF SOUTHWESTERN ECUADOR: THEIR PLACE IN THE GEODYNAMIC EVOLUTION OF THE NORTHWESTERN SOUTH AMERICA

Cédric REYNAUD, Étienne JAILLARD, Henriette LAPIERRE, Marc MAMBERTI and Georges H. MASCLE.

Tectonophysics, v. 307, p. 235-254.

CHAPTER 1: OCEANIC PLATEAU AND ISLAND ARCS OF SOUTHWESTERN ECUADOR: THEIR PLACE IN THE GEODYNAMIC EVOLUTION OF THE NORTHWESTERN SOUTH AMERICA.

Desmet (1994) presented the detailed petrology of several asociations of Ecuadorian igneous rocks. This author was the first to characterize the oceanic plateau affinity of some of the oceanic rocks accreted in Ecuador.

The first geochemical and isotopical studies of oceanic plateau formations from southwestern Ecuador are presented in this chapter by means of a paper (Reynaud et al., 1999). The petrological and geochemical features of the Piñón tholeiites of this area suggest that they represent remnants of an oceanic plateau fragment which accreted to the Andean passive margin during the Late Paleocene. Locally, these rocks are overlain by lower Upper Cretaceous sediments. Thus, they cannot belong to the Late Cretaceous Caribbean Colombian Oceanic Plateau. The Early Cretaceous Ecuadorian oceanic plateau is linked to a plume located farther southwest than the Galápagos hotspot.

OCEANIC PLATEAU AND ISLAND ARCS OF SOUTHWESTERN ECUADOR: THEIR PLACE IN THE GEODYNAMIC EVOLUTION OF THE NORTHWESTERN SOUTH AMERICA

ABSTRACT

Coastal Ecuador is made up of an oceanic igneous basement overlain by Upper Cretaceous to Lower Paleocene (≈ 98-60 Ma) volcanoclastic and volcanic rocks of island-arc affinities.

The igneous basement, known as the Piñón Formation, locally dated at 123 Ma, consists of olivine-free basalts and dolerites. Relative to N-MORB, both types of rocks exhibit high concentrations in Nb (0.3-10.75 ppm), Ta (0.03-0.67 ppm), Th (0.11-1.44 ppm), light and medium rare earth elements, and low Zr (22-105 ppm) and Hf (0.59-2.8 ppm) contents, thus showing oceanic plateau basalts affinities. Most of these oceanic plateau basalt tholeiites display rather homogenous $\varepsilon_{Nd(T=123Ma)}$ ratios (≈+7), with the exception of two rocks with higher (+10) and lower (+4.5) $\varepsilon_{Nd(T=123Ma)}$, respectively. All these basalts plot, with one exception, within the Ocean Island Basalts field. Their $(^{87}Sr/^{86}Sr)_i$ ratios are highly variable (0.7032-0.7048), probably due to hydrothermal oceanic alteration or assimilation of altered oceanic crust. The rocks of the Piñón Formation are geochemically similar to the oceanic plateau tholeiites from Nauru and Ontong Java Plateaus and to the Upper Cretaceous (92-88 Ma) Caribbean Oceanic Plateau lavas.

The basalts and dolerites of the Upper Cretaceous-Lower Paleocene island arcs show calc-alkaline affinities. The ε_{Nd} ratios (+6.1 to +7.1) of these arc-rocks are very homogenous and fall within the range of intra-oceanic island-arc lavas. The Upper Cretaceous-Lower Paleocene calc-alkaline and tholeiitic rocks from Coastal Ecuador share similar high ε_{Nd} ratios to Cretaceous intra-oceanic arc rocks from north, central and south America and from the Greater Antilles.

Since the Piñón oceanic plateau tholeiites are locally overlain by early Late Cretaceous sediments (≈ 98-83 Ma) and yielded locally an Early Cretaceous age, they do not belong to the Late Cretaceous Caribbean Oceanic Plateau. The basement of coastal Ecuador is interpreted as an accreted fragment of an overthickened and buoyant oceanic plateau.

The different tectonic units of coastal Ecuador cannot be easily correlated with those of western Colombia, excepted the Late Cretaceous San Lorenzo and Ricaurte island arcs. It is suggested that northwestern South America consists of longitudinally discontinuous terranes, built by repeated accretionary events and significant longitudinal displacement of these terranes.

INTRODUCTION

Subduction of oceanic plates occurred beneath the western margin of the South America continental plate since at least Early Jurassic times (e.g. James, 1971; Aspden et al., 1987; Jaillard et al., 1990). However, whereas no mafic complexes nor exotic oceanic terranes are known in central South America (Mégard, 1987), northwestern South America is characterized by the presence of mafic terranes of oceanic origin (e.g. Gansser, 1973; Toussaint and Restrepo, 1994). Recent works carried out in western Colombia has demonstrated that several accreted terranes are remnants of oceanic plateaus (Millward et al., 1984; Nivia, 1996; Kerr et al., 1996; 1997a; 1997b), the buoyancy of which may explain why they have not been subducted.

In Ecuador, a NNE-trending Late Jurassic-earliest Cretaceous ophiolitic suture has been mapped (Aspden and Litherland, 1992), which separates the crystalline basement of the Eastern Cordillera (Litherland et al., 1994) from the oceanic volcanic rocks of Western Ecuador (Fig. 1.1). The coastal terrane was regarded as a fragment of oceanic floor (Goossens and Rose, 1973; Goossens et al., 1977; Juteau et al., 1977), overlain by intra-oceanic volcanic arcs (Lebrat et al., 1987; Jaillard et al., 1995), and accreted to the Andean margin during Late Cretaceous (Lebrat et al., 1987), Paleocene (Daly, 1989; van Thournout et al., 1992) and/or Eocene times (Feininger and Bristow, 1980; Bourgois et al., 1990).

No detailed geochemical and isotopic studies have been carried out on the mafic rocks of Coastal Ecuador, and their nature, age and origin are yet poorly constrained. The aim of this paper is to present new results on the mineralogy, petrology, geochemical and isotopic signatures of the igneous basement in coastal Ecuador. Together with recent and current geological studies (Jaillard et al., 1997; Cosma et al., 1998; Lapierre et al., 1999), the new data allows us to refine the geological evolution and geodynamic significance of this probably composite terrane, to compare its tectonic history and significance with the oceanic plateau

fragments of Western Colombia, and to discuss its origin.

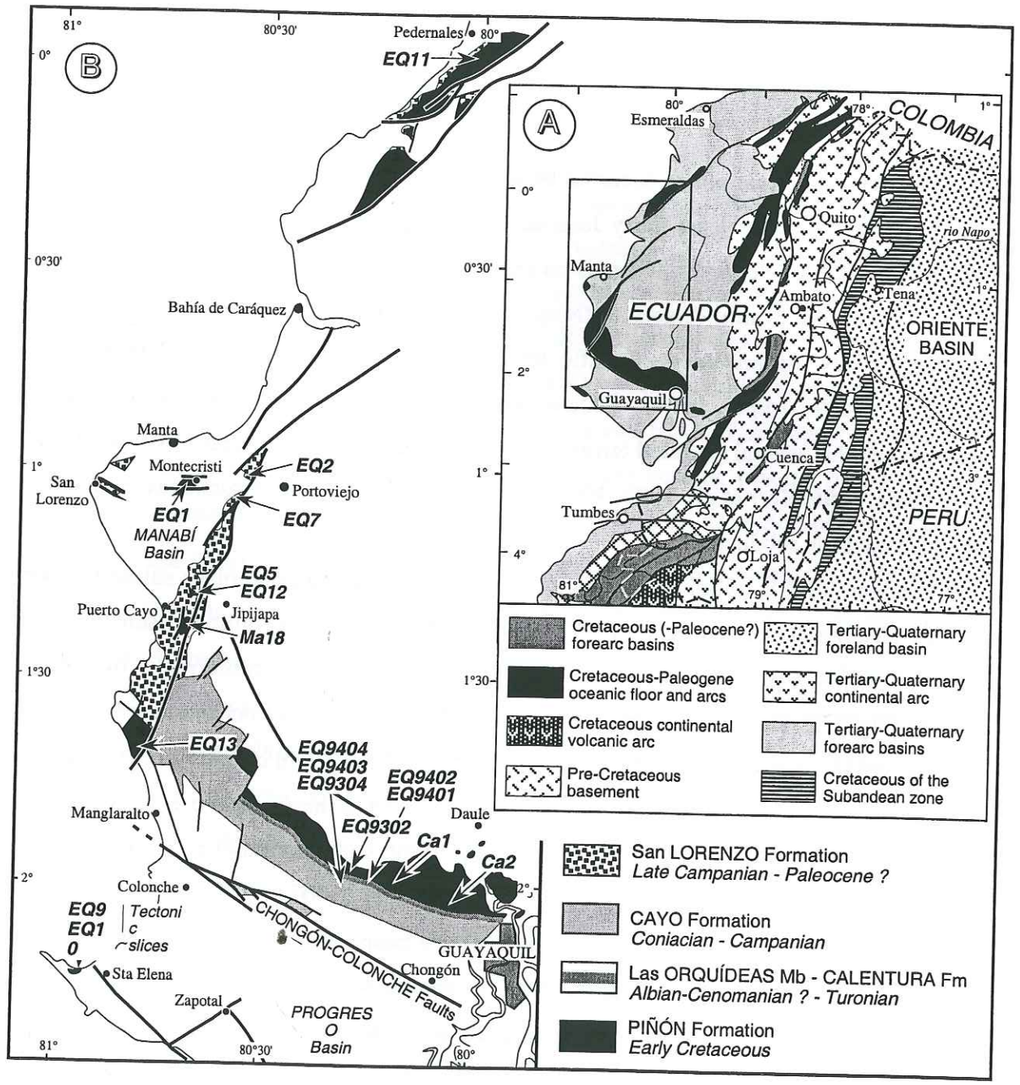

Fig. 1.1. (A) Schematic geological map of Ecuadorshowing the main geological and tectonic units and the location of the studied area. (B) Geological sketch of southern coastal Ecuador showing the distribution of the studied magmatic units and the location of the samples analyzed.

GEOLOGICAL FRAMEWORK

The Piñón Formation is regarded as the Cretaceous igneous basement of Western Ecuador, made up of tholeiitic basalt-andesitic pillow basalts and massive flows, locally associated with pillow-breccias, hyaloclastites and subordinate siliceous sediments. So far, it is considered as a piece of oceanic floor (Goossens and Rose, 1973; Juteau et al., 1977; Lebrat et al., 1987), that locally possesses island-arc affinities (Goossens et al., 1977; Henderson, 1979). The volcanic rocks are intruded by doleritic and/or gabbroic stocks. The studied samples come from two distinct geological domains of Coastal Ecuador.

In the northwestern area (Manabí, fig. 1.1 and 1.2), altered and metamorphosed basalt flows of N-type MORB composition, ascribed to the Piñón Formation, yielded unreliable K/Ar ages ranging from 110 to 54 Ma (Goossens and Rose, 1973). The Piñón Formation is of pre-Late Campanian age (≈ pre-78 Ma), since it is overlain by sediments paleontologically dated as late Campanian and cross cut by late Campanian intrusions (Pichler and Aly, 1983; Wallrabe-Adams, 1990). The northwestern area seems to be separated from the Central area by a NE- to NNE-trending fault system running East of Manta and SE of Esmeraldas (Fig. 1.1).

In the San Lorenzo area (Fig. 1.1), coarse-grained graywackes and volcaniclastic conglomerates associated with basaltic flows, ash beds, dikes and scarce thin limestone beds, are interpreted as resting on the Piñón Formation. These volcanic rocks, named the San Lorenzo Formation, are related to the activity of an intra-oceanic arc (Lebrat et al., 1987). Inter-pillow sediments of the San Lorenzo Formation are dated by late Campanian and Maastrichtian microfauna (Sigal, 1969; Faucher et al., 1971; Jaillard et al., 1995; Ordoñez, 1996). Volcanic rocks yielded K/Ar ages of 85 to 65 Ma (Goossens and Rose, 1973; Pichler and Aly, 1983) and an $^{40}Ar/^{39}Ar$ age of 72.7 ± 1.4 Ma (Lebrat et al., 1987). This succession is then unconformably overlain by fore-arc marine sediments of Middle Eocene age (Cerro, San Mateo Formations), within which the abundance of detrital quartz indicates that this area was already accreted to the continental margin (Manabí Basin, Benítez, 1995; Jaillard et al., 1995; 1997; fig. 1.2).

The Central area (Guayaquil area) is a little deformed area, where good and continuous sections can be observed, except locally, south of the Chongón-Colonche faults. In the Guayaquil outskirts (Las Orquídeas locality, Perimetral section) and in the Chogón-Colonche

Cordillera, the undated Piñón Formation is stratigraphically capped by a thin layer of pillowed phyric basalts, referred to here as the Las Orquídeas Member (fig. 1.2). Along the Perimetral section, the Las Orquídeas member is stratigraphically overlain by a 200 m-thick succession of pelagic black shales, limestones and thin-bedded volcanic or volcaniclastic intercalations (Calentura Formation), which yielded Cenomanian to Turonian microfauna, a Turonian ammonite and Turonian to Coniacian nannofossils (Thalmann, 1946; Sigal, 1969; review *in* Jaillard et al., 1995). Therefore, the Las Orquídeas Member is of pre-Cenomanian to pre-Turonian age (≈ pre-95 Ma), and the underlying Piñón Formation is most probably of pre-Late Cretaceous age (Fig. 1.2).

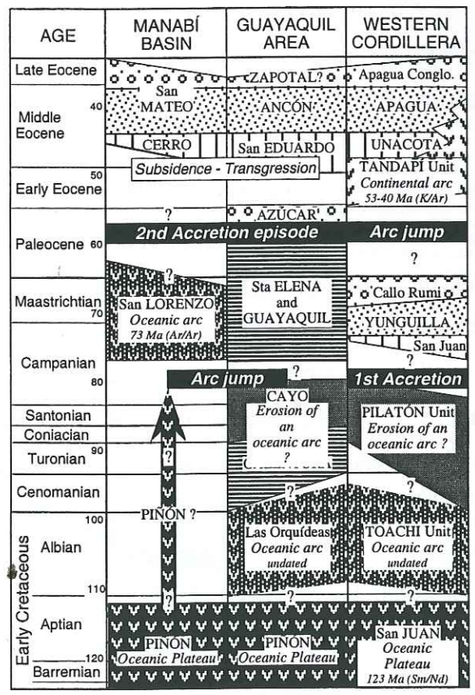

Fig. 1.2. Stratigraphic nomenclature and geodynamic setting of the Cretaceous-Tertiary rocks of western Ecuador.

The Calentura Formation is stratigraphically overlain by a 2000 m-thick turbiditic series of shales, greywackes and conglomerates (Cayo Formation). The Cayo Formation, of Coniacian to Campanian age, is interpreted as the product of the erosion of an island arc (Thalmann, 1946; Wallrabe-Adams, 1990; Benítez, 1995). It is gradually overlain by about 400 m of pelagic dark shales, cherts, siliceous tuffs and subordinate thin-bedded turbidites (Guayaquil Formation, fig. 1.2). The Guayaquil Formation, of Maastrichtian to early Late Paleocene age (Thalmann, 1946; Faucher et al., 1971; Jaillard et al., 1995), is devoid of continental sediments.

South of the Chongón-Colonche fault, the Santa Elena Formation is a strongly deformed equivalent of the Guayaquil Formation (Sinclair and Berkey, 1923; Thalmann, 1946; Jaillard et al., 1995). The Santa Elena Formation is affected by gently dipping shear planes and tight folds exhibiting penetrative axial-plane cleavage, with evidences of northward thrusting. It is unconformably overlain by a 2000 m-thick series of quartz-rich megaturbidites of latest Paleocene to earliest Eocene age (Azúcar Fm, Jaillard et al., 1995). This major tectonic event of Late Paleocene age (≈ 57 Ma) is interpreted as the result of the accretion of this area to the Andean margin (Jaillard et al., 1997).

In the whole coastal Ecuador, the Cretaceous-Paleocene volcanic and volcaniclastic rocks are unconformably overlain by a shallowing-upward sedimentary sequence of late Early Eocene to Late Eocene age (Benítez, 1995; Jaillard et al., 1995; fig. 1.2).

In this work, we shall use the same name (Piñón Formation) for the igneous basement of the Manabí and Guayaquil areas, although they are possibly not of the same age.

ANALYTICAL PROCEDURES AND LOW GRADE METAMORPHISM OF THE IGNEOUS ROCKS OF WESTERN ECUADOR

Samples have been collected from the igneous basement (Piñón Formation), the Las Orquídeas Member and the San Lorenzo and Cayo Formations (Fig. 1.1). Fourteen samples were analyzed for major, minor and trace elements (Table 1.2). Among these samples, Nd-Sr isotopic compositions were determined on nine of the less altered ones (Table 1.3). The location of these samples (Fig. 1.1) and their petrographic characteristics are listed in Table 1.1.

Table 1.1. Location and Petrographic characteristics for the Cretaceous-Paleocene igneous rocks from western Ecuador

Formation	Piñón	Piñón	Piñón	Piñón	Piñón	Piñón
Sample	EQ93.02	EQ1	EQ5	EQ10	Ca1	Ca2
Location	Las Piedras	Montecristi	Puerto Cayo	La Libertad	Sabaneta	Petrillo
Texture	Intersertal + quenched vesicular	Aphyric + Quenched	Intersertal	Ophitic	Intersertal	Intersertal
Mineralogy	Plagioclase laths and microlites + Augite Fe-Ti oxides Glass replaced by smectites	Plagioclase associated or not with augite clots titanomagnetite Abundant glass replaced by smectites	Zoned plagioclase laths subeuhedral augite titanomagnetite Glassy pods replaced by smectites	Plagioclase laths anhedral augite anhedral titanomagnetite	Plagioclase laths and microlites + Augite Fe-Ti oxides Glass replaced by smectites	Plagioclase laths and microlites + Augite minor Fe-Ti oxides
Name	Basalt	Basalt	Diabase	Diabase	Basalt	Basalt

Formation	Piñón	Piñón	Piñón	Las Orquídeas	Las Orquídeas	San Lorenzo	San Lorenzo
Sample	EQ11	EQ12	EQ13	EQ94.01	EQ94.02	EQ2	EQ7
Location	Pedernales	Puerto Cayo	Riconada	Las Orquídeas	Cerro Jordan	Cerro de Hoja	La Pila
Texture	Intersertal	Intersertal	Porhyritic + quenched	Porphyritic + quenched	Porphyritic + intersertal	Ophitic and porphyritic	Porhyritic + fluidal
Mineralogy	Plagioclase laths and microlites + clinopyroxene Fe-Ti oxides Glass replaced by smectites	Plagioclase laths Clinopyroxene abundant large titanomagnetite crystals	Plagioclase + clinopyroxene phenocrysts + microlites abundant glassy groundmass with few Fe-Ti oxides	Plagioclase + OPx + Cpx pseudomorphs groundmass recrystallized in smectites + chlorites	Mg-rich augite phenocrysts + Fe-Ti oxides Groundmass rich in plagioclase laths and microlites	Euhedral labrador + augite with Ti-rich magnetite inclusions	Labrador + zoned Ca-rich cpx phenocrysts groundmass with plagioclase microlites
Name	Basalt	Ferro-diabase	Basalt	Tholeiitic Basalt	Calc-alkaline Basalt	Calc-alkaline Diabase	Calc-alkaline Andesite

Samples N°	OCEANIC PLATEAU - PIÑON FORMATION											INTRA-OCEANIC ARC		
Name	EQ93.02** Basalt	EQ1** Basalt	EQ5** Dolerite	EQ10 Dolerite	Ca1** Basalt	Ca2 Basalt	EQ11** Basalt	EQ12 Dolerite	EQ12 Duplicate	EQ13 Basalt	MA18 Dolerite	EQ94.01** Basalt	EQ94.02** Basalt	EQ2 Diabase	EQ7** Basalt
SiO_2 wt%	52.01	48.88	48.45	48.83	50.87	51.56	50.4	54.2		48.95		57.82	63.4	52.29	52.2
TiO_2	1.06	1.23	1.61	1.58	1.55	1.08	1.36	2.1		1.16		0.24	0.23	0.91	0.95
Al_2O_3	14.89	14.39	16.1	15.2	13.2	13.75	13.93	13.34		14.86		14.83	12.93	16.22	16.32
Fe_2O_3*	12.17	12.75	14.05	12.32	14.73	12.87	14.1	16.64		12.05		9.46	8.43	11.9	12.18
MnO	0.16	0.2	0.2	0.24	0.19	0.18	0.22	0.23		0.2		0.09	0.12	0.17	0.19
MgO	7.58	8.96	6.57	6.4	6.69	7.36	7.24	3.1		8.38		8.65	5.11	5.1	4.48
CaO	7.7	10.81	9.94	11.4	8.3	9.86	9.02	5.79		11.54		4.57	7.23	8.8	9.4
Na_2O	4.3	1.89	2.34	2.95	3.91	3.68	3.1	4.09		2.5		4.29	2.31	2.88	2.92
K_2O	0.00	0.72	0.55	0.9	0.18	0.15	0.27	0.13		0.16		0.00	0.09	1.38	0.99
P_2O_5	0.13	0.18	0.19	0.17	0.18	0.14	0.18	0.29		0.16		0.05	0.13	0.34	0.39
LOI	2.99	4.45	3.18	4.32	2.72	2.15	5.94	2.81		5.64		7.63	2.24	2.16	3.75
Cr (ppm)	236.00	284.84	8.73	54.01	-	-	-	-		-		785.00	210.00	49.59	36.54
V	327.00	353.12	433.49	422.62	509.92	413.46	459.77	64.11		398.13		119.00	144.00	421.12	418.98
Sc		61.49	53.91	51.69	81.49	75.97	79.86	40.34		78.72				33.22	38.95
Ni	98.1	100.73	32.72	52.49	82.95	84.76	67.76	4.58		121.05		177.00	46.5	25.41	20.16
Rb	0.3	5.24	3.5	11.81	6.01	4.02	4.66	1.61	1.26	6.44		0.09	1.06	24.35	17.54
Rb	0.3	5.24	3.5	11.81	6.01	4.02	4.66	1.61		6.44	1.22	0.09	1.06	24.35	17.54
Sr	66.00	130.69	130.8	117.67	160.82	121.42	201.58	116.12	110.00	208.21	110.00	114.00	242.00	441.55	545.6
Y	19.6	22.26	23.16	20.45	38.38	25.92	33.58	51.02	57.01	22.69	16.9	4.5	5.8	20.45	23.5
Zr	44.00	60.09	24.75	30.68	86.39	40.81	73.32	77.07	165.00	62.67	34.00	22.00	45.00	87.97	105.94
Nb	3.13	4.16	4.29	4.18	5.34	3.87	4.66	10.75	11.71	3.92	2.69	0.63	1.28	1.22	1.42
Cs	0.01	0.00	0.00	0.18	0.11	0.05	0.03	0.01	28.21	0.13		0.01	0.16	0.46	0.56
Ba	29.00	14.9	36.35	35.5	392.35	-	-	-	23.38	-	21.00	13.00	108.00	263.95	266.7
La	2.68	3.5	4.09	3.37	5.29	3.68	4.3	9.25	9.49	3.2	2.27	1.42	2.69	10.57	13.13
Ce	7.02	9.63	10.68	9.18	14.17	9.66	11.35	24.49	25.16	8.9	6.28	2.75	6.08	24.7	30.88
Pr	1.07	1.56	1.71	1.51	2.25	1.52	1.8	3.8	3.80	1.43	1.08	0.44	0.83	3.92	4.83
Nd	5.63	8.11	8.59	7.87	11.89	8.15	9.5	19.53	18.69	7.66	5.48	2.11	3.83	17.96	22.42
Sm	1.85	2.57	2.66	2.42	3.91	2.67	3.12	6.11	5.95	2.51	1.91	0.59	1.00	4.17	5.08
Eu	0.71	0.96	1.06	0.95	1.37	1.03	1.17	2.19	2.06	0.96	0.78	0.25	0.36	1.24	1.44
Gd	2.73	3.46	3.58	3.25	5.6	3.89	4.68	8.37	7.54	3.65	2.38	0.76	1.16	4.02	4.82
Tb	0.49	0.66	0.68	0.59	1.05	0.71	0.85	1.47	1.39	0.67	0.47	0.12	0.17	0.65	0.75
Dy	3.4	4.4	4.5	4.04	7.09	4.81	5.89	9.56	9.21	4.56	3.06	0.77	1.00	3.99	4.59
Ho	0.74	0.9	0.93	0.81	1.57	1.04	1.3	1.96	2.00	0.99	0.67	0.16	0.2	0.8	0.9
Er	2.06	2.6	2.57	2.24	4.59	3.05	3.82	5.48	5.77	2.85	1.82	0.44	0.55	2.28	2.6
Tm	0.309	0.35	0.35	0.32	0.66	0.43	0.58	0.77	nd	0.42	0.28	0.066	0.083	0.33	0.37
Yb	2.05	2.53	2.27	2.01	4.62	2.99	3.9	5.17	5.57	2.78	1.74	0.44	0.54	2.18	2.41
Lu	0.319	0.38	0.35	0.31	0.72	0.47	0.61	0.77	0.87	0.41	0.27	0.075	0.093	0.35	0.37
Hf	1.33	1.89	0.96	1.09	2.76	1.54	2.24	2.49	4.63	2.07	1.18	0.59	1.17	2.53	3.07
Ta	0.242	0.58	0.25	0.32	0.4	0.28	0.33	0.67	0.74	0.3	0.18	0.033	0.092	0.03	-
Pb	0.56	0.14	0.00	0.00	0.505	0.305	0.315	0.222	0.29	0.391	2.89	0.52	1.87	2.95	3.96
Th	0.26	0.25	0.11	0.13	0.53	0.35	0.43	0.43	0.63	0.29	0.18	0.15	0.43	1.16	1.44
U	0.07	0.08	0.02	0.1	0.14	0.08	0.11	0.1	0.22	0.09	0.06	0.06	0.79	0.49	0.63
Eu/Eu*	0.97	0.98	1.04	1.05	0.89	0.97	0.93	0.93		0.96	1.11	1.14	1.02	0.93	0.89
$(La/Yb)_N$	0.94	0.99	1.29	1.2	0.82	0.88	0.79	1.28		0.83	0.88	2.31	3.57	3.48	3.91

*Total Iron reported as Fe_2O_3. **Analyzed for isotopic composition. Major elements reported on volatile free basis

Table 1.2. Major and trace-element concentrations of igneous oceanic rocks from western Ecuador.

Analytical procedures

Major and minor elements were analyzed by G. Mevelle at the Centre de Recherche Pétrographiques et Géochimiques (CRPG) of Nancy. Trace elements and rare earth elements (REE) were analyzed by ICP-MS using acid dissolution of 100 mg sample at the Laboratoire de Géochimie isotopique de l'Université Paul Sabatier in Toulouse following the procedure of Valladon et al. (unpublished report). 100 mg of powdered rocks are weighted in a Pt crucible, with 320 mg Lithium metaborate and 80 mg Lithium borate (Fluka). After careful mixing of the powders, the crucible is heated for fusion a 1000°C. After cooling, 8 ml double-distilled HNO_3 (12N) and HF are added for the dissolution of the glass. The final dilution to 30 ml of a 15ml aliquot, with MilliQ™ water and after addition of internal standards (In-Re), corresponds to a total dilution of 3000. Limits of detection are: REE and Y = 0.03 ppm, U, Pb and Th = 0.5 ppm, Hf and Nb = 0.1 ppm, Ta = 0.03 ppm, and Zr = 0.04 ppm. Standards used for the analyses were JB2, WSE Bir-1 and JR1. Analysis of sample EQ12 was duplicated following the procedure of Barrat et al. (1996).

For Sr and Nd isotopic analyses, samples were leached twice in a 2N HCl-0.1 HF mixture. For Pb isotope determinations, whole rocks were successively leached in hot 2N HCl for 20 minutes in an ultrasonic bath, rinsed with tridistilled water, leached in cold 1N HNO_3 for 20 minutes and rinsed with tridistilled water in an ultrasonic bath during 15 minutes.

Nd and Sr isotopic compositions were determined on a Finnigan MAT261 multicollector mass spectrometer at the Laboratoire de Géochimie isotopique de l'Université Paul Sabatier in Toulouse, using the analytical procedures of Lapierre et al. (1997). Correction of the mass discrimination effect was done by normalizing the $^{88}Sr/^{86}Sr$ ratio to a value of 8.3752. NBS 987 standard was measured with a $^{87}Sr/^{86}Sr$ ratio of 0.71025 (± 22). Measured $^{143}Nd/^{144}Nd$ were normalized to a value of $^{146}Nd/^{144}Nd = 0.71219$ (Wasserburg et al., 1981). Results on La Jolla standard yielded $^{143}Nd/^{144}Nd = 0.511850 \pm 8$ (mean on 39 runs) corresponding to an external reproductiblity of 0.00001.

$^{206}Pb/^{204}Pb$, $^{207}Pb/^{204}Pb$ and $^{208}Pb/^{204}Pb$ isotopic ratios were measured on a multicollector VG sector mass spectrometer at the Laboratoire de Géochimie isotopique de l'Université de Montpellier II (Table 1.3) following the analytical procedure adapted from Manhès et al. (1980). Total Pb blanks are less than 65 pg for a 100 mg sample.

Metamorphism and alteration of the igneous rocks of western Ecuador

All the igneous rocks of western Ecuador, with the exception of the arc-rocks of San Lorenzo Formation, are metamorphosed to a low grade zeolite and prehnite-pumpellyite facies, and igneous textures are always preserved. In the analyzed samples, clinopyroxene remains fresh while orthopyroxene is replaced by smectites ± chlorites. When altered, clinopyroxene is replaced by smectites, chlorites or colorless actinolite. Plagioclase is often replaced by sericite or calcite but sometimes remains fresh. However, in the arc-lavas of Las Orquídeas Member, plagioclase is albitized. Vesicles are filled by smectite, chlorite, epidote and pumpellyite, which are also present in the groundmass which sometimes include abundant chalcedony (EQ94-02; Table 1.1). Glass is systematically recrystallized in brown reddish or pale to intense green smectites.

Hydrothermal alteration of hypabyssal volcanic rocks may cause significant mobility of some major (Na, K, Ca, Si) and trace elements (Rb, Ba, Sr), while Na_2O contents (2 to 4 wt %; Table 1.2) are relatively homogeneous. K_2O (≤ 1.3 wt %; Table 1.2) and Rb (0.3 < Rb ppm < 11.8; Table 1.2) are more scattered and most likely express rock alteration. The weight loss on ignition (LOI) ranges between 2.1 and 7.6 % (Table 1.2). LOI generally positively correlates with CaO abundance due to the presence of epidote and minor calcite.

In this study, alkali (K, Rb, and Na) and alkaline earth (Sr, Ba, Ca) elements and SiO_2 are only presented as background information and only the less mobile elements Ti, Nb, Th, Ta, Zr, Hf and REE are used for the geochemical discussion.

BASEMENT OF SOUTHERN COASTAL ECUADOR (PIÑÓN FORMATION)

Petrology and mineral chemistry

The igneous components of the Piñón Formation consist of olivine-free basalts and dolerites (Table 1.1). The basalts show intersertal (EQ93-02, Ca1, EQ11) to aphyric (EQ1) textures. The intersertal basalts consist of plagioclase laths and clinopyroxene glomeroporphyric aggregates embedded in a glass-poor groundmass which contains small rounded vesicules filled with smectites + epidote ± chalcedony and quenched, plumose or dendritic clinopyroxene crystals. The size of the plagioclase laths is highly variable and range from to 0.1 to 1 mm. Fresh plagioclase shows a labradorite composition (An_{66}). Fe-Ti oxides are sometimes TiO_2-rich (24.5%). The aphyric basalts are formed of clinopyroxene

aggregates associated or not with plagioclase set in a glass-rich groundmass which includes isolated plagioclase microphenocrysts. In both lavas, Fe-Ti oxides are anhedral and the last mineral to precipitate.

The dolerites exhibit ophitic (EQ9, EQ10) to intersertal textures (EQ5) and are composed of plagioclase laths enclosed in anhedral clinopyroxene. Euhedral plagioclase is zoned with labradorite cores (An_{69}) and oligoclase rims (An_{12}). The dolerites differ with the size of the clinopyroxene and Fe-Ti oxides and the abundance of interstitial glass. Subhedral clinopyroxene and anhedral Fe-Ti oxides may occur as large crystals up to 1 cm and 0.5 cm, respectively. Oxides are titanomagnetites ($TiO_2 \leq 10$ %) with ulvospinel ($21 < TiO_2\% < 52$) fine exsolution lamellae. Orthopyroxene may occur.

The weakly zoned clinopyroxene shows similar composition in the basalts and dolerites; it is an augite (Wo_{39-43}, $En_{41-47}Fs_{9-15}$; Morimoto, 1988) with slightly Fe-enriched rims.

Geochemistry

The basalts and dolerites have restricted SiO_2, Al_2O_3, and TiO_2 ranges (Table 1.2). Basalts and dolerites have similar MgO contents (Table 1.2; Fig. 1.3) with the exception of a dolerite (EQ12) which has a lower MgO content and correlatively higher Fe_2O_3,TiO_2, Nb and Y abundances (Fig. 1.3). This rock represents the most fractionated rock of the suite (Table 1.2). At similar MgO levels, basalts and dolerites (except EQ12) have a large range of Zr and Y concentrations while their Nb contents range only between 3 and 5 ppm (Table 1.2; Fig. 1.3). TiO_2 increases while MgO decreases (Fig. 1.3). Both rocks show high Ti/V ($19.5 < Ti/V < 23$) and low La/Nb (< 1) ratios.

Basalts and dolerites show flat REE patterns ($0.8 < (La/Yb)_{CN} < 1.3$; Fig. 1.4) relative to chondrite (Sun and McDonough, 1989). However, two groups may be distinguished on the basis of the $(La/Yb)_N$ ratios. Group 1 composed of the basalts is characterized by slightly depleted LREE patterns with $(La/Yb)_{CN} < 1$ (Fig. 1.4A), whereas, Group 2 dolerites exhibit slightly LREE enriched patterns with $(La/Yb)_{CN}$ ratios > 1 (Fig. 1.4B). In both groups, small negative or positive Eu anomalies (Table 2) may reflect minor plagioclase removal or accumulation, respectively.

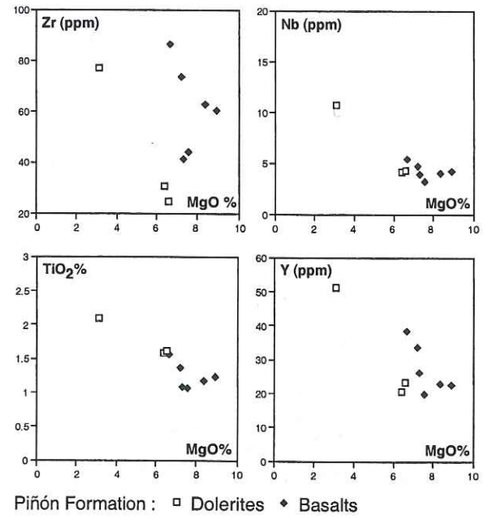

Fig. 1.3. Zr (ppm), Nb (ppm), TiO2 (wt%) and Y (ppm) vs. MgO (wt%) correlation diagrams of the basalts and dolerites of the Piñón Formation.

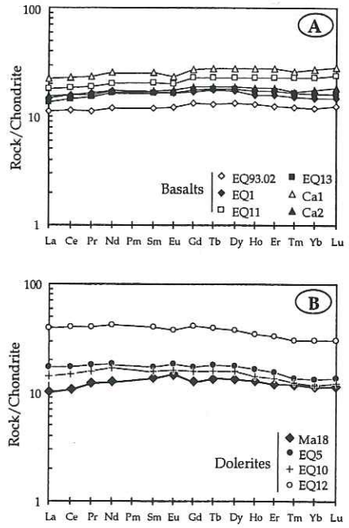

Fig. 1.4. Chondrite-normalized (Sun & McDonough, 1989) rare earth elements patterns of the basalts (A) and dolerites (B) of the Piñón Formation.

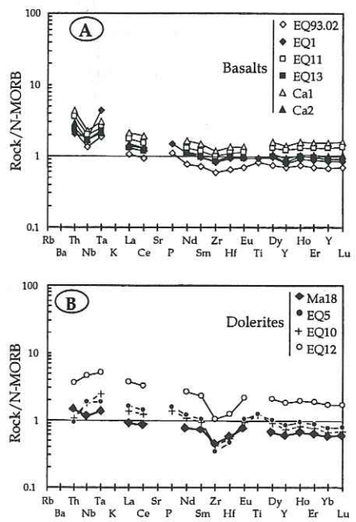

Fig. 1.5. N-MORB (Sun & McDonough, 1989) spidergrams of the basalts (A) and dolerites (B) of the Piñón Formation.

Relative to N-type MORB (Sun and McDonough, 1989; Fig. 1.5), these basalts and dolerites show (i) significant enrichments in LREE, (ii) high Nb, Ta and Th values (1.5 to 5 times the N-MORB values), and (iii) low levels in Zr and Hf (0.3 to 1 times the N-MORB values. The distinction into two groups for the igneous rocks of the Piñón Formation is also valid with respect to their N-MORB normalized trace element patterns. Group 1 is Th-, Ta- and Nb-enriched and shows a mild depletion in Zr and Hf (Fig. 1.5A). Group 2 dolerites differ from Group 1 by the lack of Th enrichment (specially marked in the EQ10 and EQ12 samples) and more marked Zr and Hf negative anomalies (Fig. 1.5B). In both Group 1 and 2, the HREE and Y contents are more or less similar to those of N-MORB or slightly higher (3 times the N-MORB values for the most fractionated rocks). Moreover, Nb/Ta and Zr/Hf ratios of these rocks are lower than those of N-MORB but U/Th is higher (Fig. 1.6). The basalts and one dolerite have a rather restricted range of Nb/U ratios ($38 < Nb/U < 52$; Fig. 1.6) which are slightly higher than those of N-MORB (Fig. 1.6), but fall within the range of oceanic mantle ($Nb/U = 47 \pm 10$; Hofmann, 1988). Two dolerites (EQ5 and EQ2) differ from the basalts by significantly higher Nb/U ratios (107 and 214; Table 1.2), which reflects, most likely, postmagmatic addition of U.

Thus, the basalts and dolerites of the Piñón Formation show oceanic plateau basalt affinities but differ on some trace element distribution (*i.e.*, LREE, Zr, Hf and Th).

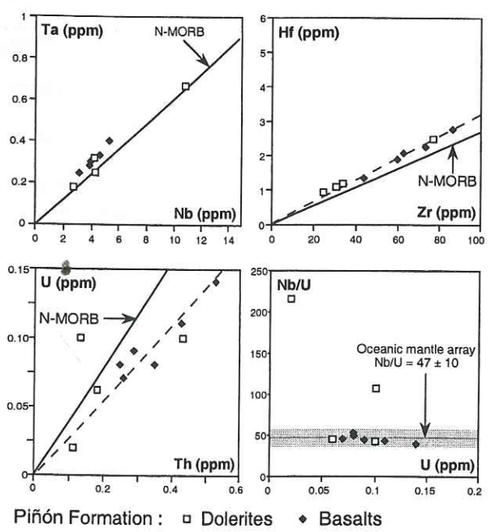

Fig. 1.6. Ta-Nb, Hf-Zr, U-Th, Nb/U-U correlation diagrams of the basalts and dolerites of the Piñón Formation. Altered samples have been omitted in the U-Th and Nb/U-U diagrams.

Nd and Sr and Pb isotopic composition

Isotopic data on the basalts and dolerites of the Piñón Formation have been corrected for in situ decay with an age of 123 Ma (see below the discussion on the age of the Piñón Formation).

Basalts and dolerites display variable ε_{Nd} ratios which range between +4.5 (Ca1) and +10 (EQ1, Table 1.3; Fig. 1.7). Two dolerites (EQ5, MA18) and two basalts (EQ93-02, EQ11) show homogeneous ε_{Nd} ratios of +7. With the exception of EQ1, being similar to N-MORB, these ε_{Nd} ratios fall within the range of ocean island basalts (OIB).

All the Piñón igneous rocks display a large range of $(^{87}Sr/^{86}Sr)_i$ (0. 70435 to 0.70466), except for two samples (EQ1 and EQ5) which have lower $(^{87}Sr/^{86}Sr)_i$ ratios (0.70321 and 0.70335, respectively; Table 1.3; Fig. 1.7).

At similar Zr/Nb ($\approx$ 15) and $(La/Yb)_{CN}$ ($\approx$ 0.8 to 0.9) ratios the basalts and one dolerite (MA18) display a large range of ε_{Nd} ratios (+10 to +4), except for dolerite EQ5 having lower Zr/Nb (5.8) and higher $(La/Yb)_{CN}$ (1.3; Fig. 1.7).

Initial lead isotopic compositions of whole rock and mineral separates display a large range in composition (Table 1.3; Fig. 1.9; Lapierre et al., 1999). EQ12 has the lowest $^{206}Pb/^{204}Pb$ ratio and plots near DMM source while Ca1 has the higher $^{206}Pb/^{204}Pb$ ratio similar to those of recent Galápagos lavas. The high $^{207}Pb/^{204}Pb$ ratios of these rocks could indicate minor amounts of pelagic sediments (Doe, 1970) in the mantle source.

EQ1 has the highest ε_{Nd} ratio (+10), reflecting derivation from the most depleted component. However, the $(^{206}Pb/^{204}Pb)i$ of this rock is higher (18.16) than those of the Piñón lavas, due to the high content of U relative to Th. Indeed, this rock does not plot on the Th/U correlation trend but is displaced towards the U side of the diagram (Fig. 1.6). This reflects the mobility of U linked to a hydrothermal event which affected EQ1. In contrast, Ca1 is characterized by the lowest ε_{Nd} (+4) and the highest $^{206}Pb/^{204}Pb$ (18.92) ratios, suggesting derivation from a more enriched source.

Formations	Samples	t (Ma)	$^{87}Rb/^{86}Sr$	$^{87}Sr/^{86}Sr$	$(^{87}Sr/^{86}Sr)_i$	εSr	$(^{147}Sm/^{144}Nd)$	$^{143}Nd/^{144}Nd$	$(^{143}Nd/^{144}Nd)_i$	εNd	$(^{206}Pb/^{204}Pb)_i$	$(^{207}Pb/^{204}Pb)_i$	$(^{208}Pb/^{204}Pb)_i$
Piñón Fm	EQ93.02	123	0.01314	0.704686 ±10	0.7046	+4.37	0.1986	0.513 ±11	0.512840	+7.03			
	EQ1	123	0.1369	0.703451±27	0.7032	-16.24	0.1916	0.513154 ±25	0.512999	+10.14	18.159	15.529	37.840
	EQ5	123	0.07738	0.703487 ± 21	0.7033	-14.25	0.1872	0.513004 ±14	0.512853	+7.29			
	EQ11	123	0.06686	0.704936 ±25	0.7048	+6.58	0.1985	0.513028 ± 8	0.512868	+7.58			
	Ca1	123	0.10809	0.704542 ±17	0.7043	-0.03	0.1988	0.51287 ± 7	0.512710	+4.49	18.923	15.566	38.431
	MA18	123					0.2107	0.513047 ± 6	0.512877	+7.76			
	EQ12	123	0.0401	0.703561 ± 12	0.70349	-12.27	0.1891	0.703561 ± 12	0.51287	+7.69	17.414	15.548	37.166
	PiO4	123	0.0148	0.703506 ±11	0.70348	-12.43	0.2119	0.513008 ± 6	0.51284	+6.98	17.898	15.595	37.825
Las Orquídeas Mb	EQ94.01	100	0.00228	0.70467 ±10	0.7046	+4.04	0.169	0.512986 ±11	0.512875	+7.14			
	EQ94.02	100	0.01266	0.704095 ±10	0.7040	-4.34	0.1578	0.512921 ±11	0.512817	+6.02			
San Lorenzo Fm	EQ7	75	0.09297	0.703541 ±19	0.7034	-13.77	0.1369	0.512961 ±16	0.512893	+6.87			

Table 1.3. 87Sr/86Sr and 143Nd/144Nd isotope ratios of the igneous oceanic rocks from western Ecuador.

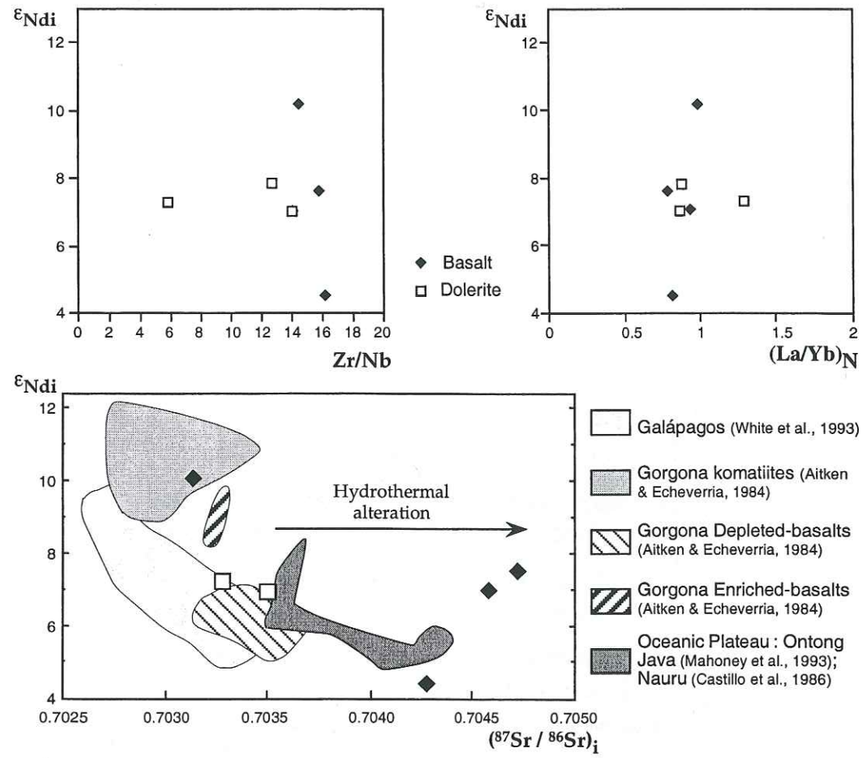

Fig. 1.7. εNdi-Zr/Nb (A), εNdi-(La/Yb)N (B) and εNdi-(87Sr/86Sr)i (C) correlation diagrams for the basalts and dolerites of the Piñón Formation (data from Aitken & Echeverria (1984) and Castillo et al. (1986),among others)

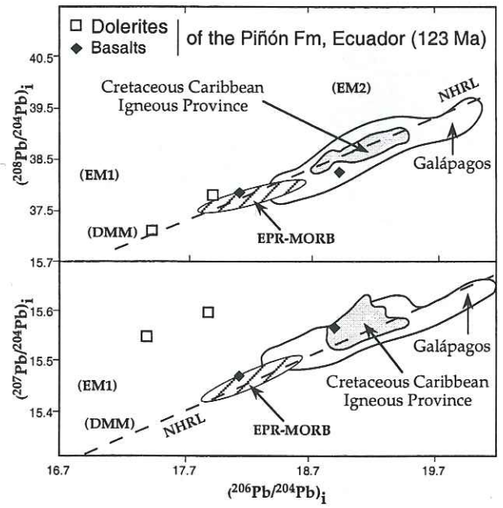

Fig. 1.8. (208Pb/204Pb)i vs (206Pb/204Pb)i and (207Pb/204Pb)i vs (206Pb/204Pb)i correlation diagrams for the basalts and dolerites of the Piñón Formation. data from Nicoya and Heradura (90 MA) igneous complexes (Costa Rica) after Hauff et al. (1997) and Sinton et al. (1997, 1998). Fields of the Gorgona picrites, komatiites, tholeiites and K-tholeiites are after Dupré & Echeverria (1984). The field of the Dumisseau basalts from Haiti is fron Sen et al. (1988). East Pacific MORB and Galápagos Island are from White et al. (1987, 1993). NHRL = North Hemisphere Line afterHart (1984).

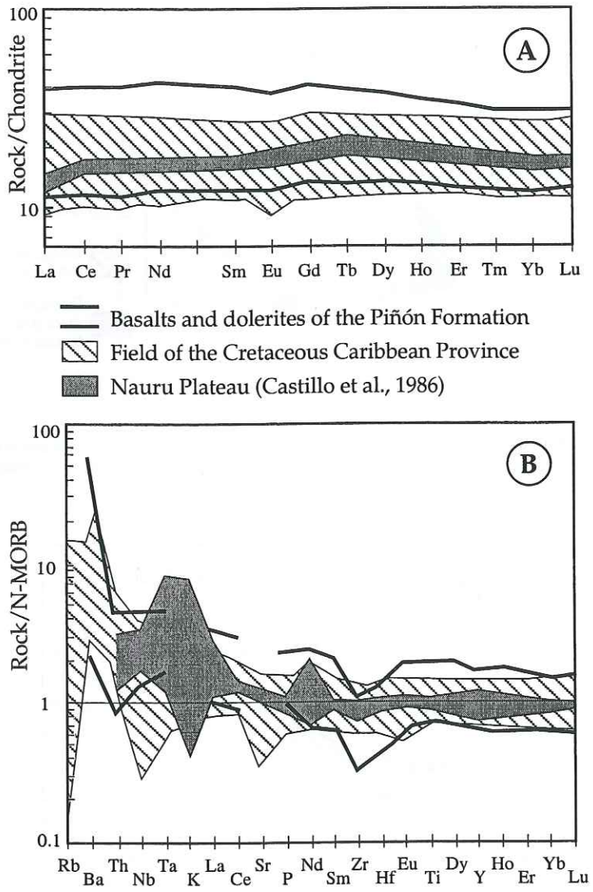

Fig. 1.9. Trace-element geochemical similarities of the basalts and dolerites of he Piñón Formation with Late Cretaceous oceanic plateau basalts from Hispaniola and western Colombia and oceanic floor basalts of the Nauru Plateau.

Summary and comparisons

The basalts and dolerites of the Piñón Formation show flat REE patterns and Ta- and Nb-enrichments relative to N-MORB. The basalts are slightly depleted in LREE, TiO_2, Ta, and Nb. relative to dolerites and some basalts show higher Th contents than the dolerites. The Piñón basalts and dolerites display a rather restricted range of ε_{Nd} (+7.03 to +7.76) and ($^{206}Pb/^{204}Pb$)i ratios (17.41 to 17.90), with the exception of two rocks. As a whole, they are interpreted as the products of an oceanic plateau.

Basalts and dolerites of the Piñón Formation are probably older than the Late Cretaceous (92-88 Ma) Caribbean-Colombian Oceanic Plateau Province (CCOP) basalts. In coastal Ecuador, the Piñón basalts are stratigraphically overlain by Cenomanian to Coniacian (99-87 Ma; Haq and Van Eysinga, 1998) pelagic sediments. Basalts and dolerites of the Piñón Formation are less radiogenic in Pb than the CCOP basalts and the Galápagos recent lavas (Fig. 1.8; Lapierre et al., 1999). This suggests that the oceanic plateau tholeiites of the Piñón Formation derived from mantle(s) source(s) depleted in isotopic Pb, compared to that of the Galápagos hotspot. So, the plume that generated the Piñón Formation oceanic plateau is likely different from, and probably older than the hotspot responsible for the formation of the CCOP and/or the Galápagos.

UPPER CRETACEOUS (-LOWER PALEOCENE ?) LAVAS (LAS ORQUÍDEAS MEMBER, CAYO AND SAN LORENZO FORMATIONS)

Petrology and mineral chemistry of the lavas and volcaniclastic sediments

The igneous rocks of the Upper Cretaceous-Lower Paleocene island arcs are mafic lavas and dolerites sampled in the Las Orquídeas Member and San Lorenzo Formation (Fig. 1.1 and 1.2; Tables 1.1 and 1.2). In southern Coastal Ecuador, the Cayo Formation consists solely of volcaniclastic sediments.

The basalts from Las Orquídeas Member are plagioclase-pyroxene phyric (Table 1.1). EQ94-01 consists of plagioclase, orthopyroxene and clinopyroxene pseudomorphs set in a glass-rich groundmass which includes tiny clinopyroxene and plagioclase and very few oxides. EQ94-02 exhibits an intersertal texture with preserved clinopyroxene phenocrysts of augitic composition (Wo_{37-42}, En_{49-52}, Fs_{8-10}) (Benítez, 1995). Fe-Ti oxides are included in the

plagioclase and augite phenocrysts and thus, represent early crystallizing crystals.

The igneous rocks of the San Lorenzo Formation are fresh compared to those of the Las Orquídeas Member. EQ2 is a dolerite (Table 1.1) which is formed of euhedral plagioclase and anhedral augite (En_{42-44}, Fs_{20-17}, Wo_{38-39}). Both plagioclase and clinopyroxene include TiO_2-rich magnetite (15 to 18 %). Plagioclase occurs as large phenocrysts up to one centimeter long and small laths and exhibits a labradorite composition (An_{52-63}) with Na-rich rims. EQ7 is a porphyritic basaltic andesite (Table 1.1) which is formed of labradorite (An_{61-67}) and zoned clinopyroxene phenocrysts. Plagioclase includes euhedral Ti-rich magnetite crystals and shows locally bytownite (An_{75}) cores. Clinopyroxene shows diopsidic cores (En_{48}, Fs_{6}, Wo_{46}; Morimoto, 1988) rimmed by augite (En_{44}, Fs_{16}, Wo_{40}).

The studied samples of the Cayo Formation are volcanic breccias and graywackes. The volcanic breccias (EQ93.03, EQ94.04; Fig. 1.1) are composed of basaltic and andesitic fragments and pyroxene phenocrysts. When preserved, the pyroxenes show clinoenstatitic (En_{64-75}, Fs_{22-32}, Wo_{2-4}) and augitic (En_{43-44}, Fs_{16-19}, Wo_{38-41}) compositions (Benítez, 1995) which fall in the orogenic basalt field of Leterrier et al. (1982) diagrams (not presented here). The basaltic fragments are orthopyroxene-clinopyroxene-plagioclase-phyric. The andesite differs from the basalts by the abundance of plagioclase phenocrysts. The graywackes (EQ94.03; Fig. 1.1) consist of basaltic fragments, and phenocrysts of augite (En_{35-44}, Fs_{15-26}, Wo_{40-45}) and plagioclase, broken or not (Benítez, 1995).

Geochemistry

The igneous rocks of the Las Orquídeas Member and San Lorenzo Formation display calc-alkaline affinities (Fig. 1.10; Table 1.2) with the exception of EQ94.01 which exhibits an arc-tholeiitic affinity (Fig. 1.10; Table 1.2). These arc-rocks are LREE-enriched ($2.31 < (La/Yb)_{CN} = 3.57$; Fig. 1.10A) and their N-MORB normalized element diagrams (Sun and McDonough, 1989; Fig. 1.10B) are very similar to those of orogenic suites. Moreover, the Las Orquídeas and San Lorenzo lavas possess a negative Nb-Ta anomaly, similar to arc related volcanic rocks.

The lavas of Las Orquídeas Member differ from the rocks of San Lorenzo Formation in that they have very low levels of Y and HREE (less than 10 times the chondritic values; Table 1.2; Fig. 1.10B), suggesting the presence of residual garnet in the mantle source.

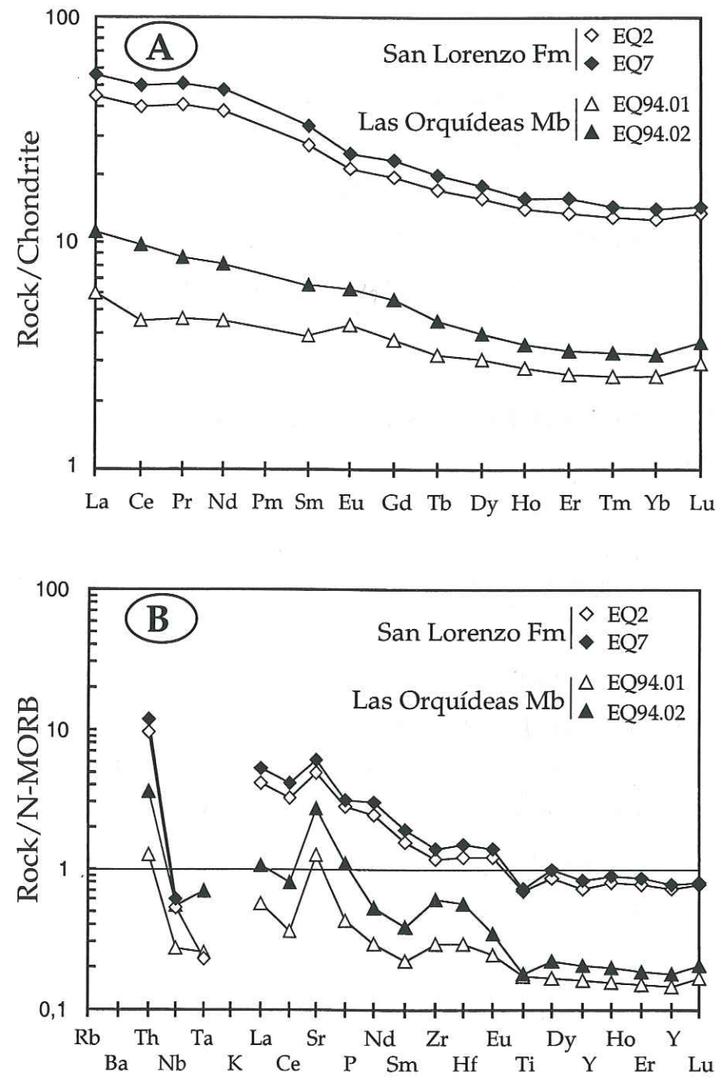

Fig. 1.10. Chondrite normalized (Sun & McDonough, 1989) rare earth elements patterns (A) and N-MORB-normalized (Sun & McDonough, 1989) spidegrams (B) of the igneous rocks of the Las Orquideas Member ans San Lorenzo Formation.

Isotopic chemistry

The ages of 100 and 75 Ma have been taken to calculate the initial $^{87}Sr/^{86}Sr$ and ε_{Nd} ratios of the igneous rocks of Las Orquídeas Member and San Lorenzo Formation, respectively (Table 1.3). The ε_{Nd} ratios of these arc-rocks range between +6.1 and +7.2 (Table 1.3).

The $(^{87}Sr/^{86}Sr)_i$ ratios range between 0.7034 and 0.7046. This large range of $(^{87}Sr/^{86}Sr)_i$ ratios could either reflect hydrothermal alteration or involvement of subducted sediments in the source or fluids released from the hydrothermally altered subducting slab.

COMPARISONS WITH THE NEIGHBOURING AREAS AND ORIGIN OF THE "PIÑÓN TERRANE"

Comparison between the Coast and the Western Cordillera of Ecuador

In the Western Cordillera, the Cretaceous-Paleogene volcanic and sedimentary rocks are in tectonic contact with the metamorphic basement of the Andean Cordillera. The stratigraphy of these Cretaceous-Paleogene series (Macuchi Formation *s.l.*, Henderson, 1979, 1981) is still unclear due to a thick Tertiary volcanic cover, and because most of the lithologic units are separated by tectonic contacts (McCourt et al., 1998). The succession of the five main lithologic units may be reconstructed as follows (Faucher et al., 1971; Kehrer and Van der Kaaden, 1979; Cosma et al., 1998).

Tectonic slices of mafic and ultramafic plutonic rocks and pillow basalts are pinched along the contact between the oceanic terranes and the continental margin. On the basis of petrographic and geochemical studies, they were interpreted as belonging to the pre-Late Cretaceous Piñón Formation (Juteau et al., 1977; Lebrat et al., 1987; Desmet, 1994; McCourt et al., 1998). Our data support this interpretation, since trace element and isotopic chemistry show that these rocks represent the deep levels of an oceanic plateau geochemically similar to the Piñón Formation (Cosma et al., 1998; Lapierre et al., 1999). Moreover, a 123 ± 13 Ma Sm/Nd internal isochron obtained from an amphibole-bearing gabbro (Lapierre et al., 1999) is consistent with the stratigraphic data from the Guayaquil area. Therefore, according to the available data, the Piñón Formation of coastal Ecuador is assumed to be of Early Cretaceous age. For this reason, an age of 123 Ma has been used for in situ decay corrections.

Undated tholeiitic pillow basalts and andesites cropping out in the western part of the Western Cordillera (Toachi beds) were developed in an intra-oceanic arc environment (Cosma et al., 1998). The Toachi beds are interpreted as overlain by graywackes (Pilatón beds) bearing Late Turonian to Coniacian inoceramid faunas, which can be correlated with the Cayo Formation of the Guayaquil area (Faucher et al., 1971; Kehrer and Van der Kaaden, 1979). Therefore, the Cretaceous succession of the Western Cordillera is comparable to that of the Guayaquil area of Coastal Ecuador (Fig. 1.2), and the Toachi beds can be correlated with the Las Orquídeas Member of the Guayaquil area, of pre-Cenomanian to pre-Turonian age (Cosma et al., 1998).

The graywackes of the Pilatón beds are locally unconformably overlain by the Maastrichtian shales and quartz-rich turbidites of the Yunguilla Formation (Faucher et al., 1971; Bristow and Hoffstetter, 1977; Kehrer and Van der Kaaden, 1979). Although the Yunguilla Formation is coeval with the Guayaquil Formation, the former contains abundant detrital quartz, which is absent in the latter (Fig. 1.2). This indicates that at least part of the Western Cordillera had been accreted to the continental margin by Maastrichtian times (Faucher et al., 1973; Kehrer and Van der Kaaden, 1979; Lebrat et al., 1987; Cosma et al., 1998). The recent dating of quartz-sandstones as early to middle Paleocene in the Western Cordillera supports this interpretation (McCourt et al., 1998). Therefore, the tectonic history of part of the Western Cordillera differs from that of the Guayaquil area, since, by the end of Maastrichtian times, part of the Western Cordillera was already accreted to the continental margin.

Volcaniclastic rocks and calc-alkaline andesites, dacites and breccias (Tandapi beds, Silante Formation) rest unconformably on the Yunguilla Formation. These volcanic rocks are dated by Tertiary radiolarians (Bourgois et al., 1990), scarce K/Ar ages (hornblende) ranging from 51.5 ± 2.5 Ma to 40 ± 3 Ma (Early to Middle Eocene, Wallrabe-Adams, 1990; Van Thournout et al., 1990), and interbedded limestones and quartz-rich turbidites which yielded Middle to Late Eocene microfossils (Henderson, 1979; Bourgois et al., 1990). Since these volcanic rocks rest on the oceanic terranes of the Western Cordillera and exhibit geochemical features of a continental magmatic arc (Cosma et al., 1998), the accretion of the Western Cordillera was achieved by Early Eocene times (Fig. 1.2). This interpretation is supported by the fact that the Cretaceous-Paleogene rocks of the Western Cordillera are unconformably overlain by a sedimentary sequence of Eocene age comparable to that of coastal Ecuador (Bourgois et al., 1990; Jaillard et al., 1995; fig. 1.2).

In summary, because of the comparable overlying Cretaceous succession and of their

similar geochemical features, we follow the previous workers in admitting that the Piñón Formation of the Guayaquil area correlates with the Early Cretaceous (≈ 123 Ma) igneous basement of the Western Cordillera, although their tectonic evolution may differ.

Comparison between Western Ecuador and Western Colombia

Recent studies carried out in Western Colombia distinguish, three distinct basaltic suites of oceanic plateau affinities (Fig. 1.11), *i.e.* the mafic igneous rocks of the Amaime Formation (> 100 Ma), Volcanic Formation (90 Ma), and Serranía de Baudó (78-73 Ma), which successively accreted to the Andean margin (Marriner and Millward, 1984; McCourt et al., 1984; Desmet, 1994; Nivia, 1996; Kerr et al., 1996, 1997b; Sinton et al., 1998).

It appears difficult to correlate the oceanic plateau basement (Piñón Formation and its plutonic roots) of the Western Cordillera and Coastal area of Ecuador with the basalts and their plutonic roots of the Amaime Formation of Colombia. Indeed, the latter formation is intruded by the Buga batholith dated at 113 ± 10 Ma (K/Ar) and 99 ± 4 Ma (Rb/Sr) (McCourt et al., 1984), indicating that the accretion of the Amaime Formation onto the margin of NW Colombia must have occurred well before 100 Ma (Kerr et al., 1997b). Early Cretaceous ages (129-104 Ma) of High Pressure metamorphic rocks associated with the Amaime Formation are interpreted as reflecting the late stages of accretion, which occurred most probably between 140-124 Ma (Aspden and McCourt, 1986; Toussaint and Restrepo, 1994). So the Amaime Formation was probably already accreted while the Piñón Formation of Ecuador erupted. Moreover, in map view, the Western Cordillera of Ecuador is not the continuation of the suture zone of Colombia (Fig. 1.11). In contrast, the Colombian suture zone is likely correlatable with the late Jurassic-earliest Cretaceous "oceanic suture", exposed along the western edge of the Eastern Cordillera of Ecuador (Aspden and Litherland, 1992; Litherland et al., 1994) and/or with the ultramafic and mafic rocks of the Raspas Complex of southwestern Ecuador (Aspden et al., 1995), the HP metamorphism of which has been dated at 132 Ma (K/Ar, Feininger, 1982; fig. 1.11).

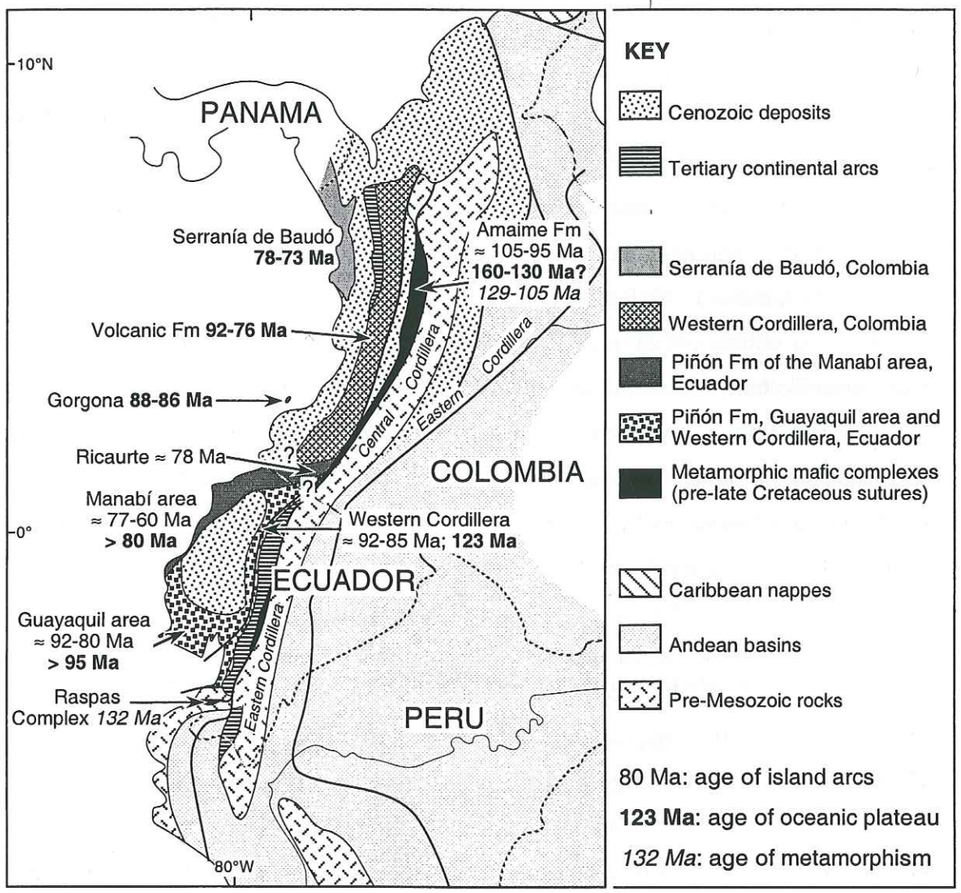

Fig. 1.11. Schematic geological map of the western Colombia and western Ecuador. Numbers indicate the age of the oceanic pateaus (bold) and island arcs (standard).

The age of the oceanic plateau basement of the northwestern area of Coastal Ecuador (Manabi area) is pre-Late Campanian because intra-oceanic arc lavas and associated pelagic sediments, both of Late Campanian-Maastrichtian age, crop out in this area (Lebrat et al., 1987). Thus, this oceanic plateau may be either coeval with the early Late Cretaceous oceanic plateau generation of Western Colombia, or coeval with the Early Cretaceous oceanic plateau of the Guayaquil area and Western Cordillera of Ecuador. More radiometric dates are necessary to distinguish between these two assumptions. The Late Campanian-Maastrichtian intra-oceanic arc (San Lorenzo Formation) can be correlated with the Campanian Ricaurte tholeiitic suite of southern Colombia, which seems to have no equivalent farther north (Spadea and Espinosa, 1996; fig. 1.11).

Finally, no equivalent of the late Late Cretaceous (≈ 78-72 Ma) oceanic plateau of westernmost Colombia (Serranía de Baudó, Kerr et al., 1997b) is known so far in Ecuador.

Therefore, with the possible exception of the northwestern area, the Ecuadorian oceanic plateau terranes are distinct from those accreted to the Colombian margin, and cannot be considered, as a whole, to belong to the Late Cretaceous Colombian-Caribbean Oceanic Plateau as defined by Kerr et al. (1997a).

A southeastern Pacific origin for the Early Cretaceous terrane of Ecuador

The 123 Ma isochron age suggests that the oceanic plateau of Coastal Ecuador is coeval with the southern Pacific large oceanic plateaus generated during the Early Cretaceous "superplume" (≈ 125-100 Ma, Larson, 1991), *i.e.*, Kerguelen, Nauru, Manihiki and Ontong Java Plateaus. More specifically, some of the Ecuadorian oceanic plateau fragments are coeval with the early igneous event of the Ontong Java Plateau, recorded at 123 Ma (Mahoney et al., 1993; Coffin and Eldholm, 1993). The overthickened and abnormally buoyant character of the basement of Western Ecuador can explain why this oceanic terrane has been accreted to, rather than subducted beneath, the Andean margin (e.g. Cloos, 1993). Moreover, the Piñón Formation forms the basement of distinct and successive Late Cretaceous island arcs of age, indicating that it behaved as a buoyant upper plate in an intra-oceanic subduction systems.

Very little is known about the plate kinematics before the latest Cretaceous. Based on fixed hotspot reference frame, Duncan and Hargraves (1984) proposed a kinematic reconstruction of the direction and velocity of the northern Farallon and southern Phoenix plates since

earliest Cretaceous times. According to this reconstruction, an arbitrary point passively transported by the Farallón Plate between 123 and 80 Ma, age of the first accretion of the Piñón terrane to the Andean margin, travelled ≈ 3500 kms northward and more than 3000 kms eastward. A point located on the present-day Galápagos 123 Ma ago would be located close to Florida on a 80 Ma reconstructed map. Although uncertainties are great in such a reconstruction, the early Cretaceous Piñón Formation cannot have been generated by the Galápagos Hotspot, and its source must be located much farther south or southwest.

The Cretaceous migration rates of the Phoenix Plate were slower than those of the Farallon Plate (Duncan and Hargraves, 1984) and accordingly, a point colliding the Ecuadorian margin 80 Ma ago must have been located about 2000 kms farther south and more than 2500 kms to the west, 123 Ma ago. Therefore, if passively transported by the oceanic plate, the early Cretaceous Piñón Formation must have been generated 3000 to 4000 kms SW of Ecuador on a 80 Ma reconstructed map, that is much closer to the Sala y Gómez Hotspot (Pilger and Handschumacher, 1981) than to Galápagos Hotspot. However, the presence of a pre-Campanian island arc products (Las Orquídeas Member, Cayo Formation, Toachi and Pilatón beds) indicates that the Piñón Formation has constituted the upper plate of an intra-oceanic subduction system, and has not been transported passively by the oceanic plate during the whole 123-80 Ma time-span. Therefore, the hotspot responsible for the generation of the Piñón Formation may have been located closer to the Ecuadorian margin. A southeastern Pacific origin of the Piñón terrane is consistent with the scarce available paleomagnetic data, which suggest that Coastal Ecuador (taken as a single terrane) has been originated 5° to the south of its present location (Roperch et al., 1987).

SUMMARY AND CONCLUSIONS

1. Petrographic, mineralogical, chemical and isotopic studies indicate that the basement of Western Ecuador is made of oceanic plateau remnants of possibly different ages. Their oceanic plateau origin may explain why these rocks have been accreted to the Andean margin, and why they supported intra-oceanic island arcs.

2. Three distinct geological domains must be distinguished in Western Ecuador. (1) In the northwestern area (Manabí area), the basement is of pre-Late Campanian age, an intra-oceanic arc developed in Late-Campanian-Maastrichtian times, and accretion occurred before the

Middle Eocene. (2) In the Central area (Guayaquil area), the basement is of Early Cretaceous age, island arcs were active during late Early Cretaceous(?) to early Late Cretaceous age, and the accretion occurred in the Late Paleocene (≈ 57 Ma). (3) In the Western Cordillera, the basement, preserved as slices in the suture zone, is of Early Cretaceous age (≈ 123 Ma), intra-oceanic arcs developed during the late Early Cretaceous(?) to early Late Cretaceous, and accretion occurred during the Late Cretaceous (≈ 80 Ma).

3. No equivalent of the Early Cretaceous oceanic plateau of Western Ecuador is thus far known in Western Colombia. However, we cannot rule out the possibility that the basement of the northwestern area of Coastal Ecuador (Manabí) is coeval to the Caribbean Plateau (≈ 92-88 Ma). Additionally, remnants of the late Cretaceous oceanic plateau of westernmost Colombia (≈ 78-72 Ma) are yet unknown in Ecuador. These observations indicate that most of the oceanic terranes of Western Ecuador do not belong to the Colombian-Caribbean Oceanic Plateau. The plume that generated the Early Cretaceous Piñón Plateau must have been located in the Southeast Pacific, far south of the present-day Galápagos Hotspot.

Acknowledgements. We are indebted to S. Benítez for his knowledge of the geology of Coastal Ecuador and his help in the collection of samples. Field works were supported by the Institut Français de Recherches Scientifiques pour le Développement en Coopération-ORSTOM (presently : Institut de Recherche pour le Développement-IRD), which funded also the analysis, together with the UPRES A 5025 (Grenoble). Thanks are due to the Laboratoire de Géochimie (UMR 5563) of the Université Paul Sabatier of Toulouse (France) for their technical assistance and to the Institut de Minéralogie et de Géologie, Université de Lausanne (Switzerland) for the mineral chemistry. A.C. Kerr and an anonymous reviewer are acknowledged for their constructive and thorough suggestions.

Chapitre 2

Ce chapitre représente une étude géochimique comparative entre différents fragments du plateau océanique Crétacé Caraïbe accrétés dans les Grandes Antilles, et ceux plus vieux (Crétacé Inférieur) accrétés en Equateur et au Mexique. Quand ce papier a été écrit, la présence en Equateur de fragments de plateau océanique plus jeunes, maintenant associés au plateau océanique Crétacé Supérieur Caraïbe, était inconnue.

Des âges Ar/Ar de 86 ± 1.4 Ma sur des amphiboles tardi-magmatiques (magnesio-hastingsite) provenant d'une roche cumulative et sur des hornblendes appartenant à une amphibolite (Lapierre et al., 1999) indiquent les roches riches en Mg et les amphibolites du Complexe Duarte en République Dominicaine sont contemporaines avec les roches formant le CCOP. Ainsi, le Complexe Duarte représente un fragment du plateau Caraïbe accrété à l'arc des Grandes Antilles. En Equateur, une isochrone interne Sm/Nd sur un gabbro à amphibole formant le sommet de l'assemblage plutonique de San Juan indique un âge de 123 Ma. Ces fragments de croûte à affinité de plateau océanique sont plus vieux que le plateau Caraïbe. Donc, les témoins de ce plateau océanique (coupe de San Juan et la Formation Piñón) présents en Equateur n'appartiennent pas au plateau océanique Caraïbe.

Toutes les roches provenant de République Dominicaine, d'Equateur et du Sud Ouest Mexique présentent des valeurs eNd homogènes similaires à celles des basaltes de plateaux océaniques. Mais les basaltes riches en Mg et les basaltes « normaux » du CCOP présentent un composant HIMU qui est absent dans les roches volcaniques et plutoniques Crétacé inférieur à affinité de plateau océaniques accrétés en Equateur.

Les âges et les compositions isotopiques des roches étudiées démontrent que deux évènements majeurs aboutissant à la formation de deux plateau océaniques sont présents dans la région péri-caraïbe et en Equateur. Le premier, Crétacé Inférieur, dérive probablement d'un point chaud situé près ou pas loin d'une ride médio océanique situé plus au sud ouest de l'Amérique du Sud, quelque part dans le Pacifique. Le deuxième, Crétacé supérieur, est probablement relié au point chaud des Galápagos (ceci est discuté dans le chapitre 7).

Chapter 2

MULTIPLE PLUME EVENTS IN THE GENESIS OF THE PERI-CARIBBEAN CRETACEOUS OCEANIC PLATEAU PROVINCE

Henriette Lapierre, Delphine Bosch, Vincent Dupuis, Mireille Polvé, René C. Maury, Jean Hernandez, Patrick Monié, Delphine Yeghicheyan, Etienne Jaillard, Marc Tardy, Bernard Mercier de Lépinay, Marc Mamberti, Alain Desmet, Francine Keller and François Sénebier

Journal of Geophysical Research, v. 105, p. 8403-8421.

CHAPTER 2: MULTIPLE PLUME EVENTS IN THE GENESIS OF THE PERI-CARIBBEAN CRETACEOUS OCEANIC PLATEAU PROVINCE

This chapter is a comparative geochemical study of the accreted fragments of the Cretaceous Caribbean oceanic plateau exposed in the Greater Antilles with those of Early Cretaceous age present in Ecuador and central Mexico. When this paper was written, the presence in Ecuador of younger oceanic plateau fragments, likely related to the Late Cretaceous Caribbean plateau was still unknown.

Ar/Ar ages of 86 ± 1.4 Ma of both late magmatic amphibole (magnesio-hastingsite) from a cumulus-enriched rock and hornblende from an amphibolite (Lapierre et al., 1999) indicate that the Mg-rich lavas and amphibolites of the Duarte Complex (Dominican Republic) are contemporaneous with the rocks of the 90-86 Ma event of the CCOP. Thus, the Duarte Complex from Dominican Republic represents an accreted fragment of the Caribbean plateau accreted to the Greater Antilles arc. In Ecuador, according to the 123 Ma age obtained from an isotropic gabbro exposed at the top of the San Juan plutonic assemblage, the crustal fragments of oceanic plateau affinity are older than the Caribbean plateau. Thus, the remnants of oceanic plateau affinity (San Juan section and Piñón Formation) exposed in Ecuador cannot belong to the Cretaceous Caribbean plateau.

All the rocks from Dominican Republic, Ecuador and western Mexico have homogeneous εNd, similar to those of oceanic plateau basalts. But the high-Mg basalts and normal basalts of the CCOP exhibit an HIMU component which is absent in the Early Cretaceous plutonic and volcanic rocks of oceanic plateau affinity exposed in Ecuador.

The ages and isotopic compositions of the studied rocks demonstrate that two major pulses of oceanic plateau magmas are present in the peri-Caribbean and Ecuador. The Early Cretaceous one probably derived from a near-ridge or ridge-centered hotspot located farther SW of South America, somewhere in the SE Pacific while the Late Cretaceous plateau was assumed to be related to the Galápagos hotspot (this assumption is now discussed in chapter 7).

MULTIPLE PLUME EVENTS IN THE GENESIS OF THE PERI-CARIBBEAN CRETACEOUS OCEANIC PLATEAU PROVINCE

ABSTRACT. The oceanic crust fragments exposed in central America, in north-western South America, and in the Caribbean islands have been considered to represent accreted remnants of the Caribbean-Colombian Oceanic Plateau (CCOP). On the basis of trace element and Nd, Sr, and Pb isotopic compositions we infer that cumulate rocks, basalts, and diabases from coastal Ecuador have a different source than the basalts from the Dominican Republic. The latter suite includes the 86 Ma basalts of the Duarte Complex which are light rare earth element (REE) -enriched and display (relative to normal mid-ocean ridge basalts, NMORB) moderate enrichments in large ion lithophile elements, together with high Nb, Ta, Pb, and low Th contents. Moreover, they exhibit a rather restricted range of Nd and Pb isotopic ratios consistent with their derivation from an ocean island-type mantle source, the composition of which includes the HIMU (high $^{238}U/^{204}Pb$) component characteristic of the Galápagos hotspot. In contrast, the 123 Ma Ecuadorian oceanic rocks have flat REE patterns and (relative to NMORB) are depleted in Zr, Hf, Th, and U. Moreover, they show a wide range of Nd and Pb isotopic ratios intermediate between those of ocean island basalts and NMORB. It is unlikely, on geochemical grounds, that the plume source of the Ecuadorian fragments was similar to that of the Galápagos. In addition, because of the NNE motion of the Farallón plate during the Early Cretaceous, the Ecuadorian oceanic plateau fragments could not have been derived from the Galápagos hotspot but were likely formed at a ridge-centered or near-ridge hotspot somewhere in the SE Pacific.

INTRODUCTION

Oceanic plateaus originate by the outpouring of large volumes of mafic magmas over oceanic crust coupled with cogenetic plutonic intrusions. Despite their volumetric importance, little is known about their overall structure and composition, especially of their deeper crustal levels. Because of their thickness, they tend to be more buoyant than normal oceanic crust [*Burke et al.*, 1978; *Nur and Ben Abraham*, 1982; *Cloos,* 1993; *Saunders et al.*, 1996] and are not easily subducted. Therefore these oceanic plateaus can potentially be obducted onto, or accreted to, continental margins [*Ben Abraham et al.*, 1981], thus increasing both the probability of preservation and accessibility of their plutonic roots.

Numerous accreted oceanic crustal fragments composed of ultramafic-mafic cumulate rocks, diabases, and basalts are exposed along the Pacific coast of Central America (Costa Rica) and South America (Colombia, Ecuador) and in the Caribbean (Venezuela, Greater Antilles, Aruba, Curaçao; fig.2.1). Their origin, age, and emplacement are still a matter of ongoing debate. Age estimates of these complexes range from Late Jurassic to Paleocene. They are interpreted as being parts of a large basaltic province, the Caribbean-Colombian Igneous Province [*Kerr et al.*, 1997a, b]

The Late Cretaceous Caribbean basaltic crust drilled during the Deep Sea Drilling Project (DSDP) Leg 15 [*Donnelly et al.*, 1973] and Ocean Drilling Project (ODP) Leg 165 [*Sigurdsson et al.*, 1997] is enriched in large ion lithophile elements (LILE) and has relatively radiogenic (Sr and Pb) isotopic characteristics [*Sen et al.*, 1988] which are consistent with derivation from a similar mantle source as that of the Galápagos hotspot. Since diabases and basalts of oceanic fragments in the islands and continent bordering the Caribbean have geochemical characteristics similar to those of the drilled rocks, *Donnelly et al.* [1990] considered these rocks to represent uplifted parts of the Caribbean-Colombian Oceanic Plateau (CCOP). Using a fixed hotspot reference frame, *Duncan and Hargraves* [1984] suggested that the CCOP was produced during the initial "plume head" phase of the Galápagos hotspot.

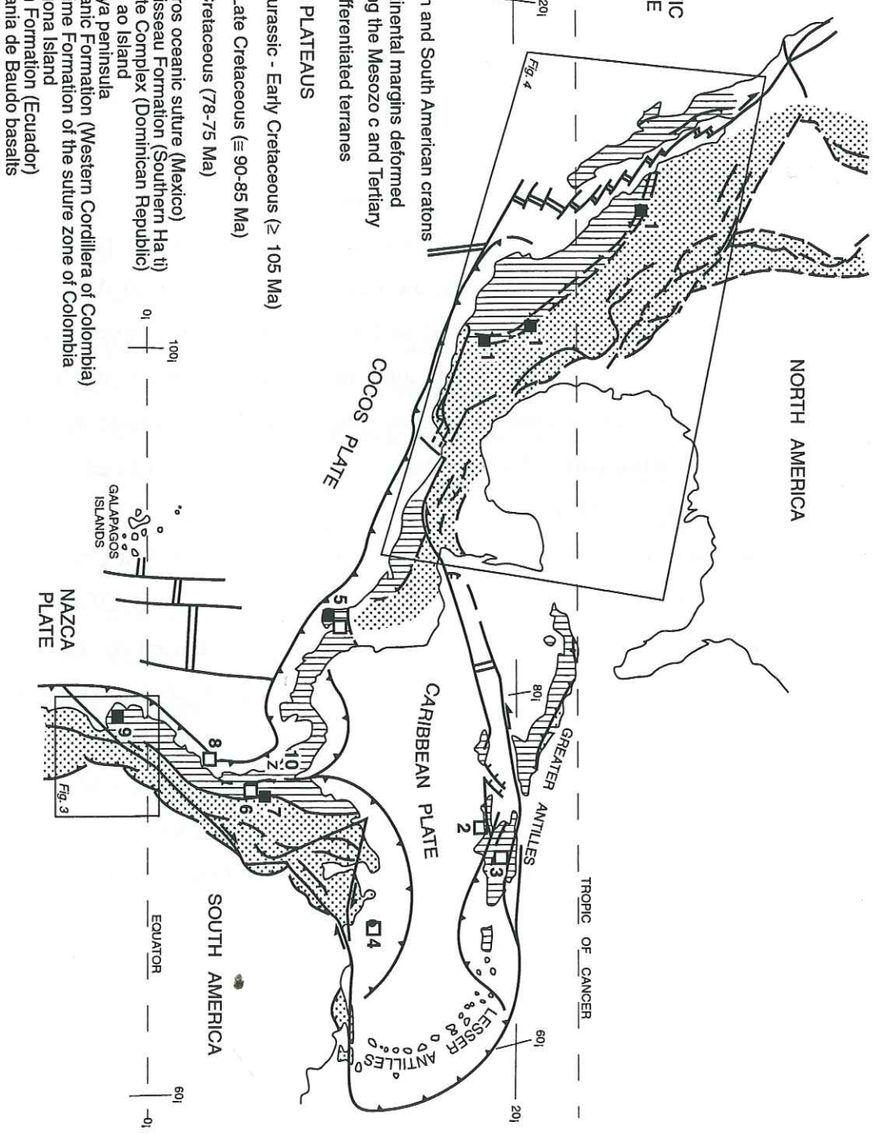

Fig. 2.1: Schematic map showing the location of the Mesozoic plateau crustal fragments exposed in western central Mexico, Costa Rica, Greater Antilles, Curaçao, Aruba, Colombia, and western Ecuador.

The CCOP is mostly made of Upper Cretaceous diabases, shallow basaltic sills, or pillowed and/or massive flows of basalts, the latter being often picritic [*Donnelly et al.*, 1973]. Exposures of these lavas are reported in southern Haiti, Curaçao, and western Colombia (including the komatiites and enriched basalts from Gorgona Island) [*Aitken and Echeverria*, 1984; *Arndt et al.*, 1996; *Kerr et al.*, 1996a, 1997a]. *Kerr et al.* [1996a, b, c, 1997a] demonstrated that the enriched tholeiites (including komatiites) from Gorgona, Curaçao, and Colombia (with the exception of the Central Cordillera [*Kerr et al.*, 1997a]) are Upper Cretaceous in age (73-91.7 Ma) and likely derived from the Galápagos hotspot. Recent Ar/Ar ages and Sr, Nd, and Pb isotopic data indicate that the enriched basalts of the Nicoya Complex from Costa Rica, now considered to be the westernmost occurrence of the CCOP, are early Late Cretaceous in age (88-92 Ma) and can also be genetically linked to the Galápagos plume [*Alvarado et al.*, 1997; *Hauff et al.*, 1997; *Sinton et al.*, 1997]. Recently, *Sinton et al.* [1998] demonstrated on the basis of $^{39}Ar/^{40}Ar$ ages that the igneous rocks of the CCOP were emplaced during two main events: 90-82 Ma and 78-68 Ma. The rocks related to the early Late Cretaceous event (90-83 Ma, specifically Turonian to Santonian) were produced by a hotspot that possibly was the Galápagos, while those emplaced during the Late Cretaceous (78-68 Ma) possibly derived from a more depleted plume source.

Exposures of mafic plutonic and volcanic rocks with enriched tholeiitic affinities exposed in western Ecuador (Piñón Formation, see Figures 2.1 and 2.3) [C. Reynaud et al., Oceanic plateau and island arcs of southwestern Ecuador: Their place in the geodynamic evolution of northwestern America, submitted to *Tectonophysics*, 1998, herein after referred to as Reynaud et al., submitted manuscript, 1998] have also been assigned to the CCOP [*Kerr et al.*, 1996b, 1997a]. However, these rocks are older than those from most of the CCOP, since they are locally overlain by early Late Cretaceous (≈ 95-90 Ma) sediments [*Jaillard et al.*, 1995; Reynaud et al., submitted manuscript, 1998]. Furthermore, in the Central Cordillera of Colombia, part of the accreted fragments of an oceanic plateau were affected by Early Cretaceous high- pressure metamorphism (K/Ar ages [*Toussaint and Restrepo*, 1994]) and are older than 120 Ma. Finally, the enriched tholeiites of the Arperos basin exposed in central and western Mexico (Fig.2. 1) [*Freydier et al.*, 1996], are geochemically similar to those of western Ecuador (see below). Moreover, they share with the rocks of western Ecuador similar Early Cretaceous age because they are stratigraphically interbedded with cherts that yielded Lower Cretaceous radiolarian faunas [*Dávila Alcocer and Martínez Reyes*, 1987].

There is presently some geochemical data (age, major, trace element, and Nd, Sr, and Pb isotopic compositions) on oceanic plateau basalts, for example, the Ontong Java plateau basalts exposed in the Solomon Islands [*Tejada et al.*, 1996] and the Upper Cretaceous komatiitic and picritic basalts from the Caribbean and northern South America. However, most of these exposures are still restricted to the volcanic levels of oceanic plateau crust, and none of them allows investigation to be made of the geochemical features of the underlying ultramafic and mafic plutonic roots of the oceanic plateau. The oceanic crustal fragments from Hispaniola and more specifically from Ecuador offer the unique opportunity to study different components of the CCOP, i.e., the Upper Jurassic oceanic crust basement and the Cretaceous ultramafic and mafic hypabyssal and volcanic rocks and their plutonic roots.

Major and trace element compositions and isotopic data, although necessary, cannot identify the parental hotspot(s) of these oceanic plateau magmas. Ages and transport directions of the allochthonous oceanic crustal fragments together with kinematics of regional plates are also required to constrain parental hotspot location.

The purpose of the present paper is to report new data on the trace element and isotopic (Sr, Nd, Pb) characteristics of selected clinopyroxene- and/or olivine-rich basalts of the Duarte Complex (Dominican Republic) and plutonic and volcanic rocks from coastal Ecuador. From the comparison of these data with our published data on basalts and diabases from westerncentral Mexico and those already available in the literature, we propose a new interpretation of the origin of the Caribbean-Colombian Oceanic Plateau.

GEOLOGICAL INFORMATION

Dominican Republic.

The Duarte Complex forms the core of the Central Cordillera of the Dominican Republic. It is bounded on both sides by arc-derived rocks of Cretaceous age and intruded by Late Cretaceous to Tertiary plutons (Fig 2.2) [*Kesler et al.*, 1977]. *Bowin* [1975] and *Palmer* [1979] proposed that this complex represents a fragment of oceanic crust. *Draper and Lewis* [1991] and *Lewis and Jiménez* [1991] consider this complex to be a Late Jurassic-Early Cretaceous ocean island or seamount modified by Late Cretaceous-Eocene island arc magmatism [*Bowin*, 1966; *Kesler et al.* 1977; *Mercier de Lépinay*, 1987; *Draper and Lewis*, 1991]. *Donnelly et al.* [1990 p. 347] consider the picrites, ankaramites, and amphibolites of

the Duarte Complex and the Upper Cretaceous unmetamorphosed mafic rocks of the Siete Cabezas to represent the "tectonized allochthon of the Caribbean Cretaceous basaltic rocks."

Detailed field mapping in the Juncalito-Janico-La Vega area allowed us to distinguish four units in the Duarte Complex (Fig. 2.2), the first three of which are particularly important geochemically in the context of the present study: (1) a thick pile of Mg-rich basalts, (2) mafic amphibolites and amphibole-epidote gneisses tectonically imbricated with the Mg-rich basalts, (3) pillowed and massive basalts stratigraphically associated with Upper Jurassic (160-149 Ma) ribbon cherts [*Montgomery et al.*, 1994], and (4) serpentinized peridotites crosscut by diabase dikes.

The olivine and clinopyroxene (cpx)-rich basalts are metamorphosed to greenschist facies and are generally intensively deformed. However, the stratigraphic bedding marked by the flow contacts and the graded bedding in the pyroclastic levels are locally preserved, and the plagioclase-free, Mg-rich lavas form massive flows, < 2 m thick, interbedded with lapilli and crystal tuffs. These flows show evidence for accumulation of olivine and clinopyroxene crystals at their base, while their tops are highly vesicular. They are often intruded by diabase dikes. In the southeastern extremity of the Central Cordillera (Fig. 2.2) the amphibolites of the Duarte Complex are tectonically overlain by the unmetamorphosed diabases, basalts, and cherts of the Siete Cabezas Formation containing Cenomanian to Santonian (97-83 Ma [*Gradstein et al.*, 1994]) radiolarians [*Mercier de Lépinay*, 1987; *Donnelly et al.*, 1990].

Ar/Ar ages of 86 ± 1.4 Ma of both late magmatic amphibole (magnesio-hastingsite) from a cumulus-enriched rock and of hornblende from an amphibolite (96VD126, see below) [*Lapierre et al.*, 1999] indicate that the Mg-rich lavas and amphibolites of the Duarte Complex are contemporaneous with the oceanic plateau tholeiites of the CCOP exposed in the Caribbean and Central America.

Ecuador.

Three main geological domains can be distinguished (Fig. 2.3). The NNE trending Andean Cordillera is predominantly composed of deformed Paleozoic to Mesozoic metamorphic rocks [*Aspden and Litherland*, 1992; *Noble et al.*, 1997] crosscut and overlain by the products of Tertiary magmatic arcs [*Aspden et al.*, 1992; *Lavenu et al.*, 1992]. Cretaceous to Paleogene continental volcanic arcs cropping out in southwestern Ecuador represent the continuation of the magmatic arc of Peru [*Jaillard et al.*, 1996].

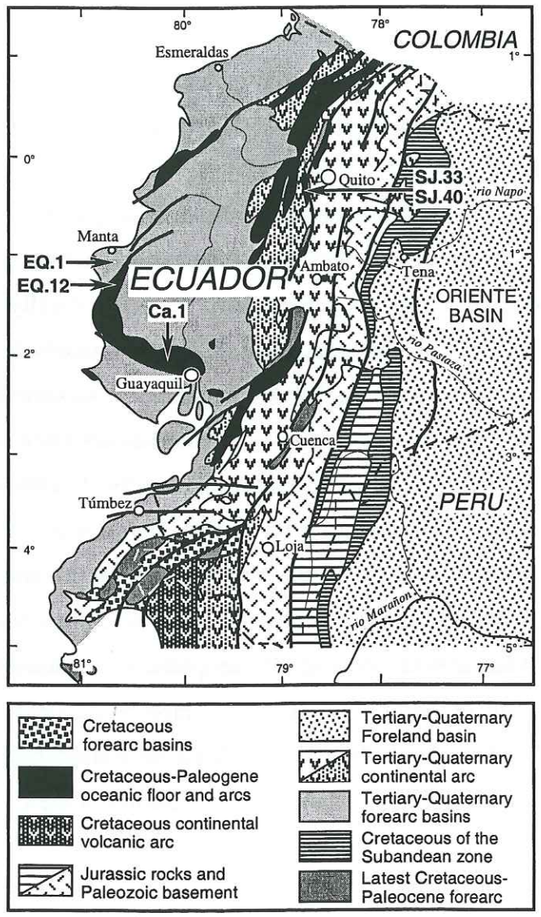

Fig. 2.3. Schematic map of Ecuador showing the location of the analyzed samples discussed in the text

The western coastal zone comprises an oceanic igneous basement, unconformably overlain by early Late Cretaceous to Paleogene intraoceanic arcs [*Lebrat et al.*, 1987; *Bourgois et al.*, 1990; R. Marksteiner and A. Alemán, unpublished report, 1991], in turn, overlain by Tertiary forearc marine sediments. The igneous basement (i.e., the Piñón Formation) consists of pillow basalts and diabases which yielded dubious K/Ar ages on plagioclase and whole rocks ranging from 110 to 54 Ma [*Goossens and Rose*, 1973]. This basement is stratigraphically overlain by undated volcanic rocks of oceanic arc origin, which are in turn overlain by pelagic sediments containing Cenomanian(?) to Turonian faunas. Thus the age of the oceanic basement of Coastal Ecuador can be regarded as pre-early Late Cretaceous.

In the eastern part of the coastal zone (i.e., the Western Cordillera) the Cretaceous-Paleogene magmatic rocks are in fault contact with the basement of the Andean Cordillera. Tectonic slices of ophiolitic series pinched along this contact were interpreted as remnants of an oceanic crust [*Juteau et al.*, 1977; *Lebrat et al.*, 1987] or an oceanic plateau [*Desmet*, 1994]. The island arcs and their oceanic basement were accreted to the margin of the South American Plate during Late Cretaceous to late Paleocene times [*Jaillard et al.*, 1997; *Cosma et al.*, 1998]. In summary, coastal Ecuador is a fragment of oceanic lithosphere of pre-Late Cretaceous age (> 91 Ma), overlain by early Late Cretaceous to Tertiary intraoceanic volcanic arc series.

Western Central Mexico.

The Guerrero volcano-plutonic arc was accreted to the continental margin of western Mexico before Cenomanian times [*Tardy et al.*, 1986]. It is presently separated from the Precambrian and Paleozoic terranes of Mexico by the Arperos oceanic suture (Fig. 2.4). In northwestern and central Mexico the Arperos suture contains scattered outcrops of submarine mafic lava flows and diabases overlain by pelagic sediments containing Early Cretaceous radiolarian fauna [*Dávila Alcocer and Martínez Reyes*, 1986].

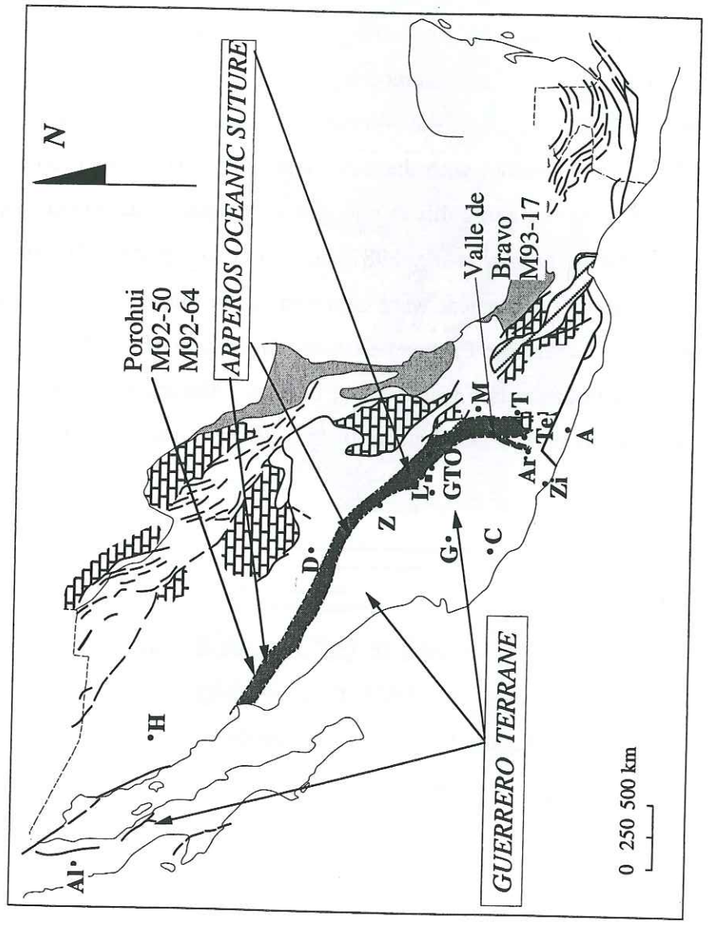

Fig. 2.4: Schematic map of the Arperos basin and the Guerrero terrane showing the location of the samples quoted in the text. A, Acapulco; Al, Alisitos; Ar, Arcelia; C, Colima; D, Durango; G, Guadalajara; GTO, Guanajuato; H, Hermosillo; L, Leon; M, Mexico city; T, Taxco; Te, Teloloapan; Z, Zacatecas; Zi, Zijuatanejo.

ANALYTICAL PROCEDURES

Diabases, and cpx- and/or olivine-rich basalts experienced hydrothermal alteration and metamorphism up to the greenschist facies. Accordingly, only those samples with well-preserved original igneous mineralogy (i.e., clinopyroxene, amphibole, and plagioclase phenocrysts) and devoid of any significant petrographic alteration features were selected for study. Phenocrysts were separated then purified by hand picking. The petrographic features of these rocks are summarized in Table 2.1. However, actinolite rims around some cpx crystals could not be completely removed.

For Sr and Nd isotopic analyses, mineral separates and host rock powders were leached in a 2 *N* HCl-0.1 *N* HF mixture. For Pb isotope determinations, mineral separates and whole rocks were successively leached in hot 2 *N* HCl for 20 min in an ultrasonic bath, rinsed with tridistilled water, leached in cold 1 *N* HNO_3 for 20 min, and rinsed with tridistilled water in an ultrasonic bath for 15 min.

Trace elements were analyzed by inductively coupled plasma mass spectrometry (ICP-MS) at the University of Grenoble after acid dissolution. Rare earth element (REE) were first separated as a group and spiked with pure Tm using procedures described by *Barrat et al.* [1996]. Standards used for the analyses were JB2, WSE BIR-1, JR1, and UBN (Table 2.2). Major element analyses were performed by ICP-optical emission spectroscopy at the Université de Bretagne Occidentale. Major and trace element analyses of the minerals and host rocks are presented in Table 2.2.

The $^{143}Nd/^{144}Nd$ and $^{87}Sr/^{86}Sr$ isotopic characteristics were determined on a Finnigan MAT261 multicollector mass spectrometer at the Laboratoire de Géochimie de l'Université Paul Sabatier (Table 2.3), using the analytical procedures of *Lapierre et al.* [1997]. The $^{206}Pb/^{204}Pb$, $^{207}Pb/^{204}Pb$ and $^{208}Pb/^{204}Pb$ isotopic ratios were measured on a multicollector VG sector mass spectrometer at the Laboratoire de Géochimie isotopique de l'Université de Montpellier II (Table 3) following the analytical procedure adapted from *Manhès et al.* [1980]. Total Pb blanks are less than 65 pg for a 100 mg sample.

Isotopic data on minerals and host rocks have been corrected for in situ decay with an age of 86 Ma (Dominican Republic samples) and 123 Ma (Ecuador samples). This is based on Ar/Ar ages measured on Duarte igneous amphiboles [*Lapierre et al.*, 1999] and on a Sm/Nd internal isochron age determined on a gabbro from Ecuador, respectively (Table 2.4).

Tab 2.2. Major and Trace Element Analyses for the Duarte Complex and Ecuadorian Minerals and Host rocks, and Arperos Basalts

	Ecuado SJ 40 Cpx	Ecuador SJ40 Amphibol	Ecuador SJ40 Plagio	Ecuador RTSJ 40 Cumulate Gabbro	Ecuador SJ33 Cumulate Peridotite	Ecuador SJ33 Duplicate	Standard UBN Ultramafic	Ecuado PI04 cpx	Ecuador PI04 RT Intersertal Diabase	Ecuador EQ12 Plagio	Ecuador EQ12 Ophitic Diabase
SiO_2				49.61*	42.96*				53.32*		54.2*
TiO_2				0.07	0.04				1.48		2.1
Al_2O_3				16.33	6.55				13.59		13.34
Fe_2O_3				6.32	12.68				15.04		16.64
MnO				0.08	0.16				0.22		0.23
MgO				12.48	32.55				6.55		3.1
CaO				14.88	6.12				8		5.79
Na_2O				0.74	0.08				3.19		4.09
K_2O				0.04	0.01				0.01		0.13
P_2O_5											0.29
LOI											
Total											
Ba, ppm	8.306	2.87	4.69	9.24	4.75	6.46	31.36	4.47	14.50	42.89	na
Cr	na	na	na	172	2480	na	na	na	58	na	bdl
Hf	bdl	bdl	bdl	bdl	bdl	bdl	0.13	bdl	2.10	1.11	2.49
Nb	0.117	0.30	0.35	bdl	bdl	bdl	0.06	1.58	4.74	bdl	10.75
Ni	na	na	na	98	962	na	na	na	69	na	na
Rb	0.16	0.16	0.19	0.34	0.21	0.16	2.91	0.099	0.24	0.89	1.61
Sr	7.50	6.41	215.87	86.61	23.32	21.73	7.68	43.66	46.21	174	116.12
Ta	bdl	bdl	bdl	bdl	bdl	bdl	0.018	0.106	0.38	bdl	0.67
V	na	na	na	99	45	na	na	na	359	na	na
Y	7.64	3.83	0.07	2.16	1.03	0.89	2.33	45.74	28.09	9.95	51.02
Zr	bdl	bdl	bdl	bdl	bdl	0.41	3.13	bdl	66.05	41.65	77.07
Pb	bdl	bdl	bdl	0.60	0.58	0.32	12.64	0.035	0.68	0.23	0.22
Th	bdl	bdl	bdl	bdl	bdl	bdl	0.07	0.341	0.33	0.17	0.43
U	bdl	bdl	bdl	bdl	bdl	bdl	0.07	0.08	0.09	0.15	0.11
La	0.139	0.044	0.089	0.068	0.073	0.068	0.31	4.316	3.756	2.32	9.25
Ce	0.424	0.183	0.168	0.175	0.166	0.155	0.749	11.422	9.992	5.17	24.49
Pr	0.103	0.045	0.021	0.036	0.033	0.029	0.107	1.827	1.555	0.75	3.8
Nd	0.69	0.325	0.092	0.206	0.184	0.175	0.569	9.571	8.04	3.61	19.53
Sm	0.431	0.187	0.02	0.122	0.069	0.077	0.2	3.494	2.818	1.06	6.11
Eu	0.156	0.099	0.102	0.096	0.039	0.042	0.077	2.022	1.028	2.23	2.19
Gd	0.689	0.368	0.02	0.193	0.113	0.117	0.317	5.003	3.412	1.29	8.37
Tb	0.17	0.079	0.003	0.046	0.023	0.024	0.059	1.079	0.709	0.23	1.47
Dy	1.25	0.604	0.014	0.35	0.165	0.164	0.406	7.514	4.783	1.47	9.56
Ho	0.3	0.146	0.003	0.088	0.038	0.038	0.096	1.774	1.107	0.33	1.96
Er	0.87	0.441	0.006	0.266	0.112	0.109	0.264	5.067	3.146	0.92	5.48
Tm	0.133	na	na	0.041	na	na	na	0.809	0.491	0.16	0.77
Yb	0.795	0.473	0.005	0.256	0.115	0.111	0.29	5.109	3.088	0.85	5.17
Lu	0.13	0.074	0.001	0.041	0.018	0.019	0.048	0.836	0.477	0.126	0.77
$(La/Yb)_N$	0.12	0.06	11.57	0.19	0.45			0.61	0.87	1.94	1.28

	Duarte 97VD55* cpx	Duarte 97VD55 RT	Duarte 96VD126* Amphibole	Duarte 96VD126 cpx	Duarte 96VD126 RT	Duarte 96VD106* cpx	Duarte 96VD106	Arpero: M93-1	Arperos M92-50	Arperos M92-64
		Cumulus-enriched			Cumulus enriched		cpx rich basalt	Basalt	Basalt	Basalt
SiO_2	51.4	48.86	38.23		46.5	50.1	45.5	44.5	43.48	44.1
TiO_2	0.65	1.04	2.96		1.5	1	1.46	0.9	1.79	2.1
Al_2O_3	3	8.04	12.3		10.79	3.9	11.55	15.1	14.06	16.5
Fe_2O_3	6.8(FeO)	11.0	16.93 (FeO)		13.11	6.52 (FeO)	12.17	8.4	7.32	10.74
MnO	0.17	0.17	0.26		0.18	0.12	0.2	0.1	0.16	0.1
MgO	16	13.72	9.83		11.25	14.45	9.65	6.4	4.61	8
CaO	20.37	14.63	11.72		12.2	22.5	10.5	12.6	14	6.3
Na_2O	0.27	0.85	2.88		2.09	0.42	0.73	4.1	3.5	3.7
K_2O	bdl	0.12	0.48		0.1		0.12	0.2	0.28	1.2
P_2O_5	bdl	0.07	bdl		0.15		0.36	0.1	0.27	0.4
LOI	bdl	bdl	bdl		2.38		4.71	7.4	10.42	7.2
Total	98.66	98.51	95.6		100.25	99.01	99.95	99.8	99.89	100.34
Ba, ppm	2.571	23.708	31.2	8.96	100	5.52	106	38.51	88.31	426
Cr	na	1925	na	na	1050	na	460	287	286	217
Hf	bdl	bdl	3.04	bdl	bdl	bdl	2.7	3.84	3	4.75
Nb	1.526	3.71	12.7	3.66	bdl	0.79	15.46	10.06	6.91	9.78
Ni	na	268	na	na	454.91	na	215.23	146	129	50
Rb	0.34	1.815	0.51	0.29	0.63	0.52	2.98	1.45	2.32	14.2
Sr	19.83	114.78	120.9	34.9	53.06	53.2	392.47	249	308	391.5
Ta	bdl	0.23	0.69	0.2	bdl	0.05	1.01	0.68	0.46	0.6
V	na	455.5	na	na	272.94	na	262.63	204	239	278
Y	10.06	13.18	17.8	14.1	9.57	13.9	18.49	33.35	25.57	28.3
Zr	bdl	na	83.8	bdl	bdl	bdl	88.47	172.8	117	170
Pb	bdl	0.48	0.87	0.27	0.548	0.4	2.938	1.06	1.23	0.85
Th	bdl	0.234	0.28	0.06	0.66	0.05	0.74	0.76	0.54	0.62
U	bdl	0.08	bdl	bdl	0.11	bdl	0.16	0.3	0.56	0.38
La	0.508	3.042	3.16	0.98	6.98	1.49	8.97	10.76	7.3	8.54
Ce	2.016	8.156	8.86	3.12	15.06	4.75	19.57	26.78	19.66	24.02
Pr	0.46	1.316	1.47	0.73	2.12	1.01	2.76	3.87	3.06	3.61
Nd	3.019	6.908	7.38	4.72	9.89	5.94	12.64	17.5	14.31	17.43
Sm	1.408	2.332	2.54	2.02	2.5	2.15	3.46	4.8	4.1	4.64
Eu	0.484	0.801	0.82	0.79	0.84	0.68	1.24	1.59	1.34	1.40
Gd	1.666	2.38	2.25	2.2	2.83	2.32	3.88	5.2	4.24	5.56
Tb	0.329	0.432	0.45	0.45	0.47	0.44	0.63	0.93	0.74	0.89
Dy	2.026	2.561	3.42	3.06	2.81	2.94	3.89	5.58	4.45	5.62
Ho	0.414	0.538	0.68	0.58	0.56	0.56	0.78	1.23	0.95	1.13
Er	1.031	1.323	1.81	1.47	1.36	1.41	2.05	3.43	2.61	3.21
Tm	0.143	0.195	0.28	0.21	0.18	0.2	0.27	0.51	0.39	0.42
Yb	0.8	1.067	1.53	1.12	1.09	1.12	1.77	3.19	2.37	2.79
Lu	0.114	0.15	0.23	0.16	0.14	0.17	0.27	0.49	0.36	0.41
$(La/Yb)_N$	0.455	2.04	1.48	0.62	4.31	0.95	3.41	2.42	2.10	2.19

Locations, samples, facies, and rock types are given. Limits of detection: Zr = 24 ppb, Nb = 5 ppb, Ta = 0.5 ppb, Hf = 1 ppb, U, Th and Pb = 0.6 ppb.
*Analytical conditions of microprobe analysis: 15 kV, 10-20 nA, focused beam, natural standards.
*Major elements reported on volatile free basis after *Desmet* [1994] and Reynaud et al. (submitted, manuscript, 1988). na, not analyzed; bdl, below detection limit.
#Zoned cpx, mean analysis is without signification. Microprobe analyses of major elements are available on request.

Tab. 2.1. Location and Descriptions of Duarte Complex (Dominican Republic), Piñón Formation (Ecuador), and Arperos Formation (Mexico) Samples

	Sample			
	96VD126	97VD55	96VD121	96VD106
Duarte Complex	Villa Altagracia Autopista Santo Domingo	Villa Altagracia Autopista Santo Domingo	Villa Altagracia Autopista Santo Domingo	South Janico road to Juancalito
Texture	cumulus-enriched	cumulus-enriched	porphyritic	porphyritic
Mineralogy	olivine pseudomorphs (5%) large cpx phenocrysts (80%) rimmed by Mg-rich Hastingsite (3%) skeletal cpx crystals interstitial glass (12%) present recrystallized to smectites	cpx large crystals (90%) interstitial glass (10%) present, recrystallized to smectites	cpx large crystals (60%) rimmed locally by actinolitic hornblende glassy groundmass (40%)	cpx large crystals (30%) in a quenched groundmass (70%) with skeletal cpx microlites glass recrystallized to smectites
Name	cpx-rich cumulative basalt	cpx-rich cumulative basalt	cpx-rich basalt	cpx-rich basalt

	Sample			
	SJ40	SJ33	EQ12	PIO4
Ecuador	Quebrada San Juan	Quebrada San Juan	Puerto Cayo	North of Guayaquil
Texture	adcumulatelayered	cumuluslayered	ophitic	intersertal
Mineralogy	preserved plagioclase (70%) cpx (25%) partly transformed to hornblende opx (5%) pseudomorphs	cumulus: olivine (60%) + cpx (35%) intercumulus: anorthite (5%)	plagioclase laths (50%) interstitial cpx (40%) Fe-Ti oxides (10%)	plagioclase laths (50%) cpx (40%) epidote + chlorite (10%)
Name	gabbro	wehrlite	diabase	diabase

	Sample		
	M93-17	M92-50	M92-64
Western Mexico Arperos	Valle de Bravo	Porohui	Porohui
Texture	porphyritic	intersertal	intersertal
Mineralogy	skeletal olivine (5%) replaced to calcite + Crspinels quenched Ti-rich cpx (15%) oxides (5%) in the groundmass (75%)	plagioclase (40%) laths and phenocrysts replaced to albite small cpx crystals (20%) groundmass (40%)	plagioclase (40%) laths and microlites cpx (20%) calcite-filled vesicles (20%) groundmass (40%)
Name	basalt	basalt	basalt

TRACE ELEMENT CHEMISTRY ON MINERAL SEPARATES AND THEIR HOST ROCKS

Dominican Republic

REE patterns of samples 96VD126 (olivine and cpx-rich basalt) and 96VD106 (cpx-rich basalt) are light REE (LREE)-enriched ($3.4 < (La/Yb)_N < 4.3$; Table 2.2 and Fig. 2.5) with low REE contents (around 10 times chondritic values). These data are in agreement with previous works [*Kerr et al.*, 1996b, 1997a]. Sample 97VD55 (cpx cumulate) differs from the others, being less enriched in LREE ($(La/Yb)_N = 2.04$). Clinopyroxenes have very similar REE_N patterns with moderate LREE depletions ($0.45 < (La/Yb)_N < 0.95$), whatever their host rock type. Amphiboles have rather flat REE patterns ($(La/Yb)_N = 1.48$). The LREE enrichment of whole rock with respect to clinopyroxene (cpx) and amphibole (amph) is consistent with the preferential partitioning of REE into the melt. The heavy REE (HREE) levels in the host rock and cpx are quite similar, with the exception of 96VD126 host rock which is more HREE-depleted than its cpx (Fig. 2.5a).

Relative to normal mid-ocean ridge basalts (NMORB) (Fig. 6), these rocks and their minerals show moderate enrichment in LILE and high Nb, Ta, and Pb contents. Their Th/U ratios ($3.34 < Th/U < 6.75$; Fig. 2.7) fall within the range of the mid-Cretaceous tholeiites from Costa Rica [Hauff *et al.*, 1997; *Sinton et al.*, 1997]. In the cumulus-enriched rocks, trace element patterns of minerals and related host rocks are more or less parallel. This is not the case for the cpx-rich basalt where the host rock is markedly enriched in Th, Ta, and Nb with respect to the cpx. Pb has similar behavior in the cpx and in its host rock. This suggests that Nb, Ta, and Pb were concentrated in the groundmass.

The Duarte Mg-rich rocks show a wide range of Nb/U and Pb/Ce ratios (Fig. 2.7) ($29.9 < Nb/U < 96.6$; $0.01 < Pb/Ce < 0.09$) but with U contents significantly lower than those of ocean island basalts (OIB) ($0.96 < U < 1.68$). Th/U is higher and Nb/Ta and Zr/Hf are generally lower than NMORB (Fig. 2.7).

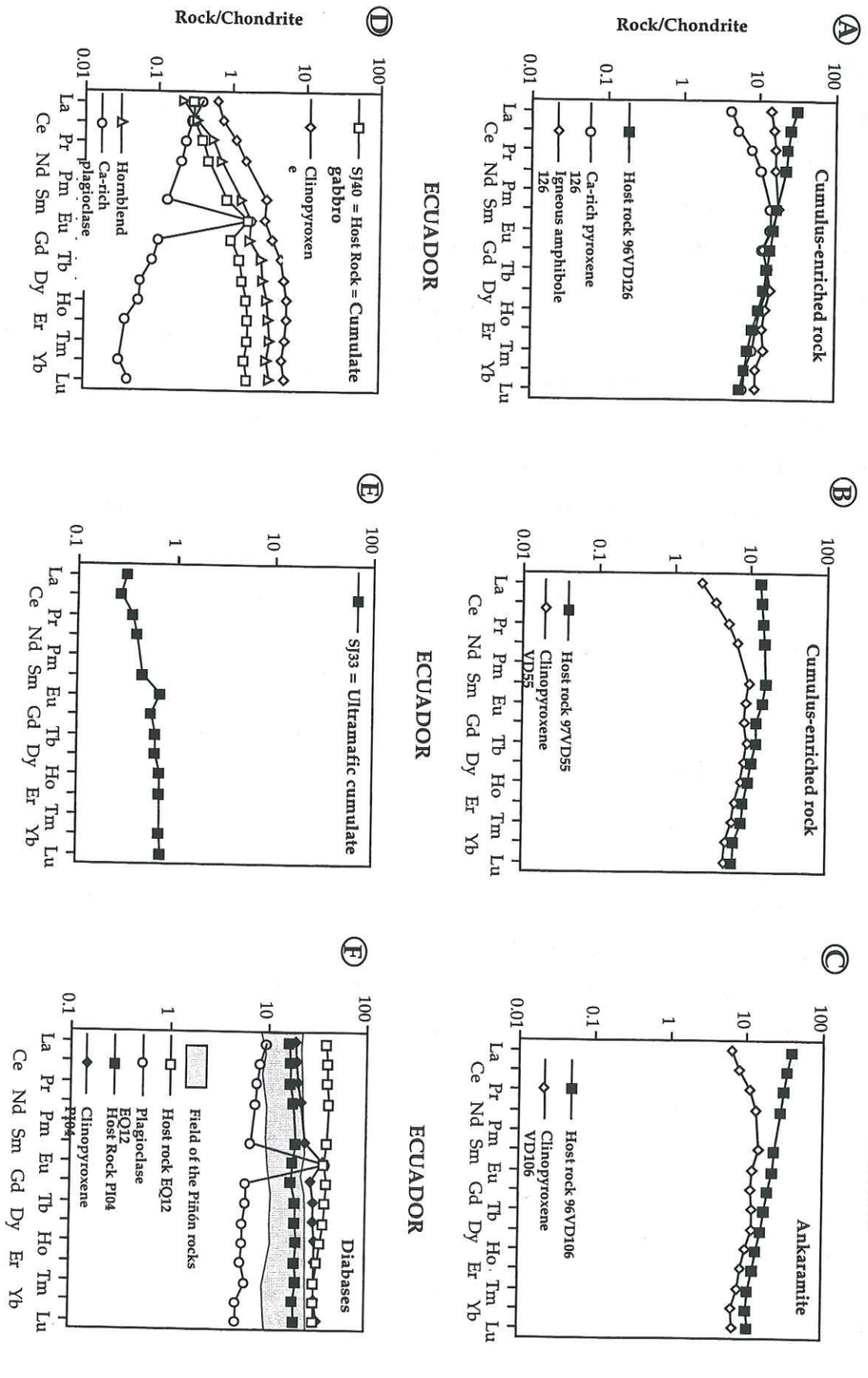

Fig. 2.5: Chondrite-normalized (*N*) rare earth element patterns of the minerals and host rocks which show oceanic plateau affinities. San Juan cumulates and Piñón diabases are from Ecuador. Cumulus-enriched picrites and ankaramites belong to the Duarte Complex from Dominican Republic. Chondrite values are from *Sun and McDonough* [1989].

Ecuador

The diabases of the Piñón Formation (Reynaud et al., submitted manuscript, 1998) differ from the Duarte cpx-rich basalt in having flat REE patterns ($0.87 < (La/Yb)_N < 1.28$; Table 2.2 and Fig. 2.5). Compared to the host rock, PIO4 cpx has similar REE abundances but differs in the degree of LREE depletion ($(La/Yb)_N = 0.61$) and is enriched in HREE. The EQ12 Ca-rich plagioclase REE concentrations are significantly lower than those of its host rock, and this mineral is LREE-enriched compared to the HREE ($(La/Yb)_N = 1.94$; Table 2.2 and Fig. 2.5).

The cumulate rocks from western Ecuador (SJ33, SJ40; Table 1) and SJ40 cpx differ from the Duarte cumulus-enriched rocks (96VD126, 97VD55) and related cpx in having significantly lower REE contents (Table 2.2; < 10 times the chondritic abundances) and a marked LREE depletion (Fig. 2.5). The whole rock SJ40 and its related cpx and hornblende have similar parallel REE patterns, characterized by a significant LREE depletion ($0.06 < (La/Yb)_N = < 0.19$; Fig. 2.5 and Table 2.2). The cpx and its host rock have the highest and lowest REE levels, respectively, which are < 10 times the chondritic values. Hornblende has lower La and Ce abundances than the host rock. Ca-rich plagioclase is LREE-enriched ($(La/Yb)_N = 11.57$; Table 2). Finally, the cumulate wehrlite is LREE-depleted ($(La/Yb)_N = 0.45$) and has negative Ce ($Ce/Ce^* = 0.51$) and positive Eu ($Eu/Eu^* = 1.24$) anomalies.

Relative to NMORB, the Piñón diabases have high Nb, Ta, and Th values, characteristic of plume-generated magmas. Moreover, their Th/U ratios are slightly higher than those of NMORB (Table 2.2 and Fig. 2.6) with the exception of EQ12. However, these rocks differ from the Duarte cumulus-enriched olivine and/or cpx-rich basalts by their lower contents of Zr, Hf, U, Th, Nb, and Ta ($38.14 < Nb/U < 52$; Table 2.2 and Fig. 2.6 and 2.7). The Pb/Ce ratios of these rocks are low ($0.008 < Pb/Ce < 0.07$) with the exception of the cumulate gabbro ($Pb/Ce = 3.45$) but generally higher than those of MORB.

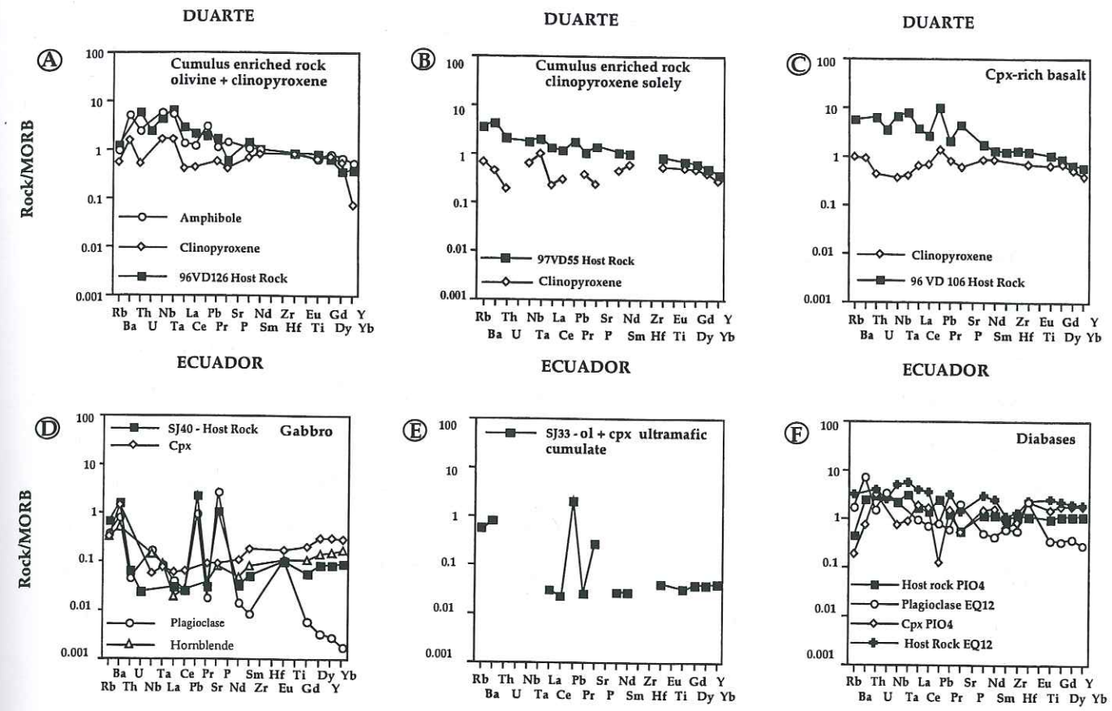

Fig. 2.6: NMORB-normalized trace element patterns for the minerals and host rocks from Dominican Republic and Ecuador. NMORB values are from *Sun and McDonough* [1989].

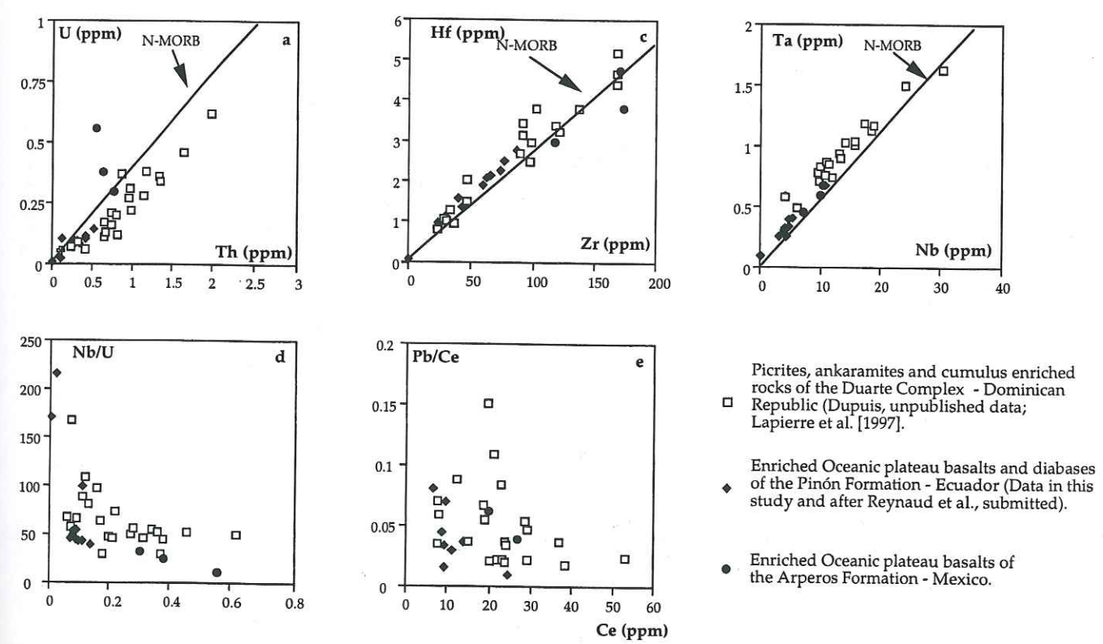

Fig. 2.7: U-Th, Hf-Zr, Ta-Nb, Nb/U-U, and Pb/Ce-Ce plots for the igneous rocks from Dominican Republic, Ecuador, and western Mexico.

Western Mexico

The Arperos basalts presented here belong to group 1 [*Freydier et al.*, 1996]. They differ from the Piñón rocks by a greater LREE enrichment relative to HREE ($(La/Yb)_N \sim 2$; Table 2.2 and Fig. 2.8) which is nevertheless smaller than that of the Duarte cpx-rich basalts.

Relative to NMORB, the Arperos basalts are enriched in Th, U, Ta, and Nb but slightly depleted in Hf and Zr. Their U, Th, Hf, and Zr abundances are higher than those of the Piñón rocks and more or less similar to those of the Duarte cpx-rich basalts (Fig. 2.6). In contrast, their Nb and Ta contents are intermediate between those of Piñón and Duarte rocks. Their Nb/U ratios (12.33 to 33.5) are lower than those of the Duarte and Piñón rocks (Fig. 2.7). Their Pb/Ce ratios are low (0.045 and 0.062) but slightly higher than those of the Piñón rocks.

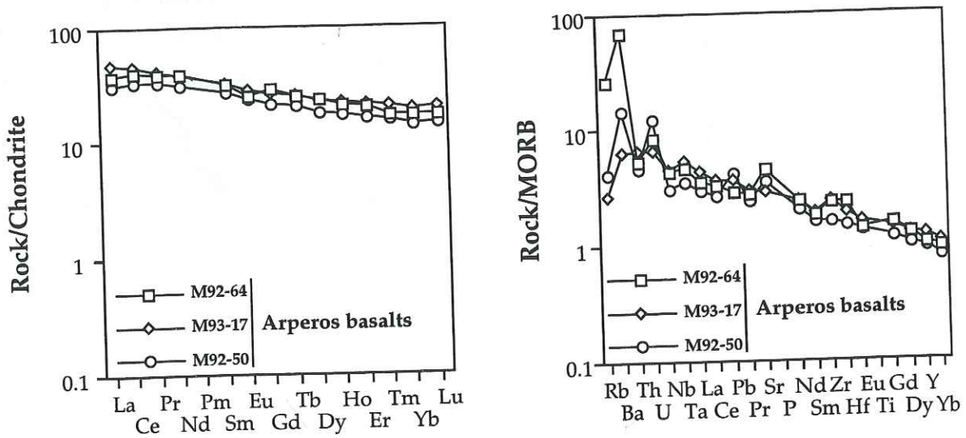

Fig. 2.8: Chondrite-normalized *(N)* rare earth and NMORB normalized trace element patterns of the basalts of the Arperos Formation (westerncentral Mexico) which show oceanic plateau affinities. Chondrite and NMORB values are from *Sun and McDonough* [1989].

Characteristics of Calculated Melts in Equilibrium with clinopyroxene

In order to determine the compositions of the cpx parent magmas, REE compositions of melts in equilibrium with these minerals were calculated using the partition coefficients of *Hart and Dunn* [1993]. The REE abundances of these calculated melts based on 97VD55 and 96VD126 cpx compositions of the Duarte basalts (Fig. 2.9) match well with those of the cpx-rich basalt 96VD106 (Fig. 2.5a). The REE composition of the calculated melt based on 97VD55 cpx composition is rather similar to those of both cpx-rich basalts. The calculated melt in equilibrium with 96VD126 cpx composition has a similar LREE-enriched pattern associated with higher REE abundances and a positive Ce anomaly, which is absent in the Mg-rich rocks. The liquid in equilibrium with the 97VD55 cpx has a composition similar to that of the cpx-rich basalt (96VD106). The higher REE abundance of the calculated melt based on 96VD126 cpx is probably related to olivine crystallization leading to a more fractionated residual liquid in the cumulus-enriched rock.

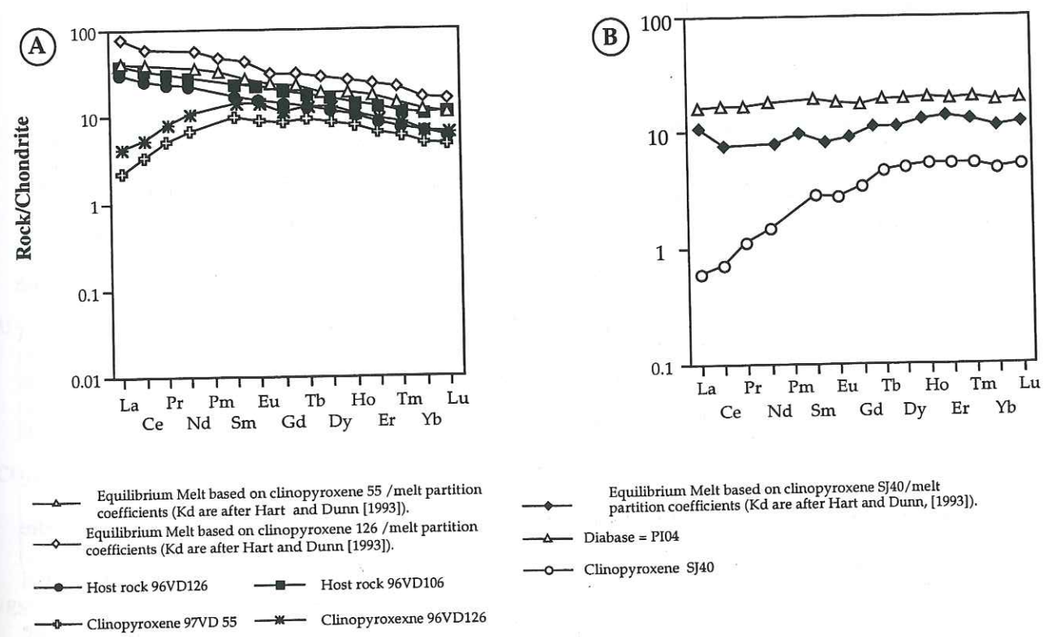

Fig. 2.9: Rare earth*N* patterns of calculated melts in equilibrium with the Duarte (Dominican Republic) and Piñón (Ecuador) clinopyroxenes. Chondrite values are from Sun and McDonough [1989].

The REE pattern of the calculated melt, based on the SJ40 cpx of the gabbro from Ecuador (using again partition coefficients from *Hart and Dunn* [1993] is more or less flat (Fig. 2.9) and similar to those of the Piñón diabases (Table 2.2 and Fig. 2.5b) but displays negative spikes for Ce and Nd which are absent in the REE patterns of the Piñón diabases. However, cpx SJ40 was probably in equilibrium with an enriched tholeiitic magma characterized by a flat REE pattern, similar to those of the Piñón diabases.

In summary, the rocks from Dominican Republic, Ecuador, and western Mexico have general oceanic plateau basalt affinities but show differences in trace element compositions. The Duarte Mg-rich rocks are enriched in LREE, Pb, Th, and U and are characterized by high Th/U ratios. Relative to NMORB, they are depleted in HREE and Y. In contrast, the Piñón diabases have flat REE patterns and are Pb, Zr, and Hf depleted. Their Th/U ratios are low. The Duarte cpx is less LREE depleted than that of Ecuador and is in equilibrium with a cpx-rich basaltic melt, similar to 96VD106. The cpx from Ecuador is in equilibrium with an enriched tholeiitic melt. The Arperos basalts exhibit intermediate geochemical features between those of the Duarte and Piñón rocks.

ISOTOPIC CHEMISTRY OF THE MINERAL SEPARATES AND HOST ROCKS

The cpx-rich basalts of the Duarte Complex

As already mentioned, all data were corrected for in situ decay assuming an age of 86 Ma for this formation. The 96VD126 cpx and its cumulate-enriched cpx-rich host rock have similar ε_{Nd} ratios (+8.34 and 8.53, respectively; Table 2.3 and Fig. 2.10) while that of the amphibole is slightly lower (7.99). In contrast, the $(^{87}Sr/^{86}Sr)_i$ of the amphibole and its host rock are exactly the same (0.70315; Table 3) and plot in the same range as the associated cpx (0.70320). The cpx-rich basalt, cumulus-enriched rocks (97VD55, 96VD121) and their constituent cpx have rather homogeneous ε_{Nd} ($+7.6 < \varepsilon_{Nd} < 6.2$; Table 3) which are significantly lower than those of the 96VD126 rock and constituent minerals. The cpx of the cpx-rich basalt (96VD106) differs from the previous rocks by having a slightly lower ε_{Nd} ratio (+5.5; Table 2.3 and Fig. 2.10), although its host rock displays ε_{Nd} (+6.4) in the same range as other sampled rocks of this complex.

Similarly, the initial Sr isotopic ratio of the 96VD106 cpx is slightly higher (0.70362; Table 3) than that of the corresponding whole rock (0.70370; Table 3). We attribute this difference to the presence of actinolite which locally rims the cpx. These Mg-rich rocks and their minerals (with the exception of the cumulus-enriched 96VD121) have homogeneous $(^{87}Sr/^{86}Sr)_i$ ($0.70315 < (^{87}Sr/^{86}Sr)_i < 0.70370$; Table 2.3 and Fig. 2.10), which probably reflects their source composition.

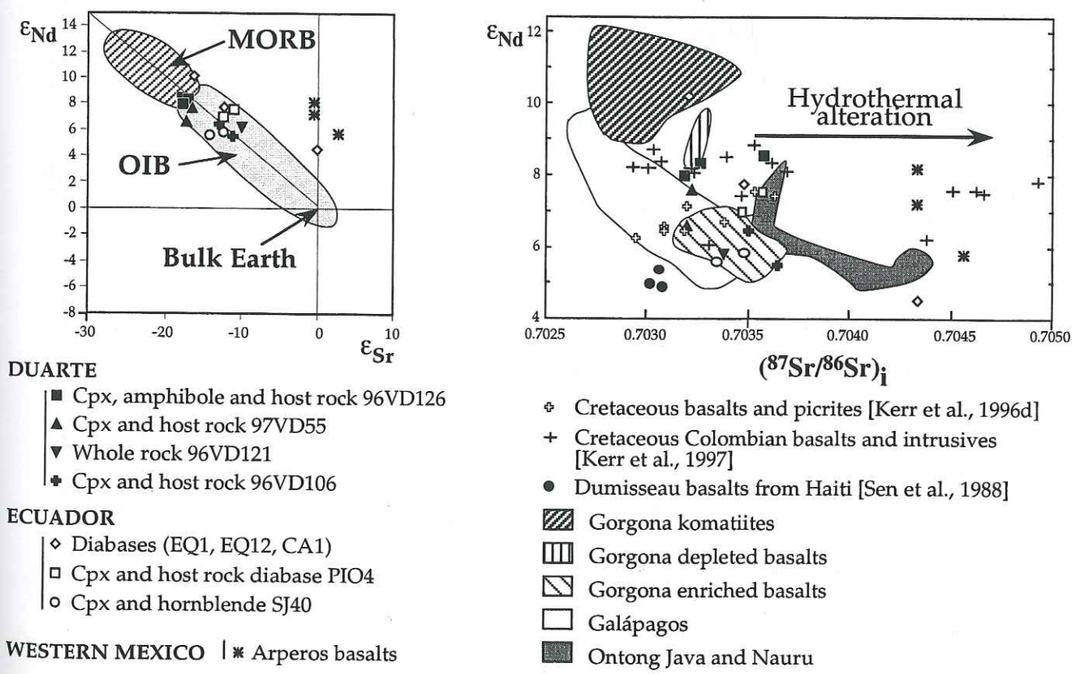

Fig. 2.10: The εNd -εSr and εNd -(87Sr/86Sr)*i* plots for the minerals and host rocks from Dominican Republic, Ecuador, and westerncentral Mexico.

Initial lead isotopic compositions of whole rocks and mineral separates from Mg-rich basalts of the Duarte Complex display a limited range of $^{206}Pb/^{204}Pb$ (18.97-19.54), $^{207}Pb/^{204}Pb$ (15.52-15.60), and $^{206}Pb/^{204}Pb$ (38.6-39.3) (Table 2.3 and Fig. 2.11). These highly radiogenic isotopic compositions fall within the range of enriched OIB signatures. Interestingly, the Duarte Complex domain falls close to or on the Northern Hemisphere Reference Line (NHRL [*Zindler and Hart*, 1986]) in the $^{207}Pb/^{204}Pb$-$^{206}Pb/^{204}Pb$ isotope diagram but on or slightly above the NHRL in the $^{208}Pb/^{204}Pb$-$^{206}Pb/^{204}Pb$ isotope diagram.

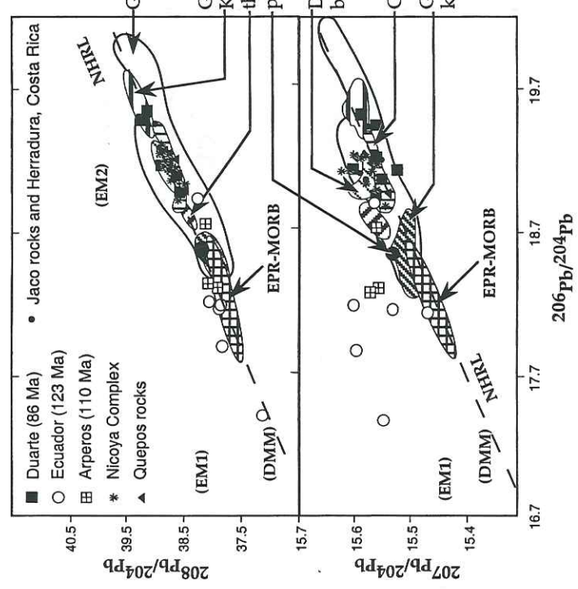

Fig. 2.11: The 208Pb-204Pb versus 206Pb-204Pb and 207Pb-204Pb versus 206Pb-204Pb correlation diagrams for the minerals and host rocks. Recalculated initial ratios have been reported for minerals and whole rocks from cumulates and clinopyroxene-rich basalts from Dominican Republic (86 Ma), gabbros and diabases from Ecuador (123 Ma), and pillow basalts from Arperos from Mexico (110 Ma). Typical analytical uncertainties are indicated by the size of the symbols. Various analytical points and data fields have been reported from the literature. Data from the Nicoya Complex, Jaco rocks and Herradura, Costa Rica (90 Ma), are after *Hauff et al.* [1997], and *Sinton et al.* [1997 and 1998]. The Gorgona picrites, komatiites; tholeiites; and K-tholeiites fields are after *Dupré and Echeverria* [1984]. The field of the Dumisseau basalts from Haiti field is from *Sen et al.* [1988]. The Galapagos lavas field is reported by*White et al.* [1993]. East Pacific MORB data and Galapagos Islands field are from *White et al.* [1987, 1993].

Tab. 2.3: Nd, Sr and Pb isotopic Analyses for the Duarte complex, Ecuadorian, and Mexican Minerals and Host Rocks.

Facies	$(^{206}Pb/^{204}Pb)i$	$(^{207}Pb/^{204}Pb)i$	$(^{208}Pb/^{204}Pb)i$	$^{143}Nd/^{144}Nd$	$^{87}Sr/^{86}Sr$	$(^{87}Sr/^{86}Sr)i$	εNd	εSr	Hispaniola
Cumulate 96VD126	19.094	15.550	38.603	0.513051± 4	0.703190±6	0.70315	+8.53	-17.77	**E-MORB 85 Ma**
Amphib. 126	19.158	15.601	38.956	0.513054± 6	0.703163±18	0.70315	+7.99	-17.77	
Cpx - 126				0.513100± 6	0.703233±13	0.70320	+8.34	-16.98	"
Ankaramite 96VD106	19.537	15.588	39.188	0.512951 ± 4	0.703520 ± 8	0.70349	+6.45	-12,87	"
Cpx 106	19.252	15.557	38.941	0.512957± 7	0.703642 ± 12	0.70362	+5.52	-11.06	"
Cumulate 96VD121	19.146	15.525	38.800	0.512936± 8	0.703867± 25	0,70370	+6.19	-9,95	"
Amphib. 121	19.466	15.563	39.267						"
Cumulate 97VD55	18.966	15.565	38.621	0.512979 ± 9	0,703234 ± 8	0,70318	+6.57	-17,34	"
Cpx 55				0.513073± 7	0.703270 ± 18	0.70321	+7.56	-16.89	
Pillow basalt M92-50	18.712	15.563	38.168	0.512997 ± 36	0.704372 ± 11	0.70432	+7.2	-0.72	**Arperos**
Pillow basalt M93-17	18.271	15.570	37.948	0.513027 ± 13	0.704435 ± 11	0.70432	+8.2	-0.70	**110 Ma**
Pillow basalt M92-64	18.304	15.558	38.099	0.512912 ± 48	0.704720 ± 8	0.70455	+5.8	+2.49	**Mexico**
Diabase PiO4	17.898	15.595	37.825	0.513008 ± 6	0.703506 ± 11	0.70348	+6.98	-12.43	**Piñon**
Cpx PiO4				0.513043± 6	0.703588 ± 10	0.70358	+7.53	-11.06	**123 Ma**
Diabase EQ12	17.414	15.548	37.166	0.513026 ± 6	0.703561 ± 12	0.70349	+7.69	-12.27	**Ecuador**
Plagio. EQ12				0.512055 ± 30	0.703327± 21				
Diabase EQ1	18.159	15.529	37.840	0.513154 ± 25	0.703451± 27	0.70321	+10.1	-16.24	
Diabase CA1	18.923	15.566	38.431	0.512870 ±7	0.704542 ± 17	0.70435	+4.49	-0.03	
Gabbro SJ40	18.193	15.602	38.100						
Plagio. SJ40	18.126	15.473	37.890	0.512822 ± 18	0.703162 ± 7	0.70316	+4.62	-17.01	
Cpx. SJ40				0.513079 ± 11	0.703588± 10	0.70348	+5.84	-12.44	
Amphib. SJ40				0.513046 ± 16	0.703473± 20	0.70335	+5.59	-14,33	
Ultramafic SJ33				0.512822 ± 14	0.703448 ± 13	0.70282	+3.17	-13.69	

Pb isotope ratios were corrected with a mass discrimination factor of 0.13% per atomic mass unit relative to values of the NBS-981 standard measured during this period: $^{206}Pb/^{204}Pb = 16.936 \pm 0.006$, $^{207}Pb/^{204}Pb = 15.494 \pm 0.006$ and $^{208}Pb/^{204}Pb = 36.721 \pm 0.013$. Pb isotope ratios 2σ uncertainties are assumed to be less than 0.15%.

Basalts, Diabases, and Cumulate Gabbro from Ecuador and Mexico

In an attempt to obtain a reliable constraint on the age of the Piñón suite, we determined a Sm/Nd internal isochron on the SJ13 amphibole gabbro (Table 4). The three experimental points (whole rock, plagioclase, and amphibole) yield a regression age of 123±13 Ma with a $^{143}Nd/^{144}Nd$ initial ratio of 0.512875±37 (mean square of weighted deviation, MSWD = 2.05) [*Ludwig*, 1987] (Fig. 2.12). This age is interpreted as corresponding to the crystallization of the cumulate gabbro in the oceanic plateau section, now exposed in Ecuador. It also indicates that plateau-building eruptions occurred in the Ecuadorian province as early as 123 Ma. Meanwhile, the rather large uncertainty of this age needs to be refined by additional analyses.

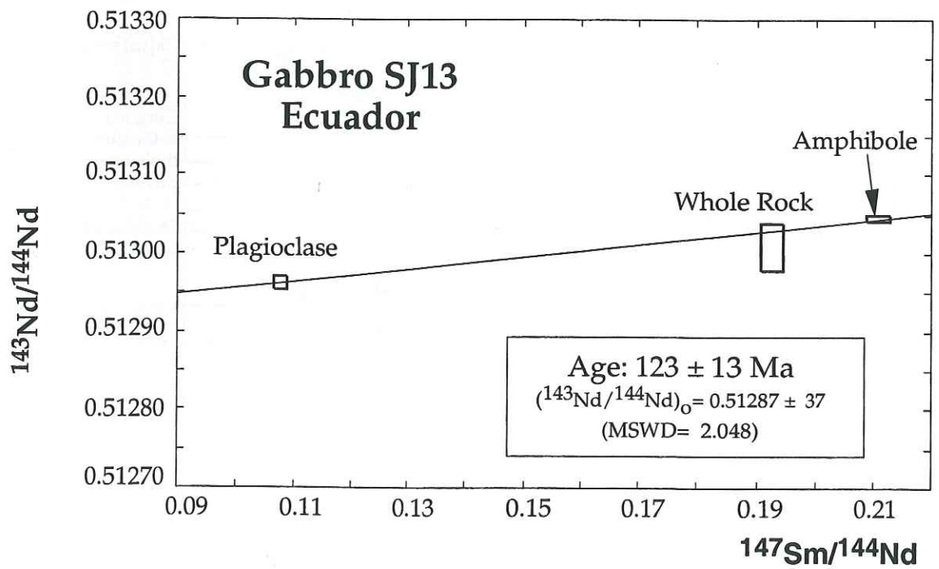

Fig. 2.12: Sm/Nd isochron plot for minerals and whole-rock from the Ecuadorian SJ13 Gabbro. The regression analysis [Ludwig, 1987] yields T = 123 ± 13 Ma, (143Nd/144Nd)o = 0.512875 ± 37, εNdo = +7.76, and MSWD = 2.05 for plagioclase, whole rock and Amphibole.

Tab. 2.4: Sm and Nd Contents and $^{143}Nd/^{144}Nd$ Ratios From SJ13 Whole Rock, Amphibole, and Plagioclase Concentrates

Sample	Nd, ppm	Sm, ppm	$^{147}Sm/^{144}Nd$	$^{143}Nd/^{144}Nd$
SJ13 whole rock	8.40	2.68	0.193	0.513008±29
SJ13 plagioclase	0.99	0.18	0.108	0.512962±08
SJ13 amphibole	27.59	9.63	0.211	0.513045±04

The Sm and Nd concentrations have been determined by isotope dilution using a mixed ^{149}Sm and ^{146}Nd enriched solution. Sm/Nd errors are 1%

In common with the minerals and host rocks of the Duarte Complex the diabases, basalts, gabbro, and associated cpx from Ecuador and Mexico share rather similar homogeneous ε_{Nd} ratios that range between +8 and +5.8 (Table 3) (Reynaud et al., submitted manuscript, 1998). The SJ40 plagioclase has a slightly lower ε_{Nd} (+4.62, Table 3). However, a diabase (EQ1) and a basalt (CA1) from Ecuador have higher (ε_{Nd} = +10) and lower ε_{Nd} (+4.5) ratios, respectively (Table 2.3 and Fig. 2.10). This suggests that the basalts and diabases from Ecuador and Mexico might be derived from different mantle sources and/or different blends of depleted NMORB and enriched OIB magma types.

In the ε_{Nd} versus ε_{Sr} diagram (Fig. 2.10), all these rocks fall within the "mantle array," and their $(^{87}Sr/^{86}Sr)_i$ likely reflects the source composition, with the exception of three basalts from western Mexico (M92-64, M93-17, and CA1). The shift of the Sr isotopic ratios of these three rocks toward the radiogenic side of the mantle plot reflects an enrichment in radiogenic Sr (Fig. 2.10), probably induced by seawater contamination through hydrothermal process or contamination with pelagic sediment [*Kerr et al.*, 1997b].

Lead initial isotopic compositions of whole-rocks and mineral separates from basalts and cumulate gabbros from Ecuador and Mexico have a large range of $^{206}Pb/^{204}Pb$ and $^{208}Pb/^{204}Pb$ ratios (Table 2.3 and Fig. 2.11). Basalt EQ1 has a markedly lower $^{206}Pb/^{204}Pb$ ratio and plots near the depleted mantle morb (DMM) source. In contrast, CA1 has a significantly higher $^{206}Pb/^{204}Pb$ ratio similar to those of recent Galápagos lavas. The Ecuador samples define a nearly horizontal domain located slightly above the NHRL in the $^{207}Pb/^{204}Pb$ diagram. These high $^{207}Pb/^{204}Pb$ ratios could reflect a contamination of their mantle sources by pelagic sediments [*Doe*, 1970] and/or altered oceanic crust.

In summary, all samples from Dominican Republic, Ecuador, and western Mexico have fairly homogeneous ε_{Nd} (+5.5 to +8), similar to those of oceanic plateau basalts. The cpx of the Duarte cumulus-enriched basalt has slightly higher ε_{Nd} (+8.5). Finally, one mafic rock of the Piñón Formation has the highest ε_{Nd} (+10), similar to those of NMORB. A comparison of initial Pb isotopic signatures measured (on mineral separates and host rocks) on cumulus-enriched Mg-rich basalts from the Duarte Complex, on gabbros and diabases from Ecuador, and on Arperos basalts from Mexico emphasize a contribution from a more depleted mantle source for Ecuador than for the Duarte Complex. Mg-rich basalts from the Dominican Republic (Duarte) have a Pb isotopic range consistent with that of the Galápagos HIMU plume component and similar to the Gorgona tholeiites and Costa Rican lavas [*White et al.*, 1993; *Dupré and Echeverria*, 1984; *Hauff et al.*, 1997; *Sinton et al.*, 1997]. The Ecuadorian and Mexican basalts and cumulate gabbros have a Pb isotopic signature intermediate between NMORB and OIB components.

DISCUSSION: PRESENCE OF THREE DISTINCT MAGMATIC SUITES IN THE CCOP

A major difficulty in constraining the geochemical and isotopic characteristics of oceanic plateau igneous rocks arises from the low grade metamorphism or hydrothermal alteration that these rocks suffered either during their magmatic emplacement and cooling in a submarine environment and/or during their subsequent tectonic emplacement. These processes resulted in the mobility of Rb, Sr, and U, as suggested by the variable behavior observed for these elements in most spidergrams (Fig. 2.6), despite the fact that in this study we have deliberately chosen to focus our geochemical and isotopic investigations on a restricted number of samples and host minerals showing minimum alteration. However, the observation that most whole rock REE patterns fit with those calculated from the compositions of separated primary cpx indicates that the REE distribution was not significantly affected by postmagmatic processes. In addition, the analysis of separates of unaltered primary minerals allows us to check that the corresponding bulk rock compositions did not suffer noticeable Nd and Pb (and, in most cases, Sr) isotopic changes related to hydrothermal alteration (i.e., 96VD126 and SJ40, Table 3).

On the basis of ages, rock types, and geochemical and isotopic results the ultramafic-mafic oceanic crustal fragments currently regarded as belonging to the CCOP appear to belong to three distinct magmatic suites. The Upper Cretaceous suite (92-86 Ma) comprising the Gorgona basalts is the best known and geochemically well characterized. It makes up the basement of the Caribbean Sea and part of the numerous accreted oceanic crustal fragments exposed along the Pacific coast of Central America (Costa Rica) and South America (Colombia) and in the Caribbean (Dominican Republic, most of Duarte Complex; Curaçao, and Aruba; fig. 2.1). The basalts and diabases have LREE-enriched to flat REE patterns and differ from NMORB by their enrichments in Ti, Nb, Th, and Ta. Initial radiogenic Nd isotope ratios have a rather restricted compositional range (ε_{Nd} = +6 to +9.5 [*Sen et al.*, 1988; *Kerr et al.*, 1996b, 1997b; *Alvarado et al.*, 1997; *Hauff et al.*, 1997; *Sinton et al.*, 1997]). Similarly, all these rocks have a Pb isotopic signature consistent with the field defined by the recent Galápagos Islands, suggesting the contribution of a HIMU component (Fig. 2.11).

The age of the second suite, composed of the Ecuadorian and Mexican oceanic rocks, is Early Cretaceous (123-91 Ma). The corresponding rocks have a wide range of initial radiogenic Nd and Pb isotopic ratios, intermediate between OIB and NMORB components. The Ecuadorian igneous rocks, compared to those of the Dominican Late Cretaceous Duarte Complex, are depleted in the most incompatible elements.

Finally, in the Duarte and Nicoya Complexes (Fig. 2.1), slices of Upper Jurassic oceanic rocks are tectonically associated with the Upper Cretaceous oceanic plateau tholeiites. Indeed, these Upper Jurassic basalts and diabases from Dominican Republic differ from the Duarte cpx-enriched and/or cpx-poor basalts because they are depleted in LREE and in most incompatible trace elements [*Lapierre et al.*, 1999]. Thus these basalts and diabases are interpreted as remnants of the Late Jurassic Caribbean oceanic crust formed at a ridge and possibly close to a hospot.

In Costa Rica, Upper Jurassic radiolarian cherts were probably deposited on the top of oceanic crust [*Sinton et al.*, 1997]. In Hispaniola, slices of Upper Jurassic oceanic crust are tectonically associated with the Late Cretaceous Duarte Complex (see section 6).

In summary, at least two major pulses of oceanic plateau magmas occurred in the CCOP: Late Cretaceous (88-92 Ma) and Early Cretaceous (100-123 Ma). The Late Cretaceous cpx-rich basalts share the HIMU affinity of the Galápagos hotspot, while those of the Early Cretaceous plutonic and volcanic rocks are intermediate between depleted and HIMU mantle sources.

GEODYNAMIC IMPLICATIONS

The presence of two distinct oceanic plateau suites in the crustal fragments of the peri-Caribbean realm raises two questions.

1. Are these suites derived from two distinct hotspots possessing different signatures, as suggested by *Kerr et al.* [1997a], or solely from the Galápagos one?

2. If they are both derived from the Galápagos hotspot, is the present-day geographic location of the Ecuadorian and Mexican Early Cretaceous oceanic terranes consistent with the locations of the Galápagos plume and South America and the direction of Farallón plate motion during the Early Cretaceous, respectively?

If both suites are linked to the Galápagos plume this implies that (1) the activity of the Galápagos plume began at least in Early Cretaceous times (or even before); (2) its isotopic composition has changed markedly with time from low to high $^{206}Pb/^{204}Pb$ values; (3) it was

heterogeneous and different parts were tapped in different places; and (4) its location was possibly close to or on a ridge, similar to that of the Iceland plume; [*Kerr et al.*, 1995]). It has been proposed that many of the Pacific plateaus (i.e., Shatsky, Ontong Java, Manihiki) may have been formed above long-lived, near-mid-ocean ridge or ridge-centered Cretaceous hotspots (140-65 Ma) [*Mahoney*, 1987]. Moreover, the Pb isotopic composition of the hotspot may change with time, i.e., the source of the Ontong Java plateau lavas shows an evolution with time from lower to higher $^{206}Pb/^{204}Pb$ ratio [*Mahoney et al.*, 1993].

The Ecuadorian and Mexican igneous terranes (1) could reflect an early stage of the Galápagos hotspot activity which would have lasted from 123 Ma to 86 Ma, or (2) could have formed from a possible precursor which would have been only active during a short time at the early Cretaceous or alternatively could have formed somewhere other than at the Galápagos hotspot.

Some plate tectonic constraints are important in this discussion. For example, the development of a magmatic arc through Ecuador and Colombia during the Jurassic suggests that the Farallón plate was subducting southeastward under the northwestern margin of South America [*Aspden et al.*, 1987; *Jaillard et al.*, 1995]. However, during the latest Jurassic (≈ 140-135 Ma) the activity of the continental magmatic arc stopped in Ecuador and Colombia and a new magmatic arc developed along the Peruvian margin [*Aspden et al.*, 1987; *Jaillard et al.*, 1995]. This feature suggests that the subducting motion of the Farallón Plate beneath South America drastically changed toward a NNE motion during the latest Jurassic, and this motion persisted until Late Cretaceous times (≈ 80 Ma) [*Jaillard et al.*, 1995]. If the Ecuadorian Early Cretaceous oceanic or older plateau fragments had been derived from the Galápagos hotspot, they should be presently located far NNE from the present-day Galápagos Islands. Therefore they are more probably linked to an another hotspot, which was located much farther southwest of the South American plate than the Galápagos. In contrast, the Early Cretaceous accreted oceanic plateau fragments from western Mexico could have formed at the Galápagos hotspot.

The Late Cretaceous (92-86 Ma) crustal oceanic fragments exposed presently in Costa Rica (Nicoya Peninsula), in the Caribbean region (Dominican Republic, Curaçao, Aruba), and in the Western Cordillera of Colombia are characterized by a rather large range of ε_{Nd} ratios (+9 to +6) and a limited range of lead isotopic compositions that fall within the field of the recent Galápagos Islands. This suggests that the Late Cretaceous (92-86 Ma) oceanic fragments were most probably linked to the igneous activity of the Galápagos plume, whereas the hotspot from which the oldest fragments were derived remains unknown. More data are needed to

geochemically characterize the fragments of the CCOP and to understand its chronological and geodynamic development.

CONCLUSIONS

The oceanic plateau fragments of the CCOP exposed in central Mexico, Dominican Republic, and coastal Ecuador belong to two distinct suites which differ in their age and trace element and isotopic chemistry.

1. The minerals and cumulus-enriched host rocks of the Duarte Complex (Dominican Republic), dated at 86 ± 1.4 Ma, have LREE-enriched patterns; moderate enrichments in large ion lithophile elements (LILE); high Nb, Ta, and Pb contents; homogeneous ε_{Nd} ratios (+8 to +5) and radiogenic Pb isotopic compositions, very similar to the Galápagos HIMU component. They are geochemically similar to the Late Cretaceous mafic and ultramafic rocks (with the exception of the Gorgona komatiites, picrites from SW Colombia [*Kerr et al.*, 1997a]) of the CCOP and likely derived from the Galápagos hotspot.

2. The Early Cretaceous (> 91 Ma) diabases and basalts (Piñón Formation) and cumulate gabbros (123 Ma) from western Ecuador differ from the Duarte Mg-rich rocks by flat REE patterns and lower Pb, Zr, Hf, Th, and U contents. The Lower Cretaceous basalts and diabases from Mexico (Arperos Formation) exhibit intermediate trace element compositions between the Duarte and Piñón rocks. Both Ecuadorian and Mexican rocks have also a wider range of ε_{Nd} and Pb isotopic ratios that range between those of NMORB or depleted plume and HIMU sources. Geochemical constraints alone are not really conclusive because there is ample evidence for geochemical variability of magmas originating from a single plume but derived from variable melting degrees of heterogeneous sources [*Arndt et al.*, 1996; *Kerr et al.*, 1996a]. These geochemical features of the Ecuadorian and Mexican mafic rocks suggest that they derived from a ridge-centered, or near ridge hotspot.

The Caribbean-Colombian plateau was likely formed during two major pulses of Late Cretaceous and Early Cretaceous, respectively. The Late Cretaceous pulse is likely linked to the Galápagos hotspot whereas that of Early Cretaceous probably derived from a near-ridge hotspot, located farther SW of South America, somewhere in the SE Pacific.

Acknowledgments. We would like to thank R. J. Arculus for his very helpful comments on the manuscript, P. Brunet (UMR 5563) who did all the Sr-Nd TIMS analyses, and J. Cotten (UMR 6538) for ICP-AES analyses. This work was funded by the CNRS teams UPRES-A 5025, UMR 6526, UMR 6538, UMR 5567, UMR 5563 and has benefited from MENESR-DSPT3, FNRS 21-31216.91 grants to R. C. Maury and J. Hernandez, respectively.

Chapitre 3

Ce chapitre est consacré aux études pétrograhiques et géochimiques de roches plutoniques et volcaniques en provenance de la Cordillère Occidentale. Ces roches présentent des affinités de plateau océaniques et appartiennent au plateau océanique Crétacé Inférieur (papier soumis à Journal of Petrology). Les roches volcaniques et plutoniques sont présentes le long de deux coupes. Des basaltes en coussin et des coulées massives intrudés par des intrusions gabbroïques forment la coupe de Merced-Multitud. La coupe de San Juan comportent des roches cumulatives basiques et ultrabasiques intrudées par des dykes basiques.

Les données des éléments majeurs, traces et terres rares et isotopiques sur roches totales et minéraux séparés nous ont permis de caractériser les affinités magmatiques des différents faciès des deux coupes. Des datations Sm/Nd ont été effectuées sur les dolérites de la coupe de Merced-Multitud, mais sans succès. Les roches cumulatives de la coupe de San Juan montrent des anomalies négatives en Ta et Nb. Ainsi, elles pourraient appartenir à une séquence d'arc insulaire. Dans le but de prouver qu'elles appartiennent bien à un contexte de plateau océanique, nous avons sélectionner différents critères qui permettent de discriminer les intrusions appartenant à un plateau océanique de celles d'autres contexte géodynamiques.

Chapter 3

THE EARLY CRETACEOUS SAN JUAN PLUTONIC SUITE, ECUADOR: A MAGMA CHAMBER IN AN OCEANIC PLATEAU

Marc Mamberti, Henriette Lapierre, Delphine Bosch, Etienne Jaillard, Jean Hernandez and Mireille Polvé.

Submitted to Journal of Petrology

CHAPTER 3: THE EARLY CRETACEOUS SAN JUAN PLUTONIC SUITE, ECUADOR: A MAGMA CHAMBER IN AN OCEANIC PLATEAU

This chapter is devoted to the petrology and geochemistry of the volcanic and plutonic rocks from the Western Cordillera which belong to the Early Cretaceous oceanic plateau (paper sumitted to Journal of Petrology). The volcanic and plutonic rocks are exposed along two sections. The Merced-Multitud section consists of pillowed and massive basaltic flows, dolerites and shallow level gabbroic intrusions. The San Juan section consists of cumulate mafic and ultramafic cumulates intruded by mafic dykes.

Major, trace element and isotopic data on whole rock and mineral separates are used to characterize the magmatic affinities and the mantle sources of the San Juan and Merced-Multitud rocks. Sm/Nd dating has been attempted on the dolerites of the Merced-Multitud section, but without success.

The San Juan cumulate rocks show negative Nb and Ta anomalies. Thus, they could represent arc-plutonic rocks. In order to proove that they did really belong to an oceanic plateau, we selected criteria that discriminate intrusions of oceanic plateaus from those of other tectonic settings and used them to evaluate the San Juan sequence.

THE EARLY CRETACEOUS SAN JUAN PLUTONIC SUITE, ECUADOR: A MAGMA CHAMBER IN AN OCEANIC PLATEAU

ABSTRACT: Two sections through an oceanic plateau are preserved in tectonic slices in the Western Cordillera of Ecuador (South America). The Merced-Multitud section is composed mainly of volcanic rocks while the San Juan section is a sequence of mafic-ultramafic cumulates. To establish that the plutonic rocks belonged to an oceanic plateau, we developed criteria that discriminate intrusions of oceanic plateaus from those of other tectonic settings. The mineralogy and crystallization sequence of the cumulates are similar to those of intra-plate magmas. Clinopyroxene predominates throughout and orthopyroxene is only a minor component. Rocks of intermediate composition are absent and hornblende is restricted to the uppermost massive gabbros. The peridotite is very depleted in LREE whereas the gabbros have flat or slightly enriched LREE patterns. The composition of the basaltic liquid in equilibrium with the peridotite, calculated using olivine compositions and REE contents of clinopyroxene, contains between 16 and 8 % MgO and has a flat REE pattern. This melt is geochemically similar to the Merced-Multitud rocks. The rocks have a narrow range of ε_{Nd} (+8 to +5) and Pb isotopic ratios that fall in the field of oceanic plateau basalts. These data suggest that the two sequences represent the plutonic and volcanic components of an Early Cretaceous oceanic plateau which accreted in the Late Cretaceous to the Ecuadorian margin.

KEY WORDS: Ecuador; cumulate and isotropic textures; oceanic plateau; mantle source; plutonic rocks.

INTRODUCTION

Despite the enormous size of oceanic plateaus, very little is known about their overall structure and composition, especially about their deep crustal levels. Most major plateaus (Ontong Java, Nauru, Manihiki) are located in deep waters within the Pacific ocean and their deeper parts are inaccessible. Deep-sea drilling has penetrated only their uppermost volcanic levels, which represent a minute fraction (< 0.5%) of their total volume (Saunders et al., 1996; Storey et al., 1991; Mahoney et al., 1993; Coffin & Heldhom, 1993).

The best way to study the internal structure and composition of an oceanic plateau is to analyze the fragments of plateaus exposed through accretion and/or obduction onto upper plate margins. The best known examples are the 2 to 3 km-thick slices of volcanic rocks obducted on the Solomon islands, which are thought to have formed part of the Ontong Java plateau (Neal et al., 1997; Parkinson et al., in press), and the fragments of the Caribbean oceanic plateau accreted along the Pacific coast of Central and South America and the Greater Antilles (Kerr et al., 1994, 1996, 1997, 1998; Sinton et al., 1997, 1998; Reynaud et al., 1999; Hauff et al., 2000; Lapierre et al., 1997, 2000). Most of these fragments which consist of basalts and dolerites intruded by shallow level gabbros, probably represent the uppermost levels of an oceanic plateau. Among the very few examples that are thought to come from the interior of oceanic plateaus are the ultramafic and mafic cumulates associated with komatiites and picrites of the Colombian oceanic plateau (Kerr et al., 1997; Spadea et al., 1987; Révillon et al., 2000), and gabbros and peridotites of the Solomon islands (Parkinson et al., in press).

On the basis of different crustal sections, Kerr et al. (1997, 1998) developed a description of the internal structure of the 90 Ma Caribbean plateau. In their model, large layered intrusive bodies are located just above or below the Moho. Those within the crust are plagioclase-rich cumulates, while the deeper levels are composed of peridotites, pyroxenites and olivine gabbros. To test this model, we require more detailed information on the petrological and geochemical characteristics of intrusions that may represent relict magma chambers. In some of the examples listed above there is little doubt that the intrusions are comagmatic with oceanic plateau basalts. This is the case for the intrusions of Gorgona Island, which have highly unusual chemical compositions that link them definitively to the ultramafic lavas. However, in cases in which segments of a plateau are accreted to a continent where they are intruded by calc-alkaline magmas, it becomes difficult to establish whether an intrusion is related to oceanic or subduction-related magmatism.

In this paper, we present the petrological and geochemical characteristics of two suites of rocks from the Western Cordillera of Ecuador. The first suite is composed of pillow basalts, dolerites and shallow level gabbroic intrusions while the second suite consists of cumulate ultramafic to mafic intrusive rocks. Because the geodynamic environment of the cumulate rocks is difficult to establish solely on the basis of their geochemistry, we have developed a set of criteria that help to discriminate cumulate rocks belonging to an oceanic plateau from those developed in an intra-oceanic island arc setting. Before using these criteria, we test them against the features of plutonic complexes for which the tectonic environment is well constrained. We then use them to evaluate the geodynamic setting of the Ecuadorian ultramafic-mafic rocks and show that they did indeed form part of an oceanic plateau. Finally, we will propose a petrogenetic model for the intrusive suites and use this model to develop a better description of the internal structure and evolution of an oceanic plateau.

GEOLOGICAL SETTING

Ecuador comprises three main morphological domains (Fig. 3.1). The first, the "Oriente" Basin, represents the present-day foreland basin of the Andean orogeny. The second, the Ecuadorian Andes, comprises two cordillera, crosscut and overlain by the products of Tertiary-Recent magmatic arcs (Aspden and Litherland, 1992; Lavenu et al., 1992). The Eastern Cordillera consists of deformed Paleozoic to Mesozoic metamorphic rocks (Litherland et al., 1994); the Western Cordillera of oceanic terranes that accreted to the Andean margin in the Late Santonian to Eocene (Jaillard et al., 1997; Cosma et al., 1998; Hughes and Pilatasig, in press). The third domain, the Coastal Zone, consists of basalts and dolerites of oceanic plateau affinity, overlain by Late Cretaceous island arc rocks (Goossens and Rose, 1973; Lebrat et al., 1987; Jaillard et al., 1995; Reynaud et al., 1999).

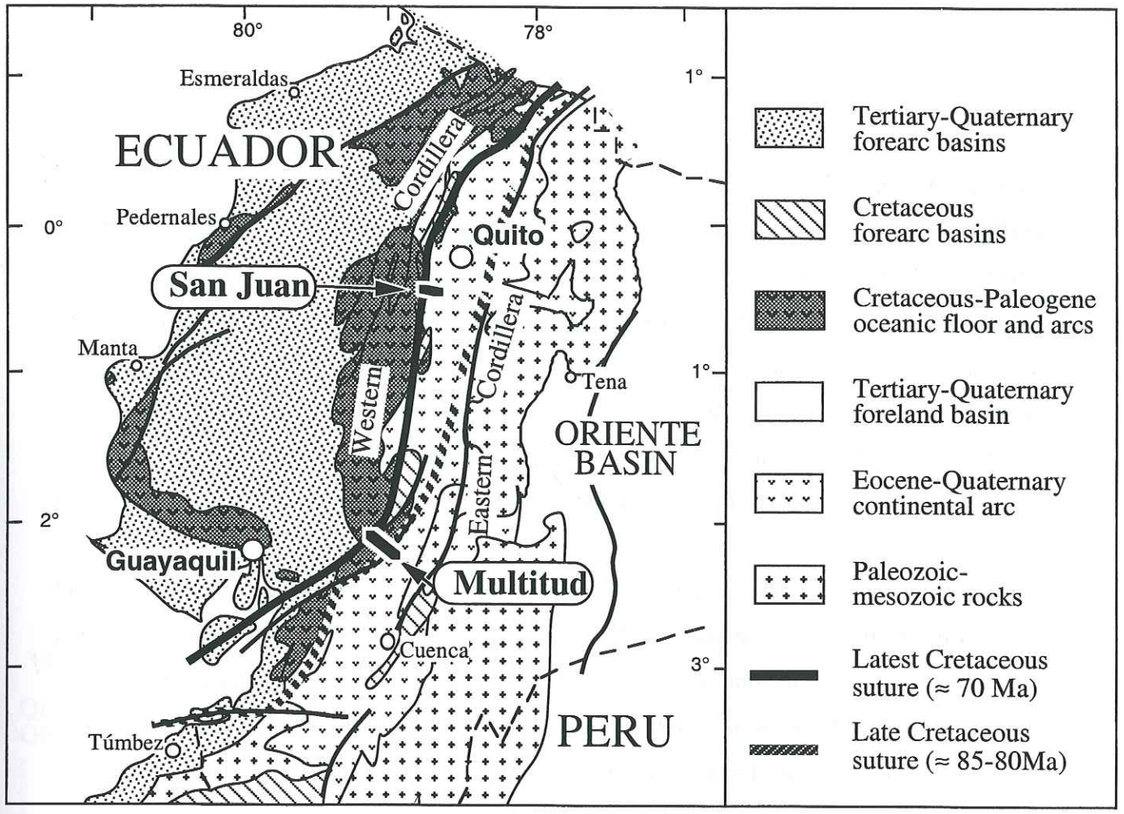

Fig. 3.1. Schematic geological map of Ecuador showing the main geological and tectonic units.

Two lithological associations have been recognized in the accreted oceanic terranes. Type 1 is composed of massive and pillowed mafic flows, tuffs and greywackes intruded by shallow level gabbros and dolerites. This type is widely exposed on the coast (Piñón Formation, Reynaud et al., 1999; Fig. 3.1) and in the Western Cordillera, where it is called the Pallatanga unit (Dunkley and Gaibor, 1998; Hughes and Pilatasig, in press). A section through the Pallatanga unit at Merced-Multitud, one of the localities described in this paper, is situated in the Western Cordillera (Fig. 3.1). The lower part of the section consists of alternating pillowed and massive basaltic flows; the upper part of doleritic and gabbroic intrusions. Locally, the volcanic flows are interbedded with fine-grained tuffs and greywackes (Fig. 3.2a).

The second lithological association (Type 2) consists of cumulate peridotites and gabbros intruded by mafic dykes. This type is well exposed along the 2000-m-thick San Juan section, one of several tectonic slices pinched in a Late Cretaceous suture near the crest of the Western Cordillera. The section has been interpreted by Juteau et al. (1977) as a remnant of an oceanic crust, and by Desmet (1994) and Lapierre et al. (2000) as part of an oceanic plateau.

The San Juan section represents a complete cumulate suite with massive dunites at the base, grading upwards through layered wehrlites and gabbros into isotropic amphibole-gabbros (Fig. 3.2b).

The two lithologic sequences are pre-Late Cretaceous in age. South of Multitud, the Pallatanga unit (Type 1) is associated with Early Cretaceous ammonites (Pratt et al., 1998). In the coastal zone, the Piñón Formation is regarded as pre-Late Cretaceous, since it forms the basement of undated volcanic arc rocks, which in turn are stratigraphically overlain by pelagic sediments containing early Late Cretaceous faunas (Jaillard et al., 1995). An amphibole-bearing gabbro from the San Juan section (Type 2) has been dated by Lapierre et al. (2000) who obtained an internal Sm-Nd isochron age of 123 ± 13 Ma. This Early Cretaceous age is unknown in the Caribbean-Colombian oceanic plateau where the main volcanic pulse occurred during the late Cretaceous (90-86 Ma).

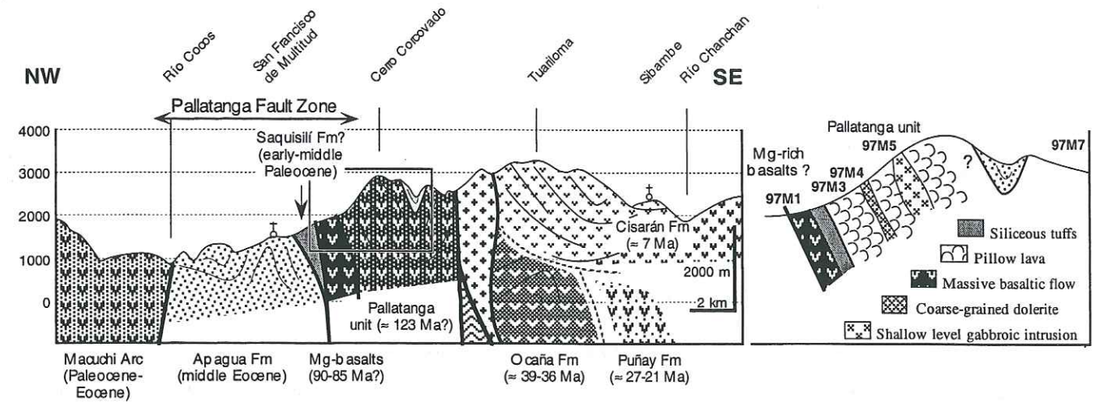

Fig. 3.2a: Schematic cross section of the Merced-Multitud sequence showing the different components of the uppermost levels of the Early Cretaceous Ecuadorian oceanic plateau.

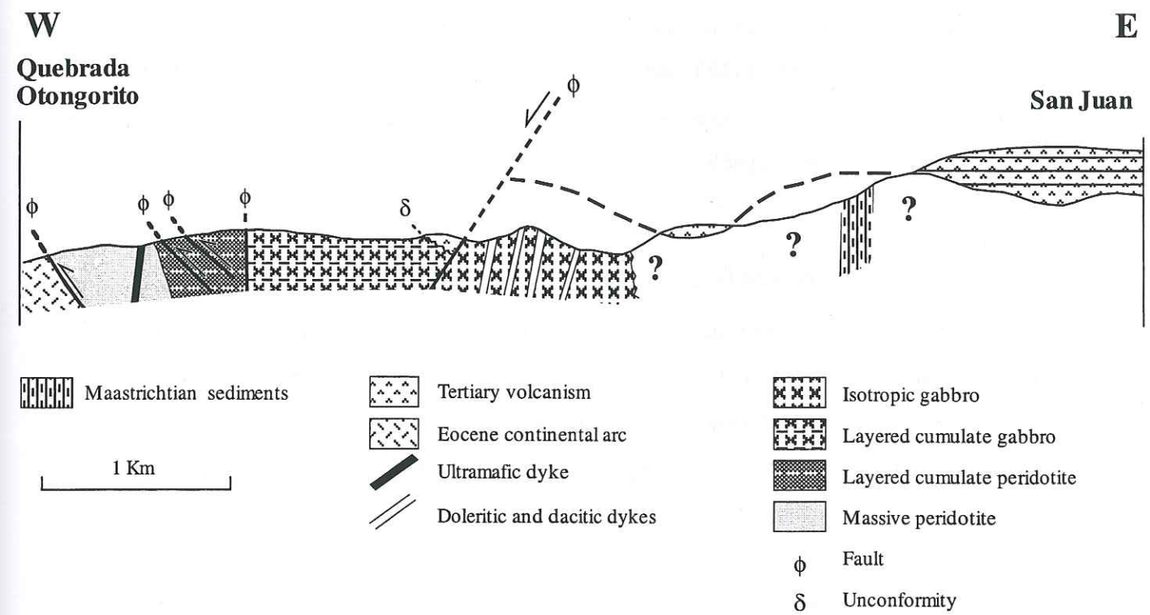

Fig. 3.2b: Schematic cross section of the San Juan plutonic sequence showing the different components of the deep levels of the Early Cretaceous Ecuadorian oceanic plateau.

PETROLOGY AND MINERAL CHEMISTRY OF THE MERCED-MULTITUD AND SAN JUAN SECTIONS

Merced-Multitud section (Type 1)

The Merced-Multitud section (Type 1, Fig. 3.2a) comprises massive and pillowed basalts intruded by isotropic gabbro and dolerite. The isotropic gabbro (97M5) has an ophitic texture with 1-2 cm long, frond-like pyroxenes and <1 cm sized plagioclase laths, embedded in an abundant matrix of late crystallizing acicular Ti-rich magnetite and micropegmatitic quartz. The dolerite (97M4) differs from the gabbro only in its finer grain size and more abundant micropegmatitic quartz. In both rocks, plagioclase is totally replaced by albite (An < 5). Pyroxene remains fresh in the gabbro and has a Fe-rich augitic composition (Wo_{36}, En_{39}, Fs_{25}), with the exception of a few crystals of Ca-rich diopside (Wo_{45}, En_{37}, Fs_{17}).

The basalts (97M1, 97M3, 97M7) are composed of plagioclase, clinopyroxene and olivine phenocrysts set in a smectite-rich groundmass. Clinopyroxene and olivine are replaced by actinolite and calcite, respectively.

San Juan section (Type 2)

Four units are recognised in the San Juan section (Type 2), each bounded by NE-trending normal or reverse faults (Fig. 3.2b). From top to base the units are:

(1) fine- to coarse-grained, isotropic, amphibole-bearing gabbros (97SJ13) intruded by pegmatitic gabbros, and swarms of basaltic, doleritic and felsic dykes. Locally, plagioclase in the gabbros exhibits an igneous lineation. An upper faulted contact separates gabbros from overlying recent felsic tuffs.

(2) layered cumulate olivine gabbros (97SJ1, 97SJ3) and two-pyroxene gabbros (97SJ4, 97SJ9) intruded by rare, thin basaltic dykes.

(3) layered cumulate fine-grained peridotites (97SJ6, 97SJ8, 97SJ10, 98SJ4) with locally abundant clinopyroxene or interstitial plagioclase. Clinopyroxene-rich rocks are coarse grained.

(4) massive partially serpentinized peridotites (98SJ2) crosscut by gabbroic and ultramafic dykes (98SJ3), locally affected by shear zones.

Four rock types have been distinguished on the basis of textures, mineralogy and modal compositions. Listed in order of decreasing abundance they are: (1) cumulate peridotites, (2) layered olivine-clinopyroxene gabbros, (3) isotropic amphibole gabbros, (4) dykes. The petrographic characteristics of the plutonic rocks are summarised in Table 3.1.

All the rocks are hydrothermally altered. Although olivine cores are preserved in some peridotites and gabbros, most grains are intensely fractured and almost completely serpentinized. Orthopyroxene is commonly replaced by chlorite and/or smectite. In contrast, clinopyroxene is preserved in most samples, except in some peridotites and gabbros in which it is replaced by actinolite. Plagioclase is fresh in the gabbros but is variably altered in peridotites and dolerites. In peridotites, it is replaced by a microcrystalline association of hydrogarnet and epidote. Fe-Ti oxides are preserved in gabbros.

Peridotite

The peridotites are massive or layered. The dunites (98SJ2) are unlayered and consist of very fine grained serpentinized olivine, euhedral chromite grains (0.50 < Cr# = Cr/Cr+Al < 0.57), with interstitial diopside (En_{48}, Fs_5, Wo_{47}) (Morimoto, 1998). When preserved, cumulus olivine is forsteritic (Fo_{89-91}). Wehrlites (98SJ4, 97SJ8, 97SJ10) are layered with mineral banding formed of olivine and clinopyroxene and local interstitial, late-crystallising plagioclase. Their texture is mesocumulate with cumulus olivine and clinopyroxene as the intercumulus phase. Olivine composition is very constant (Fo_{84}) with no chemical variations between core and rim. The pyroxene is diopside (Wo_{45-48}, En_{44-47}, F_{5-7}) with a very uniform composition. When preserved, plagioclase is always bytownite (An_{87-88}), regardless the type of associated mineral (olivine or clinopyroxene). Variations in the wehrlite are expressed by the abundance of the plagioclase and the presence of diopside exsolutions within the diopside. The wehrlites contain isolated layers predominantly of plagioclase with some cumulus olivine (97SJ6).

Layered gabbro

The layered gabbros contain two pyroxenes with or without olivine. The olivine gabbros (97SJ2, 97SJ3) are adcumulates with olivine, plagioclase and clinopyroxene as cumulus phases and orthopyroxene and plagioclase as the intercumulus phase. Olivine included in the pyroxenes is forsteritic and less Mg-rich (Fo_{75}) than that of the wehrlites. Among the cumulus crystals, plagioclase predominates and displays an adcumulate texture.

Sample	97SJ1	97SJ3	97SJ4	97SJ6	97SJ8
Texture Mineralogy	Meso- to heteradcumulate Plagioclase cumulus (70%) Olivine cumulus (2%) Cpx (20%) Intercumulus Opx pseudomorphs (10%)	Meso to heteradcumulate Plagioclase cumulus (70%) Olivine cumulus (2%) Cpx (20%) Intercumulus Opx pseudomorphs (10%)	Mesocumulate Plagioclases in cumulus(65%) Preserved Cpx and Opx (30%) in cumulus Late and early crystallizing Ti- and V-rich magnetite (5%)	Layered heteradcumulate Mineral banding Olivine (50%) Cpx (40%) Plagioclases intercumulus (10%)	Layered heteradcumulate Olivine (60%) Cpx (30%) Plagioclases intercumulus (5%) Oxide (<1%)
name	Olivine Gabbro	Olivine Gabbro	Two pyroxene gabbro	Plagioclase-rich wehrlite	Wehrlite

Sample	97SJ9	97SJ10	97SJ11	97SJ12	97SJ13
Texture Mineralogy	Meso- to heteradcumulate Plagioclase cumulus (60%) Cpx cumulus (30%) Intercumulus Opx pseudomorphs (10%)	Layered heteradcumulate Olivine (70%) Cpx (20%) Plagioclases intercumulus (5%) Oxide (<1%)	Ophitic Plagioclases Cpx replaced by chlorite Interstitial quartz Ti magnetite	Intersertal-ophitic Plagioclase phenocrists Quartz phenocrists Epidote Ti magnetite	Granular Plagioclase (50%) Amphibole with pyroxene core (50%)
Name	Two pyroxene gabbro	Wehrlite	Dolerite	Rhyolite	Gabbro

Sample	98SJ2	98SJ4
Texture Mineralogy	Heteradcumulate Olivine (90%) Cpx (5%) Oxide (5%)	Layered heteradcumulate Olivine (65%) Cpx (30%) Plagioclases intercumulus (5%) Oxide
Name	Dunite	Wehrlite

Table 3.1: Petrographic descriptions of the San Juan cumulate rocks.

The olivine-free gabbros (97SJ4 and 97SJ9) show two distinctly different facies. 97SJ9 differs from the olivine gabbros solely by the absence of olivine. 97SJ4 differs significantly from the other gabbros by the crystal sequence and the exceptional preservation of orthopyroxene (clinoenstatite; Wo_{28}, En_{71}, Fs_{1}). In this rock, both pyroxenes crystallized before the plagioclase. Two generations of Fe-Ti oxides are present. The early crystallizing oxides consist of small euhedral crystals included in the pyroxenes while the late ones occur as large interstitial grains.

Regardless the gabbro lithologies, both clinopyroxene (Wo_{45-47}, En_{44-45}, Fs_{8-9}) and plagioclase (An_{84-88}) have uniform and constant compositions that do not differ from those in the wehrlites.

Amphibole bearing gabbro (97SJ13)

These unlayered rocks are coarser grained than the cumulate gabbros and contain more sodic plagioclase composition (An_{52-44}). This mineral forms large (< 1 cm) crystals bounded by brown pleochroic Mg-rich amphibole. Inclusions of clinopyroxene and smaller plagioclase crystals are common. The amphibole is Mg-rich hornblende (Leake et al., 1997).

ANALYTICAL METHODS

All the igneous rocks are hydrothermally altered and metamorphosed to greenschist facies, but the plutonic rocks are less altered than the basalts. For this reason, only samples with well-preserved igneous mineralogy (i.e., clinopyroxene, amphibole, and plagioclase) and devoid of significant petrographic alteration were selected for chemical analysis. Minerals were separated then purified by hand picking. Most mineral separates were 99% pure, but actinolite rims around some clinopyroxene crystals could not be completely removed.

For Sr and Nd isotopic analyses, mineral separates and host rock powders were leached in a mixture of 2 N HCl and 0.1 N HF. For Pb isotope determinations, mineral separates and whole rocks were successively leached in hot 2 N HCl for 20 minutes in an ultrasonic bath, rinsed with triple-distilled water for 15 min in an ultrasonic bath.

Major-element analyses were performed by X-ray fluorescence at the Department of Geology of the Australian National University (Canberra) and at the Institut de Minéralogie et Pétrographie de l'Université de Lausanne (Switzerland). After acid dissolution, trace elements were analysed by inductively coupled plasma mass spectrometry (ICP-MS) at the University of Grenoble (France) using a Tm spike following procedures described by Barrat et al. (1996). Standards used for the analyses were JB2, WSE, BIR-1, JR1, and UBN. Major and trace element analyses of the minerals and host rocks are presented in Tables 3.2 and 3.3.

The $^{143}Nd/^{144}Nd$ and $^{87}Sr/^{86}Sr$ isotopic characteristics were determined on a Finnigan MAT261 multicollector mass spectrometer at the Laboratoire de Géochimie de l'Université Paul Sabatier (Toulouse, France; Table 3.4), following the analytical procedures described by Lapierre et al. (1997). The chemical separation of Pb was done following the procedure modified from Manhès et al. (1978). Total Pb blanks are less than 65 pg for a 100 mg sample. Pb isotopic ratios were measured on a VG P54 magnetic sector ICPMS at the Ecole Nationale Supérieure de Lyon (France; Table 3.4).

The complete isotopic data set has been corrected for in-situ decay assuming an age of 123 Ma, based on the age of the (97SJ13) gabbro (Lapierre et al., 2000).

Samples	98SJ2	97SJ6	97SJ8*	97SJ8	97SJ10*	97SJ10	98SJ4	97SJ1	97SJ3	97SJ4	97SJ9	97SJ13	98SJ3	97M5	97M4
Name	Dunite	Wehrlite	Wehrlite	Wehrlite	Wehrlite	Wehrlite	Wehrlite	Gabbro	Gabbro	Gabbro	Gabbro	Gabbro	Ultramafic Dyke	Gabbro	Dolerite
SiO2	40.7	47.01	46.90	-	44.53	-	42.82	48.15	48.13	48.05	48.21	52.38	40.57	51.10	58.76
TiO2	0.03	0.10	0.09	-	0.06	-	0.04	0.06	0.06	0.20	0.06	0.42	0.02	1.83	1.68
Al2O3	1.60	8.39	7.85	-	6.81	-	7.34	23.33	22.80	6.47	22.32	20.40	1.02	12.68	10.83
Fe2O3	10.65	7.40	7.75	-	10.17	-	9.58	3.79	3.80	14.61	3.64	6.10	11.37	15.42	16.54
MnO	0.17	0.14	0.14	-	0.17	-	0.15	0.08	0.08	0.23	0.08	0.11	0.17	0.21	0.29
MgO	45.79	24.22	25.08	-	30.59	-	32.76	8.14	7.97	23.64	8.04	5.77	46.80	4.88	1.16
CaO	1.07	12.39	11.91	-	7.51	-	7.30	16.30	16.06	6.21	16.55	12.08	0.04	8.33	5.54
Na2O	0.00	0.32	0.26	-	0.14	-	0.00	1.06	1.07	0.42	1.07	2.60	0.00	3.21	3.26
K2O	0.01	0.01	0.01	-	0.02	-	0.00	0.01	0.02	0.17	0.01	0.12	0.00	0.30	0.18
P2O5	0.01	0.00	0.00	-	0.00	-	0.01	0.02	0.01	0.00	0.02	0.02	0.01	0.13	0.40
LOI	13.11	3.54	5.43		6.88		8.39	0.92	1.04	0.38	0.86	0.74	3.34	1.91	1.36
Ba	2.85	4.18	-	3.83	-	5.38	3.55	6.57	15.2	33.9	5.57	113.1	5.56	29.5	65.5
Rb	0.14	0.10	0.30	0.29	0.4	0.32	0.13	0.13	0.25	4.07	0.31	1.50	0.10	4.91	2.07
Sr	3.89	29.2	32.3	33.6	21	24.9	13.0	108.9	110.7	42.9	113.7	154.9	2.68	93	51
Ta	nd	nd	nd	nd	0.01	nd	nd	bd	bd	0.02	bd	0.02	nd	0.41	0.86
Th	nd	nd	nd	nd	0.01	nd	nd	bd	bd	0.01	0.40	bd	0.11	nd	0.29
Zr	nd	1.20	nd	1.27	2.10	2.03	nd	0.65	0.79	6.99	1.25	19.6	0.40	76.9	131
Nb	nd	bd	nd	0.03	0.30	0.22	nd	0.02	0.05	0.45	0.40	0.55	nd	5.70	12.92
Y	nd	3.22	3.70	3.71	1.90	1.95	nd	2.20	2.50	5.34	3.16	17.2	0.21	32.4	68.9
Hf	nd	0.05	nd	0.05	0.05	0.07	nd	0.02	0.03	0.22	0.04	0.63	0.01	1.82	3.97
V	-	151.6	435.3	-	82	-	-	67	67	72	105	176.9	-	481	-
Cr	5647	2274	2447	-	1390	-	3447	493.8	489	1828	719	389	6629	-	344
Ni	1843	607	660	-	733	-	1080	139.5	129	680	128	63	2230	53	108
Co	124.1	54.1	-	91.3	21.6	111.7	113.6	37.8	35.9	118.3	34.5	21.8	124.7	48.0	22.3
Pb	0.12	0.08	-	0.15	-	0.49	0.11	0.12	0.29	0.90	0.13	4.40	0.09	0.10	0.24
U	nd	0.01	nd	0.01	0.12	0.13	nd	nd	nd	0.09	nd	0.03	nd	0.06	0.15
La	0.02	0.08	0.10	0.08	0.17	0.13	0.04	0.24	0.22	1.59	0.24	1.42	0.02	4.30	7.68
Ce	0.06	0.29	0.29	0.28	0.36	0.33	0.14	0.60	0.54	3.14	0.63	4.23	0.07	11.90	21.7
Pr	0.01	0.06	-	0.06	-	0.06	0.02	0.08	0.08	0.38	0.10	0.78	0.01	1.86	3.50
Nd	0.06	0.39	0.33	0.38	0.32	0.23	0.15	0.38	0.36	1.48	0.48	4.19	0.04	9.76	18.62
Sm	0.03	0.20	0.13	0.21	0.15	0.12	0.06	0.13	0.12	0.38	0.16	1.49	0.01	3.33	6.24
Eu	0.01	0.10	0.06	0.10	0.06	0.07	0.04	0.13	0.09	0.13	0.10	0.59	0.01	1.17	2.49
Gd	0.06	0.32	0.26	0.34	0.19	0.18	0.10	0.19	0.20	0.51	0.26	1.92	-	4.22	8.58
Tb	0.01	0.07	-	0.07	-	0.04	0.02	0.04	0.04	0.10	0.05	0.37	0.00	0.82	1.59
Dy	0.08	0.50	0.48	0.52	0.31	0.28	0.14	0.31	0.34	0.72	0.44	2.50	0.03	5.45	10.6
Ho	0.02	0.12	0.12	0.12	-	0.07	0.03	0.07	0.08	0.17	0.11	0.57	0.01	1.23	2.33
Er	0.06	0.34	0.36	0.35	0.22	0.19	0.10	0.21	0.25	0.52	0.31	1.60	0.02	3.38	6.63
Tm	-	-	-	-	-	-	-	-	-	-	-	-	-	-	-
Yb	0.07	0.33	0.34	0.34	0.23	0.20	0.10	0.22	0.24	0.57	0.31	1.56	0.03	3.15	6.32
Lu	0.01	0.05	0.05	0.05	0.03	0.03	0.02	0.03	0.04	0.09	0.05	0.23	0.01	0.50	1.00
(La/Yb)n	0.4	0.48	-	0.47	-	0.66	0.44	0.74	0.62	1.88	0.52	0.58	1.21	0.92	0.82
(La/Sm)n	0.17	0.39	-	0.2	-	0.43	0.28	1.16	1.15	2.63	0.94	0.55	0.56	0.81	0.77

Table 3.2: Major (wt%) and trace element (ppm) analyses for the San Juan and Merced-Multitud samples. Nd: not detected, -: not analysed, * samples analysed in ANU (Canberra)

Samples	97SJ10	97SJ3	97SJ13	97SJ13	97M5	97M5
Name	Cpx	Cpx	Plagio	Amph	Cpx	Plag
Localité	San Juan	San Juan	San Juan	San Juan	Multitud	Multitud
SiO2	52.56	51.74	54.55	46.81	49.92	69.1
TiO2	0.15	0.21	-	1.75	0.51	-
Al2O3	2.72	2.79	28.30	7.31	2.63	18.74
Fe2O3	-	-	-	9.92	1.81	-
FeO	4.03	5.67	0.40	6.36	14.55	1.25
MnO	0.02	0.04	-	0.30	0.44	-
MgO	16.99	15.58	-	13.72	12.84	-
CaO	22.33	22.84	10.70	11.12	16.47	0.66
Na2O	0.31	0.34	5.44	1.30	0.21	11.14
K2O	-	-	0.14	0.08	-	0.06
Total	99.10	99.20	99.53	100.59	99.38	100.95
Ba	0.91	5.73	86	29.54	4.01	35.37
Rb	0.11	0.10	1.43	0.49	0.08	5.89
Sr	4.21	9.67	223	17.60	9.42	108
Ta	bd	0.01	0.03	0.07	0.33	0.10
Th	0.21	0.03	0.05	0.08	0.07	0.10
Zr	2.22	4.71	1.23	37	43.46	60.95
Nb	0.04	0.10	0.05	1.47	4.71	0.82
Y	3.91	8.76	0.88	71	59.29	5.40
Hf	0.10	0.20	0.04	1.85	1.94	1.54
Co	87	51.64	5.87	70	81.19	3.14
U	0.01	0.02	0.02	0.03	0.06	0.19
La	0.18	0.26	1.44	2.44	2.51	0.89
Ce	0.50	1.16	2.41	11.48	10.33	2.04
Pr	0.11	0.25	0.28	2.70	2.06	0.29
Nd	0.60	1.43	0.92	16.22	11.67	1.37
Sm	0.29	0.58	0.17	6.35	4.91	0.42
Eu	0.15	0.22	0.43	1.38	0.91	0.68
Gd	0.41	0.87	0.23	7.97	6.74	0.57
Tb	0.09	0.18	0.03	1.63	1.38	0.11
Dy	0.66	1.31	0.14	11.24	9.41	0.77
Ho	0.15	0.31	0.03	2.59	2.10	0.19
Er	0.45	0.93	0.08	7.33	6.09	0.57
Tm	-	-	-	-	-	-
Yb	0.44	0.95	0.08	7.14	6.12	0.58
Lu	0.07	0.14	0.01	1.08	0.97	0.09

Table 3.3: Major (wt%) and trace element (ppm) analyses for the San Juan and Merced-Multitud mineral separates.

RESULTS

Merced-Multitud sequence (Type 1)

Chemical data for the basalts (samples 82119, 82126, 82106) are available in Lebrat et al. (1987) and only the isotropic gabbro and one of the dolerites were analysed in our study (Table 3.2).

As can be seen from Table 3.3, the basalts have slightly higher MgO contents (~ 8.5 %) but lower TiO_2 and Fe_2O_3 than the dolerite and gabbro. All samples have similar flat rare-earth element (REE) patterns (Fig. 3.3), but the basalts are distinguished from the dolerite and gabbro by lower REE contents and negative Eu anomalies. All samples of mafic rocks have higher-than-chondritic ratios of Nb or Ta to La (Fig. 3.3). The isotropic gabbro and its mineral separates (clinopyroxene and plagioclase) have very similar ε_{Nd} ratios (~+7) which fall in the range of ocean-island or oceanic-plateau basalts.

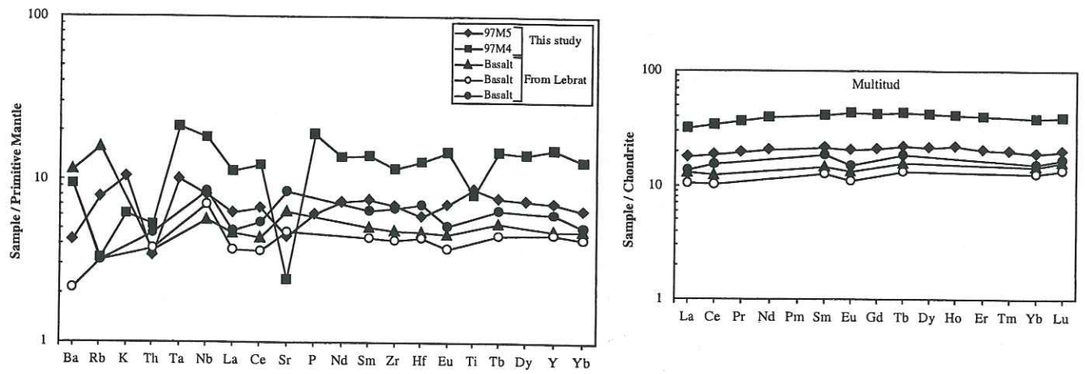

Fig. 3.3: Chondrite- and primitive mantle-normalized (Sun & McDonough, 1989) rare earth element patterns and multi-element diagrams for basalts, dolerite and isotropic gabbro of the Merced-Multitud sequences. Samples 82119, 82126 and 82106 are basalts from Lebrat et al. (1987).

San Juan sequence (Type 2)

Mobility of major and trace elements

Before interpreting of the chemistry of the San Juan igneous rocks in terms of magmatic processes, we have to assess the possible chemical effects of element mobility during hydrothermal alteration and metamorphism. The rocks have low to moderate values of loss-on-ignition (0.4 to 5.4%), with the exception of the dunite and two wehrlites in which most of the olivine is serpentinized (LOI = 8.4 to13.1%; Table 3.3).

Light rare-earth elements (LREE) such as cerium are regarded as being relatively immobile during alteration of rocks of mafic to ultramafic compositions in the absence of Ca-rich fluids (Humphris, 1984). In Fig. 3.4, Ce is plotted against Ba, Sr, and Rb, elements that are considered to be very mobile during alteration and low grade metamorphism. Ba shows positive correlation, suggesting that Ba is relatively immobile. Sr correlates with Ce in the peridotites but remains constant as Ce increases in the gabbros. These trends reflect the crystallisation of clinopyroxene followed by the accumulation of plagioclase. Rb does not correlate with Ce, suggesting that this element was mobile during the alteration that affected the San Juan cumulate rocks.

Magmatic aspects

Major and trace element analyses of the cumulate rocks are reported in Table 3.3 and plotted in Figs. 3.4 to 3.8.

Plots of Al_2O_3, CaO, SiO_2, and FeO versus MgO (Fig. 3.5) show that: (1) the San Juan ultramafic rocks were derived from the accumulation of olivine followed by clinopyroxene and plagioclase, (2) the gabbros are formed by the accumulation of plagioclase followed by the crystallisation of clinopyroxene. The gabbros 97SJ4 and 97SJ13 do not follow the general trend. The two-pyroxene gabbro 97SJ4 is distinguished from the other gabbros by evidence of cumulus orthopyroxene as indicated by higher SiO_2 and MgO, and lower CaO contents. The hornblende-gabbro 97SJ13 has much higher TiO_2, SiO_2, and lower MgO and represents a differentiated gabbroic melt (Fig. 3.6).

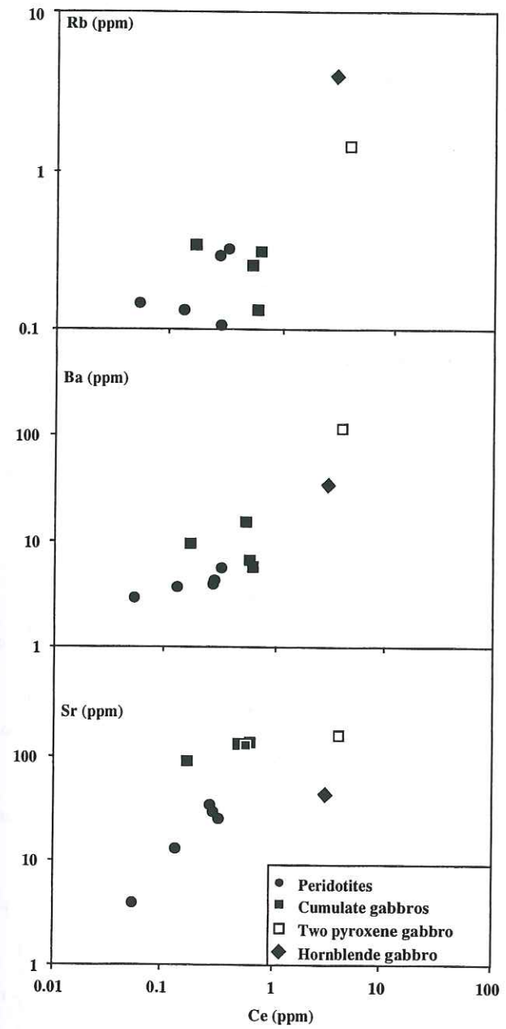

Fig. 3.4: Rb (ppm), Ba (ppm) and Sr (ppm) vs Ce (ppm) correlation diagrams of the San Juan peridotites and gabbros.

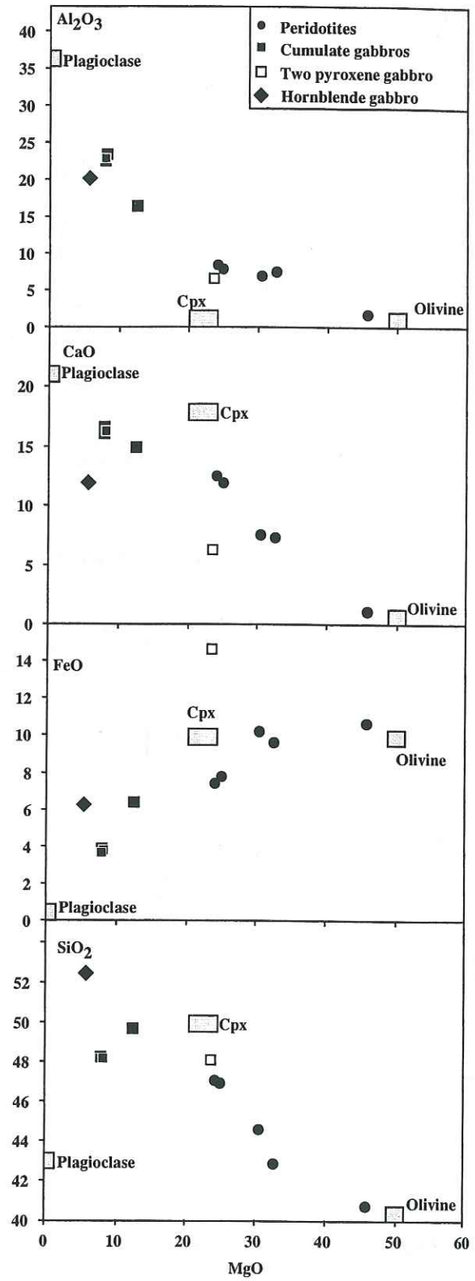

Fig. 3.5: Al2O3 (wt%), CaO (wt%), SiO2 (wt%) and FeO (wt%) vs MgO (wt%) correlation diagrams of the San Juan peridotites and gabbros.

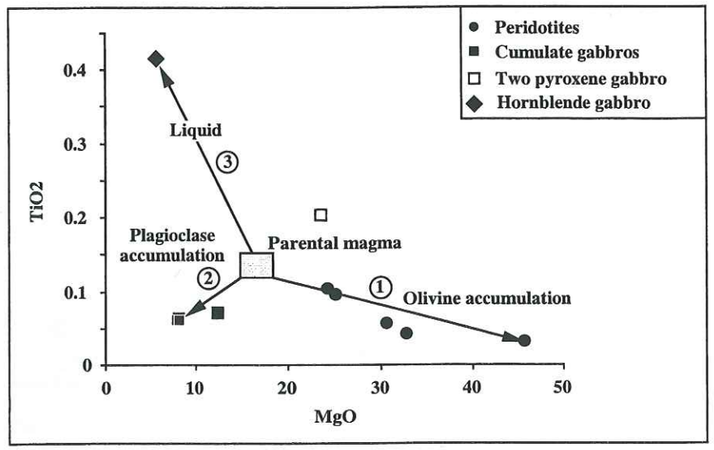

Fig. 3.6: TiO2 (wt%) vs MgO (wt%) correlation diagram of the San Juan peridotites and gabbros.

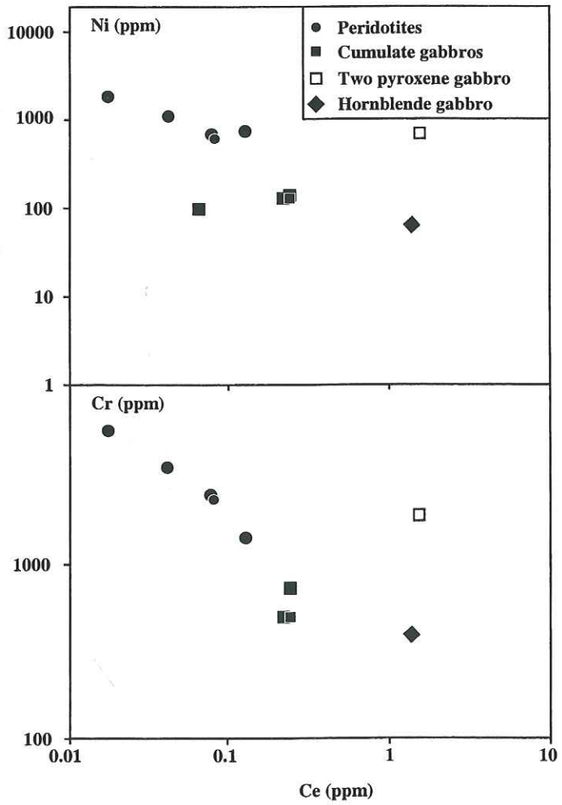

Fig. 3.7: Cr (ppm) and Ni (ppm) vs Ce (ppm) correlation diagrams of the San Juan peridotites and gabbros. Diamond represents an evolved gabbroic liquid derived from the parental magma after removal of olivine and plagioclase.

Trace-element abundances in the mineral fractions and host peridotites and gabbros are presented in Fig. 3.8. All the peridotites are markedly depleted in light relative to heavy REE, with the exception of 97SJ10 which shows a slight enrichment in La and Ce relative to Nd. Compared to its wehrlitic host rock, the clinopyroxene 97SJ10 has higher REE contents (near chondritic values) and is less depleted in LREE. 97SJ10 and 98SJ4 are distinguished from the other peridotites by their marked positive Eu anomalies.

Trace-element contents in peridotites are very low. Most of the wehrlites and the clinopyroxene from sample 97SJ10 exhibit marked depletion in Nb, Ta, Zr and Hf relative to the REE. The exception is the 97SJ10 whole-rock sample, which has near-chondritic ratios of the two sets of elements.

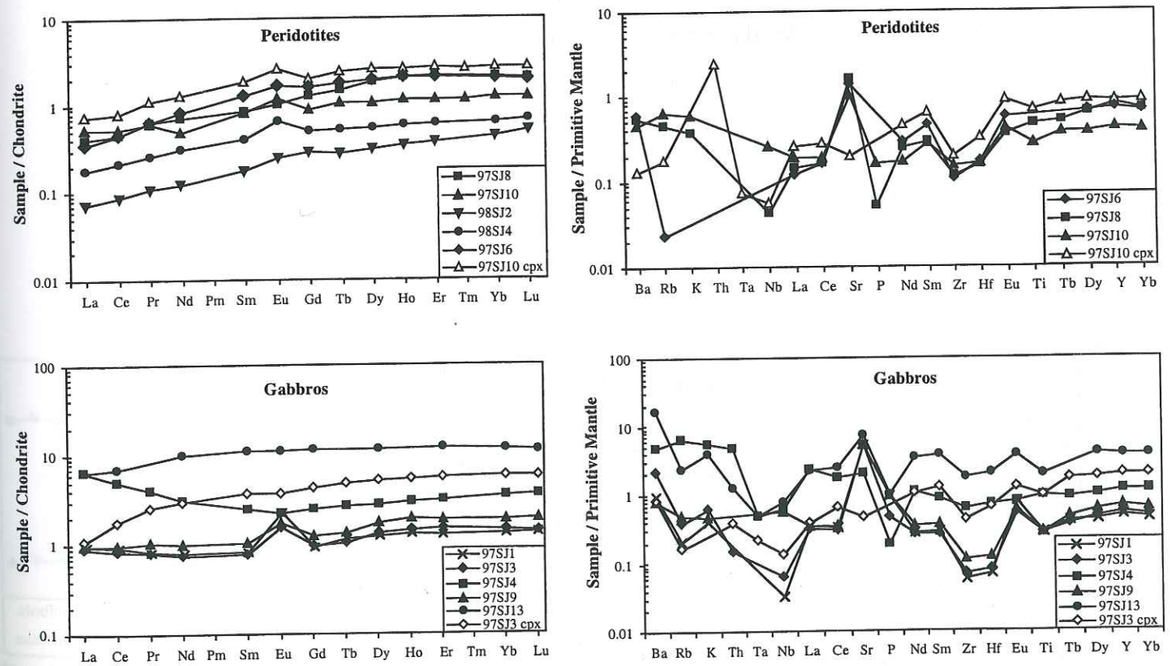

Fig. 3.8: Chondrite- and primitive mantle-normalized (Sun & McDonough, 1989) rare earth element patterns and multi-element plots for peridotites, gabbros and mineral separates of the San Juan sequence.

Three gabbros (97SJ1, 97SJ3 and 97SJ9) have flat REE patterns and marked Eu positive anomalies. Compared to its host rock, the clinopyroxene from 97SJ3 is depleted in LREE. 97SJ4 and 97SJ13 are LREE-enriched and LREE-depleted, respectively. The REE pattern of the 97SJ13 hornblende differs from its host rock by higher REE contents, a marked LREE-depletion and a negative Eu anomaly (Fig. 3.9). In contrast, the 97SJ13 plagioclase is strongly enriched in LREE and has a large positive Eu anomaly.

The gabbros also show relative depletion of Ta, Nb, Zr Hf and Ti, and coupled with enrichment of Ba and Sr. The exception is sample 97SJ4, which does not have these anomalies. The hornblende gabbro 97SJ13 and its amphibole and plagioclase separates have the highest trace element abundances (Fig. 3.9). Plagioclase from 97SJ13 exhibits negative Nb, Zr and Hf anomalies and is enriched in Sr and Eu. Amphibole from the same sample is enriched in Nb and Ta and depleted in Sr. The whole-rock sample 97SJ4 shows a positive Ti anomaly and a less marked depletion in Zr and Hf. The high Ti and Fe contents (Table 3.3) of this rock is expressed by the presence of abundant Ti-rich magnetites.

The ultramafic dyke (98SJ3), which cuts across the massive peridotites, has a major-element composition similar to the 98SJ2 dunite (Table 3.3; Fig. 3.10), but its REE pattern is flat, in contrast to the depleted pattern of the peridotites.

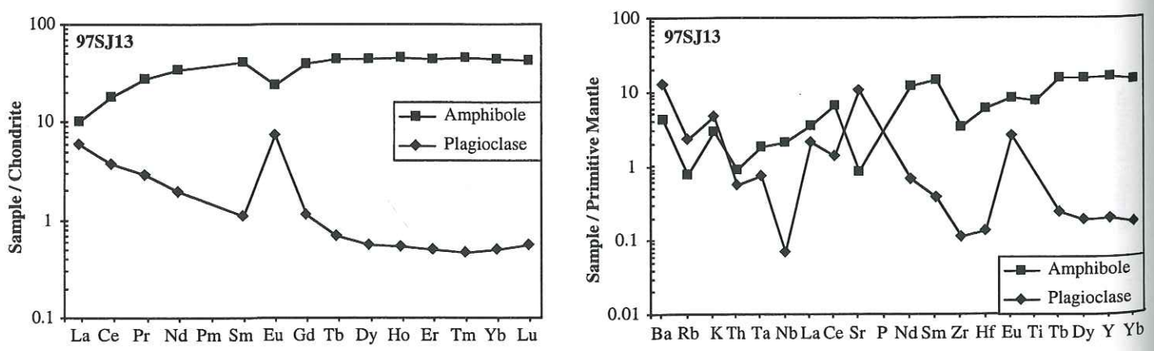

Fig. 3.9: Chondrite- and primitive mantle-normalized (Sun & McDonough, 1989) rare earth element patterns and multi-element diagrams for amphibole and plagioclase of the 97SJ13 isotropic gabbro.

050 036624 3

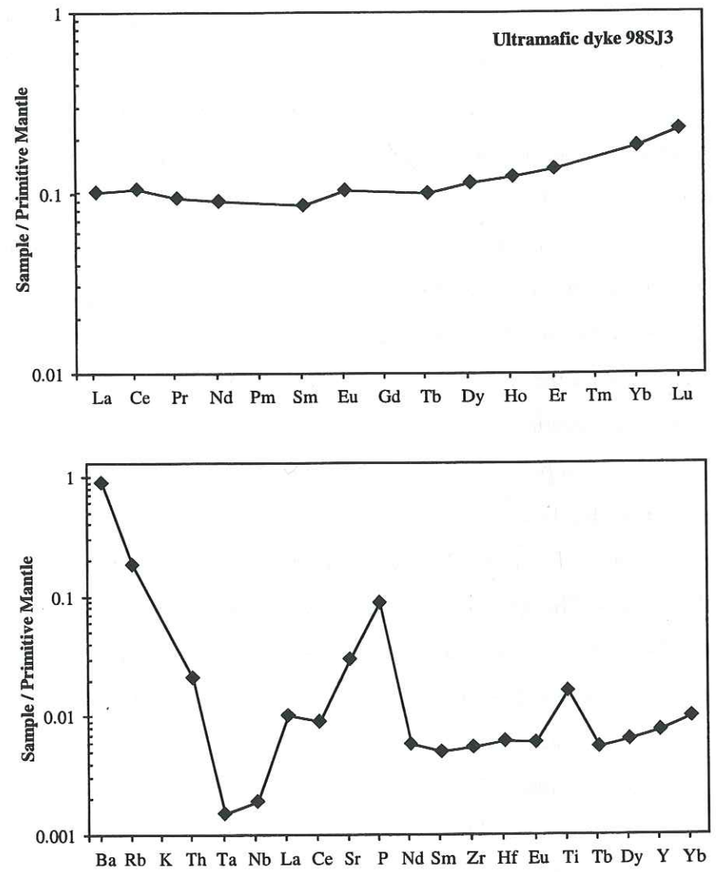

Fig. 3.10: Chondrite- and primitive mantle-normanlized (Sun & McDonough, 1989) rare earth element patterns and multi-element diagram for the San Juan ultramafic dyke.

Nd, Sr, Pb isotopic chemistry

The wehrlites have a rather restricted range of ε_{Nd_i} values, from +5.4 to +8.1 (Table 3.4 and Fig. 3.11). These values are marginally higher than those of the gabbros (+5.2 to +7.5). Plagioclase and amphibole separated from sample 97SJ13 have uniform ε_{Nd} ratios (+7.7 and +7.3) which are slightly higher than that of their host rock (+6.9). Clinopyroxene from 97SJ10 has an ε_{Nd} ratio of +3.0, significantly lower than its host rock (+6.5). This is probably linked to the presence of actinolite that was not completely removed during mineral separation.

All the wehrlites exhibit a limited range of initial $^{87}Sr/^{86}Sr$ ratios (0.703205 to 0.703250), except for the plagioclase-rich wehrlite (97SJ6) which has a higher ratio (0.703412). The gabbros exhibit a large range of initial $^{87}Sr/^{86}Sr$ (0.703293 to 0.704088) which all are higher than those of the peridotites. In the ε_{Nd}-$^{87}Sr/^{86}Sr$ diagram (Fig. 3.12), the wehrlites plot in the Galápagos field and within the mantle array (with the exception of 97SJ6). The gabbros plot on the right side of the diagram, at higher initial $^{87}Sr/^{86}Sr$, probably because of hydrothermal alteration or metamorphism.

Initial lead isotopic compositions of whole rocks and mineral separates from cumulate peridotites and gabbros are broadly homogeneous (Table 3.4) and fall at the boundary between more radiogenic Pb from East Pacific Ridge MORB and less radiogenic samples of the Galápagos (Fig. 3.13). The gabbro 97SJ13 and its related plagioclase have the highest ($^{206}Pb/^{204}Pb$)i and ($^{208}Pb/^{204}Pb$)i ratios, and clinopyroxene separated from the wehrlite 97SJ10 has the lowest (Table 4; Fig. 3.13). Pb isotope ratios of wehrlites (97SJ8, 98SJ4) and olivine-gabbro (98SJ9) are very similar. The San Juan suite domain falls close to the northern hemisphere reference line of Zindler & Hart (1986) in the $^{208}Pb/^{204}Pb$-$^{206}Pb/^{204}Pb$ diagram (Fig. 3.13) but slightly above in the $^{207}Pb/^{204}Pb$-$^{206}Pb/^{204}Pb$ plot, because of the high $(^{207}Pb/^{204}Pb)_i$ of 97SJ10 cpx and of the two wehrlites.

In summary, the basalts, dolerites and isotropic gabbros from the Merced-Multitud sequence exhibit petrological and geochemical features of oceanic plateau basalts. The San Juan cumulates derive from the accumulation of olivine, succeeded by clinopyroxene and plagioclase. Rocks of intermediate to felsic compositions are absent. Orthopyroxene and amphibole are restricted to the uppermost gabbroic levels. The Nd and Pb ratios of the San Juan cumulates fall in the range of within plate intra-oceanic basalts.

Name	Dunite	Wehrlite	Wehrlite	Wehrlite	Wehrlite	Gabbro	Gabbro	Gabbro	Gabbro	Gabbro	Dacite	Ultramafite	Dolerite	97SJ13 amph	97SJ13 Pl	97SJ10 cpx
Samples	98SJ2	97SJ6	97SJ8	97SJ10	98SJ4	97SJ1	97SJ3	97SJ4	97SJ9	97SJ13	97SJ12	98SJ3	98SJ5	123	123	123
t (Ma)	123	123	123	123	123	123	123	123	123	123	123	123	123			
87Rb/86Sr		0.017852	0.025798	0.055086	0.029232	0.003451	0.006535	0.274514	0.007888	0.028006	0.006991		0.009214			
87Sr/86Sr	0.704676±20	0.703443±14	0.703295±15	0.703301±21	0.703295±8	0.703124±8	0.704099±16	0.703941±11	0.703307±11	0.703702±13		0.705305±12	0.703311±8	0.705040±13	0.704646±10	0.705176±12
(87Sr/86Sr)i		0.703412	0.703250	0.703205	0.703244	0.703844	0.704088	0.703461	0.703293	0.703653			0.703295			
ESr		**-13.40**	**-15.70**	**-16.34**	**-15.78**	**-7.26**	**-3.80**	**-12.7**	**-15.08**	**-9.97**			**-15.06**			
147Sm/144Nd		0.219259	0.396775	0.283414	0.257258	0.357278	0.201538	0.155233	0.201538	0.214831	0.155700		0.192294	0.236703	0.111721	0.288282
143Nd/144Nd		0.513073±15	0.512981±8	0.513040±9	0.512960±26	0.513089±5	0.513011±12	0.512871±15	0.513025±6	0.513008±9	0.512089±8		0.513051±6	0.513045±4	0.512962±9	0.512860±40
(143Nd/144Nd)i		0.512897	0.512662	0.512812	0.512757	0.512801	0.512848	0.512746	0.512863	0.512835	0.511964		0.512896	0.512855	0.512872	0.512628
εNd		**8.13**	**5.94**	**6.48**	**5.41**	**6.28**	**7.18**	**5.20**	**7.48**	**6.94**	**-10.07**		**8.13**	**7.31**	**7.66**	**2.89**
(206Pb/204Pb)m		18.48		18.40	18.40				18.57	18.61			18.42		18.58	18.28
(206Pb/204Pb)i		18.42		18.31	18.31				18.60	18.53					18.52	18.17
(206Pb/204Pb)i*		18.40		18.38	18.38			18.56	18.53	15.51			-		18.56	18.23
(207Pb/204Pb)m		15.59		15.53	15.53			15.54	15.51	15.51					15.54	15.53
(207Pb/204Pb)i		15.59		15.53	15.53				15.51	15.51			15.55		15.53	15.53
(207Pb/204Pb)i*		15.59		15.53	15.53			15.54	15.51	15.51			-		15.54	15.53
(208Pb/204Pb)m		38.17		38.01	38.01			38.05	38.13	38.13					38.17	38.00
(208Pb/204Pb)i		38.16		38.00	38.00				38.12	38.12			38.17		38.13	37.90

Table 3.4: Nd, Sr and Pb isotopic compositions for the San Juan rocks and mineral separates. (m): ratios measured; (i): recalculated initial ratios based on the U, Th and Pb contents determinated by ICP-MS (refer Table 2); (*): initial ratios recalculated using the Pb and U abundances determinated on the basis of the measured Nb/U and Ce/Pb ratios and assuming that Nb and Ce have not been mobilized (Hofmann et al., 1986).

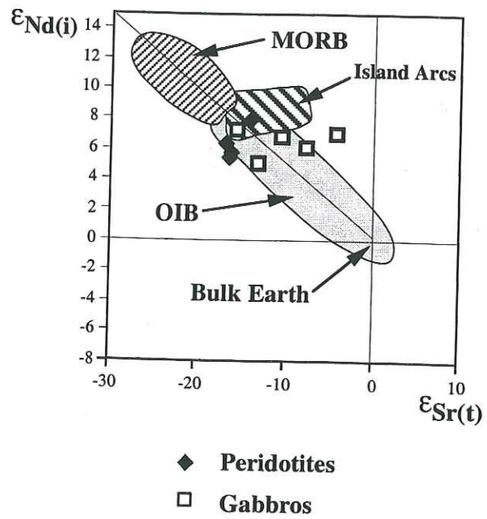

Fig. 3.11: εNd(i) - εSr(t) correlation diagram of the San Juan plutonic rocks.

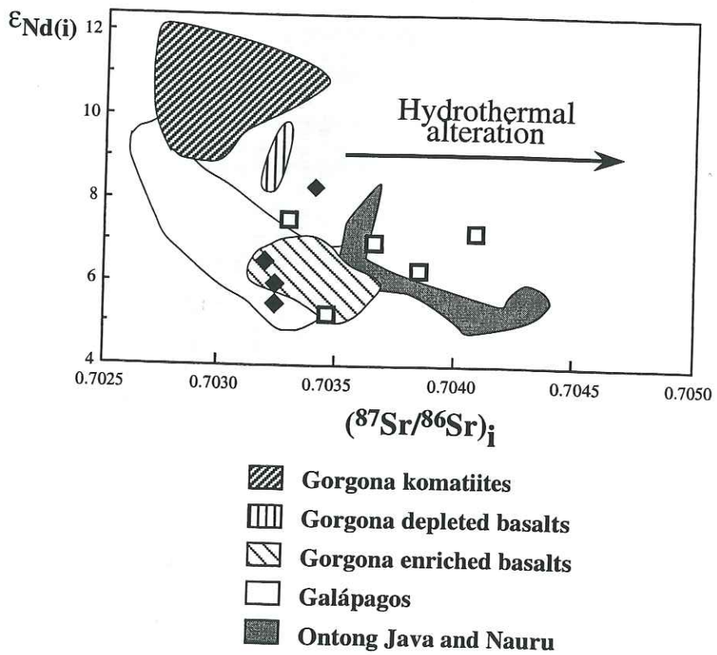

Fig. 3.12: εNd(i) vs (87Sr/86Sr)i diagram of the San Juan plutonic rocks. Fields of volcanic rocks from Gorgona (Aitken & Echeverria, 1984), Galápagos (White et al., 1993), Ontong Java (Mahoney et al., 1993) and Nauru (Castillo et al., 1986) are given for comparison.

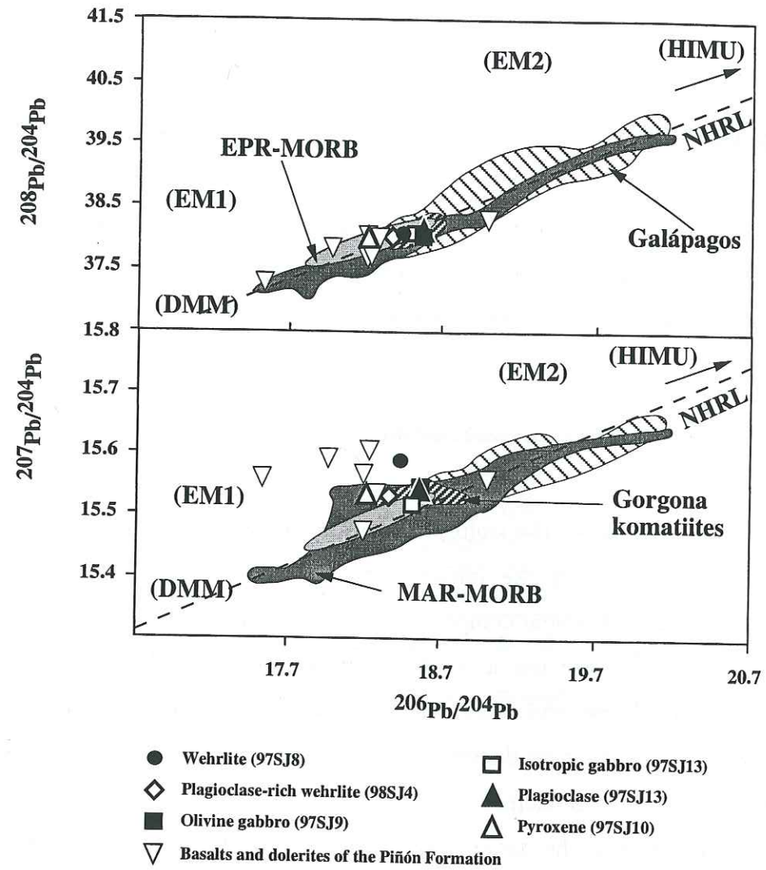

Fig. 3.13: $^{208}Pb/^{204}Pb$ vs $^{206}Pb/^{204}Pb$ and $^{207}Pb/^{204}Pb$ vs $^{206}Pb/^{204}Pb$ diagrams for peridotites, gabbros and mineral separates from the San Juan sequence. Basalts and dolerites from the Piñón Formation are reported after Reynaud et al., 1999 and Lapierre et al., 2000. The "Northern Hemisphere Reference Line" (NHRL) and the field from some mantle reservoirs are reported after Zindler & Hart (1986). East Pacific Rise (EPR) MORB and Mid Atlantic Ridge (MAR) MORB data and Galapagos Islands field are from White et al. (1987). The Gorgona field is reported after White et al. (1993).

DISCUSSION

In this section we will focus on two questions: (1) the nature of the magmatic liquids and interpretation of the major- and trace-element compositions of the cumulate rocks; (2) the tectonic setting in which the intrusions were emplaced.

Compositions of magmatic liquids

With the exception of the isotropic gabbros and dolerites from the upper sections of Merced-Multitud suite, all the intrusive rocks are cumulates. This complicates the interpretation of their chemical compositions. To infer the nature of the liquids from which they crystallized, we must use a combination of mineral compositions and whole-rock compositions. The major and incompatible trace element compositions of the San Juan cumulate rocks depend both on the nature of the predominent minerals and the partitioning of REE and incompatible trace elements in these minerals.

The composition of the basaltic liquid in equilibrium with the cumulate peridotite and olivine-gabbros can be estimated from the forsterite contents of the olivine grains in these rocks. The Mg/Fe ratio of the liquid is determined using the partition coefficient of 0.3 from Roeder and Emslie (1970) and the MgO content is calculated using the FeO^{total} of the whole rock. Calculated MgO contents range from 16 % in dunites to 2 % in certain gabbros.

To determine the REE compositions and Nb abundances of melts in equilibrium with clinopyroxenes we used partition coefficients of Hart and Dunn (1993). The calculated melts are compared to the composition of dolerites from the Merced-Multitud section and the Piñón Formation, which are interpreted to represent the uppermost levels of the Lower Cretaceous oceanic plateau (Reynaud et al., 1999; Lapierre et al., 2000). As seen in Fig. 3.14, the calculated melts have flat HREE patterns with abundances similar to or lower than those of the mafic rocks. The LREE are slightly enriched. The La/Nb ratios of the melts in equilibrium with clinopyroxene separates from wehrlites, cumulate and isotropic gabbro ranges from 0.44 to 1.64.

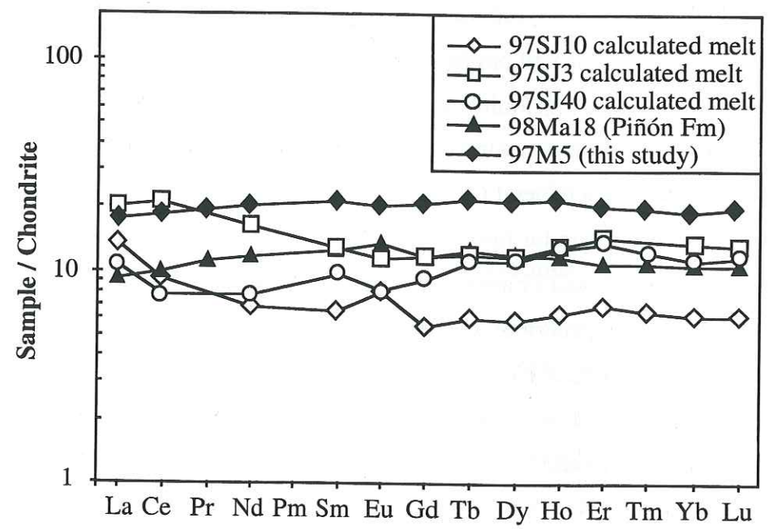

Fig. 3.14: Chondrite-normalized REE patterns of calculated melts from the cpx of San Juan wehrlite and olivine-gabbro. These calculated melts are compared to dolerites (97MA18 and 97M5).

Before trying to explain the trace element distribution in the San Juan cumulates, we must first estimate the abundance of trapped liquid in these rocks. It is possible to do this using the measured compositions and modal abundances of the cumulus minerals and by making an assumption about the composition of the trapped liquid. In the procedure presented in Table 3.2 and 3. 6, we have assumed that the isotropic gabbro of the San Juan suite represents the liquid. The results of the calculations show that the abundances of trapped liquid in the cumulate peridotite range between 5 and 20 %.

The relative concentrations of trace-elements such as the REE, Nb and Zr in the cumulates will depend on the proportion of trapped liquid and the nature of the cumulus minerals. Their overall levels will be controlled mainly by the relative proportions of minerals such as olivine and plagioclase, with which these elements are incompatible, and the amount of trapped liquid. The relative abundances, on the other hand, will be influenced by the amount of clinopyroxene, a mineral for which the partition coefficients vary significantly. As is well known, the HREE are far more compatible in clinopyroxene than the LREE; what is less appreciated is that Nb and Zr are significantly less compatible than the REE. The mantle-normalized trace-element pattern of a clinopyroxene-rich cumulate is therefore characterized by negative anomalies for these elements.

These effects are illustrated by the trace element composition of the wehrlite 97SJ10, which contains about 20 modal % of clinopyroxene and 70 % of olivine. We estimate that this sample contained about 5% trapped liquid. It is seen in Fig. 3.8 that the clinopyroxene and whole rock have similar LREE-depleted patterns but that REE abundances in the whole rock are lower than in the clinopyroxene. The differences in abundances are explained by the relatively small amount of the trapped liquid and the high proportion of olivine, which contains no REE and lowers concentrations in the cumulate rock. The marked negative Nb and Zr anomalies in both the clinopyroxene and whole rock can be explained in the same way. Both elements are less compatible than the REE and are present in very low concentrations in the clinopyroxene, which controls the composition of the cumulate.

The trace-element chemistry of the cumulate gabbros depends on the relative abundances of plagioclase and clinopyroxene. Because the LREE are more compatible than the HREE in plagioclase, a cumulus gabbro rich in this mineral will have a relatively flat REE pattern. This is seen in the samples 97SJ1, 97SJ3 and 97SJ9, which are characterized by flat REE patterns. The compatible nature in plagioclase of Eu and Sr results in marked positive anomalies for these elements.

Criteria that discriminate between intrusions in oceanic plateaus, normal oceanic crust and island arcs

The geodynamic environment in which cumulate intrusive rocks were emplaced is difficult to establish when spatial relations with cogenetic basalts are obscured by later tectonic events. In such cases it is unclear whether an intrusion was once part of normal oceanic crust, or part of an oceanic plateau, or related to subduction magmatism. To distinguish between these possibilities, we need to develop criteria to establish the tectonic setting in which the intrusions were emplaced.

There are three broad types of criteria: (1) geodynamic setting and broad lithological associations; (2) mineralogy and major-element compositions; (3) trace-element and isotope compositions.

Geodynamic setting and lithological associations.

Even in cases in which the tectonic environment is obscured by later events, it is often possible to gain some insights from structural relationships and the identification of diagnostic lithological associations. For example, oceanic ridges and plateaux are made up dominantly of monotonous, commonly pillowed tholeiitic basalts associated with pelagic sediment whereas subduction related units contain a more diverse calc- alkaline rocks whose compositions range from basalt to rhyolite.

Magma compositions and crystallization sequences.

The parental magmas of volcanic and intrusive rocks from different settings differ significantly in composition because of differences in the nature of their sources and conditions of melting. Magma at mid-ocean ridge is essentially anhydrous. Because of the absence of lithosphere beneath the ridge, the degree of melting is relatively high and melting takes place a relatively shallow depths. Under these conditions, the aluminous phase (plagioclase) is unstable and totally enters the melt. The resultant magma is rich in Al, with relative low Fe and Na and relatively high Mg. This type of magma will crystallize olivine first (like any melt produced by melting of peridotite) and this phase will be joined early in the crystal sequence by plagioclase. The expected crystallization sequence is olivine → plagioclase → cpx → opx. The first two phases are those commonly observed as phenocrysts in mid-ocean ridge basalts.

The parental magma of an oceanic island or oceanic plateau forms at greater depth because the melting takes place beneath the oceanic lithosphere. This magma may be poorer in Al because this element is partially retained in aluminous ortho- or clinopyroxene. It is richer in Fe (because of the higher pressure) and in Na (because of lower degree of partial melting). The second silicate phase to crystallize (after olivine) is clinopyroxene, and plagioclase crystallizes relatively late. The expected sequence is olivine → (chromite) → cpx → plagioclase → (opx) as could be inferred from the phenocryst assemblage in oceanic island basalts.

The parental magma of island arc magma forms in the presence of water. This changes the relative stabilities of the major phases, reducing the stability of the olivine compared to that of plagioclase and orthopyroxene. During crystallization, olivine is joined early by both orthopyroxene and plagioclase and Fe-Ti oxides are early and abundant. The expected sequence is olivine → plagioclase → Fe-Ti oxide → opx → cpx → hydrous minerals. Again, this sequence can be confirmed from phenocryst assemblages in volcanic rocks from island arcs.

Trace elements and isotopes.

The source of mid-ocean ridge basalts is depleted both in terms of trace elements and isotopes. The degree of partial melting is high and the only residual phases are olivine and orthopyroxene. These minerals do not fractionate incompatible trace elements and the primary magma inherits the trace-element depletion of the source. Normal MORB are depleted in LREE and other incompatible elements and their Nd isotope ratios are very high ($\varepsilon Nd = +10$ to +12).

Basalts of oceanic islands and plateaus form at greater depth from a less depleted source. During the melting that forms oceanic island basalts (OIB), clinopyroxene ± garnet are residual and the magma is less depleted in incompatible trace elements than the source. REE patterns are flat to enriched in incompatible elements, depending on the nature of the source and the conditions of melting. Basalts in oceanic plateaux generally have flat REE patterns but the most Mg-rich melts (picrites and komatiites) may be enriched or depleted in LREE. The isotopic compositions of OIB span a very large range of values from moderately depleted to strongly enriched, in contrast to the compositions of basalts from oceanic plateaus which are more uniform and only slightly less depleted than MORB.

Arc-basalts come from a source with distinctive characteristics. Their REE patterns vary from depleted to enriched and they display characteristic negative Nb and Ta anomalies in mantle-normalized plots. These anomalies are absent in N-MORB and plume-related basalts. The Nd isotope compositions of arc-basalts are similar to those of OIB.

Test cases

Before using these criteria to evaluate the nature of San Juan suite, we will test them against the characteristics of several intrusions for which the tectonic setting is well known.

Intrusions at mid-ocean ridges

Because of their inaccessibility, very few studies of intrusions at ocean ridges have been undertaken. Until 1975, the only available plutonic samples were collected during dredging. More recently, drilling and submersible sampling of cliffs along transform faults has yielded samples of mafic cumulates and higher-level gabbros from three main regions: the MARK area on the Mid-Atlantic Ridge (Cannat et al, 1995; Casey, 1997; Kempton and Hunter, 1997), Hess Deep in the East-Pacific (Francheteau et al., 1990, 1992; Pedersen et al., 1996), and Site 735B of ODP Leg 118 in the Indian Ocean (Dick et al., 1991).

The predominants rocks from both areas are gabbros, norites and troctolites in which clinopyroxene and plagioclase are cumulus phases and olivine is an interstitial phase. The lower portions of some sections contain serpentinized peridotites and cumulate gabbros.

The gabbroic rocks exhibit a large range of REE patterns. Some are strongly depleted in LREE, others are slightly enriched in these elements. Niobium contents are below detection limits (Pedersen et al., 1996). Clinopyroxenes separated from the gabbros have a narrow range in REE contents (Gillis, 1996) and are depleted in LREE with a negative Eu anomaly. The $^{143}Nd/^{144}Nd$ ratios of the gabbros have values typical of MORB (Pedersen et al., 1996).

Ophiolites

Complete sections through oceanic crust, as exposed in well-known ophiolites such as Cyprus and Newfoundland, are now thought to represent remnants of back-arc basins. The principal arguments are the identification of geochemical features typical of subduction-related rocks, such as low TiO_2 contents (< 1.5%) and negative Nb anomalies. In contrast, the ophiolites of Oman have been interpreted as coming from true oceanic crust.

The cumulate sections of the Maqsad massif in the Oman ophiolite (Benoit et al., 1996; Benoit, 1997) consist of troctolites, olivine gabbros, norites, pyroxenites and dunites. These rocks are generally similar to those of ocean ridges but are characterised by a greater abundance of orthopyroxene in both the gabbroic and ultramafic sections and by the presence of brown (magmatic) amphibole in the uppermost gabbroic levels. The crystal sequence in the ultramafic cumulates is olivine --> clinopyroxene --> plagioclase ± orthopyroxene.

Rare-earth element patterns range from flat to depleted, with or without Eu anomalies. All the cumulate rocks exhibit negative Nb and Zr anomalies of variable magnitude. ε_{Nd} values of the intrusive rocks ranges from +6 to +10. Two types of basalts have been distinguished in the Oman ophiolite. The lower basalts display N-MORB affinities while the upper basalts are characterized by negative Nb anomalies, features of arc-tholeiites. Negative Nb and Zr anomalies in the cumulate rocks are absent in N-MORB-type basalts that immediately overlie the plutonic sections. These basalts are interpreted as cogenetic with the intrusive cumulate rocks. Thus, the negative Nb anomalies observed in the Oman cumulate rocks are probably due to fractionation during clinopyroxene accumulation.

Intrusions in oceanic islands

Few samples of intrusions in oceanic islands are available, and most of those that exist are from intrusions with a clearly alkalic character that is very different from the magmas that fed oceanic plateaus. One source of information comes from suites of xenoliths found in alkaline volcanic rocks on islands such as Hawaii and Kerguelen (Grégoire et al., 1998). Samples believed to come from the lower crust contain plagioclase- or spinel-rich assemblages and Fe-rich mafic minerals. In such suites, the mineral assemblages are olivine, clinopyroxene, orthopyroxene, plagioclase (spinel) and Fe-Ti oxides. Crystallization sequences are olivine --> spinel --> clinopyroxene --> orthopyroxene --> plagioclase in the ultramafic rocks and spinel --> clinopyroxene --> orthopyroxene --> plagioclase in the gabbros. Intrusions of tholeiitic character on the Kerguelen Archipelago consist of gabbros and olivine, clinopyroxene and plagioclase cumulates (Giret and Beaux, 1984).

Ultramafic to mafic xenoliths from Kerguelen display low REE abundances at near chondritic values. Their normalised patterns are usually flat but rare examples are either slightly LREE-enriched or LREE-depleted. They are interpreted as cumulates of the Kerguelen tholeiitic-transitional basaltic series. The clinopyroxenites and metagabbroic xenoliths have higher REE concentrations and display convex upward REE, a feature that was

attributed by Grégoire et al. (1998) to metasomatic enrichment in the middle REE. They represent high-pressure cumulates of alkaline magmas produced during the recent phases of the Kerguelen plume. The εNd values of these xenoliths span a large range, from + 4 to –2 (Vance et al., 1989; Mattielli, 1996)

Intrusion in an oceanic island arc: the Chilas complex of Kohistan

The Chilas complex is interpreted as the plutonic part of a Cretaceous oceanic arc (Bard, 1983; Khan et al., 1989, 1993). The volcanic sequence is typical of an island arc comprising basalt, andesite, dacite and rhyolite of arc-tholeiitic affinity intruded by numerous large to small gabbroic to granitic plutons (Collins et al., 1998). The Chilas intrusive complex itself comprises two distinct rock associations: the gabbroic Main Facies Zone, and the ultramafic-mafic-anorthosite cumulate association.

The Main Facies Zone, which forms at least 85% of the complex, consists of diverse rock types – gabbro (50-55%), diorite (40-45%) and minor granite. In the gabbronorites cumulus orthopyroxene is ubiquitous and abundant (20-30%), olivine is absent, hornblende is always present in minor quantities, and magnetite forms 2 to 4 % of the rock. The Main Facies Zone rocks display remarkably uniform and distinctive trace-element patterns. The LREE are slightly enriched, negative Nb anomalies are ubiquitous, and Ba, Rb, K and Th are strongly enriched relative to the less incompatible elements (Kausar, 1998). ε_{Nd} values are uniform and relatively low (+2.8 to +2.9) (Khan et al., 1997).

The ultramafic-mafic-anorthosite association is composed of cycles of layered to massive olivine, orthopyroxene, clinopyroxene ± plagioclase cumulates. All ultramafic samples are very poor in incompatible elements and the abundances of Rb, Ba, Th and Nb are below detection limits. Wehrlites are characterized by depletion of LREE but gabbros have generally flat REE patterns with positive Eu, Ba and Rb anomalies and negative Nb anomalies. The ε_{Nd} values of the cumulate ultramafic and mafic rocks are slightly higher than in the gabbronorites (+3.5 to +4).

Conclusion

From this review we conclude that the best criteria to identify the tectonic setting of mafic-ultramafic intrusions are the broad lithological associations and the mineralogy of the cumulus sequences. The presence of abundant calc-alkaline intermediate to felsic rocks

clearly identifies an arc setting, such rocks being rare or absent in the oceanic environments. Orthopyroxene is the key diagnostic mineral, being abundant in cumulates from island arcs, present in minor quantities in oceanic crust and ophiolites, but rare to absent from oceanic intraplate magmatism. In places where this mineral is reported, as in the xenolith suites from the Kerguelen Archipelago, it is associated with spinel and other high-pressure phases. Its presence there may indicate crystallization in the lower parts of the volcanic pile. Hydrous minerals are also characteristic of arc-related rocks, but magmatic amphibole is also present in evolved late-stage rocks in ophiolites and oceanic islands.

Also useful are trace-element and isotope compositions, but their interpretation is not always unambiguous. Neodymium isotope ratios of intraplate volcanics are lower than those of ocean-ridge basalts, but similar to arc basalts (Sr and Pb isotopes are not readily applicable to variably altered rocks). The interpretation of trace-element data is complicated by the accumulation process. A plagioclase cumulate has a flatter REE pattern than the magma from which it crystallizes and is characterised by positive anomalies of Ba, Sr and Eu; a clinopyroxene cumulate has a more depleted pattern and negative Nb and Ta anomalies. Fractionation of Nb (and geochemically similar Ta) from other incompatible elements is particularly important because this process influences the interpretation of negative Nb anomalies, normally a clear signature of a subduction setting. Because Nb is less compatible in pyroxene than the LREE and Th ($KD_{Nb}^{cpx\text{-}liq} = 0.0077$ cf $KD_{La}^{cpx\text{-}liq} = 0.0536$; Hart and Dunn, 1993), a pyroxene cumulate may show negative anomalies that were not present in the host magma. These effects must be taken into account during the interpretation of the trace-element patterns of mafic and ultramafic cumulates.

Plutonic rocks from the Caribbean and Ontong Java plateaus

There is little doubt about the tectonic environment of the ultramafic cumulates and mafic intrusions from Gorgona Island (Echeverria, 1980). These rocks share the distinctive geochemical and isotopic characteristics of associated mafic and ultramafic lavas, such as strong depletion of incompatible elements and moderate to high ε_{Nd} values (Révillon et al., 2000). The majority of the intrusive rocks are olivine, clinopyroxene and plagioclase orthocumulates. Orthopyroxene is absent. On the basis of distinctive textures thought to indicate relatively rapid cooling (abundant small olivine crystals and rare grains with skeletal

habits), Révillon et al. (2000) concluded that the intrusions were emplaced at high levels of the Caribbean oceanic plateau.

The Bolívar-Rio Frio complex in west-central Colombia consists of cumulate ultramafic and mafic rocks tectonically imbricated with basalts and sediments (Nivia, 1996; Kerr et al., 1998). Ultramafic ortho- and adcumulates, in places distinctly layered (Desmet, 1994), are overlain by gabbros. The rocks have harzburgitic to noritic compositions, commonly with a high proportion of orthopyroxene to olivine. An upper unit of isotropic gabbro contains abundant amphibole and pegmatoid textures. From the crystallisation sequence and the abundance of orthopyroxene and hydrous minerals, the geodynamic setting of the Bolívar-Rio Frio complex appears more like that of an island arc than an oceanic plateau.

Gabbros from Santa Isabel are associated with thin fault-bounded slices of upper mantle peridotite and pillow basalts that are thought to form part of the Ontong-Java oceanic plateau. The mafic rocks range in composition from troctolite through olivine-gabbro to two-pyroxene gabbro. Magmatic amphibole has never been described in these gabbros. All these gabbros exhibit negative Nb anomalies. The REE patterns range from strongly LREE-depleted to enriched and their $\varepsilon_{Nd}(T)$ values range from +5.7 to +7.8. On the basis of these results, the setting is ambiguous (Fig. 3.15).

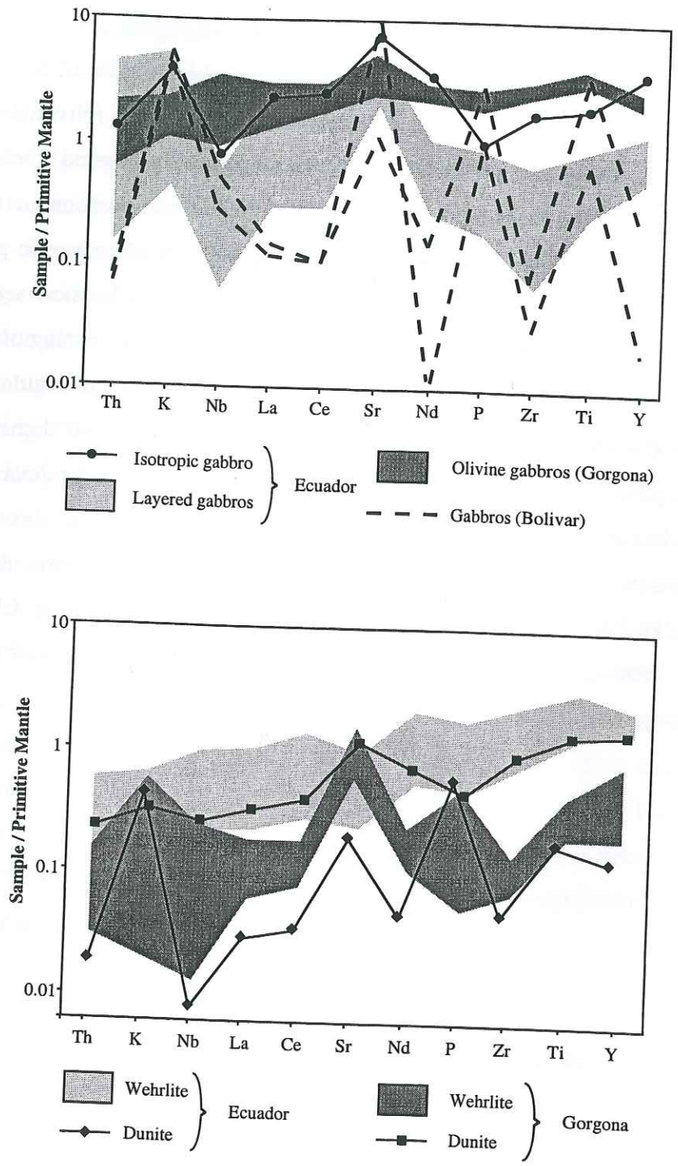

Fig. 3.15: Primitive mantle-normalized (Sun & McDonough, 1989) multi-element plots showing the compositional range of isotropic and layered gabbros, and dunites and wehrlites from Ecuador (this study) compared to the gabbros from Gorgona (Révillon, 1999; Révillon et al., 2000), and Bolivar (Kerr et al. 1998).

Criteria that demonstrate that the San Juan sequence belongs to an oceanic plateau

Geodynamic setting and broad lithological associations.

Although island arc sequences are associated with other segments of the Caribbean plateau (e.g.in Ecuador where the Piñón plateau is overlain by arc sequences, Reynaud et al., 1999), typical island arc rock associations have never been reported within the Multitud or San Juan sequences. The supracrustal sequences of the Western Cordillera (Merced-Multitud section) and along the Pacific coast (Piñón Formation) consist of mafic volcanic and hypabyssal rocks, intercalated with pelagic sediments. Evolved calc-alcaline suites of basalt, andesite, dacite and rhyolite are absent.

Mineral assemblages and crystallization sequences:

The mineralogy of the San Juan rocks is similar to that of intraplate rocks. Orthopyroxene is only a very minor component in the San Juan gabbros and the ultramafic cumulates are dominated by olivine and clinopyroxene. Amphibole is restricted to the uppermost massive gabbro. The crystallization sequence is olivine (chromite) → cpx → plagioclase → opx.

Trace element and isotopic compositions:

The relatively flat REE patterns are typical of rocks from oceanic plateaus and distinct from the depleted patterns of MORB and the more enriched patterns of oceanic island and arc basalts. The trace element anomalies measured in certain samples are either a result of alteration or a feature related to the accumulated minerals. Thus the negative Nb-Ta anomalies, which are present in certain ultramafic rocks but not in the basalts, are related to the accumulation of clinopyroxene and do not indicate a subduction setting.

Nd isotopic compositions are not discriminant because the Nd isotope compositions of oceanic plateau basalts overlap those of recent Pacific MORB, ophiolites and arc-rocks. Sr isotopic data cannot be applied to the San Juan plutonic rocks because alteration has modified their $^{87}Sr/^{86}Sr$ ratios.

What is the relationship between the two sequences and the structure of the oceanic plateau

Because of Andean deformation, the primary relationships between the San Juan and Merced-Multitud igneous suites are unclear. Although both sequences are now 250 km apart, most authors consider that they belong to the same tectonic unit, since both are probably of Early Cretaceous age, and accreted during the same pre-Maastrichtian collision episode (Lebrat et al., 1987; Dunkley and Gaibor, 1998; Hughes and Pilatasig, in press). Two questions must then be asked: are the two sections genetically linked, and do they represent different levels in an oceanic plateau?

In a former section, we calculated melt compositions based on clinopyroxenes separated from San Juan intrusive rocks. These melts have trace-element patterns similar to those of the shallow level gabbros and basalts of both the Merced-Multitud section and the Piñón Formation which indicates that the Merced-Multitud tholeiites could represent melts in equilibrium with the San Juan rocks. Moreover, the melt composition calculated from olivine in the wehrlite contains 8% MgO, which is similar to that of the less differentiated basalts of the Piñón Formation (MgO ≈ 9%, Reynaud et al., 1999) and from Merced-Multitud area (MgO ≈ 8.5%, Lebrat et al., 1987). Finally, the rather restricted and similar range of εNd values (+8.1 to +5.2) of rocks from both sequences supports a comagmatic relationship.

The majority of Lower Cretaceous rocks from Western Cordillera are basaltic in composition, and do not represent primary mantle melts. Basalts from Ontong Java plateau not only have trace element ratios similar to the basalts, dolerites and shallow-level gabbros of the Piñón Fm and Pallatanga unit, but display a similar range in MgO contents (Mahoney et al., 1993; Neal et al., 1997). Neal et al. (1997) estimated that the hidden cumulates related to the Ontong Java basalts consist primarily of early olivine and later clinopyroxene, with lesser amounts of plagioclase, orthopyroxene and spinel. Farnetani et al. (1996) proposed that high seismic velocities near Moho levels are due to the presence of crystal cumulates (chiefly olivine) that formed through large-scale fractionation of primary picritic magmas. Moreover, they suggested that these picritic melts underwent further crystal fractionation to produce gabbroic intrusions as they evolved to the basaltic compositions of the erupted lavas. As a result, these authors have proposed a structure of an oceanic plateau with olivine and clinopyroxene cumulates near to and below the Moho, with pyroxene-rich intrusions in the

lower part of the crust and more plagioclase-rich gabbros closer to the surface. The structure of an oceanic plateau predicted by these authors corresponds to what we observe in Ecuador. The basaltic flows and hypabyssal intrusions of the Merced-Multitud area correspond to evolved magmas in the upper part of the plateau; the mafic-ultramafic cumulates of the San Juan region to intrusions at a deeper level of the plateau.

CONCLUSION

(1) A set of criteria has been developed to establish the tectonic setting of mafic-ultramafic intrusions and to identify intrusions that form parts of an oceanic plateau. The more important criteria are the broad lithological associations and the mineralogy of the cumulus sequences.

(2) Mafic and ultramafic volcanic and intrusive rocks exposed in the high parts of the Western Cordillera of Ecuador are shown, using these criteria, to represent different levels of an oceanic plateau. The diagnostic features are the absence of evolved calc-alkaline suites, the crystallization sequence of the cumulate rocks which is similar to that of intraplate rocks and the presence of basalts with flat REE patterns.

(3) Negative Nb and Zr anomalies in clinopyroxene and host peridotites and gabbros are believed to result from the exclusion of these elements from the structure of cumulus clinopyroxene. They do not indicate a subduction environment.

(4) The studied sections represent two parts of an Early Cretaceous oceanic plateau which accreted in the Late Cretaceous on the Ecuadorian margin. The basaltic flows and hypabyssal intrusions of the Merced-Multitud area correspond to evolved magmas in the upper part of the plateau; the mafic-ultramafic cumulates of the San Juan region to intrusions at a deeper level of the plateau.

ACKNOLEDGEMENTS

We would like to thank N. T. Arndt for his very helpful comments and for all the time he spent in correcting the manuscript. This research has been supported by grants from INSU-CNRS (Intérieur de la Terre) Contribution N° and FNRS N° 20-50812.97 to M. Polvé and J.

Hernandez, respectively. Thanks to Pierre Brunet who did all the Sr-Nd TIMS analyses and to François Sénebier who did all the mineral separates.

Chapitre 4

Pendant le Crétacé Supérieur – Paléocène Inférieur, des terrains océaniques (plateaux océaniques et arcs insulaires) viennent s'accréter le long de la marge Andine. Chaque accrétion est marquée par la présence de sédiments d'origine continentale caractérisés par la présence de quartz. Les terrains accrétés sont formés de basaltes, de basaltes riches en Mg, d'ankaramites et de picrites et affleurent aussi bien dans la Cordillère Occidentale que sur la côte. Au niveau de la Cordillère, ces différentes roches sont en contact faillé avec les roches du plateau océanique Crétacé Inférieur et situées systématiquement plus à l'ouest. Nous avons essayé de dater différents faciès en utilisant plusieurs méthodes (Pb/Pb et Sm/Nd). Dans ces roches, seuls les clinopyroxènes sont préservés. Les plagioclases sont absents dans les les roches les plus magnésiennes ou complètement remplacés par de l'albite ou de la smectite. Nous avons donc couplé les clinopyroxènes avec les roches totales pour obtenir un âge. Pour obtenir une bonne isochrone avec des rapports Sm/Nd différents, nous avons essayé de prendre différentes granulométries de clinopyroxènes. Malgré cela, aucun âge cohérent n'a été obtenu.

Cependant, Boland et al. (communication personnelle) ont trouvé des faunes Santoniennes dans des radiolarites associées à des basaltes en coussins à affinité de plateau océanique. Ainsi, cette séquence composées de basaltes et basaltes riches en Mg présente un âge Crétacé Supérieur plus récent que ceux du Crétacé Inférieur caractérisés précédemment en Equateur (San juan et Merced-Multitud). De plus, les faciès pétrographiques et la géochimie des roches du plateau océanique Crétacé Supérieur, développés dans ce chapitre, sont très différents de ceux des roches du plateau océanique Crétacé Inférieur.

Chapter 4

ACCRETED FRAGMENTS OF THE LATE CRETACEOUS CARIBBEAN-COLOMBIAN PLATEAU IN ECUADOR

Marc Mamberti, Henriette Lapierre, Delphine Bosch, Etienne Jaillard, Raynald Ethien, Jean Hernandez and Mireille Polvé.

Submitted to Journal of Geology

CHAPTER 4: ACCRETED FRAGMENTS OF THE LATE CRETACEOUS CARIBBEAN-COLOMBIAN PLATEAU IN ECUADOR

During the Late Cretaceous and Early Paleocene, material of oceanic plateau and island arc affinities accreted to the Ecuadorian margin. After each accretional event, the oceanic rocks were sealed by continental-derived sediments. Basalts, Mg-rich basalts, ankaramites and picrites crop out west of the accreted Early Cretaceous oceanic plateau, in fault contact with the Lower Cretaceous rocks, and are exposed both in the western Cordillera and along the coast. We have tried to date these roccks using different methods (Pb/Pb, Sm/Nd). In these rocvks, the only preserved mineral is clinopyroxene. Plagioclase is absent in the most magnesium-rich rocks or completely replaced by albite or smectite. So clinopyroxene remained the only mineral which coupled with the whole rock could give an age. In order to obtain the best isochron regression line with very different Sm/Nd ratios from only clinopyroxene, we have tried to date these rocks using different granulometries of clinopyroxene separates. Unfortunately, no coherent ages have been obtained.

By chance, radiolarite faunas found in inter-basaltic pillow sediments yielded a 89 Ma age (Cenomanian-Turonian). The basalts have an oceanic plateau affinity. Thus the Mg-rich and Mg-poor basaltic sequence of oceanic plateau affinity is Late Cretaceous in age and younger than the Lower Cretaceous one previously characterized in Ecuador (San Juan and Merced-Multitud sections, Pinon Formation). Moreover, the petrology and geochemistry of the Upper Cretaceous oceanic plateau basalts and picrites, developed in this chapter, are very different from those of the Lower Cretaceous oceanic plateau rocks.

ACCRETED FRAGMENTS OF THE LATE CRETACEOUS CARIBBEAN-COLOMBIAN PLATEAU IN ECUADOR

ABSTRACT

The eastern part of the Western Cordillera of Ecuador includes fragments of an Early Cretaceous (≈ 123 Ma) oceanic plateau accreted around 85-80 Ma (San Juan-Multitud unit). West of this unit and in fault contact with it, another oceanic plateau sequence (Guaranda unit) is marked by the occurrence of picrites, ankaramites, basalts, dolerites and shallow level gabbros. A comparable unit is also exposed in northwestern coastal Ecuador (Pedernales unit).

Picrites have LREE-depleted patterns, high εNd and very low Pb isotopic ratios suggesting that they were derived from an extremely depleted source. In contrast, the ankaramites and Mg-rich basalts are LREE-enriched and have radiogenic Pb isotopic compositions similar to the Galápagos HIMU component; their εNd are slightly lower than those of the picrites. Basalts, dolerites and gabbros differ from the picrites and ankaramites by flat REE patterns and lower εNd; their Pb isotopic compositions are intermediate between those of the picrites and ankaramites. The ankaramites, Mg-rich basalts, and picrites differ from the lavas from the San Juan-Multitud Unit by higher Pb ratios and lower εNd.

The Ecuadorian and Gorgona 88-86 Ma picrites are geochemically similar. The Ecuadorian ankaramites and Mg-rich basalts share with the 92-86 Ma Mg-rich basalts of the Caribbean-Colombian oceanic plateau (CCOP) similar trace element and Nd and Pb isotopic chemistry. This suggests that the Pedernales and Guaranda units belong to the Late Cretaceous CCOP. The geochemical diversity of the Guaranda and Pedernales rocks illustrates the heterogeneity of the CCOP plume source and suggests a multi-stage model for the emplacement of these rocks. Stratigraphic and geological relations strongly suggest the Guaranda unit was accreted in the Late Maastrichtian (≈ 68-65 Ma).

INTRODUCTION

The margins of the Caribbean plate and the western margin of northern South America include accreted oceanic sequences (Gansser, 1973), most of which have oceanic plateau affinity (Fig. 4.1). These oceanic plateau remnants, however, differ in their petrology,

geochemistry and age. It is commonly accepted that oceanic fragments accreted in central America, in the Caribbean islands and in north-western South America represent remnants of the Late Cretaceous Caribbean-Colombian Oceanic Plateau (CCOP, Donnelly et al., 1990; Kerr et al., 1996a; 1996b; Sinton et al., 1997).

Three magmatic events have been recognized in the CCOP (Sinton et al., 1998). The oldest of 92-86 Ma age (Turonian-Coniacian) is the most widespread and volumetrically important. A volumetrically secondary and less widespread event occurred at 78-72 Ma (Campanian). This event is known in Coastal Colombia (Serranía del Baudó), Curaçao, Beata Ridge (Révillon et al., 2000a), near the Hess Escarpment and possibly in Haiti. The third event is represented by younger OIB-type basalts of 63 Ma (Paleocene) outcropping in the Quepos Peninsula (Costa Rica, Hauff et al., 1997). Moreover, among all the best-known oceanic plateaus of Mesozoic age, the CCOP is the only one where komatiites have been described and studied (Aitken and Echeverria, 1984; Arndt et al., 1997; Révillon et al., 2000b). The picritic and komatiitic basalts from Gorgona and Colombia are related to the older and major 92-86 Ma pulse (Sinton et al., 1997; Kerr et al., 1997a; 1997b).

However, northwestern South America also includes oceanic terranes of older ages, accreted between the Late Jurassic and the Late Cretaceous. A Late Jurassic-Early Cretaceous suture, containing metamorphosed oceanic and continental rocks, has been identified in Colombia (McCourt et al., 1984; Aspden and McCourt, 1986; Toussaint and Restrepo, 1994) and in Ecuador (Litherland et al., 1994; Gabriele et al., 1999; Bosch et al., in press). On the other hand, remnants of an Early Cretaceous oceanic plateau, distinct from the CCOP have been recently discovered in Ecuador (Reynaud et al., 1999; Lapierre et al., 2000).

In order to understand the genesis and emplacement of the magmatic products related to a mantle plume, and to reconstruct the tectonic and geodynamic history of the buildup of this part of the Andes, we undertook the geochemical survey of the oceanic terranes accreted in western Ecuador.

The main aims of this paper are : (i) to present new trace element and isotope (Sr, Nd Pb) data from the picrites and Mg-rich basalts from the Western Cordillera and coastal zone of northwestern Ecuador; and (ii) to compare these rocks with both the Early Cretaceous fragments of oceanic plateaus exposed in Ecuador and with the 90-86 Ma lavas exposed on different parts of the CCOP.

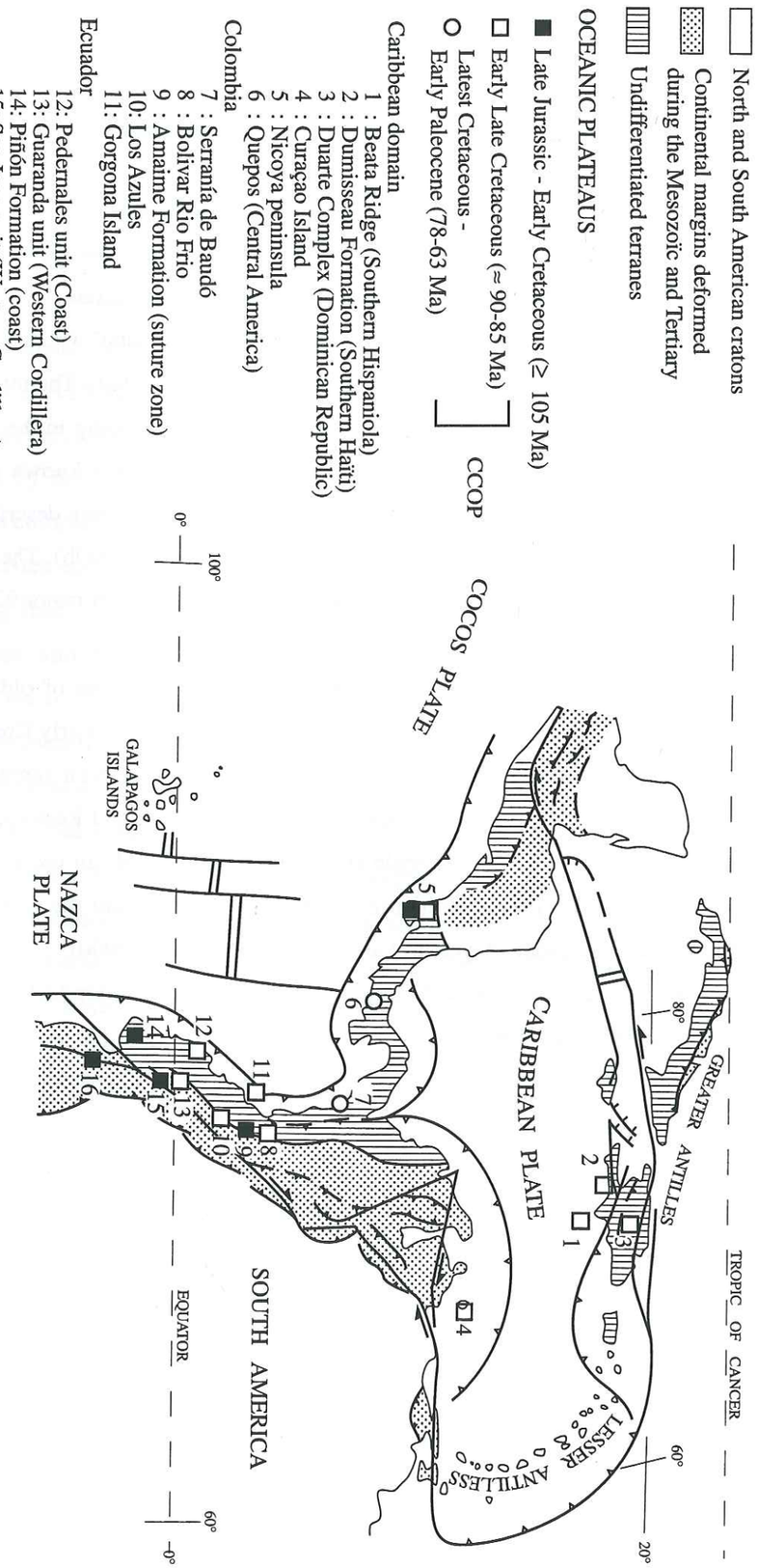

Fig. 4.1: Schematic map showing the location of the Mesozoic plateau crustal fragments exposed in Costa Rica, Greater Antilles, Curaçao, Colombia, and western Ecuador.

GEOLOGICAL SETTING

The Coast and Western Cordillera of Ecuador are characterized by the presence of oceanic terranes accreted to the Andean margin between the Late Santonian-Campanian (85-80 Ma) and the Eocene (≈ 40 Ma) (Feininger and Bristow, 1980; Lebrat et al., 1987; Jaillard et al., 1997; Cosma et al., 1998; Hughes et al., 1999; Boland et al., 2000).

The coastal zone of Ecuador consists of Cretaceous basalts and dolerites with oceanic plateau affinity (Piñón Formation) overlain by Late Cretaceous island arc rocks (Goossens and Rose, 1973; Lebrat et al., 1987 ; Jaillard et al., 1995; Reynaud et al., 1999). Although the age of the Piñón Formation is poorly constrained (K/Ar ages range from 180 Ma to 54 Ma, Goossens and Rose, 1973; Pichler and Aly, 1983; Malone et al., 1999), stratigraphic relations indicate that it is pre-Late Cretaceous in age (pre-95 Ma, Reynaud et al., 1999).

According to McCourt et al. (1998), Pratt et al. (1998), Dunkley and Gaibor (1998), Hughes et al. (1999), and Boland et al. (2000), the Western Cordillera of Central Ecuador comprises several tectonic units including, from West to East, Paleogene island arc lavas and sediments (Macuchi unit), Late Cretaceous volcaniclastic and oceanic sediments, and Cretaceous oceanic magmatic rocks (Pallatanga unit; Fig. 4.2). Part of the latter has been recently interpreted as representing remnants of an Early Cretaceous oceanic plateau (Lapierre et al., 2000; Mamberti et al., submitted).

On the basis of their tectonic setting and geochemical signatures, we distinguish remnants of two Cretaceous oceanic plateau within the Pallatanga unit of the Central Ecuador.

1) The first oceanic plateau crops out in the eastern part of the Western Cordillera of Central Ecuador (0°-3°30'S), and comprises two sequences. The San Juan sequence consists of tectonic slices of cumulate peridotites and gabbros intruded by mafic dykes, dated as Early Cretaceous (≈ 123 Ma, Lapierre et al., 2000). The Multitud sequence is composed of massive and pillowed mafic flows, graded-bedded tuffs and greywackes intruded by shallow levels gabbros and dolerites (Merced-Multitud cross section : Lebrat et al., 1985; Dunkley and Gaibor, 1998; Mamberti et al., submitted). It is associated farther south with a Late Jurassic?-Early Cretaceous ammonite (Pratt et al., 1998). These sequences will be referred to as the San Juan-Multitud unit, of Early Cretaceous age, tentatively correlated with the Piñón Formation of the coastal zone (Lebrat et al., 1987; Dunkley and Gaibor, 1998; Reynaud et al., 1999).

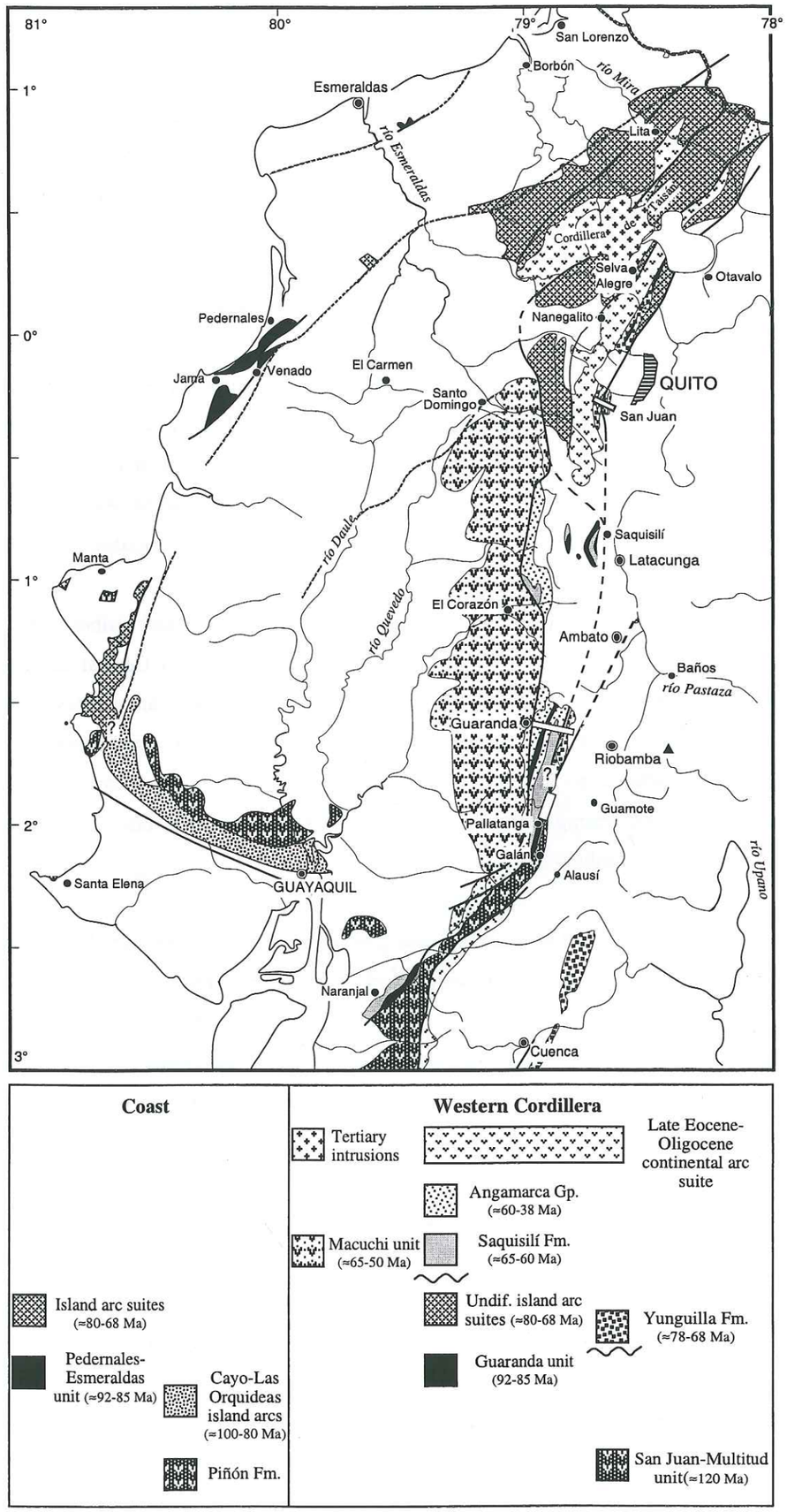

Fig. 4.2: Schematic geological map of Western Ecuador showing the main geological and tectonic units.

2) The second type of oceanic plateau rocks is exposed in the high parts of the Western Cordillera and in northwestern Coastal Ecuador.

- In the Western Cordillera of Central Ecuador, they are located immediately west of, and in fault contact with, the San Juan-Multitud unit. They consist of ankaramites, picrites and Mg-rich basalts often associated with deformed pelagic black cherts or limestones. In this paper, they will be referred to as the Guaranda unit (western part of the Pallatanga unit of McCourt et al., 1998). According to the sections, these rocks are in fault contact with quartz-bearing turbidites of Late Campanian-Early Maastrichtian (Yunguilla Formation; Sigal et al., 1969), Early to Middle Paleocene (Saquisilí Formation; Hugues et al., 1999), or Early Tertiary age (Angamarca Group, McCourt et al., 1998), or stratigraphically overlain by the Paleocene Saquisilí Formation (Jaillard, unpublished data).

- In Western Cordillera of North Ecuador, Boland et al. (2000) mention in a similar structural position, oceanic rocks dated by Santonian radiolarians, associated with Campanian-Maastrichtian island arcs rocks.

- In northwestern coastal Ecuador (Pedernales and Esmeraldas areas), the magmatic substratum of this forearc zone is made of picrites, pillow basalts and hyaloclastites associated with dolerites and isotropic gabbros, which are comparable with those of the Western Cordillera. We will refer to these Mg-rich volcanic rocks as the Pedernales unit.

Five sections have been studied. The Guaranda, Pallatanga and Galán sections belong to the Western Cordillera (2°-2°30'S: Fig. 4.2), whereas the Pedernales and Esmeraldas sections are located on the coastal zone of northwestern Ecuador (0°30'S-1°N; Fig. 4.2).

Three rock types have been distinguished in the Guaranda cross-section on the basis of petrographic observations: pillow basalts, ankaramites and picrites (Fig. 4.3). The pillow basalts are pinched between the Early Tertiary Angamarca turbidites to the east and the picrites and ankaramites to the west. The picrites and ankaramites occur as a pile of massive sheeted flows gently dipping to the east. Picrites are located at the base of the section while the ankaramites are present at the top. The thickness of the flows ranges between one and four meters. These flows show evidence of accumulation of clinopyroxene and/or olivine at their base while their tops are highly vesicular. The rounded or flattened up to 4 centimeter-sized vesicules are filled with calcite in the ankaramites and smectites in the picrites.

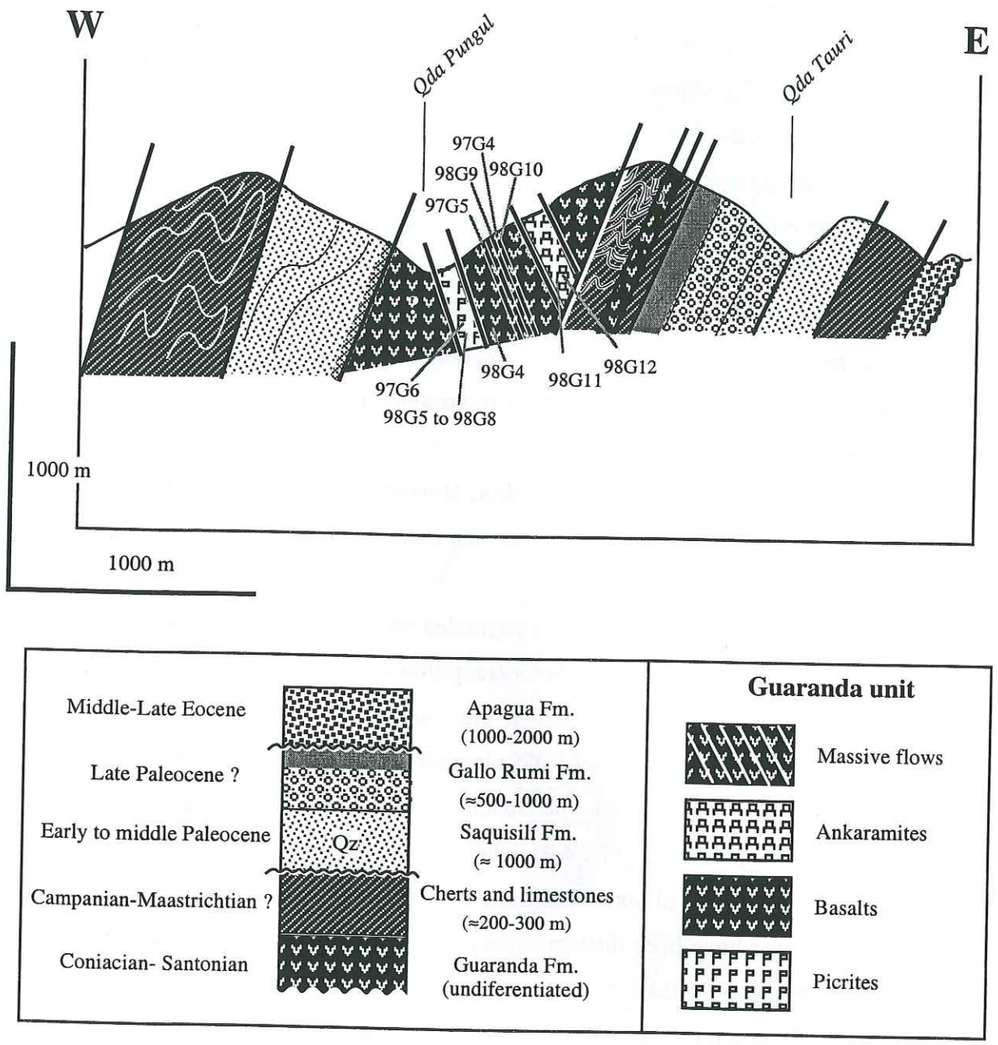

Fig. 4.3: Schematic Guaranda cross section showing the different components of the uppermost levels of the oceanic plateau.

The highly faulted Pallatanga cross-section comprises basalts and dolerites. The Galán cross-section is composed of basalts and pillow lavas associated with dolerites. The Galán and Pallatanga cross-sections are located in a dextral transcurrent fault zone. The oceanic rocks are often in fault contact with the Maastrichtian Yunguilla Formation to the east, and are associated to the west with black, micaceous cherts and siltstones, most probably related to the Paleocene Saquisilí Formation (Pallatanga), or with the coarser-grained quartz-rich turbidites of the Angamarca Group (Galán).

The Pedernales and Esmeraldas cross-sections are characterized by hyaloclastites, which contain centimeter-sized rounded glass fragments of basaltic ($7.19 > MgO_{wt\%} > 8.91$) and picritic ($MgO_{wt\%} > 20$) compositions. They are associated with pillow basalts, dolerites and isotropic gabbros. Pillow basalts with glassy rims and basaltic hyaloclastites are exposed near Venado (15 km south of Jama; Fig. 4.2). The relations between the picritic hyaloclastites and the pillow basalts remain unknown. The most continuous section of the basaltic succession (less than 700 meters long) is located along the El Cármen-Pedernales road (Fig. 4.2). This section consists of pillow basalts interlayered with columnar-joint massive flows. Siliceous sediments occur as pillow matrix. Lava flows are gently dipping to the southwest and are unconformably overlain by fine-grained greywackes, cherts and pelites of Eocene age. Dolerites and isotropic gabbros occur as small stocks or dykes crosscutting the lava flows.

PETROLOGY AND MINERALOGY

We distinguished two groups of rocks in two main groups on the basis of their petrographic features. The first group consists of basalts, ankaramites, dolerites and isotropic gabbros and is exposed in all the studied sections. The second group is composed of picrites, which are restricted to the Guaranda cross section.

Igneous rocks from the Western Cordillera

Mg-rich basalts, ankaramites and dolerites

Three rock-types have been distinguished on the basis of the texture, mineralogy and modal compositions. They are the following, listed in decreasing abundance: (1) the Mg-rich basalts, (2) the ankaramites and (3) the dolerites. All the rocks have variably suffered a low-grade hydrothermal alteration. Olivine is totally replaced by serpentine, smectite or calcite.

Plagioclase is completely transformed into albite, chlorite or epidote. In contrast, clinopyroxene is generally well preserved in all rock-types but is partially replaced by actinolite in the groundmass.

The Mg-rich basalts (98P3, 98P7, 98P8, 98P10) occur as massive flows and display aphyric to porphyritic textures. When aphyric (98P3, 98P7), the matrix is composed of clinopyroxene and plagioclase microlites with sometimes, olivine pseudomorph microcrysts. The oxides are the last to crystallize. When the texture is porphyritic (98P8, 98P10), the basalts are composed of olivine and clinopyroxene phenocrysts and microlites of clinopyroxene and plagioclase in the mesostasis. The euhedral habits of the olivine pseudomorphs are always preserved. Differences between samples are expressed by the olivine abundance (6 to 12%) and size (0.5 to 2 mm). Pyroxene is essentially diopside (Wo_{40-45}, En_{47-49}, Fs_{6-7}) and represents the predominant phase (between 50 to 60% in the matrix). It occurs either as isolated phenocrysts or as glomeroporphyritic clots (< 5%). Plagioclase forms essentially microlites. The rare pillow-lavas (98P10, 97G2) exhibit aphyric or intersertal texture with plagioclase laths and clinopyroxene microcrysts in a silicified matrix.

Ankaramites (98G9, 98G10, 98G11, 98G12, 97G4, 98G4) differ from the Mg-rich basalts by the presence of abundant and large (up to 2 cm-sized) clinopyroxene phenocrysts (5 to 10%). Their fine-grained groundmass includes abundant clinopyroxene, plagioclase and olivine microcrysts. 98G4 differs from the other rocks by the presence of abundant altered plagioclase microlites.

Dolerite (97P18) exhibits an ophitic texture and is formed of millimeter-sized plagioclase laths cemented by clinopyroxene and late crystallizing oxides. Its groundmass is largely recrystallized into secondary quartz, epidote, and smectite with chlorite and calcite-filled veins

Picrites

The picrites (97G5, 97G6, 98G5, 98G6, 98G7, 98G8) are formed of clinopyroxene microphenocrysts with olivine pseudomorphs. Clinopyroxene has a diopside composition (Wo_{44-48}, En_{47-51}, Fs_{5-10}). The matrix is essentially composed of clinopyroxene microcrysts and few needle-shape Fe-Ti oxides. The modal composition of the olivine ranges between 20 to 50%. All the picrites are highly vesicular with quartz, or calcite or smectites-filled large vesicles.

Igneous rocks from northwestern coastal Ecuador

The Pedernales and Esmeraldas sections are composed of hyaloclastites, pillow basalts, dolerites and isotropic gabbros.

The hyaloclastites (99PE16, 99PE19, 99ES1, 99ES5) consist of glass partially replaced by palagonite, which contains centimeter-sized, rounded picritic to basaltic fragments. The basaltic fragments are either composed of plagioclase and clinopyroxene microcrysts enclosed in a more or less altered glassy matrix or are aphyric with preserved glass. Clinopyroxene and plagioclase microcrysts are quenched. The picritic fragments consist of quenched olivine and Cr-spinel enclosed in a preserved glass. The petrology, geochemistry and dating of the picrite is the subject of a distinct paper (Mamberti et al., in preparation).

The pillow lavas (97PE5, 97PE6, 99PE22) are composed of clinopyroxene and plagioclase phenocrysts enclosed in a groundmass formed of abundant quenched plagioclase and clinopyroxene microlites. Plagioclase (up to 0.8 millimeters long) is altered to albite and exhibits bow tie and/or dendritic quenched textures. Clinopyroxene clusters into glomeroporphyritic aggregates and is sometimes replaced by calcite (97PE5 and 97PE6). Sample 99PE21 represents the glassy matrix of the pillows.

Basalts (97PE13, 99PE15, 99PE20) are aphyric with rare clinopyroxene, olivine (only in 97PE13) and plagioclase phenocrysts. Olivine is completely altered to smectite. Plagioclase is replaced by albite and epidote. The matrix is transformed into smectite and prehnite and locally is crosscut by calcite- and quartz-filled cracks.

The dolerites (97PE14, 99PE24, 99PE25, 99ES8) and isotropic gabbro (99PE11) exhibit ophitic textures with plagioclase phenocrysts. Most of these rocks consist of millimeter-sized plagioclase laths cemented by clinopyroxene and late crystallizing oxides. 97PE14 differs from the other dolerites by the presence of olivine microcrysts partially or completely replaced by serpentine. When the core of olivine is preserved, it is a forsterite Fo_{73-75}. Clinopyroxene composition ranges from diopside to augite (Wo_{43-46}, En_{43-48}, Fs_{9-12}). When plagioclase is preserved, it has a bytownite and labrador composition (An_{80-82} and An_{65}, respectively). The late crystallizing oxides fill the space in between the clinopyroxene and plagioclase. 99PE11 differs from the dolerites (99PE24 and 99PE25) by a coarser grain size.

ANALYTICAL METHODS

All the igneous rocks have variably experienced hydrothermal alteration. Thus, only the samples with well-preserved original igneous mineralogy (i.e., clinopyroxene, olivine, and plagioclase) and devoid of any significant alteration were selected for study. Minerals were separated and then purified by hand picking.

For Sr and Nd isotopic analyses, mineral separates and whole-rocks were leached in a 2 N HCl-0.1 N HF mixture. For Pb isotope determinations, mineral separates and whole rocks were successively leached in hot 2 N HCl for 20 min in an ultrasonic bath, and rinsed with tridistilled water in an ultrasonic bath for 15 min.

Major element analyses were performed by X-ray fluorescence at the Institut de Minéralogie et Pétrographie de l'Université de Lausanne (Switzerland). Trace elements were analyzed by inductively coupled plasma mass spectrometry (ICP-MS) at the University of Grenoble after acid dissolution. Trace elements are spiked with pure Tm using procedures described by Barrat et al. (1996). Standards used for the analyses were JB2, WSE, BIR-1, JR1, and UBN. Major and trace element analyses of host rocks and their mineral separates are presented in Tables 4.1 and 4.2.

The $^{143}Nd/^{144}Nd$ and $^{87}Sr/^{86}Sr$ isotopic data were determined on a Finnigan MAT261 multicollector mass spectrometer at the Laboratoire de Géochimie de l'Université Paul Sabatier (Table 4.3), using the analytical procedures of Lapierre et al. (1997). The chemical separation of lead was done following the procedure modified from Manhès et al. (1978). Total Pb blanks are less than 65 pg for a 100 mg sample. The Pb isotopic ratios were measured on the MC-ICP-MS P54 at the Ecole Nationale Supérieure de Lyon (Table 4.3). The complete isotopic data set has been corrected for in situ decay assuming an age of 90 Ma, based on the age of the CCOP oceanic plateau rocks.

Sample	99PE19	99PE20	99PE21	99PE22	97PE5	97PE6	97PE13	99ES1	99ES5	99ES8	97G5
Name	Hyaloclastic Basalt	Basalt	Glass	Pillow	Pillow Basalt	Pillow Basalt	Lava Basalt	Hyaloclastic	Hyaloclastic	Dolerite	Picrite
Locality	Pedernales	Pedernales	Pedernales	Pedernales	Pedernales	Pedernales	Pedernales	Esmeraldas	Esmeraldas	Esmeraldas	Guaranda
SiO_2	52.9	52.3	52.6	51.8	50.3	51.4	51.5	50.9	50.6	50.1	43.7
TiO_2	1.34	1.30	1.07	0.99	0.99	1.03	1.16	1.03	1.14	0.92	0.78
Al_2O_3	14.1	13.9	14.8	14.6	14.4	14.9	13.3	15.2	15.1	14.3	10.2
FeO	12.8	13.1	12.8	10.8	11.1	9.8	11.9	11.7	12.7	11.1	13.5
MnO	0.25	0.24	0.31	0.21	0.22	0.18	0.28	0.21	0.23	0.16	0.21
MgO	7.40	7.60	7.48	8.73	8.42	7.64	7.79	8.45	8.91	8.69	19.85
CaO	8.89	9.29	8.12	10.49	11.24	12.91	11.23	10.70	9.51	12.22	10.87
Na_2O	1.33	1.70	2.22	2.15	3.03	1.90	2.29	1.23	0.92	2.04	0.39
K_2O	0.87	0.52	0.55	0.22	0.22	0.20	0.55	0.45	0.69	0.30	0.05
P_2O_5	0.11	0.11	0.07	0.08	0.07	0.05	0.14	0.08	0.08	0.08	0.09
Cr_2O_3	0.01	0.01	0.03	0.03	-	-	-	-	-	-	0.24
NiO	0.01	0.01	0.01	0.01	-	-	-	-	-	-	0.10
LOI	5.91	4.15	3.69	2.07	3.14	2.13	2.79	4.69	8.12	1.01	5.49
Total	100	100	100	100	100	100	100	100	100	100	100
Ba	468.49	93.45	33.47	7.75		25.9	133	33	996	128	19.9
Rb	9.55	4.74	4.70	1.02	2.57	0.82	9.59	7.76	12.45	1.52	0.77
Sr	648	247	249	162	166	87	577	448.0	765	103	14.6
Ta	0.24	0.24	0.20	0.23	0.22	0.23	0.24	0.20	0.22	0.33	0.07
Th	0.23	0.23	0.20	0.19	0.23	0.24	0.21	0.19	0.21	0.17	0.05
Zr	58.0	58.3	46.8	46.4	51.1	52.1	55.8	53.33	61	45	29.5
Nb	3.39	3.52	3.14	3.08	3.26	3.30	3.75	3.25	3.83	2.94	1.63
Y	24.8	25.2	23.3	20.6	21.4	20.4	23.8	20.99	24.7	19.06	15.0
Hf	1.60	1.69	1.33	1.36	1.45	1.50	1.58	1.35	1.41	1.27	0.88
V	434	420	394	335	-	-	-	363	372	297	245
Cr	71	76	223	169	-	-	-	394	392	289	1246
Ni	77	76	107	103	-	-	-	130	134	128	837
Co	43.4	42.1	45.4	43.0	47.0	42.3	46.6	47	54	44	100
U	0.10	0.08	0.07	0.07	0.13	0.09	0.10	0.06	0.09	0.05	0.02
Pb	0.38	0.41	0.48	0.33	0.41	0.55	0.38	0.27	0.59	260	0.39
Sc	80	86	101	63	-	-	-	72	91	44	29
Cu	120	108	76	94	-	-	-	142	139	98	3
Zn	100	101	85	82	-	-	-	79	82	61	84
La	2.99	3.03	2.37	2.55	2.67	2.71	2.89	2.65	2.91	2.42	1.12
Ce	7.97	8.32	6.46	6.73	7.24	7.37	7.92	7.08	7.72	6.29	3.59
Pr	1.28	1.29	1.03	1.06	1.15	1.17	1.25	1.12	1.25	1.03	0.68
Nd	6.43	6.48	5.26	5.36	5.90	5.90	6.40	5.87	6.31	5.32	3.90
Sm	2.22	2.16	1.81	1.82	1.94	1.95	2.14	2.02	2.15	1.85	1.53
Eu	0.86	0.84	0.77	0.69	0.76	0.76	0.83	0.73	0.83	0.68	0.57
Gd	3.17	3.12	2.64	2.57	2.66	2.64	2.93	2.69	2.70	2.59	2.06
Tb	0.59	0.61	0.52	0.48	0.49	0.48	0.54	0.51	0.53	0.46	0.37
Dy	3.85	3.92	3.45	3.21	3.33	3.26	3.66	3.38	3.54	3.22	2.36
Ho	0.86	0.90	0.81	0.73	0.74	0.71	0.82	0.79	0.74	0.68	0.50
Er	2.56	2.57	2.31	2.10	2.13	2.04	2.36	2.02	2.09	1.85	1.39
Tm	-	-	-	-	-	-	-	-	-	-	-
Yb	2.49	2.51	2.17	2.00	2.02	1.95	2.25	2.08	2.16	1.94	1.20
Lu	0.38	0.41	0.35	0.33	0.32	0.31	0.36	0.32	0.34	0.30	0.18
(Ce/Yb)n	0.83	0.86	0.77	0.87	0.93	0.98	0.91	0.88	0.92	0.84	0.78
(La/Sm)n	0.85	0.89	0.82	0.88	0.87	0.88	0.85	0.83	0.85	0.83	0.53
(La/Yb)n	0.81	0.82	0.74	0.86	0.89	0.94	0.86	0.86	0.91	0.84	0.73

Sample	97G6	98G5	98G6	98G7	98G8	97G2	99PE11	99PE24	99PE25	97PE14	98G10
Name	Picrite	Picrite	Picrite	Picrite	Picrite	Dolerite	Doleritic Gabbro	Dolerite	Dolerite	Dolerite	Ankaramite
Locality	Guaranda	Guaranda	Guaranda	Guaranda	Guaranda	Guaranda	Galán	Pedernales	Pedernales	Pedernales	Guaranda
SiO_2	44.6	44.9	42.9	47.1	44.6	53.6	51.1	49.4	49.6	66.4	49.0
TiO_2	0.56	0.54	0.83	0.56	0.78	1.47	1.67	0.88	1.08	0.43	1.15
Al_2O_3	7.1	7.0	10.8	7.6	10.3	15.3	14.4	14.7	15.8	10.0	12.1
FeO	11.6	11.1	12.1	10.3	11.6	13.6	13.4	10.5	11.1	5.5	11.5
MnO	0.18	0.18	0.20	0.17	0.20	0.19	0.23	0.16	0.19	0.10	0.19
MgO	27.26	27.29	22.21	23.04	21.53	6.25	5.54	8.87	7.20	7.06	10.46
CaO	7.89	8.33	10.05	10.38	10.09	5.30	9.89	13.28	11.84	9.15	11.70
Na_2O	0.05	0.02	0.24	0.21	0.36	3.88	3.08	1.97	2.81	1.19	3.35
K_2O	0.03	0.01	0.01	0.02	0.01	0.23	0.46	0.13	0.22	0.23	0.14
P_2O_5	0.05	0.04	0.06	0.05	0.06	0.12	0.14	0.06	0.09	0.02	0.25
Cr_2O_3	0.42	0.37	0.43	0.31	0.36	0.02	0.01	0.04	0.01	-	0.08
NiO	0.24	0.23	0.16	0.18	0.13	0.01	0.01	0.02	0.01	-	0.03
LOI	7.10	7.06	5.96	5.32	6.37	7.16	1.92	-0.02	1.99	3.26	1.89
Total	100	100	100	100	100	100	100	100	100	100	100
Ba	15.69	5.14	5.68	8.20	5.63	39.2	30.6	19.5	23.9	23.2	49.6
Rb	1.42	1.44	0.60	0.53	0.48	2.74	4.00	1.47	1.22	8.75	0.81
Sr	31.01	25.1	11.6	12.0	11.4	172	118	121	133	139	152
Ta	0.04	0.04	0.06	0.04	0.05	0.24	0.34	0.16	0.21	0.10	0.34
Th	0.04	0.03	0.04	0.03	0.04	0.26	0.33	0.15	0.21	0.10	0.25
Zr	24.76	22.6	33.4	24.6	32.5	60.0	66.6	38.3	49.2	26.2	58.0
Nb	0.60	0.56	0.80	0.62	0.84	4.06	5.25	2.35	3.08	1.53	7.57
Y	8.76	8.20	12.2	8.90	12.2	25.5	29.6	18.6	21.5	13.0	17.4
Hf	0.72	0.65	0.96	0.71	0.94	1.66	1.96	1.15	1.40	0.82	1.55
V	193	179	278	196	282	551	411	272	321	-	341
Cr	1952	1298	2630	1554	1910	161	35	231	65	-	519
Ni	1346	1178	867	995	841	87	48	129	87	-	220
Co	90.68	88.2	72.9	79.0	74.4	50.4	39.7	49.0	45.1	42.5	60.5
U	0.01	0.01	0.01	0.01	0.01	0.12	0.11	0.05	0.07	0.04	0.08
Pb	0.62	0.09	0.09	0.09	0.08	0.37	0.16	0.33	0.44	0.24	0.91
Sc	25	61	75	65	81	83	54	45	46	-	52
Cu	-	11	62	48	18	103	16	80	151	-	91
Zn	72	63	76	62	71	117	58	87	72	-	95
La	0.65	0.58	0.87	0.61	0.83	3.63	3.36	2.25	3.56	1.44	3.50
Ce	2.13	2.00	2.99	2.13	2.93	9.94	10.21	6.14	8.73	4.05	8.50
Pr	0.42	0.38	0.57	0.41	0.57	1.60	1.68	0.99	1.32	0.66	1.37
Nd	2.53	2.28	3.44	2.49	3.42	7.94	8.91	4.99	6.30	3.41	7.04
Sm	1.01	0.92	1.36	0.99	1.38	2.70	2.85	1.74	2.09	1.18	2.30
Eu	0.38	0.36	0.57	0.39	0.50	0.96	1.11	0.71	0.81	0.52	0.83
Gd	1.36	1.25	1.87	1.39	1.89	3.10	3.89	2.32	2.75	1.68	2.78
Tb	0.25	0.23	0.34	0.25	0.34	0.64	0.72	0.46	0.51	0.32	0.49
Dy	1.59	1.44	2.15	1.58	2.18	4.26	4.73	2.86	3.35	2.11	3.10
Ho	0.31	0.30	0.46	0.33	0.46	0.92	1.07	0.65	0.74	0.47	0.63
Er	0.80	0.80	1.20	0.88	1.21	2.48	3.00	1.81	2.11	1.33	1.61
Tm	-	-	-	-	-	0.40	-	-	-	-	-
Yb	0.75	0.72	1.06	0.78	1.07	2.65	2.85	1.68	1.95	1.27	1.52
Lu	0.11	0.11	0.16	0.12	0.16	0.40	0.44	0.27	0.31	0.19	0.22
(Ce/Yb)n	0.73	0.72	0.73	0.71	0.71	0.97	0.93	0.95	1.16	0.83	1.44
(La/Sm)n	0.41	0.40	0.40	0.39	0.38	0.85	0.74	0.81	1.07	0.77	0.96
(La/Yb)n	0.58	0.55	0.55	0.53	0.52	0.92	0.80	0.91	1.23	0.77	1.55

Sample	98G11	98G12	97G4	98G4	98G9	98P3	98P7	98P8	98P10	99PE15	99PE16
Name	Ankaramite	Ankaramite	Ankaramite	Ankaramite	Ankaramite	Basalt	Basalt	Basalt	Pillow Basalt	Basalt	Hyaloclastite Basalt
Locality	Guaranda	Guaranda	Guaranda	Guaranda	Guaranda	Pallatanga	Galán	Galán	Galán	Pedernales	Pedernales
SiO_2	48.4	43.4	47.6	48.0	46.6	53.4	48.9	50.8	53.0	52.0	52.1
TiO_2	1.11	1.38	1.28	1.28	0.98	1.30	0.98	0.92	1.27	1.28	0.98
Al_2O_3	11.7	14.6	12.2	11.2	8.89	14.1	14.6	14.1	13.3	14.2	14.4
FeO	10.6	12.7	12.6	12.6	12.5	12.0	12.0	11.0	11.7	12.9	10.8
MnO	0.18	0.20	0.20	0.19	0.20	0.19	0.20	0.19	0.21	0.20	0.18
MgO	9.93	8.47	12.11	12.99	17.44	8.18	9.00	8.95	6.78	7.19	8.37
CaO	15.44	18.02	11.26	11.49	12.51	5.93	11.22	10.25	9.49	7.87	11.39
Na_2O	2.21	0.81	1.67	1.42	0.42	4.54	2.95	3.54	4.09	0.84	1.10
K_2O	0.10	0.10	0.76	0.57	0.03	0.17	0.04	0.08	0.04	3.43	0.44
P_2O_5	0.17	0.21	0.10	0.11	0.08	0.10	0.08	0.08	0.11	0.11	0.08
Cr_2O_3	0.11	0.05	0.16	0.12	0.23	0.02	0.04	0.04	0.02	0.02	0.04
NiO	0.02	0.02	0.06	0.06	0.09	0.01	0.01	0.01	0.01	0.01	0.01
LOI	1.34	2.38	2.89	2.57	3.93	2.76	2.56	3.10	2.61	5.76	6.05
Total	100	100	100	100	100	100	100	100	100	100	100
Ba	44.8	16.43	133	116	6.62	47.51	21.72	27.23	16.33	77.79	30.97
Rb	0.54	0.68	11.82	7.71	0.51	2.35	0.75	0.71	0.18	20.94	7.44
Sr	267	757	85.5	61.8	14.6	128	78.5	86.9	101	205	192
Ta	0.30	0.40	0.18	0.21	0.27	0.23	0.18	0.24	0.23	0.24	0.20
Th	0.23	0.34	0.22	0.25	0.21	0.24	0.18	0.17	0.20	0.22	0.19
Zr	54.2	72.0	51.0	69.0	27.1	60.6	49.3	45.1	59.3	56.1	43.7
Nb	6.45	9.44	3.22	4.48	3.25	4.34	3.44	3.61	3.51	3.58	2.87
Y	17.0	20.6	19.4	17.0	8.25	24.5	20.3	18.1	23.8	23.5	18.8
Hf	1.51	1.95	1.48	1.78	0.76	1.72	1.31	1.27	1.71	1.57	1.23
V	353	317	355	318	290	437	334	334	418	430	357
Cr	668	321	989	742	1282	134	243	247	132	111	241
Ni	167	172	388	400	588	98	109	108	87	75	103
Co	54.0	57.3	73.9	72.0	75.1	44.5	49.4	43.8	41.2	41.9	40.9
U	0.07	0.12	0.08	0.08	0.05	0.08	0.06	0.06	0.08	0.08	0.05
Pb	1.51	3.23	0.44	0.27	0.27	0.36	0.32	0.30	0.37	0.39	0.30
Sc	52	45	32	55	68	85	74	73	58	75	80
Cu	217	111	26	18	13	90	63	64	110	106	91
Zn	83	83	104	94	81	102	90	81	102	98	80
La	3.57	4.80	3.87	3.69	2.43	3.37	2.57	2.29	2.85	2.89	2.36
Ce	8.17	11.11	10.45	10.02	7.01	8.58	6.64	5.90	7.56	7.74	6.27
Pr	1.37	1.81	1.62	1.64	1.16	1.36	1.05	0.94	1.23	1.24	0.98
Nd	7.13	9.20	7.69	8.54	6.11	7.04	5.42	4.86	6.46	6.25	5.05
Sm	2.31	2.89	2.24	2.68	2.02	2.36	1.87	1.63	2.19	2.09	1.70
Eu	0.86	1.05	0.85	0.96	0.77	0.90	0.68	0.62	0.74	0.82	0.66
Gd	2.81	3.34	2.82	3.16	2.54	3.17	2.50	2.25	3.07	2.90	2.36
Tb	0.50	0.59	0.50	0.52	0.45	0.61	0.48	0.43	0.59	0.56	0.45
Dy	3.11	3.72	3.19	3.22	2.71	4.17	3.29	2.95	4.10	3.70	3.00
Ho	0.63	0.75	0.66	0.63	0.54	0.91	0.72	0.67	0.90	0.83	0.67
Er	1.57	1.93	1.79	1.55	1.43	2.43	1.97	1.79	2.51	2.44	1.91
Tm	-	-	-	-	-	-	-	-	-	-	-
Yb	1.47	1.79	1.46	1.36	1.25	2.54	2.08	1.88	2.66	2.37	1.88
Lu	0.22	0.26	0.20	0.20	0.18	0.39	0.33	0.30	0.41	0.37	0.30
(Ce/Yb)n	1.44	1.60	1.85	1.91	1.45	0.88	0.83	0.81	0.74	0.85	0.86
(La/Sm)n	0.98	1.04	1.09	0.87	0.76	0.90	0.86	0.88	0.82	0.87	0.88
(La/Yb)n	1.64	1.81	1.79	1.83	1.31	0.90	0.84	0.82	0.73	0.82	0.85

Table 4.1: Major (wt%) and trace element (ppm) analyses for the Guaranda, Galán and Pedernales samples. -: not analysed.

Sample	97G4	98G4	98G4-2	98G9	98G12	98G12	97G5	97G6	98G5	98G7	98G7
Host Rock	Cpx	Cpx	Cpx	Cpx	Cpx	Cpx	Cpx	Cpx	Cpx	Cpx	Cpx
	Ankaramite	Ankaramite	Ankaramite	Ankaramite	Ankaramite	Ankaramite	Picrite	Picrite	Picrite	Picrite	Picrite
Fraction (µm)	100/125	80/100	100/125	125/160	80/100	100/125	100/125	100/125	100/125	80/100	100/125
Ba	18.85	29.86		2.38	2.29		-	-	5.20	6.26	
Rb	3.12	1.59		0.07	0.11		0.27	0.57	0.54	0.40	
Sr	13.58	24.22		11.78	32.45		12.59	22.85	21.17	15.76	
Ta	0.00	0.07		0.01	0.03		0.01	0.03	0.06	0.05	
Th	-	0.08		0.01	0.02		0.00	0.02	0.04	0.04	
Zr	9.55	35.55		10.94	17.79		10.54	25.01	29.35	29.18	
Nb	0.07	1.09		0.09	0.57		0.09	0.47	0.85	0.69	
Y	7.77	-		-	-		8.55	10.31	-	-	
Hf	0.44	1.35		0.55	0.92		0.49	0.76	1.01	0.99	
Co	44.11	-		-	-		38.58	82.32	-	-	
U	-	0.04		0.01	0.02		-	-	0.02	0.02	
Zn	18.94	-		-	-		16.62	34.05	-	-	
La	0.24	1.12		0.31	0.49		0.17	0.54	0.68	0.74	
Ce	0.91	3.53		1.20	1.84		0.66	1.89	2.24	2.58	
Pr	0.22	0.66		0.26	0.40		0.18	0.37	0.43	0.51	
Nd	1.70	4.15		1.91	2.74		1.33	2.30	2.81	3.33	
Sm	0.81	1.62		0.91	1.20		0.71	0.99	1.18	1.33	
Eu	0.33	0.65		0.38	0.48		0.29	0.42	0.50	0.56	
Gd	1.22	2.31		1.46	1.87		1.16	1.39	1.76	1.98	
Tb	0.20	0.39		0.25	0.32		0.20	0.25	0.31	0.34	
Dy	1.46	2.59		1.70	2.18		1.48	1.71	2.12	2.36	
Ho	0.28	0.51		0.32	0.42		0.30	0.36	0.43	0.47	
Er	0.72	1.32		0.82	1.05		0.78	1.00	1.16	1.26	
Tm	2.71	0.18		0.11	0.14		2.69	2.73	0.16	0.17	
Yb	0.60	1.09		0.63	0.83		0.64	0.86	0.99	1.09	
Lu	0.08	0.16		0.10	0.13		0.10	0.13	0.16	0.17	
(Ce/Yb)n	0.40	0.84		0.49	0.57		0.27	0.57	0.58	0.61	
(La/Sm)n	0.18	0.44		0.21	0.25		0.15	0.34	0.36	0.35	
(La/Yb)n	0.27	0.69		0.33	0.39		0.18	0.42	0.46	0.46	
$^{143}Nd/^{144}Nd$		0.513052	0.513054	0.513086	0.513011	0.512991				0.513171	0.513179
2σ		±8	±22	±21	±25	±16				±16	±12
$^{147}Sm/^{144}Nd$		0.236020	0.236020	0.288067	0.264794	0.264793				0.241491	0.241492
$(^{143}Nd/^{144}Nd)i$		0.512913	0.512915	0.512916	0.512855	0.512835				0.513029	0.513037
ε(Nd)i		7.63	7.67	7.69	6.50	6.11				9.88	10.04

Table 4.2: Major (wt%), trace element (ppm), and isotopic analyses for the Guaranda mineral separates.

GEOCHEMISTRY

Major and trace elements

The degree of alteration of the analyzed rocks is more or less important. The loss of ignition (LOI, Table 4.1) varies between 1.3% and 7.1%. This geochemical study is based on the most immobile elements like the rare earth (REE) and high field strength elements (HFSE).

Major and trace element analyses of the samples from each group are reported in Table 4.1. Ankaramites and basalts exhibit a large range of MgO contents (6.78 to 17.44 wt%). In contrast, the dolerites and isotropic gabbro show a narrow range of MgO concentrations (5.5 to 8.9 wt%). The picrites differ from the basalts and ankaramites by significantly higher MgO contents (between 19.9% and 27.3 wt%). The major element plots (Fig. 4.4) confirm the distinction into two groups. The dolerites, basalts and ankaramites cluster into one package characterized by the highest contents in Al_2O_3 and SiO_2 (Fig. 4.4). Among the latter, CaO exhibits the largest range of abundances. This likely expresses alteration processes (i.e., calcite-filling vesicles or cracks). However, the ankaramites have the highest CaO contents (up to 18 %) probably related to the abundance of the clinopyroxene phenocrysts. Mafic rocks have also a wide range of trace element concentrations (TiO_2, Ni, Cr and Zr; Fig. 4.4) at approximatively constant MgO level (6-7 %). All the rocks including the picrites have relatively similar FeO concentrations (Fig. 4.4).

The picrites display a linear trend in all diagrams. They have the highest Cr and Ni contents, which correlate with the highest MgO values. Their abundance in incompatible trace elements like Zr and Ta are the lowest of the analyzed rocks. The most MgO-enriched picrite is relatively depleted in SiO_2, TiO_2, Al_2O_3 and CaO. In the Ni and Cr versus MgO plots (Fig. 4.4), the mafic rocks and picrites exhibit a nice correlation trend where the picrites and dolerites represent the less and the most differentiated rocks of this suite, respectively. This reflects the key role of olivine and clinopyroxene in the crystal fractionation of these rocks.

In the La versus Nb diagram (Fig. 4.5), the basalts and the ankaramites plot in the E-MORB field, while the picrites cluster in the N-MORB field. This confirms that picrites are more depleted in incompatible elements compared to the basalts.

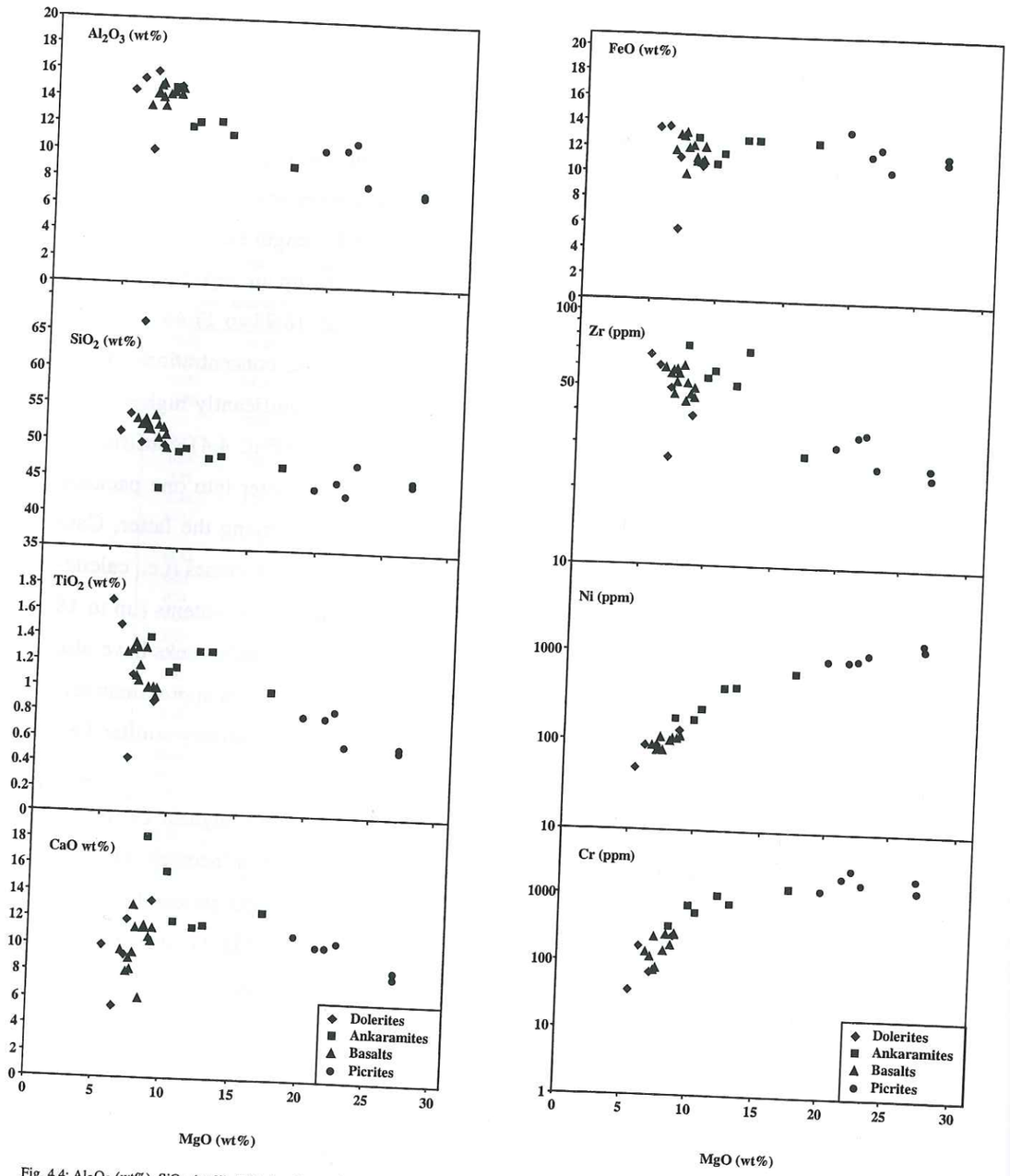

Fig. 4.4: Al_2O_3 (wt%), SiO_2 (wt%), TiO_2 (wt%), CaO (wt%), FeO (wt%), Zr (ppm), Ni (ppm), and Cr (ppm) vs MgO (wt%) correlation diagram of dolerites, ankaramites, basalts and picrites.

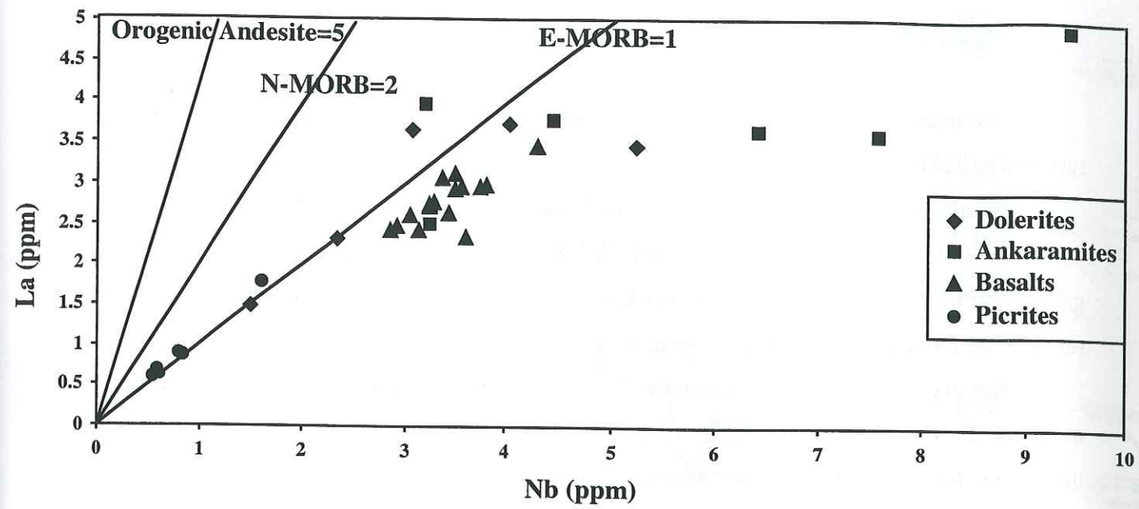

Fig. 4.5: La (ppm) vs Nb (ppm) correlation diagram of dolerites, ankaramites, basalts and picrites.

REE compositions of the igneous rocks and their host minerals

The trace element concentrations including the REE of the mafic and picritic rocks are reported in Table 4.1.

Basalts and dolerites have nearly flat REE patterns (Sun and McDonough, 1989) (Fig. 4.6) with (La/Yb)n ratios ranging between 0.73 and 0.94 (with the exception of the isotropic gabbro 99PE25, with a 1.23 higher ratio). Compared to the basalts, the dolerites have a wider range of REE contents and appear to be more fractionated.

Basalts and dolerites exhibit similar flat spiderdiagrams characterized by positive Sr and negative Th anomalies. The observed positive and negative anomalies of the large ion lithophile elements (LILE) reflect the alteration and/or low grade metamorphism experienced by these rocks. The isotropic gabbro (99PE25) differs from the dolerites by negative anomalies in Ti and P and lower contents in all the trace elements (Fig. 4.6).

Ankaramites exhibit light (L)REE-enriched patterns (Fig. 4.6; 1.8 < (La/Yb)n < 1.3). Compared to the basalts and dolerites, the ankaramites differ by a depletion in Heavy (H)REE and Y, and by an enrichment in Nb and Ta. The positive or negative Sr anomalies reflect plagioclase accumulation or removal. Clinopyroxene separates from four ankaramites (97G4, 98G4, 98G9, 98G12) are depleted in LREE [0.27 < (La/Yb)n < 0.69] and have lower REE contents compared to their host rocks (Fig. 4.6).

The picrites have low REE contents and hamped-shaped patterns, slightly depleted in LREE relative to the HREE (0.52 < (La/Yb)n < 0.73) (Fig. 4.6). The picrites exhibit negative anomalies in Th and Sr. They have low abundances in incompatible trace elements like Ta, Nb, Zr and Hf but show Ta and Nb positive anomalies. Clinopyroxenes separates from four picrites (97G5, 97G6, 98G5, 98G7) have, like those of the ankaramites, lower REE contents than their host rocks but are more depleted in LREE than those of the ankaramites (Fig. 4.7; 0.18 < (La/Yb)n < 0.46).

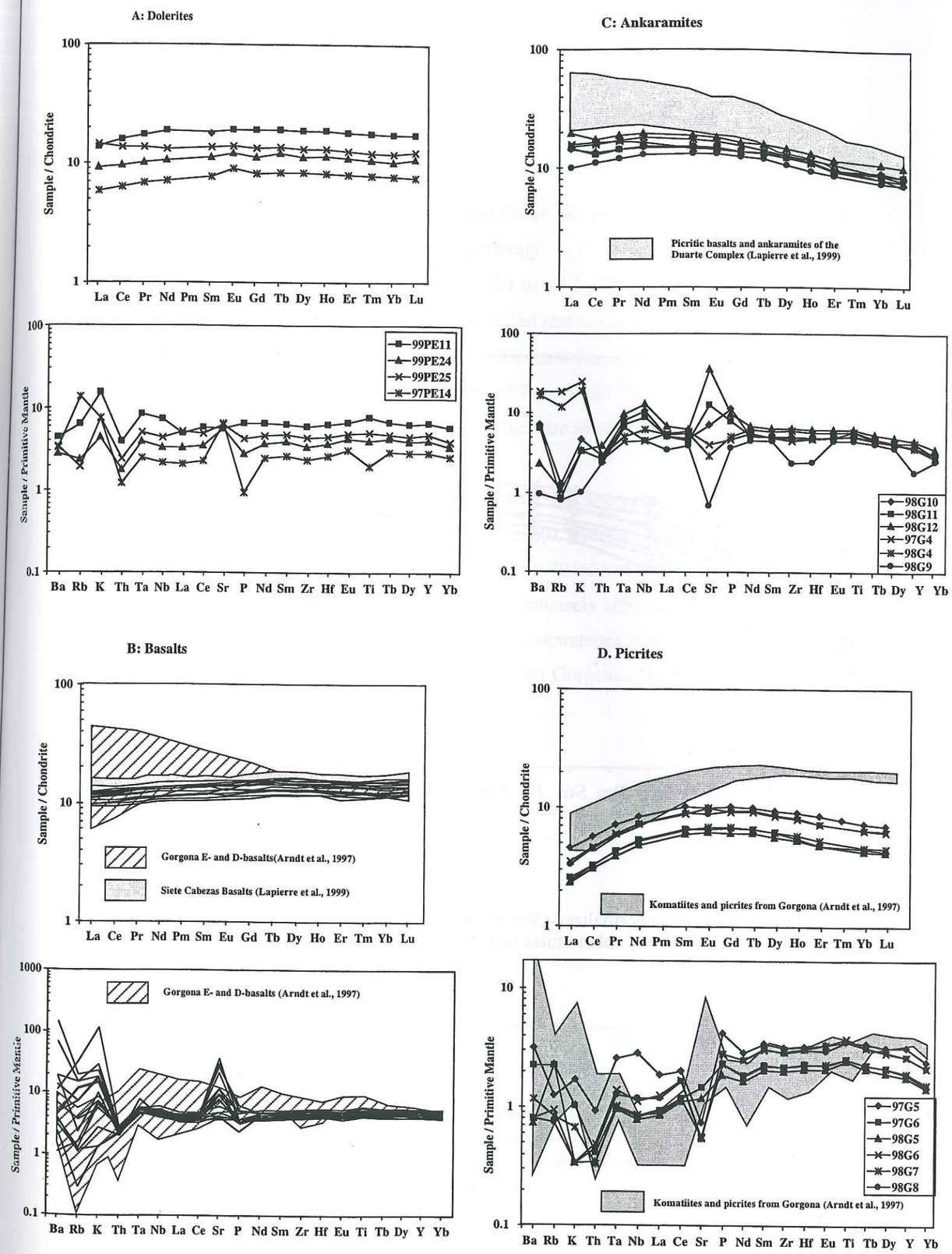

Fig. 4.6: Chondrite- and primitive-normalized (Sun & McDounough, 1989) rare earth element patterns and multi-element plots for dolerites (A), basalts (B), ankaramites (C), and picrites (D).

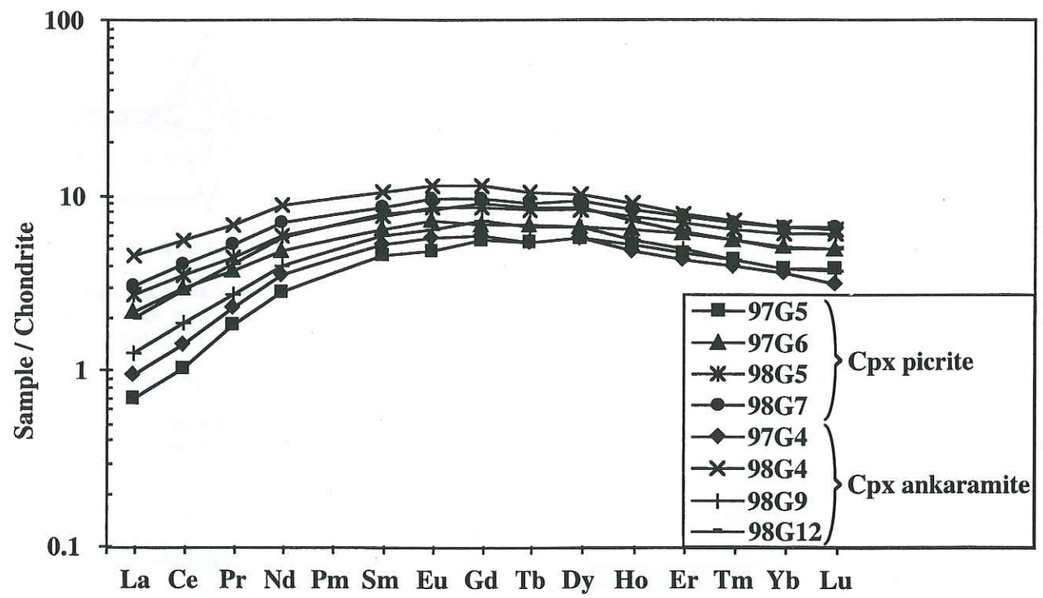

Fig. 4.7: Chondrite-normalized (Sun & McDonough, 1989) rare earth element patterns for cpx of picrites and ankaramites from Guaranda cross section.

Nd, Sr and Pb isotopic chemistry

The isotopic compositions of Nd, Sr and Pb of the studied rocks and their mineral separates are reported in Tables 4.2 and 4.3, respectively.

The basalts have the lowest εNd values (+6.1 to +9.2). The clinopyroxene separates of the ankaramites and whole rocks have rather similar and restricted range of εNd i (+7.0 to +8.2) which are slightly higher than those of the basalts (Tables 4.2 and 4.3). The picrites exhibit the highest and largest range of εNd values (between +7.7 to +10.2). The clinopyroxene separates from the picrite (98G7) have also the highest εNd which are similar with that of the whole rock (Tables 4.2 and 4.3; Fig. 4.8; +9.88 and +10.04)

The ankaramites exhibit a restricted range of ($^{87}Sr/^{86}Sr$)i ratios (0.70301 to 0.70348) while the Sr ratios of the picrites are lowest ($^{87}Sr/^{86}Sr$)i (0.70297 to 0.70311) (Table 4.3). The basalts span a large range of ($^{87}Sr/^{86}Sr$)i (0.70416 to 0.70469) which are the highest of the studied rocks and suggest that the basalts were more intensely affected by alteration than the picrites and ankaramites (Fig. 4.8). In figure 4.8, the ankaramites plot in the Galápagos field and near that of the depleted and enriched basalts from Gorgona. The picrites cluster in the Gorgona komatiites field.

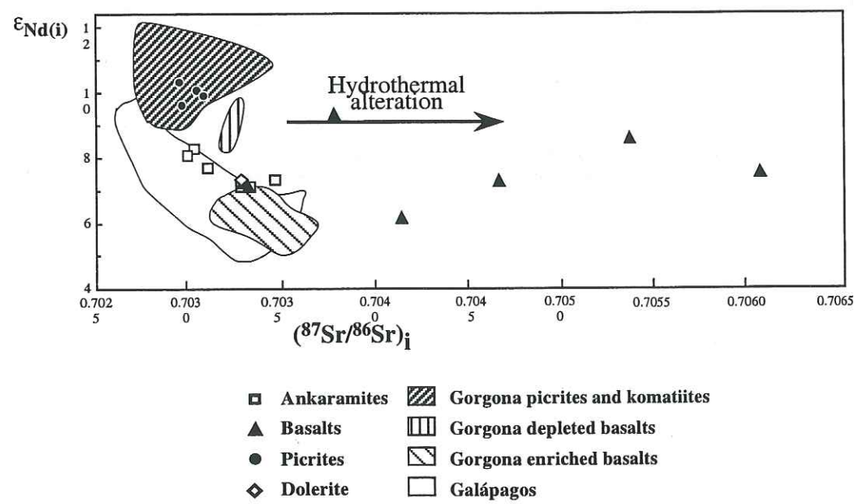

Fig. 4.8: The εNd -($^{87}Sr/^{86}Sr$)*i* plots for ankaramites, picrites and basalts from the Guaranda cross section.

Sample	Name	$(^{206}Pb/^{204}Pb)i$	$(^{207}Pb/^{204}Pb)i$	$(^{208}Pb/^{204}Pb)i$	$(^{87}Sr/^{86}Sr)m$	2σ	$^{87}Rb/^{86}Sr$	$(^{87}Sr/^{86}Sr)t$	ε (Sr)i	Sm	Nd	Sm/Nd	$(^{143}Nd/^{144}Nd)m$	2σ	$^{147}Sm/^{144}Nd$	$(^{143}Nd/^{144}Nd)i$	ε(Nd)i
97G2	Dolerite	19.24	15.55	38.79						2.70	7.94	0.34					
99PE11	Gabbro									2.85	8.91	0.32					
97PE14	Dolerite				0.705110	±6	0.18247	0.704877	6.85	1.18	3.41	0.35	0.513017	±12	0.21172	0.512892	7.22
99PE24	Dolerite									1.74	4.99	0.35					
99PE25	Dolerite	18.80	15.56	38.40	0.703632	±6	0.02657	0.703598	-11.30	2.09	6.30	0.33					
99ES8	Dolerite																
97G4	Ankaramite	18.81	15.52	38.46	0.703568	±9	0.39982	0.703057	-18.99	2.24	7.69	0.29	0.513046	±9	0.17612	0.512942	8.20
98G4	Ankaramite	18.58	15.53	38.39	0.703476	±9	0.36080	0.703015	-19.59	2.68	8.54	0.31	0.513043	±5	0.18969	0.512931	7.98
98G9	Ankaramite	19.59	15.59	39.12	0.703261	±12	0.10152	0.703131	-17.93	2.02	6.11	0.33	0.513030	±7	0.19956	0.512913	7.62
98G10	Ankaramite	19.71	15.61	39.19	0.703327	±8	0.01539	0.703307	-15.43	2.30	7.04	0.33	0.512999	±7	0.19796	0.512882	7.03
98G11	Ankaramite	19.67	15.61	39.19	0.703487	±18	0.00581	0.703480	-12.99	2.31	7.13	0.32	0.513009	±5	0.19541	0.512894	7.25
98G12	Ankaramite	19.65	15.60	39.17	0.703352	±8	0.00260	0.703349	-14.84	2.89	9.20	0.31	0.512994	±5	0.19016	0.512882	7.02
97PE5	Pillow				0.705007	±6	0.04503	0.704949	7.88	1.98	5.87	0.34					
97PE6	Pillow				0.703385	±7	0.02925	0.703348	-14.86	1.92	5.84	0.33	0.513001	±9	0.19833	0.512884	7.06
97PE13	Basalt				0.706341	±8	0.16745	0.706127	24.60	2.15	6.47	0.33	0.513023	±7	0.20042	0.512905	7.47
98P3	Basalt				0.704760	±15	0.05336	0.704692	19.18	2.36	7.04	0.33	0.513010	±12	0.20240	0.512891	7.19
98P7	Basalt	18.98	15.58	38.54						1.87	5.42	0.35	0.513059	±6	0.20886	0.512936	8.07
98P8	Basalt	18.82	15.59	38.40						1.63	4.86	0.34	0.513060	±7	0.20312	0.512940	8.16
98P10	Pillow				0.704169	±10	0.00521	0.704162	-3.29	2.19	6.46	0.34	0.512954	±9	0.20515	0.512833	6.07
99PE15	Basalt									2.09	6.25	0.33					
99PE16	Hyaloclastite	19.01	15.56	38.63	0.703940	±6	0.11203	0.703797	-8.48	1.70	5.05	0.34	0.513115	±34	0.20324	0.512995	9.23
99PE19	Basalt	18.34	15.60	38.08	0.706320	±8	0.04265	0.706265	26.56	2.22	6.43	0.34					
99PE20	Basalt	18.86	15.55	38.56	0.705482	±7	0.05549	0.705411	14.44	2.16	6.48	0.33					
99PE21	Glass	18.66	15.59	38.39	0.706138	±7	0.05446	0.703315	-15.32	1.81	5.26	0.34	0.513012	±7	0.20795	0.512890	7.17
99PE22	Pillow	18.94	15.51	38.51	0.705430	±6	0.01824	0.705407	14.37	1.82	5.36	0.34	0.512074	±7	0.2047	0.512954	8.48
99ES1	Hyaloclastite	18.27	15.59	37.98													
99ES5	Hyaloclastite	18.56	15.57	38.32													
97G5	Picrite	18.31	15.46	38.05						0.91	3.18	0.29	0.513021	±10	0.17302	0.512919	7.74
97G6	Picrite				0.703133	±12	0.12656	0.702971	-20.20	0.65	2.05	0.32	0.513160	±10	0.19171	0.513047	10.24
98G5	Picrite	18.71	15.55	38.64	0.703201	±13	0.16646	0.702988	-19.96	0.92	2.28	0.40	0.513155	±15	0.24396	0.513011	9.54
98G6	Picrite	18.31	15.48	38.11	0.703257	±13	0.14851	0.703067	-18.84	1.36	3.44	0.39	0.513174	±9	0.23836	0.513034	9.98
98G7	Picrite	18.40	15.49	38.10	0.703274	±13	0.12916	0.703109	-18.25	0.99	2.49	0.40	0.513169	±22	0.24149	0.513027	9.85
98G8	Picrite	18.29	15.49	38.06			0.11262			1.38	3.42	0.40	0.513178	±7	0.24443	0.513034	9.99

Table 4.3: Nd, Sr and Pb isotopic compositions for the Guaranda, Pallatanga, Pedernales and Esmeraldas rocks and mineral separates.
(m): ratios measured; (i): initial recalculated ratios (90Ma) based on the U, Th and Pb contents determinated by ICP-MS (refer Table 1).

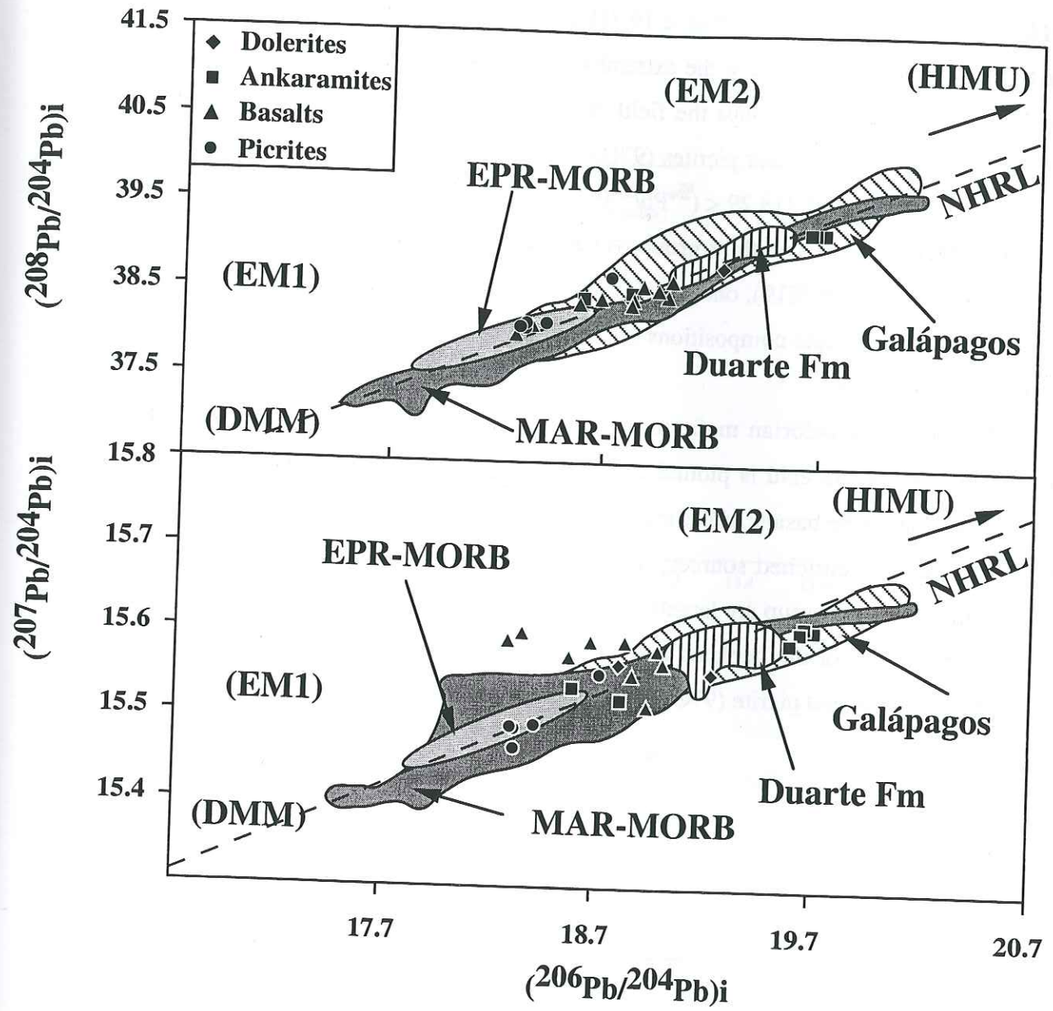

Fig. 4.9: $(^{208}Pb/^{204}Pb)i$ vs $(^{206}Pb/^{204}Pb)i$ and $(^{207}Pb/^{204}Pb)i$ vs $(^{206}Pb/^{204}Pb)i$ diagrams for dolerites, ankaramites, basalts and picrites. The "Northern Hemisphere Reference Line" (NHRL) and the field from some mantle reservoirs are reported after Zindler & Hart (1986). East Pacific Rise (EPR) MORB and Mid Atlantic Ridge (MAR) MORB data and Galapagos Islands field are from White et al. (1987). The Duarte field is reported after Lapierre et al. (1997).

Lead initial isotopic compositions of the whole rocks are reported in Table 4.3 and cluster into three groups in the Pb/Pb correlation diagrams (Fig. 4.9). The first group, constituted by the most radiogenic Pb samples, consists of the ankaramites (98G9, 98G10, 98G11, 98G12) ($19.59 < (^{206}Pb/^{204}Pb)i < 19.71$) and plots into two distinct fields, one located close to the Galápagos lavas and at the extremity of the more radiogenic samples of the Duarte Complex, and the second overlaps the field of the Mid-Atlantic Ridge (MAR)-MORB. The second group, composed of four picrites (97G5, 98G6, 98G7, 98G8) and one basalt (99PE19) is the least radiogenic in Pb ($18.29 < (^{206}Pb/^{204}Pb)i < 18.40$). This group plots in the East Pacific Rise (EPR)-MORB field. The third group which is composed of all the dolerites and basalts (with the exception of 99PE19), one picrite (98G5) and two ankaramites (97G4 and 98G4), is characterized by Pb isotopic compositions ($18.56 < (^{206}Pb/^{204}Pb)i < 19.01$) intermediate between the groups 1 and 2.

Most of the Ecuadorian mafic to ultramafic lavas display a linear but discontinuous trend in diagrams where εNd is plotted against MgO, (La/Yb)n and $(^{206}Pb/^{204}Pb)i$ (Fig. 4.4). This suggests that (i) the basalts, dolerites, and one picrite (98G5) could derive from the mixing of both depleted and enriched sources; (ii) the variations of the MgO content and (La/Yb)n ratios within each rocks group are largely dependant on the partial melting percentages. The Pb isotopic compositions of the depleted and enriched sources end-members could be similar to those of the most depleted picrite (97G6) and enriched ankaramite (98G12; Table 4.3).

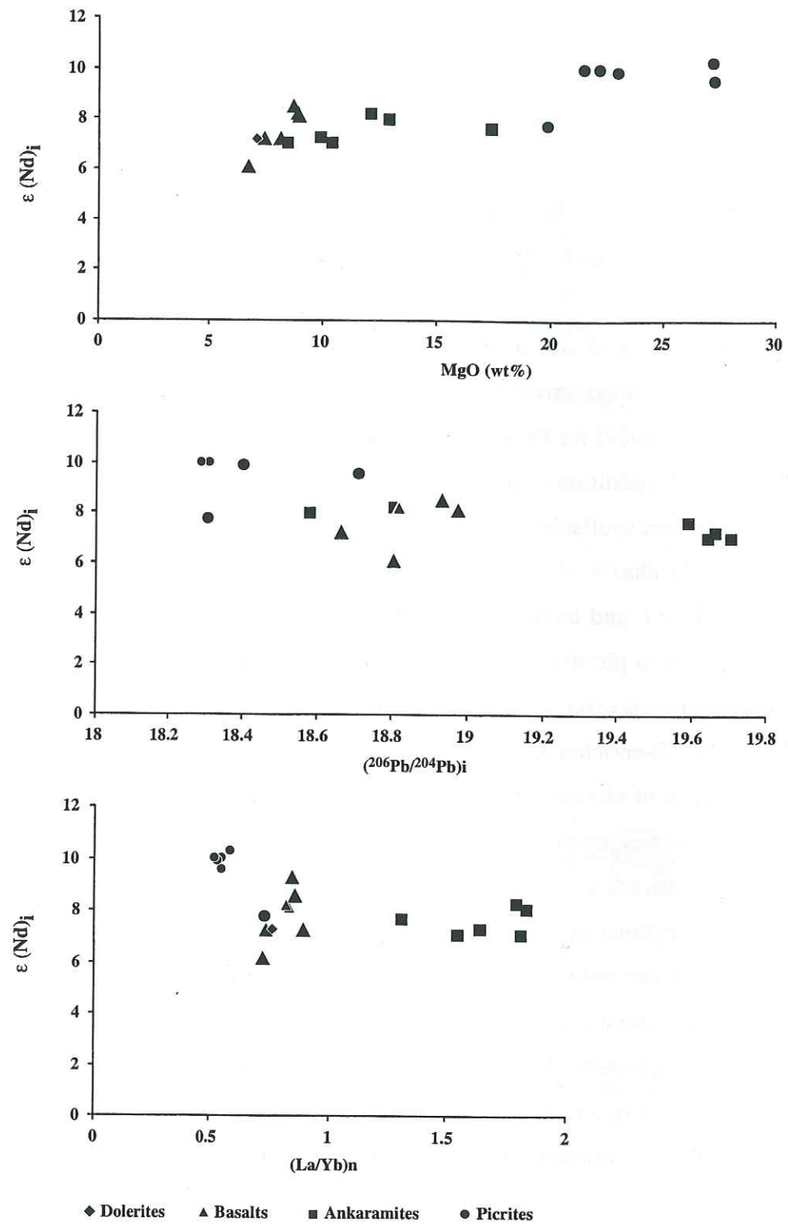

Fig. 4.10: εNd vs MgO (wt%), $(^{206}Pb/^{204}Pb)i$, and (La/Yb)n correlation diagrams for ankaramites, basalts and picrites from Guaranda and Pedernales sequences.

Calculated melts in equilibrium with the clinopyroxenes

Eight clinopyroxenes were separated from ankaramitic and picritic host rocks. The trace element compositions of the clinopyroxene separates (including the REE) are reported in Table 4.2.

The REE compositions of the parent melts in equilibrium with the clinopyroxene separates from picrites and ankaramites were calculated using the partition coefficients of Ulmer (1989) and Shimizu (1982) for the picrites, and of Hart and Dunn (1993) for the basalts. It was difficult to choose the partition coefficient for the ankaramites because such coefficients for ankaramitic melts are not available in the literature. So, we used, for the ankaramites, the partition coefficients for basalts.

Picritic (Fig. 4.11-A). and ankaramitic (Fig. 4.11-B). melts in equilibrium with the clinopyroxene separates from picrites and ankaramites share in common with the host rocks similar LREE-depleted patterns (except for 97G5). However, these theoretical melts differ from the lavas by a slightly LREE-enrichment ($1.02 < (La/Yb)n < 1.11$) and higher REE abundances This is due to the presence of olivine that leads to a dilution of the REE contents in the host rock. This reflects also the key role of clinopyroxenes in controlling REE abundances of the Ecuadorian picrites and ankaramites.

Two rocks are exceptions and illustrate the complexity of using partition coefficients. The REE composition of the calculated melts using picrite 97G5 and ankaramite 98G4 clinopyroxene separates match only with the host rocks on the basis of the partition coefficients for basalt and picrite, respectively. This is the opposite of what we should expect. This is probably linked to differences in temperature and/or pressure for condition of crystallization of these two rocks (97G5, 98G4), compared to the others picrites and ankaramites.

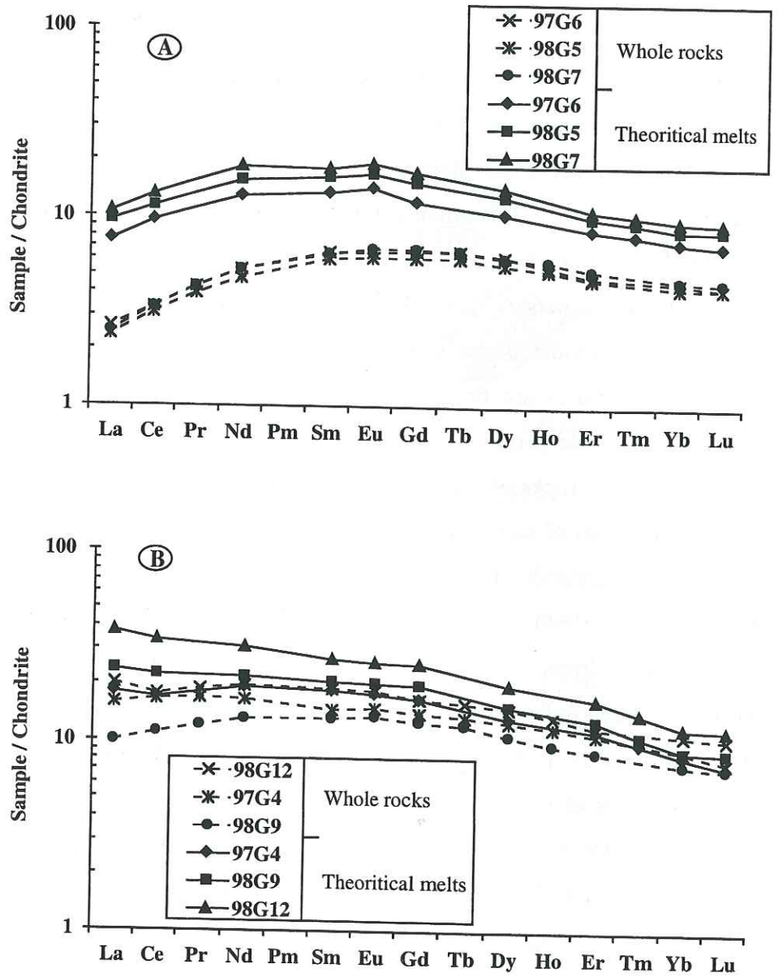

Fig. 4.11: Chondrite-normalized REE patterns of calculated melts from the cpx of Guaranda picrites (A) and ankaramites (B). The melts are calculated using partition coefficients for picrite and ankaramite (Shimizu, 1982; Ulmer, 1989; Hart & Dunn, 1993).

DISCUSSION

Comparison with the nearby Early Cretaceous and Late Cretaceous oceanic plateau sequences

The two crustal fragments of oceanic plateau affinity exposed in Ecuador differ in terms of lithologies and isotopic compositions of their igneous components, and likely represent crustal fragments of two distinct oceanic plateaus.

The Early Cretaceous crustal fragments exposed in the Western Cordillera consist of cumulate ultramafic and mafic rocks (San Juan sequence) and isotropic gabbros, dolerites and basalts (Merced-Multitud sequence). The pre-late Cretaceous Piñón Formation from the Coastal zone is tentatively considered coeval with the San Juan-Multitud unit.

Picrites and ankaramites are never present in the Piñón Formation and Multitud sequence. Conversely, cumulate peridotites and gabbros have never been observed associated with these types of extrusive rocks of the Guaranda and Pedernales units. However, basalts, dolerites and isotropic gabbros of both crustal fragments display flat REE patterns and Nb, Ta, and Th positive anomalies (relative to the primitive mantle) like all the well known oceanic plateau basalts (Kerr et al., 1996b; Neal et al., 1997). The main difference between the two Ecuadorian oceanic plateau fragments lies in the Nd and Pb isotopic compositions. The Piñón Formation and the San Juan and Multitud sequences span a very large range of εNd ratios (from +10 to +4.5, Reynaud et al., 1999; Lapierre et al., 2000) and rather restricted Pb isotopic ratios that fall in the fields of the Mid Atlantic Ridge (MAR) or East Pacific Rise (EPR). Conversely, with the exception of the Guaranda picrites, the basalts, dolerites and all the ankaramites of the Guaranda and Pedernales units have significantly higher Pb isotopic ratios compared to the range described for Piñón rocks (Fig. 4.12).

The Guaranda and Pedernales units appear to be petrologically and geochemically similar to the Upper Cretaceous (92-86 Ma) lavas of the CCOP. These volcanic rocks can be subdivided into two main groups. Group 1 consists of highly depleted komatiites and picrites (Gorgona, Colombia; Fig 4.6) characterized by high εNd and very low Pb ratios. Group 2 encompasses all the other lavas exposed in the Caribbean (Colombia, Costa Rica, Hispaniola, Curaçao), i.e., picrites, Mg-rich basalts, ankaramites, and basalts. This second group is characterized by flat to LREE-enriched patterns, εNd ranging between +6 and +9.5 and (Fig. 4.8) Pb isotopic signature consistent with the field defined by the recent Galápagos Islands (Fig. 4.9), suggesting the contribution of a HIMU component.

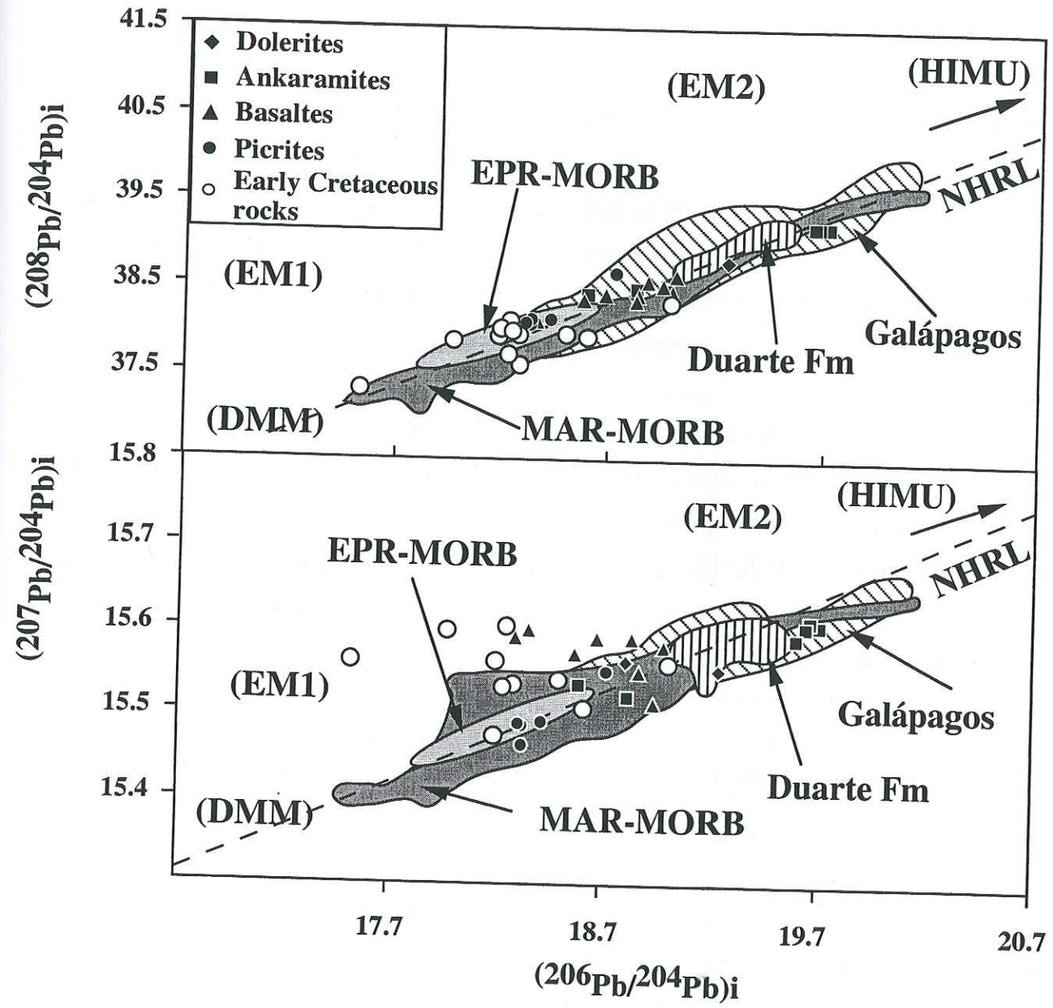

Fig. 4.12: Pb isotopic ratios comparison between Early Cretaceous rocks (Lapierre et al., 2000; Mamberti et al., submitted) and the studied rocks. The "Northern Hemisphere Reference Line" (NHRL) and the field from some mantle reservoirs are reported after Zindler & Hart (1986). East Pacific Rise (EPR) MORB and Mid Atlantic Ridge (MAR) MORB data and Galapagos Islands field are from White et al. (1987). The Duarte field is reported after Lapierre et al. (1997).

The picrites of the Guaranda unit share with the CCOP Group 1 similar Nd and Pb isotopic compositions (Fig. 4.8 and 4.9) but differ from the Gorgona picrites in that they are less depleted in LREE, have lower REE abundances, especially in HREE, and are enriched in Nb and Ta (Fig. 4.6). The ankaramites, Mg-rich basalts, dolerites and basalts of the Guaranda and Pedernales units exhibit the same trace element patterns and Sr, Nd and Pb isotopic geochemistry as the CCOP Group 2 rocks (Figs. 4.8 and 4.9).

In summary, the picrites, ankaramites and associated mafic rocks from the Guaranda and Pedernales units of Ecuador differ from the Lower Cretaceous oceanic plateau (Piñón Formation, San Juan-Multitud unit) by the presence of depleted picrites and the contribution of a HIMU component in their genesis. They likely belong to the Late Cretaceous major event of the CCOP, of which they would represent the most southerly remnants accreted to the South American margin.

One may wonder whether the two distinct oceanic plateau successions of Ecuador may represent two distinct basaltic pulses within the same plateau, as described for the Ontong Java Plateau (OJP) (Neal et al., 1997). However, on one hand picrites and ankaramites have never been described in the OJP, and on the other hand the Early Cretaceous plateau fragments and Late Cretaceous CCOP remnants always belong to distinct tectonic units. Therefore, we assume that the two oceanic plateau successions of Ecuador do not belong to the same plateau.

Spatial and temporal relationships between picrites, ankaramites, dolerites and basalts

Field relationships in the Guaranda section allow us to specify that the picrites are stratigraphically overlain by the ankaramites, and that the time span between picrite and ankaramite eruptions was very short. We have no evidence for the stratigraphic relations between the basalts and the more-mafic lavas. The pillow basalts and dolerites are either the uppermost levels of the volcanic pile or the lateral variations of the ankaramites. The pillow matrix of the Pedernales basalts consists of siliceous pelagic sediments suggesting that these pillowed flows represent the shallower levels of the oceanic plateau crust. The most likely stratigraphic succession for the Ecuadorian complete sequence would be picrites overlain by ankaramites, which are in turn overlain by the pillow basalts and dolerites. This is in agreement

with the hypothetical cross-section through the Caribbean oceanic plateau proposed by Kerr et al. (1998).

Trace-element signatures of lavas from the Guaranda and Pedernales units vary widely from almost enriched LREE patterns in ankaramites to extremely depleted patterns in picrites. Basalts and dolerites exhibit much more homogeneous geochemical features which are those of most oceanic plateaus (flat REE patterns). Trace-element variations within each group of rocks are linked to differences in the partial melting percentages. These contrasting features are also present in the isotopic geochemistry of these rocks. The picrites derived from an extremely depleted source, with initial εNd ranging from +10.2 to +7.7 and low Pb isotopic ratios. The source of the ankaramites is less depleted with initial εNd ranging from +8.2 to +7, and highly radiogenic Pb isotopic compositions suggesting a HIMU component contribution. The basalts and dolerites have the most homogeneous enriched source with initial εNd ranging from +9.2 and 6.1. Their Pb isotopic compositions are intermediate between those of the depleted picrites and enriched ankaramites.

Multi-stage model for the emplacement of the Ecuadorian picrites, ankaramites and basalts

In view of the close spatial and temporal relationships between the picritic, ankaramitic and basaltic magmas, it appears obvious that the source of the Ecuadorian magmas was originally heterogeneous at a small scale. As previously proposed by Révillon et al. (2000b), and shown in Figure 4.13, a multi-stage model can potentially explain the stratigraphic succession from picrites to basalts through ankaramites, and the contrasting geochemical and isotopic features of these plume-related rocks.

The Ecuadorian picrites likely derived from the narrow, hot central core of the plume and ascended directly to the surface without being trapped in intermediate magma chambers. These ultramafic melts derived from an extremely depleted source with high partial melting ratios (20 to 25 %; Révillon et al., 2000b). The ankaramitic melts were more probably extracted from an enriched source located at the edge of the plume. The rather high MgO contents (17.4 < MgO % < 8.5) of these rocks suggests that most of them ascended like the picrites directly to the surface. The trace element variations of the ankaramites (especially the LREE-enrichment) are likely linked to the differences in the partial melting percentages, which are significantly lower than in the picrites. The depleted and enriched sources of the plume likely derive from

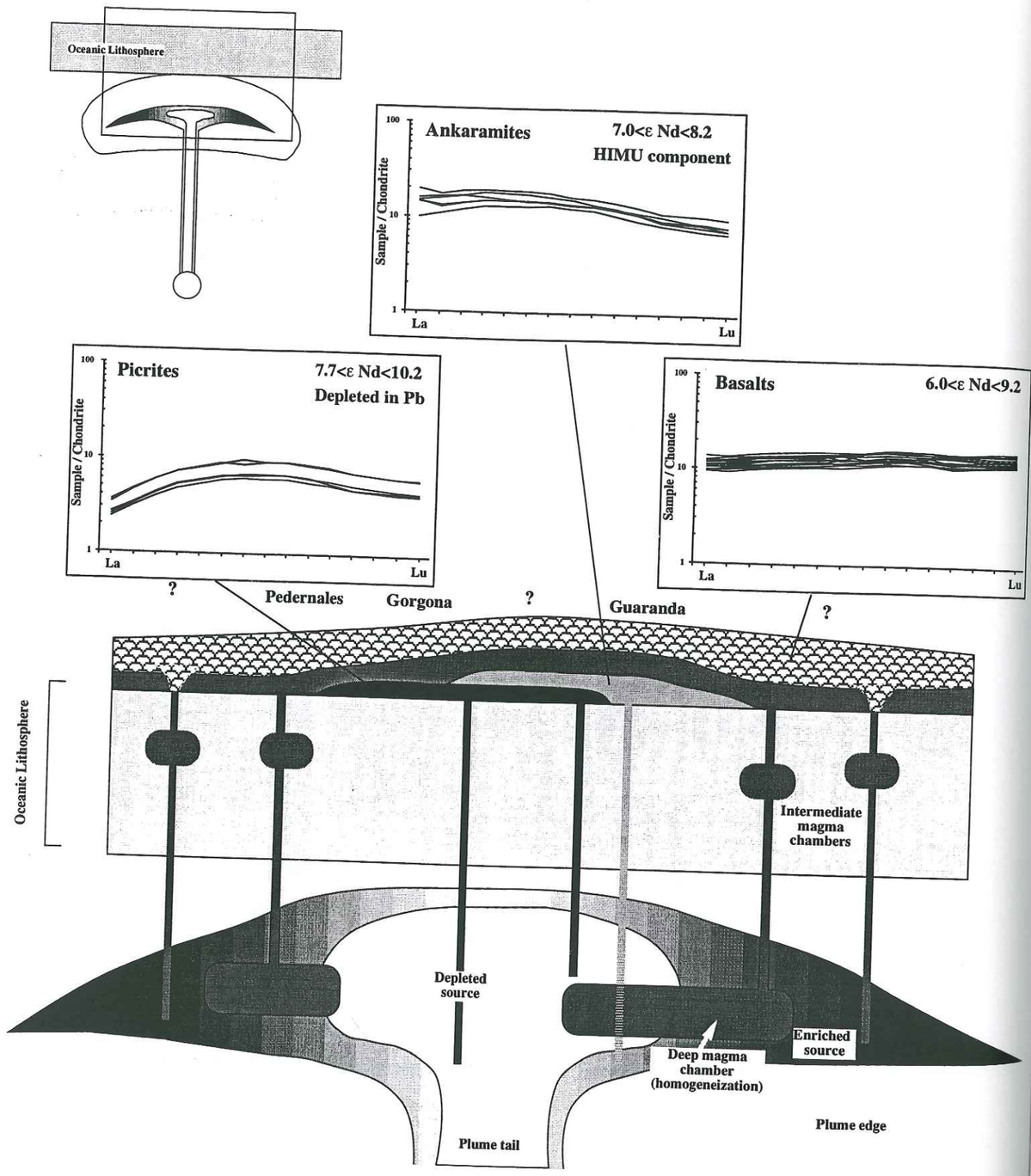

Fig. 4.13: Spatial and temporal relationships between the picritic, ankaramitic and basaltic magmas.

recycled oceanic lithosphere (ultramafic and mafic cumulates and hydrothermalized basalts; Révillon, 1999).

The origin and emplacement of the basalts, dolerites and gabbroic stocks are probably very different from that of the picrites and ankaramites. These rocks are the last to be emplaced. Their trace element and isotopic compositions are very homogeneous and do not depart from other oceanic plateau basalts. Thus, they are not any more representative of individual plume source components. This change with time in the chemistry of the oceanic plateau lavas from depleted ultramafic melts to very homogeneous basalts through enriched ankaramites indicates that (i) the magmatic system above the plume evolved and (ii) the successive batches of magma mixed and fractionated in deep or intermediate level magma chambers, to generate the later basalts and dolerites.

Komatiites, picrites and ankaramites occur only in the CCOP and are not known in large Mesozoic oceanic plateaus like the Ontong Java where only geochemically homogeneous basalts have been described (Mahoney et al., 1993; Neal et al., 1997). This indicates that in the Caribbean-Colombian province, the deeper sections of the plateau have been uplifted and exposed thanks to subsequent erosion, allowing direct sampling and study of the depleted and enriched plume components.

Age and tectonic history of the two oceanic plateau sequences

The oceanic terranes accreted to the Andean margin of Ecuador can be characterized by their age, magmatic affinities of their igneous components, their geodynamic environment, and the date of their accretion to the margin. The age of this accretion can be estimated by means of stratigraphic and tectonic relationships. Especially, the first appearance of detrital quartz in sediments which unconformably overly the oceanic terrane can be taken as an evidence of their accretion to the continental margin. Four oceanic plateau associations are present in Ecuador: the Piñón Formation, the San Juan-Multitud, Guaranda and Pedernales units.

The Piñón Formation of the Guayaquil area has been accreted in the Late Paleocene (≈58 Ma, Jaillard et al., 1995, 1997).

The San Juan-Multitud unit represents fragments of an oceanic plateau of Early Cretaceous age (Pratt et al., 1998; Lapierre et al., 2000, Mamberti et al., submitted). Since it is the easternmost accreted Cretaceous terrane, its accretion occurred most likely before the other ones. The San Juan-Multitud unit is often associated with quartz-bearing turbidite series of Late

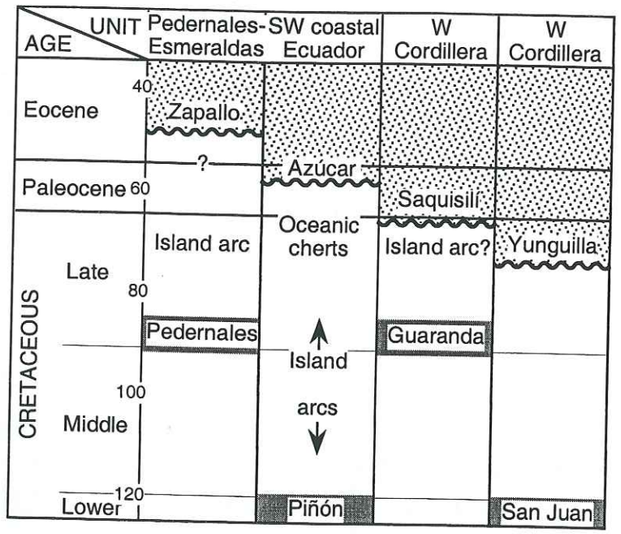

Fig. 4.14: Chronostratigraphic sketch of some accreted oceanic terranes of western Ecuador. Shaded area: oceanic plateaus; dotted areas: quartz-rich deposits; heavy lines: inferred accretion episodes.

Campanian-Early Maastrichtian age (Fig. 4.14; Yunguilla Formation, Thalmann, 1946; Sigal, 1969; Bristow and Hoffstetter, 1977). Since the Yunguilla Formation is not observed upon the Guaranda and Pedernales oceanic units, and is more deformed than the subsequent quartz-rich turbidites, we assume that the deposition of the Yunguilla Formation sealed the accretion of the San Juan-Multitud unit, and was deformed by the subsequent accretion of the Guaranda unit. The San Juan-Multitud unit accreted, therefore, between 85 and 80 Ma (Late Santonian-Early Campanian, Reynaud et al., 1999; Hughes and Pilatasig, in press).

The Guaranda unit appears to be the southern extension of the dismembered CCOP and may be considered as Turonian-Coniacian in age (92-86 Ma). It is exposed west of the San Juan-Multitud unit and therefore, has been accreted later than the Early Cretaceous oceanic plateau fragments. Hughes et al. (1999) defined a little deformed, fine-grained, quartz-rich turbidites series of Early to Middle Paleocene age (Saquisilí Formation), which is tectonically associated with the Guaranda unit along the Pallatanga and Guaranda sections. 10 km south of the Guaranda section (Cerro Calderón, 7383-98090), the Saquisilí Formation stratigraphically overlies oceanic rocks of the Guaranda unit. The presence of detrital quartz and micas in these turbidites, together with the lack of remnants of the Yunguilla Formation on the Guaranda unit, indicate that the accretion of the Guaranda unit took place after deposition of the Yunguilla Formation, and before deposition of the Saquisilí Formation, i.e. during the Late Maastrichtian (≈ 69-65 Ma; Fig. 4.14).

The interpretation of a Late Maastrichtian accretionary event is supported by (i) the local deposition of thick breccias of Middle Maastrichtian age in some forearc zones (Jaillard et al., 1998; 1999), (ii) the occurrence of a thermal event around 75-65 Ma in the Eastern Cordillera of Ecuador (Aspden et al., 1992; Litherland et al., 1994), (iii) a regional depositional hiatus of Late Maastrichtian-Early Paleocene age in this part of the margin (Jaillard, 1997; Jaillard et al., 1998; 1999), and (iv) the arc jump from the Campanian-Maastrichtian San Lorenzo island arc (Lebrat et al., 1987) to a continental arc of latest Maastrichtian-Paleocene age (Sacapalca Formation, Jaillard et al., 1996; Hungerbühler, 1997).

The Pedernales unit is probably part of the CCOP of Turonian-Coniacian age. Since it is unconformably overlain by quartz-rich marine sediments of Early to Middle Eocene age (Fig. 4.14; Faucher et al., 1971; Deniaud, 2000), it was already accreted to the Andean margin by the Mid Eocene. Note that Boland et al. (2000) proposed that the terrane located East of Esmeraldas-Pedernales (Naranjal terrane) accreted in the Early Eocene (≈ 55-50 Ma).

In summary, the available geological data suggest that western Ecuador comprises fragments of at least two distinct oceanic plateaus: (i) an Early Cretaceous plateau, part of

which (San Juan-Multitud unit) was accreted in the Late Santonian-Early Campanian (≈ 85-80 Ma), and (ii) an oceanic plateau similar to the Turonian-Coniacian CCOP (≈ 92-85 Ma), locally overlain by a Campanian-Maastrichtian oceanic arc. The Turonian-Coniacian oceanic plateau accreted to the ecuadorian margin during at least two episodes, of Late Maastrichtian, and pre-Middle Eocene age, respectively.

CONCLUSIONS

Crustal fragments of oceanic plateau affinity exposed in Ecuador belong to two distinct oceanic plateaus. They differ in their rock lithologies, isotopic chemistry of their igneous components, and most probably in their age and timing of accretion.

The oldest plateau sequence, of Early Cretaceous age (≈ 123 Ma), consists of ultramafic and mafic cumulate rocks and pillow basalts and dolerites, intruded by gabbroic stocks. All the igneous rocks have low Pb isotopic ratios and display a rather large range of εNd (from +10 up to +4) but most values cluster at +7. This suggests that the Early Cretaceous oceanic plateau rocks derived from a rather depleted mantle source. This sequence accreted to the Ecuadorian margin during the Late Santonian-Early Campanian (≈ 85-80 Ma).

The youngest plateau sequence (≈ 90 Ma) is composed of picrites, ankaramites, Mg-rich basalts, basalts, dolerites and shallow level gabbros. The LREE-depleted picrites derived from a depleted source, characterized by high εNd ratios and very low Pb isotopic ratios. In contrast, the LREE-enriched ankaramites and Mg-rich basalts differ from the picrites by lower εNd and higher radiogenic Pb isotopic compositions, and are very similar to the Galápagos HIMU component. The basalts, dolerites and gabbros exhibit homogeneous εNd (+6 to +9), and Pb ratios intermediate between those of the picrites and ankaramites. The ankaramites and Mg-rich basalts differ from the Early Cretaceous igneous rocks by higher $^{206}Pb/^{204}Pb$ ratios. The Ecuadorian picrites, ankaramites and Mg-rich basalts bear striking similarities with those of the Late Cretaceous (92-86 Ma) Caribbean-Colombian Oceanic Plateau, of which this sequence may represent an accreted fragment. Fragments of this plateau have been identified in the Western Cordillera of Central Ecuador (Guaranda Unit) and in the northern part of coastal Ecuador (Pedernales-Esmeraldas unit). Parts of this Late Cretaceous oceanic plateau collided with the Ecuadorian margin in the Late Maastrichtian (≈ 70-65 Ma).

The field observations and geochemical data support a multi-stage model for the emplacement of the Late Cretaceous plume-related rocks. Moreover, the temporal evolution from depleted picrites to homogeneous mildly enriched basalts through highly enriched

ankaramites indicates that the heterogeneity and specific isotopic features of the mantle plume source vanish with time. In contrast with the picrites and ankaramites, which ascended directly to the surface, the basaltic melts were stocked in deep or intermediate magma chambers where they mixed and fractionated.

ACKNOWLEDGEMENTS

This research has been supported by grants from INSU-CNRS (Intérieur de la Terre) Contribution N° and FNRS N° 20-50812.97 to M. Polvé and J. Hernandez, respectively. Thanks to François Sénebier who did all the mineral separates. We would like to thank P. Telouk and the "service Commun National du MC-ICPMS de l'Ecole Normale de Lyon", as well as P. Brunet (UMR-5563), who carried out all the Sr-Nd TIMS analyses.

Chapitre 5

Des hyaloclastites de composition picritique et basaltique affleurent sur la côte de l'Equateur au niveau de Pedernales. Elles sont associées à des basaltes en coussin, des dolérites et des gabbros isotropiques et présentent de hauts rapports isotopiques du plomb (présence d'un composant HIMU) similaires à ceux présents dans les basaltes du plateau océanique Crétacé Supérieur décrits dans le chapitre précédent.

Une picrite très bien préservée est présente dans la coupe de Pedernales. Elle est constituée d'olivine et de magnésio-chromite. Certaines olivines sont dendritiques et traduisent des vitesses de refroidissement rapides. Cette picrite est appauvrie en éléments les plus incompatibles et présente de grandes similitudes géochimiques avec les picrites et komatiites de l'île de Gorgone. Richard J. Walker a essayé de dater cette roche par isochrone interne Re/Os sur olivine, magnésio-chromite, verre et roche totale, mais les rapports isotopiques de ces différents composants étaient trop proches pour obtenir un âge correct.

Chapter 5

ULTRA-DEPLETED PICRITE IN ECUADOR: REMNANT OF THE CCOP PLUME HEAD.

Marc Mamberti, Richard J. Walker, Stephan Eggins, Henriette Lapierre, Jean Hernandez, Delphine Bosch, Etienne Jaillard & Mireille Polvé.

In preparation for Earth and Planetary Science Letters

CHAPTER 5: ULTRA-DEPLETED PICRITE IN ECUADOR: REMNANT OF THE CCOP PLUME HEAD.

Hyaloclastites composed of picritic and basaltic fragments are exposed near Pedernales, Ecuador. They are associated in the field with pillow basalts, dolerites and isotropic gabbros which have high Pb ratios (presence of an HIMU component) of the Upper Cretaceous oceanic plateau basalts described in the previous chapter.

This exceptionally well preserved picrite is solely composed of quenched olivine crystals and magnesiochromite, and has depleted geochemical features similar to the Gorgona high-Mg lavas. Richard J. Walker tried to date this rock by an internal Re/Os isochron on olivine, magnesiochromite, glass and whole rock, but the isotopic ratios of the different components are too similar to obtain a good regression isochron line.

ULTRA-DEPLETED PICRITE IN ECUADOR: REMNANT OF THE CCOP PLUME HEAD.

INTRODUCTION

Picrites and komatiites have a world-wide distribution. Komatiites are essentially located in Archean greenstone belts (Nisbet, 1982; Viljoen & Viljoen, 1982; Barley & Bickle, 1982, Arndt 1994), but modern analogues are described in Gorgona island (Gansser et al., 1979; Echeverria, 1980; Arndt et al., 1997). Both rock types are ultramafic igneous rocks (high MgO contents) but differ by the spinifex texture of komatiite olivine and the MgO content of the rock (Le Bas, 2000). They are often associated with highly Mg-rich basalts. Note that picrites, komatiites and basalts are often associated whatever their age, Archean or Mesozoic. Komatiites and picrites are generally more depleted and less evolved than the basalts.

Previous works on modern komatiites and picrites (Kerr et al. 1996; Arndt et al., 1997; Révillon et al., 2000) suggest that ultramafic igneous rocks are formed in the hot axial region of mantle plumes. The liquidus temperatures of the magnesian parental liquid range between 1360°C and 1700°C (Arndt et al., 1997; Thompson & Gibson, 2000) that is 400°C hotter than the temperatures calculated for the Phanerozoic mantle plumes. These calculated thermal informations are essentially based on the forsterite composition of the olivine.

Most of the picrites and komatiites exhibit more depleted rare earth element and isotopic compositions than the associated basalts, suggesting that the picrite-komatiite-basalt association reflects the heterogeneity of the mantle source (Kerr et al., 1996; Arndt et al., 1997). The variations in REE and isotopic compositions of the different magmas produced by the same plume suggest complex melting processes in the mantle source. In contrast, Anderson (1994) suggests that the enriched chemistry of magmas associated with MgO-rich melts is an attribute of the shallow mantle and not of the plume, and that the eruptability of high-MgO magmas may be controlled by lithospheric conditions and melt viscosity. The previous work shows the difficulty of applying a model for mantle plumes and some questions about the temperature, the composition, the conditions of rising and the heterogeneity of the source are controversial.

Why is the Ecuadorian picrite an exceptional rock ? The picrite is an ultramafic lava composed only of olivine and Mg-chromite embedded in a fresh glassy matrix. Skeletal olivine exhibits quench texture with evidence of rapid raising of the picritic magma. Because of the primitive feature of this Mg-rich melt, the petrology and chemistry of this rock is important for understanding the nature of the mantle plume and the thermodynamic conditions (temperature, pressure) during the magma genesis.

The aim of the paper is to show that the exceptional character of the Ecuadorian picrite, and provide information about the genesis and ascent of Mg-rich melts. We argue that this ultramafic ultra-depleted lava represents the products of the hottest parts of the mantle plume.

PETROGRAPHY

The picrite, subject of this study, was collected from hyaloclastites, exposed near Pedernales in north-western Ecuador. The hyaloclastites are associated with pillow basalts and consist of vesicle-free glass which contains centimeter-sized rounded fragments with picritic and basaltic compositions.

The picrite contains 20-25 % of mm-sized olivine phenocrysts ($Fo_{90-92.4}$) in a glass matrix which includes quenched dendritic olivine microphenocrysts and microlites and spinel (photos). The glassy matrix of the hyaloclastite is partly replaced by palagonite. Locally, the rims of the some picritic fragments are slightly palagonitized.

Olivine is Cr-rich ($0.10 < Cr_2O_3 < 0.19$; Table 5.1) and exhibits homogeneous composition within a single grain. Olivine phenocrysts contain Cr-rich spinels and abundant rounded and elongated melt inclusions (5 to 30 microns).

Cr-spinel is a magnesiochromite the composition of which remains constant whatever the spinel is included in (olivine or glass). Its Cr number ($0.6 < Cr/(Cr+Al) < 0.54$; Table 5.1) is the same than that of the Gorgona komatiites. In the Cr/(Cr+Al) versus Mg/(Mg+Fe) plot (Fig. 5.1), the Cr-spinel falls in the harzburgite field.

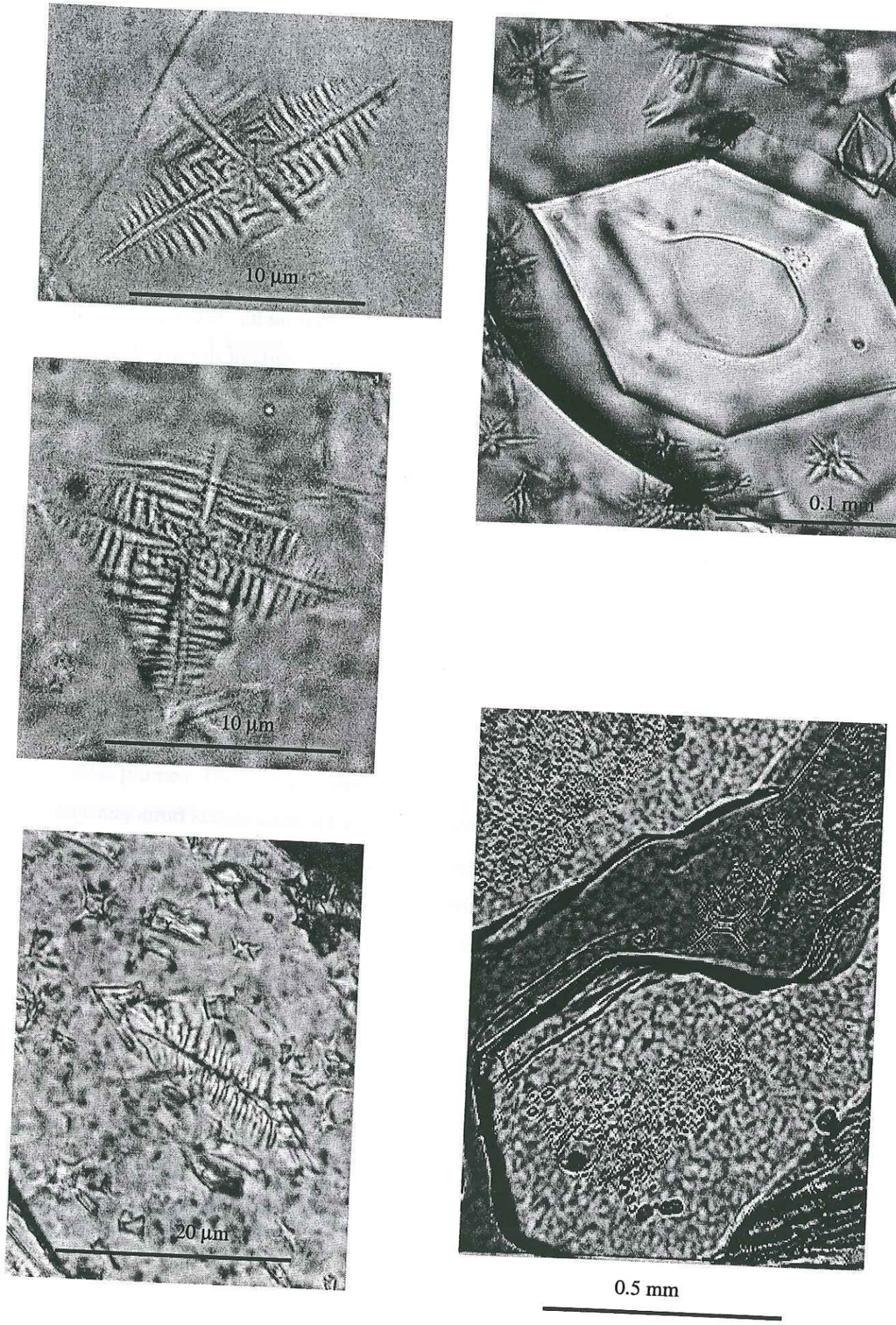

Photos: Various olivine morphologies in the Ecuadorian picrite.

Mineral	Chromite					Olivine				
SiO2	0.1	0.12	0.17	0.08	0.13	40.95	40.94	40.52	40.85	41.09
TiO2	0.21	0.17	0.15	0.19	0.16	0.01	0.01	0.01	0.01	0.01
Al2O3	19.62	19.43	21.78	19.99	20.67	0.1	0.1	0.07	0.09	0.1
Cr2O3	41.16	45.43	44.21	40.36	42.91	0.19	0.17	0.1	0.14	0.15
FeO	22.34	18.28	16	22.74	18.64	7.79	8.32	9.91	8.92	7.93
MnO	0.42	0.4	0.44	0.35	0.45	0.17	0.1	0.16	0.12	0.12
MgO	14.11	15.08	15.88	14.23	15.17	50.36	49.83	48.73	49.44	50.16
CaO	0.08	0.06	0.06	0.12	0.07	0.32	0.32	0.38	0.34	0.33
NiO	0.21	0.24	0.26	0.24	0.24	0.44	0.44	0.37	0.42	0.44
Sum Ox%	98.25	99.21	98.95	98.29	98.43	100.34	100.24	100.24	100.34	100.32
Mg*	0.53	0.60	0.64	0.53	0.59	0.924	0.914	0.898	0.908	0.919
Cr*	0.58	0.61	0.58	0.58	0.58					

Table 5.1: Selected microprobe analyses of chromite and olivine from Pedernales picrite. Analyses were carried at the University of Lausanne.

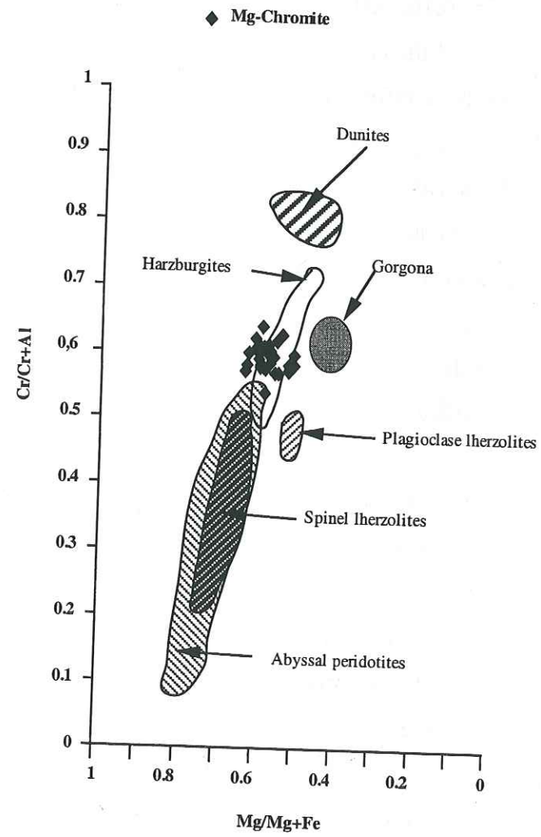

Fig. 5.1: Cr/(Cr+Al) versus Mg/(Mg+Fe) correlation diagram for the magnesiochromite from Ecuador. The Gorgona field is reported after Echeverria (1980).

GEOCHEMISTRY

Whole rock major element composition of the picrite is that of a highly MgO-rich melt (MgO = 21.20 %), depleted in Al_2O_3 (10.56 %) and TiO_2 (0.25 %; Table 5.2). According to the recent IUGS revised nomenclature of high-Mg volcanic rocks (LeBas, 2000) based solely on the major element compositions, the studied picrite falls in the komatiite field. However, this picrite does not show spinifex texture typical of komatiites. That is why we consider this highlyMg-rich rock as a picrite.

The glassy matrix and melt inclusions have similar major-element compositions, i.e. MgO = 10.4 %, Al_2O_3 = 14.7%, CaO = 13%; Table 5.2). On the basis of the Fo of olivine and MgO content of the whole rock and glass, the estimated % of olivine is 21.6 %.

The trace element chemistry of the whole rock and glass are extremely depleted in all incompatible elements. Nb (0.16; 0.10 ppm, respectively) and Zr (7.9; 9 ppm, respectively) are largely lower than those of the N-MORB (Hofmann, 1988). The very low $(La/Yb)_N$ ratios (0.12 and 0.06, respectively) confirm the depleted character of this rock, compared to N-MORB (Fig. 5.2). The Ecuadorian picrite exhibits high Sm/Nd (0.55) and $(^{143}Nd/^{144}Nd)_i$ (0.512980) ratios (Table 5.3). These ratios are significantly higher than those of various basalts and picrites (Fig. 5.3) and slightly lower than those of the Gorgona komatiites (Fig. 5.3). Conversely, the Pb ratios are low [$(^{206}Pb/^{204}Pb)i$ = 38.04; $^{207}Pb/^{204}Pb)_i$ = 15.58; Table 5.3]. These Nd and Pb isotopic compositions are comparable to those of MORB and indicate that this picrite derives from a depleted source (Fig. 5.4). In contrast, the $^{87}Sr/^{86}Sr$ ratio is higher than those of MORB and likely expresses the sea water hydrothermal alteration which affects locally the glassy matrix of the picrite.

The whole rock is Os-rich and Re-poor (Table 5.4). The Os content can be correlated with the high MgO of the whole rock and the presence of spinels, like magnesiochromite which incorporates Os (201ppb). Olivine contains 7.8 ppb of Os. The strong partitioning between Re and Os in crust relative to the mantle, makes Os a powerful tracer for olivine-chromite bearing rocks and helps to discriminate between source components and interaction of oceanic lithosphere in the genesis of plume-related rocks. Previous investigations show that plume-related magmas have a large range of γOs (from to –3 to +40). This large range of values of γOs reflects the nature of recycled material involved in the plume-source. The Ecuadorian picrite has a subchondritic Os isotopic composition (γ Os = -0.2; $^{187}Os/^{188}Os$ = 0.12656; Table 4). A combination of Os, Nd and Pb isotope data has been used to study the possible interaction of oceanic lithosphere in the genesis of this picrite. The Ecuadorian

picrite falls in the DMM field in both diagrams where γOs is correlated with εNd and $^{206}Pb/^{204}Pb$.

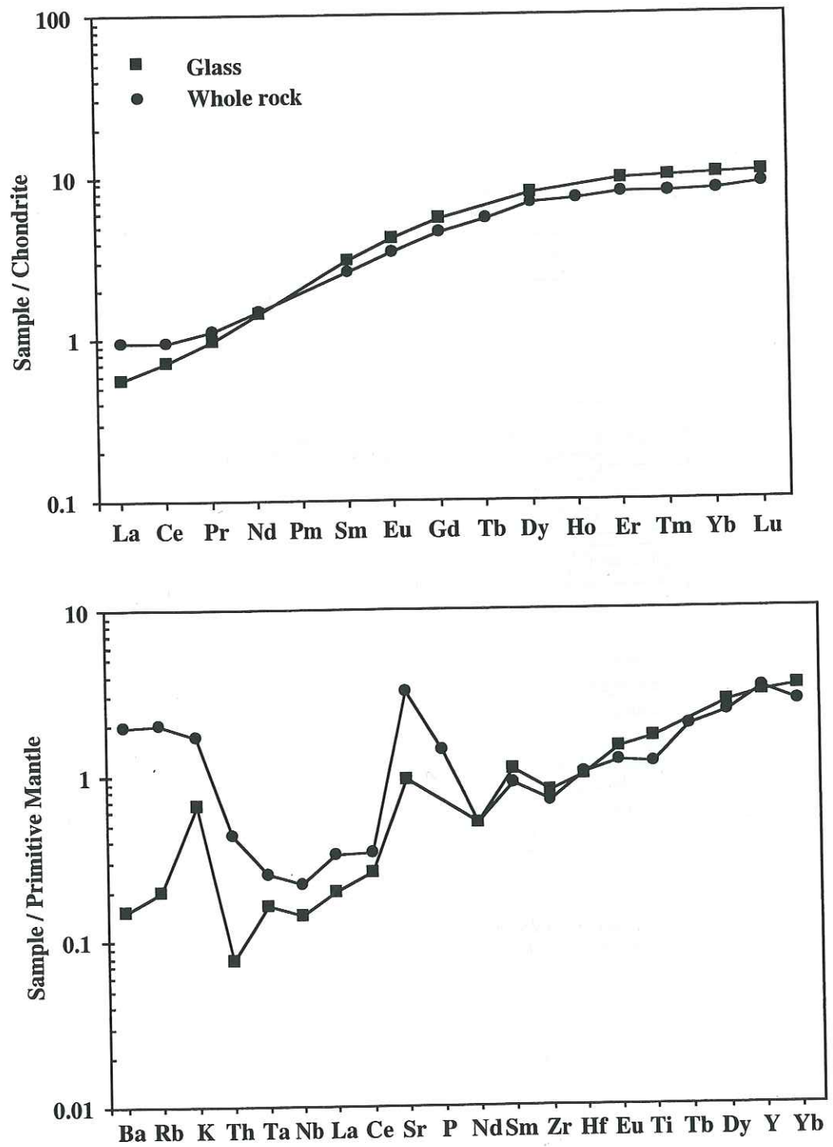

Fig. 5.2: Chondrite- and primitive mantle-normanlized (Sun & McDonough, 1989) rare earth element patterns and multi-element diagram for the glass and the whole rock.

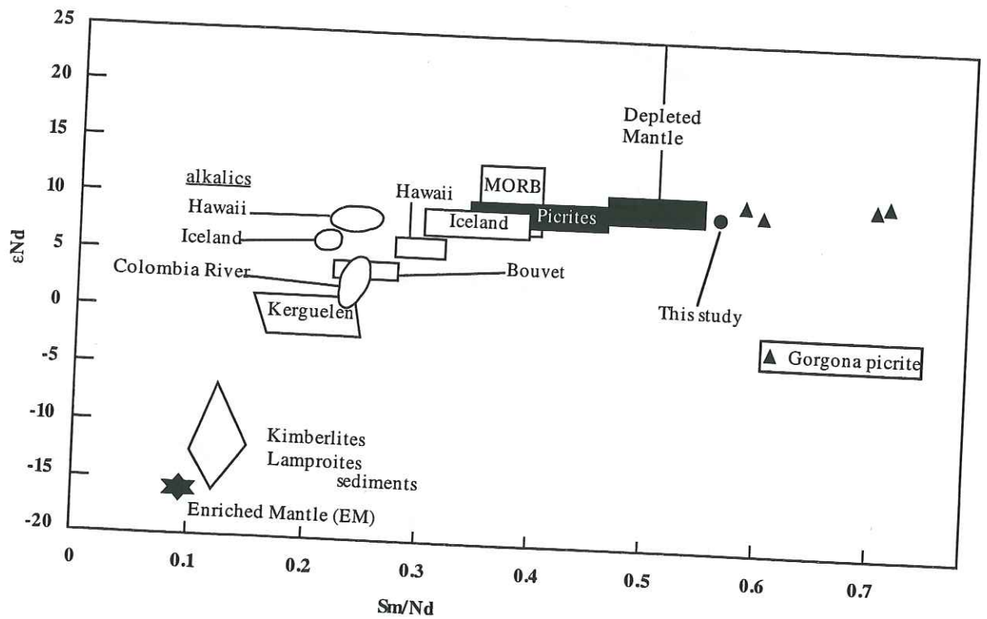

Fig. 5.3: εNd versus Sm/Nd of various basalts and picrites. Compositions of endmembers are from Anderson, 1982, 1983, 1985. Gorgona field (picrite and komatiite) from Révillon et al., 2000.

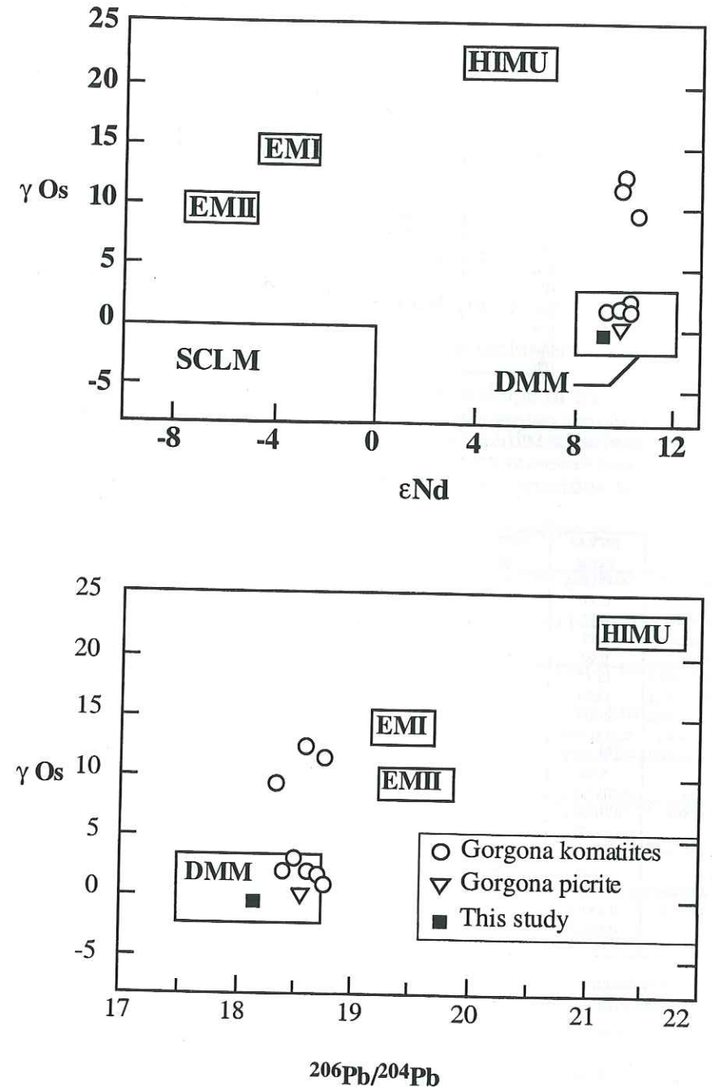

Fig. 5.4: γ Os versus εNd and $^{206}Pb/^{204}Pb$ for the Ecuadorian picrite. Gorgona picrites and komatiites are reported after Walker et al. (2000).

N°Ech.	99PE13 Picrite	99PE13 Glass matrix
SiO2	41.93	47.20
TiO2	0.23	0.35
Al2O3	9.60	14.19
Fe2O3	10.17	9.94
FeO		
MnO	0.16	0.18
MgO	19.26	11.39
CaO	7.90	11.96
Na2O	1.08	0.99
K2O	0.05	0.02
P2O5	0.03	-
Cr2O3	0.32	0.11
NiO	0.13	0.05
LOI	8.35	-
Total	99.21	96.37

N°Ech.	99PE13 Picrite	99PE13 Glass
Ba	13.82	1.053
Rb	1.27	0.13
Sr	66.5	20.0
Ta	0.01	0.0067
Th	0.04	0.0065
Zr	7.85	8.98
Nb	0.16	0.103
Y	15	14.3
Hf	0.31	0.309
V	*175*	185.5
Cr	*1902*	
Ni	*830*	
Co	92	
U	0.02	0.002
Sc	97	38.0
Cu	*17*	
Zn	*59*	
Pb	0.22	10.22

N°Ech.	99PE13 Picrite	99PE13 Glass
La	0.23	0.14
Ce	0.61	0.46
Pr	0.11	0.10
Nd	0.71	0.69
Sm	0.40	0.47
Eu	0.20	0.24
Gd	0.92	1.12
Tb	0.21	
Dy	1.76	2.02
Ho	0.42	
Er	1.32	1.60
Tm	0.20	
Yb	1.33	1.68
Lu	0.22	0.27

Table 5.2: Major (in wt%) and trace element (in ppm) analyses of theEcuadorian picrite. Major elements were measured by XRF; trace elements by XRF(italics) or ICP-MS (plain text). LOI: Loss on ignition. Major elements of the glass by electronic microprobe; trace elements by ICP-MS laser ablation.

N°Ech. Nom	99PE13 Picrite	99PE13 Glass
(Ce/Yb)n	0.12	0.07
(La/Sm)n	0.37	0.18
(La/Yb)n	0.12	0.06
Mg number	0.82	0.73
Cr number	0.90	
(206Pb/204Pb)i	18.13	
(207Pb/204Pb)i	15.58	
(208Pb/204Pb)i	38.04	
143Nd/144Nd	0.513179±6	
(143Nd/144Nd)i	0.512980	
ε(Nd)i	8.94	
87Sr/86Sr	0.703757±7	
(87Sr/86Sr)t	0.703686	
ε(Sr)t	-10.05	
Re (ppb)	0.146	0.066
Os (ppb)	2.858	1.809
187Os/188Os	0.12656	0.12633
187Re/188Os	0.24569	0.17530
Initial 7/8	0.12620	0.12607
γOs	-0.2	-0.3

Table 5.3: Isotopic compositions of the Whole rock and glass from the Ecuadorian picrite.

	Re (ppb)	Os (ppb)	$^{187}Os/^{188}Os$	$^{187}Re/^{188}Os$	$(^{187}Os/^{188}Os)i$	γ_{Os}
99PE13 WR Picrite	0.1458	2.858	0.12656	0.2457	0.12620	-0.2
99PE13 Olivine	0.0153	7.827	0.12618	0.0094	0.12617	-0.2
99PE13 Glass	0.0658	1.809	0.12633	0.1753	0.12607	-0.3
99PE13 Chromite	1.5001	201.4	0.12592	0.0359	0.12587	-0.4

Table 5.4: Re Os isotopic composition of the whole rock (WR), olivine, glass and chromite from the Ecuadorian picrite.

TEMPERATURE OF THE PICRITIC MELT

Olivine Morphology.

The presence of quenched olivine and the lack of degassing vesicles suggest that these hyaloclastites were formed under shallow water level. The dendritic and skeletal shapes of some of these crystals provide evidence of extremely rapid cooling The picrite also contains magnesio-chromite (Cr# 0.60 - 0.54), which is in inclusion in the olivine and thus, appears to be the first to crystallize. The diversity in size and shape of the olivine is the result of different growth conditions. The skeletal olivine indicates that the rock is quenched.

Investigation of olivine morphology (Photos) provides useful informations about the cooling rate crystallization and the degree of supercooling at which particular shape grew. The diversity of the olivine morphology in the Ecuadorian picrite shows the complexity of the cooling history of the rock. The largest olivine phenocrysts are skeletal and exhibit melt inclusions and glass filling gulfs. Quenched dendritic olivine microcrysts occur also in the glassy matrix. They exhibit different morphologies which are similar to those formed during experiments at one atmosphere (Donaldson, 1975; 1976). We have tried to estimate the temperature and cooling rates of the Ecuadorian picrite by comparison of the shape and size of the quenched olivine microcrysts with those obtained by experiments (Donaldson, 1975; 1976). We estimated that the olivine from the picrite crystallized between 10 and 80 °C below the liquidus temperature and at degrees of supercooling between 5 to 1450 °C/hr (Donaldson, 1976). The large cooling rate and the estimated degrees of supercooling can be explained by the quick raising of the picrite to the surface. Dendritic olivine crystals similar to the feather olivine in the Donaldson classification (1976) indicate that the picritic melt cooled at 1450°C/hr, so the temperature of the melt where the dendritic olivine crystallized was at least 1450°C. The quick cooling of the picrite is likely due to the submarine volcanic activity and the fragmentation of the volcanic rock. This quick cooling is also evidenced by the lack of other mineral phases like clinopyroxene and plagioclase.

This diversity of olivine morphology shows the evolution of the magma during its ascent to the surface. The most Mg-rich olivine phenocrysts grew first during the magma ascent and cooling, followed by the less magnesian olivine phenocrysts while the quenched microcrysts and dendritic olivine formed during the eruption.

MgO CONTENT OF THE PARENTAL MELT

We estimated the MgO content of the parental melt in equilibrium with the picrite using the forsterite content of olivine and FeO total abundance of the whole rock. The calculated Mg/Fe ratio of the liquid is determined using a partition coefficient of 0.03 (Rœder and Emslie, 1970). The Rœder and Emslie, (1970) partition coefficient is similar to that calculated for the picrite (0.34), on the basis of MgO-FeO contents (assuming Fe3+/(total Fe) = 0.15; Aitken, 1983) of the picrite and the highest MgO content of the olivine. The calculated MgO content of the parental melt ranges from 20.6 (Fo_{92}) to 15 (Fo_{90}). This highest MgO content (20.6) approaches that of the whole rock (21.20 %). This indicates that the most Mg-rich olivine is in equilibrium with the whole rock which can be considered as a primitive melt. Thus, we have a direct access to the different informations about a primitive melt produced in a mantle plume.

LIQUIDUS TEMPERATURE

If we assume that the whole rock represents the parental primitive melt, we could used the MgO content to estimate the temperature of this melt. Using the following relationship from Nisbet (1982): T(°C)= 20 * MgO + 1000; the liquidus temperature is 1410°C (with forsterite 92) and 1300°C (with forsterite 89). This temperature corresponds to that calculated for the Gorgona picrite which ranges between 1360°C and 1400°C (Arndt et al., 1997). Li et al. (1995) have shown that high temperatures are required to precipitate Cr-rich olivine (Cr_2O_3 > 0.1%). Cr_2O_3 content of the olivine in the studied picrite ranges between 0.1 and 0.19% and brings evidence of the high temperature of the liquid in which the olivine crystallized

COMPARISON WITH GORGONA PICRITES AND KOMATIITES

Petrography

The first detailed descriptions of Gorgona picrites have been given by Aitken & Echeverria (1986). The picrites are in blocks and consist of abundant euhedral, non-skeletal olivine phenocrysts, magnesiochromite and titanomagnetite embedded in a variolitic matrix consisting of fine grained acicular crystals of clinopyroxene (augite and pigeonite) and plagioclase. Olivine is the dominant phase with a composition ranging from 92.3 to 90.1. Olivine from Gorgona picrites is similar in composition with that of the Ecuadorian picrite. The main difference between the Gorgona and Ecuadorian picrites is the presence of acicular clinopyroxene and plagioclase in the Gorgona matrix.

Spinels from the Gorgona picrites crystallized after olivine while in the Ecuadorian Mg-rich melt, magnesiochromite appears before olivine. Compared to the studied picrite, Gorgona magnesiochromite presents the same Cr number but differs by lower Mg number (Echeverria, 1980).

Major, trace element and isotopic chemistry

The Ecuadorian and Gorgona picrites are Mg-rich (27.87 < MgOwt% < 21.20; Arndt et al., 1997; Révillon et al., 2000) and have similar major element compositions. Moreover, these rocks are more magnesian than the Gorgona komatiites (23.9 < MgO % < 13.2). The estimated eruption temperature for the Gorgona komatiites varies between 1450 to 1500°C (Echeverria, 1980; Arndt et al., 1997) and is slightly higher than that estimated for the Ecuadorian picrite, which ranges between 1300 and 1410°C.

The glass compositions of the Gorgona picrites are comparable to those reported from the spinifex komatiites but differ from those of the Ecuadorian picrite by lower MgO abundance and higher Al_2O_3 and CaO contents

A comparison of REE and trace elements of Gorgona and Ecuadorian picrites is reported in figure 5.5. The Gorgona analyses are from Révillon et al. (2000). Both rocks exhibit a large depletion in LREE relative to the HREE and low incompatible trace elements (Nb, Ta). They have also similar (Ce/Yb)n ratios (0.07 < Ce/Yb)n < 0.12).

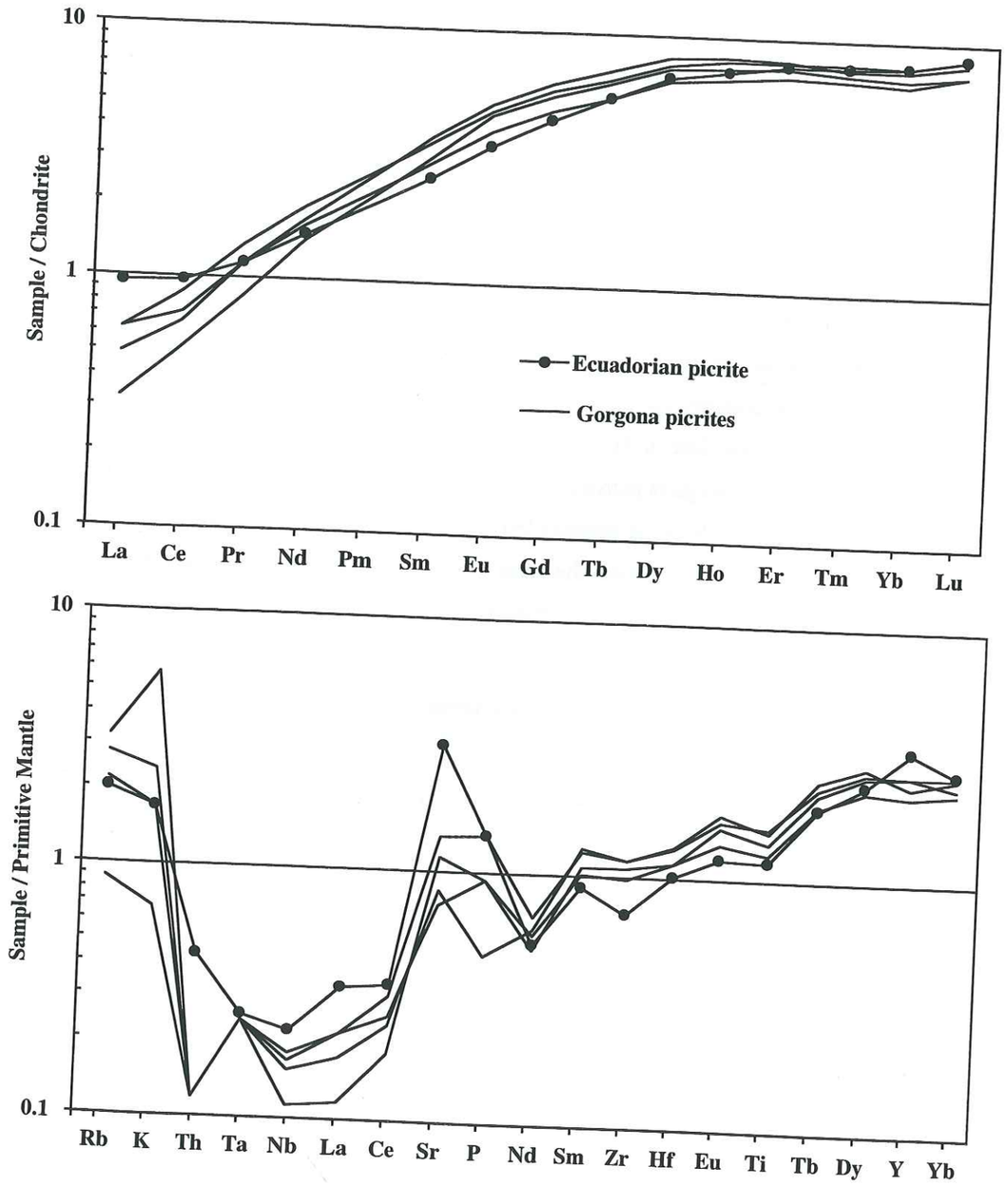

Fig. 5.5: Chondrite- and primitive mantle-normanlized (Sun & McDonough, 1989) rare earth element patterns and multi-element diagram for the Pedernales and Gorgona picrites. Gorgona picrite data are reported after Révillon et al. (2000).

The initial Nd isotopic compositions of the Gorgona picrites range between 0.512975 and 0.513060. In the εNd versus Sm/Nd diagram, picrites from Gorgona and Ecuador plot near the depleted mantle field but the Gorgona picrites have higher Sm/Nd ratios compared to that of Ecuadorian picrite. Picrites from both localities have low Pb and Os isotopic ratios ($18.13 < (^{206}Pb/^{204}Pb)i < 18.56$; $0.12656 < {}^{187}Os/^{188}Os < 0.13052$; Dupré & Echeverria, 1986; Walker et al, 2000) but the Ecuadorian picrite is less radiogenic in Pb and Os than those from Gorgona (Fig 5.4). The γOs of the Ecuadorian picrite is lower than those of the Gorgona picrites. Walker et al. (2000) proposed that the komatiites and picrites with chondritic Os compositions derived primarily from the ultramafic portion of recycled material while the ^{187}Os-enriched komatiites derived from recycled basaltic crust.

In summary, the main difference between the Gorgona and Ecuadorian picrites is the presence of acicular augite, pigeonite and plagioclase in the matrix of the Gorgona Mg-rich volcanics. This suggests that compared to the Gorgona Mg-rich volcanics, the Ecuadorian picrite has higher cooling rates and ascended more rapidly to the surface. However, these petrological differences between the Gorgona and Ecuadorian picrites have no effect on the major and trace element chemistry of these rocks. Indeed, picrites from both localities have high MgO contents and are very depleted in LREE and in the most incompatible elements. Moreover, these rocks have similar Nd, Sr and Pb isotopic chemistry suggesting that they derived from a very depleted mantle source but the Ecuadorian picrite differs by lower Os isotopic composition. This subchondritic Os isotopic composition of the Ecuadorian picrite indicates that this rock derives from the melting of the ultramafic part of a recycled material or from a depleted mantle MORB source (DMM), but in any case from recycled basaltic crust.

DISCUSSION

1 – Origin. What are the processes required to produce depleted rocks? Ultra-depleted primary melt has been found in an olivine from the Mid-Atlantic Ridge (Sobolev and Shimizu, 1993). The authors suggest that such melt is produced by critical melting at small degree of partial melting where just a part of the liquid is extracted towards the surface. Thus, the trapped liquids retained in the residue are depleted in incompatible trace elements. This melting process is named critical melting by Maaloe (1982). Thompson & Gibson (2000) have found a high magnesian olivine ($Fo_{93.3}$) in a basalt-picrite dyke linked to the Tristan mantle plume. These authors suggest that these olivines were formed under high temperatures

(1700°C), derived from an unerupted komatiitic melt located beneath the Moho and then carried to the upper crust levels by less Mg-rich magmas. In this case, these olivines are not in equilibrium with the whole rock. It is not the case, for the Ecuadorian picrite. Indeed we have shown in a previous section, that olivine in the picrite was in equilibrium with the host lava.

Geochemical and isotopical compositions of the Ecuadorian picrite show that this rock derived from a highly depleted hot mantle source. The petrological and geochemical observations indicate that the high MgO content, and the large LREE-depletion of this picrite are not due to olivine accumulation but to the primitive characters of the melt. Moreover, the MgO contents of the calculated liquid and whole rock are similar. Thus, this picrite represents a primary melt produced at the initial time of melting of the mantle source. This Mg-rich liquid was immediately extracted from the source and raised through the oceanic lithosphere to erupt in the seawater. During the magma ascent, olivine crystallized but the rapid raising generated a large diversity in the olivine morphology.

2. The presence of ultramafic lavas in the Gorgona island (Kerr et al., 1994, 1996; Arndt et al., 1997; Révillon et al., 2000), Colombia (Spadea et al., 1989; Kerr et al., 1996, 1997, 1998), Costa Rica (Alvarado et al., 1997) and now in Ecuador, reflects the presence of an abnormal thermal event in the Late Cretaceous. The Late Cretaceous Caribbean magmatism is not the only case known in the Pacific. A magmatic pulse of similar age is reported in the Ontong Java oceanic plateau (Mahoney, 1993). During the Late Cretaceous, a thermal event occurred and led to an important production of oceanic crust correlated with a rapid accretionary rate ridge (greater than 10cm/year). 90 Ma coincides with the paroxysm magmatism of the Caribbean plateau with a maximum of the sea level elevation who generated the highest marine transgression of the Phanerozoic times (Hancock, 1979; Haq et al., 1987). These 90 Ma events are linked with a world-wide thermal event and the development of carbonate platforms, in particular in the Caribbean area. Generally, ultramafic lavas, like picrites and komatiites are seldom exposed because they are trapped in the deeper parts of the crust. In the case of the Caribbean plateau, the eruption of komatiites and picrites suggests that they represent the initial magmatic products of the oceanic plateau and that the oceanic crust, basement of the oceanic plateau, was probably thin enough to allow their eruption.

3 – The presence of picrites and komatiites scattered in various localities of the Caribbean area is related first to the multi phased accretion of the CCOP to the northern

margin of South America, and second to the fragmentation and deformation of the Caribbean plate during Tertiary to Recent times. Alvarado et al. (1997) suggested that the picrites and komatiites from these different localities have a common origin. It is commonly considered that the Mg-rich and depleted lavas derived from the hottest parts of the mantle plume, while the enriched basalts are produced by different melting processes in a cooler region of the plume. So, the picrites and komatiites of the CCOP represent the remnants of the ascending plume head. Two hypothesis can be proposed to explain their scattered occurrences. (1) They belong to the same oceanic plateau and were emplaced during a single and same event and their present day geographic distribution is due only to tectonic events. (2) They could also represent the remnants of different and contemporaneous small plumes linked to the plume head of a superplume trapped in the transition zone (Brunet & Yuen, 2000).

Chapter 6

PETROLOGY AND GEOCHEMISTRY OF A LATE CRETACEOUS ISLAND ARC IN THE WESTERN CORDILLERA FROM ECUADOR

CHAPTER 6

PETROLOGY AND GEOCHEMISTRY OF A LATE CRETACEOUS ISLAND ARC IN THE WESTERN CORDILLERA OF ECUADOR

INTRODUCTION

During Jurassic times, the paleo-Pacific plate was subducting beneath the South American plate and arc-magmas emplaced in Colombia and Ecuador. The remnants of this arc are presently found along the Subandean zone of Ecuador. During the Cretaceous and Paleocene, subduction stopped beneath the Ecuadorian margin. The late Cretaceous and Paleocene magmatic arcs exposed now in Ecuador are exotic and developed somewhere in the Eastern Pacific. These accreted intra-oceanic arcs, together with their oceanic plateaus, played a key role in the continental growth of the northwestern margin of South America during Mesozoic and Tertiary times.

Accretions of oceanic plateaus to the Ecuadorian margin frequently triggered arc jumps in the oceanic realm. Therefore, after the Santonian-Campanian accretion (≈ 85-80 Ma), the Albian(?)-Santonian island arcs were relayed by Campanian-Maastrichtian intra-oceanic arcs, and the latter were succeeded by a Paleocene(?)-Middle Eocene island arc after the Late Maastrichtian accretion episode (≈ 70-65 Ma).

This short chapter is devoted to a Campanian-Maastrichtian arc-suite from the Western Cordillera of Ecuador. We will first present the petrology and geochemistry of the Upper Cretaceous arc-rocks. Then, we will compare these Upper Cretaceous arc-rocks with those of similar ages exposed in Colombia, the Caribbean and central America.

GEOLOGICAL NOTES

The presence of subduction-related rocks among the accreted oceanic terranes of western Ecuador has been long recognized [Lebrat et al., 1987; Bourgois et al., 1990; Wallrabe-Adams, 1990; Reynaud et al., 1999]. These arc-rocks are exposed in the Western Cordillera and along the coast.

In the Western Cordillera of Central Ecuador, recent geological studies and mapping by Hughes and Pilatasag (in press) have identified and date the Macuchi arc-terrane of Paleocene(?)-Middle Eocene age, which has been considered so far as Late Cretaceous. The Macuchi arc accreted to the Ecuadorian margin during Middle to Late Eocene times (~ 38 Ma; Hughes and Pilatasag, in press).

In the Western Cordillera of Northern Ecuador, Boland et al. (2000) identified (i) a Santonian oceanic basement (Pallatanga unit) overlain by a Campanian-Maastrichtian island arc (Río Cala unit), and (ii) a large-scale island arc terrane of Campanian-Maastrichtian age (Naranjal unit), accreted near the Early-Middle Eocene boundary (≈ 48-50 Ma). Since the latter unit constitutes the NE-ward extension of the Pedernales-Esmeraldas area of coastal Ecuador, the igneous basement of the Naranjal unit is most probably part of the Late Cretaceous Caribbean oceanic Plateau (see chapter 4).

In the southern coastal zone (Guayaquil, Manta), the Early Cretaceous oceanic plateau (Piñón Formation) is overlain by Late Cretaceous igneous and volcaniclastic rocks related to the activity of successive island arcs. The oldest arc (Las Orquídeas Member) is undated and exhibits tholeiitic affinities (Reynaud et al., 1999). It is succeeded by the Cenomanian-Campanian Cayo arc, the volcanic remnants of which are found only as reworked blocks and pebbles in a thick sequence of greywackes (Benítez, 1995). In the Guayaquil area, the Early Cretaceous oceanic plateau and related arcs accreted to the continental margin during the Late Paleocene (Jaillard et al., 1995; 1997). The third and youngest arc, known in the Manta area as the San Lorenzo Formation, is of Campanian-Maastrichtian age (Lebrat et al., 1987; Ordoñez 1996) exhibits calc-alkaline affinities (Lebrat et al., 1987; Reynaud et al., 1999). In the Manta area, since the Manabí basin recorded a regional unconformity between Maastrichtian and Middle Paleocene deposits (Deniaud, 2000), the accretion may have occurred in Late Maastrichtian or Early Paleocene times. Note that the eastern part of the Campanian-Maastrichtian Naranjal island arc of the western Cordillera appears to represent the NE-ward extension of the Manta area of coastal Ecuador. The arc-igneous rocks and their basement are overlain by marine sediments deposited in two generations of fore-arc basins of Eocene, and latest Oligocene - Pliocene age, respectively (Benítez, 1995; Jaillard et al., 1995; Deniaud, 2000).

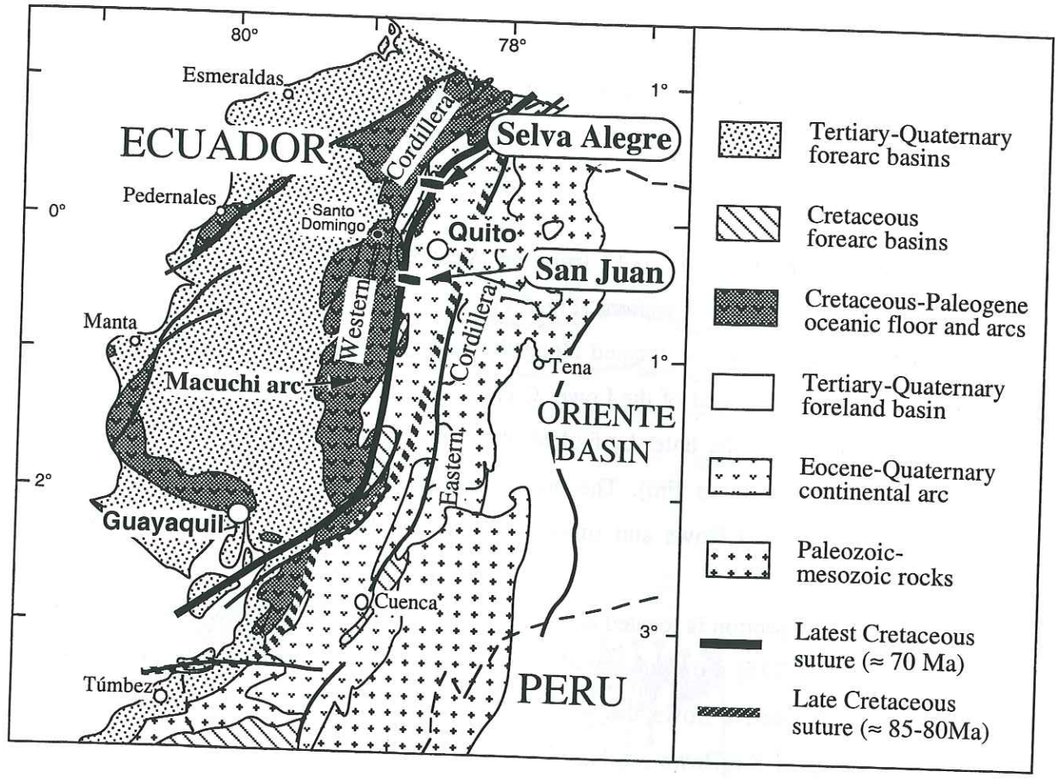

Fig. 6.1. Schematic geological map of Ecuador showing the main geological and tectonic units.

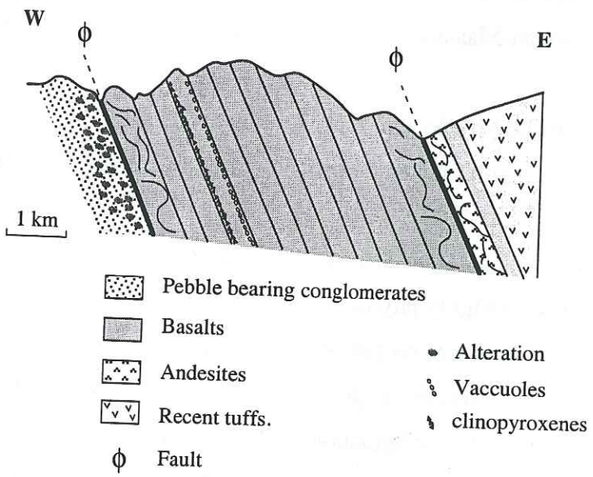

Fig. 6.2: Schematic cross section of the Selva Alegre sequence showing the different components of the island arc.

THE LATEST CRETACEOUS RÍO CALA ISLAND ARC

Petrology

The Late Cretaceous arc-rocks from the Western Cordillera have been sampled for petrological studies along two sections (Fig. 6.1).

The southern section is located along the old Quito-Santo Domingo. road The arc-volcanic rocks crop out west of the Lower Cretaceous San Juan ultramafic-mafic cumulates, and are separated from the latter by faulted blocks of Tertiary volcaniclastic sediments and andesitic breccias (Silante Fm). The arc-volcanic rocks (98SJ6 to 98SJ10) consist of predominantly massive flows and subordinate pillowed-flows. They are clinopyroxene-phyric.

The northern section is located along the Otavalo-Selva Alegre road (Fig. 6.2). The arc-rocks (98OT4-98OT15) crop out roughly four to five kilometers long and consist of one to two meters thick massive flows, dipping steeply to the east. Sometimes, the flows are almost vertical. The top of the flows are highly vesicular with small plagioclase phenocrysts. In contrast, the base of the flows are highly phyric with large and abundant clinopyroxene phenocrysts associated locally with millimetric-sized altered olivine. To the east, the arc-lavas are in fault contact with Tertiary andesitic breccias, whereas to the west, they are in fault contact with Campanian-Maastrichtian greywackes which also dip steeply to the east (Boland et al., 2000).

Although separated by 65 km, these two outcrops are assumed to belong to the same unit, because of their similar tectonic postion, and comparable petrological and geochemical features.

Two rock types have been distinguished on the basis of the presence or absence of olivine. All the lavas are highly phyric with large clinopyroxene (up to centimeter-sized) with or without olivine. Olivine size ranges between 0.5 to 1 mm and plagioclase occurs solely as microliths in the matrix. Olivine and plagioclase are seldom preserved. Olivine is replaced by smectite and serpentine while plagioclase is chloritised. Clinopyroxene is always preserved but often fractured. When present, Fe-Ti oxides cluster in the matrix and therefore, are the last to crystallized.

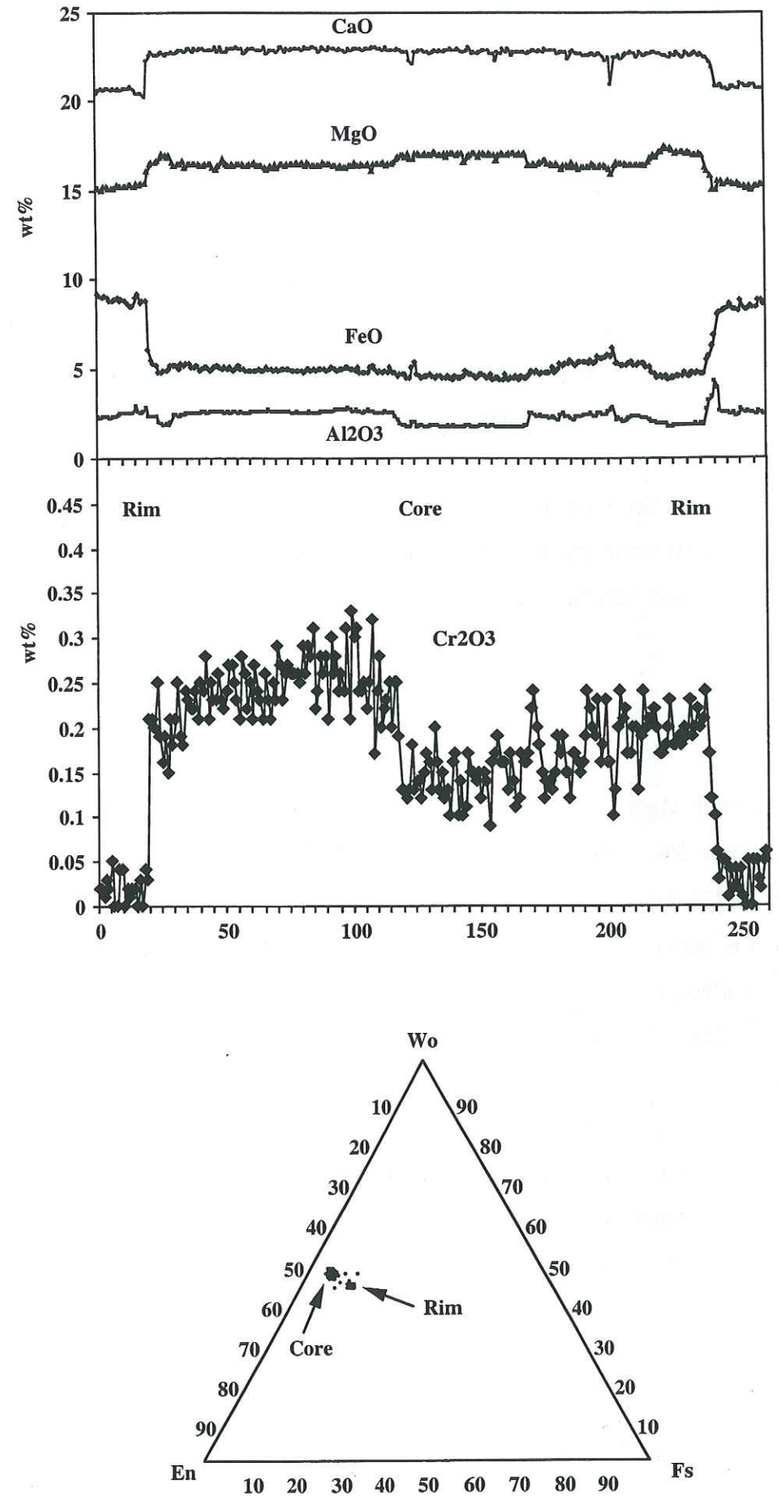

Fig. 6.3: Chemical variations from core to rim in clinopyroxene from Otavalo.

The olivine-free basalts include abundant clinopyroxene. The clinopyroxene phenocrysts are up to two centimeters-sized but this mineral occurs also as 0.2 millimeter-sized microphenocrysts in the matrix. Clinopyroxene exhibits diopsidic composition ($En_{48.6}$; $Wo_{47.8}$; $Fs_{4.6}$) but the phenocrysts show chemical variations_from core to rim (Fig. 6.3). Compared to the rims, cores are more MgO-, CaO-, Cr_2O_3-rich. These variations are examplified in the 98OT13 clinopyroxene (Fig. 6.3). However, the MgO-, CaO-, Cr_2O_3 variations do no show linear trends. This suggests that the growth of the largest clinopyroxene phenocrysts did not occur in melts with homegeneous compositions. The cores were likely formed in Mg-rich melts while the rims developed in more differentiated magmas.

The *olivine-basalts* differ from the clinopyroxene-rich, olivine-free lavas by less abundant and smaller clinopyroxene grains. Although clinopyroxene is also a diopside, it does not exhibit chemical differences between core and rim.

Geochemistry

On the basis of their MgO contents, the volcanic rocks exposed along the San Juan section are basalts (MgO > 5%; Table 6.1). These rocks are TiO_2- (< 0.8) and K_2O- (< 0.11) poor and Al_2O_3-rich. 98SJ7 differ from the other two samples by very high Mg, and by flat REE patterns (98SJ9 et 98SJ7) or slightly enriched in LREE (98SJ8) (Fig. 6.4). Their primitive-mantle normalized multi-element plots have the systematic negative Nb and Ta anomalies of arc-rocks. Their Sr and Eu negative or positive anomalies indicate plagioclase accumulation or removal.

The volcanic rocks sampled along the Selva Alegre section are less magnesian than those of San Juan. Olivine basalts have higher MgO contents (~ 8 %) than the clinopyroxene-rich lavas, which have more andesitic compositions (MgO < 5 %). Basalts and andesites are TiO_2-poor (< 1%) and Al_2O_3-rich (>14.6%). Alkalis contents (Na_2O+K_2O) range from 4.5 to 8 % (Table 6.1).

N°Ech.	98OT4	98OT5	98OT6	98OT7	98OT8	98OT9	98OT10	98OT11	98OT12	09OT13	98OT14	98sj7d	98sj8d	98sj9d	98SJ5
Nom	Basalt	Basalt	Basalt	Basalt	Basalt	Basalt	Basalt	Basalt	Basalt	Ankaramite	Ankaramite	Basalt	Basalt	Basalt	Basalt
SiO2	52.78	53.15	52.77	51.40	50.25	-	53.14	52.30	51.45	53.18	52.68	52.64	50.42	53.27	55.45
TiO2	0.99	0.84	0.80	0.75	0.73	-	0.84	0.87	0.99	0.81	0.82	0.34	0.43	0.85	0.90
Al2O3	17.16	16.44	15.19	14.60	14.98	-	17.50	18.25	16.94	16.45	16.75	13.39	14.72	15.43	15.15
FeO	9.23	8.65	8.97	8.90	9.41	-	8.63	8.88	9.54	8.33	8.37	8.62	9.90	11.98	12.57
MnO	0.16	0.18	0.17	0.15	0.17	-	0.14	0.15	0.16	0.17	0.16	0.17	0.26	0.19	0.20
MgO	3.36	5.15	6.53	8.07	8.74	-	5.45	4.78	4.87	6.23	6.19	12.96	11.29	5.41	4.17
CaO	9.05	7.41	9.21	10.57	10.73	-	9.03	8.64	10.01	8.41	10.19	9.73	10.02	8.51	8.43
Na2O	4.43	2.34	3.87	2.49	2.82	-	3.28	3.34	3.85	3.22	2.36	1.90	2.70	4.20	2.87
K2O	2.28	5.44	2.15	2.78	1.90	-	1.56	2.35	1.85	2.77	2.09	0.03	0.02	0.03	0.15
P2O5	0.55	0.39	0.33	0.29	0.26	-	0.42	0.45	0.34	0.43	0.39	0.06	0.11	0.11	0.11
LOI	2.32	2.76	2.62	3.23	2.57	-	1.86	1.80	2.78	2.21	2.25	2.22	3.75	3.43	1.25
Total	100.00	100.00	100.00	100.00	100.00	-	100.00	100.00	100.00	100.00	100.00	99.85	99.87	99.99	100.00
Ba	337	1724	459	524	604	298	521	708	852	800	609	32.93	14.32	8.33	51.18
Rb	31.34	110.8	47.99	54.50	46.40	33.24	33.04	54.00	41.57	57.90	46.90	0.68	0.36	0.42	0.49
Sr	-	557	370	318	652	-	-	-	-	630	765	92.89	147.29	20.67	154.04
Ta	0.15	0.16	0.15	0.13	0.12	0.14	0.19	0.21	0.23	0.20	0.19	0.03	0.05	0.03	0.05
Th	3.05	2.03	1.79	1.61	1.57	1.26	2.12	2.23	1.29	2.98	2.57	0.15	0.64	0.18	0.25
Zr	126	89.17	80.39	71.11	62.89	60.37	94.33	95.77	70.19	108.2	100.6	26.17	32.67	35.66	36.97
Nb	5.14	3.28	2.96	2.64	2.38	2.67	3.80	3.15	3.12	4.01	3.89	0.45	0.68	0.49	0.77
Y	23.67	19.96	18.91	17.80	15.33	12.75	18.67	19.81	20.50	18.71	20.57	8.52	8.05	17.20	20.34
Hf	3.11	2.36	2.19	1.94	1.81	1.61	2.52	2.43	1.80	2.80	2.66	0.71	0.89	1.03	1.22
V	341	298	326	278	344	-	339	356	347	283	279	202	246	417	-
Cr	15	89	182	346	133	-	78	63	41	109	55	726	561	61	-
Ni	5	19	38	52	39	-	21	20	30	33	25	247	187	26	-
Co	26.08	26.68	33.67	36.61	42.32	23.38	27.75	28.21	32.96	30.67	30.33	45.44	47.27	36.25	42.72
U	1.35	0.73	0.63	0.55	0.57	0.49	0.82	0.86	0.54	1.03	0.88	0.05	0.22	0.07	0.10
Sc	28	23	28	38	45	-	37	31	29	30	30	63	85	64	-
Cu	133	73	64	57	44	-	92	92	99	69	68	22	18	27	-
Zn	97	67	65	79	61	-	82	83	87	70	69	82	136	97	-
La	27.38	17.56	15.89	14.70	13.23	11.21	18.00	18.48	11.26	22.92	20.46	1.69	6.42	2.27	2.97
Ce	57.80	39.82	34.85	32.00	29.43	24.30	39.56	42.01	26.14	49.14	44.04	4.48	16.12	5.68	7.88
Pr	7.74	5.41	4.79	4.38	4.02	3.35	5.42	5.70	3.60	6.41	5.78	0.73	2.44	0.93	1.25
Nd	32.77	22.86	20.18	18.72	17.37	14.45	23.31	23.93	15.53	26.49	24.11	3.63	11.14	4.84	6.13
Sm	6.85	4.77	4.29	3.99	3.87	3.11	4.81	4.97	3.59	5.22	4.93	1.05	2.31	1.58	1.95
Eu	1.95	1.47	1.30	1.23	1.19	0.89	1.35	1.62	1.33	1.51	1.47	0.30	0.63	0.65	0.77
Gd	6.16	4.26	4.06	3.85	3.76	3.07	4.64	4.37	3.67	4.45	4.36	1.20	1.93	2.07	2.42
Tb	0.81	0.60	0.57	0.53	0.50	0.41	0.60	0.66	0.60	0.60	0.61	0.21	0.27	0.39	0.45
Dy	4.52	3.38	3.16	3.00	2.74	2.29	3.34	3.36	3.39	3.17	3.44	1.39	1.57	2.73	3.08
Ho	0.87	0.60	0.64	0.60	0.54	0.46	0.67	0.69	0.73	0.64	0.70	0.30	0.32	0.63	0.71
Er	2.21	1.86	1.78	1.65	1.42	1.17	1.74	1.86	2.03	1.73	1.92	0.82	0.85	1.73	2.04
Tm	-	-	-	-	-	-	-	-	-	-	-	-	-	-	-
Yb	2.18	1.72	1.63	1.52	1.26	1.16	1.75	1.77	1.99	1.56	1.79	0.92	0.87	1.90	2.05
Lu	0.34	0.27	0.26	0.25	0.20	0.19	0.28	0.28	0.30	0.25	0.28	0.15	0.14	0.31	0.32
(Ce/Yb)n	6.86	5.99	5.54	5.45	6.06	5.43	5.86	6.14	3.41	8.17	6.38	1.27	4.82	0.77	1.00
(La/Sm)n	2.52	2.32	2.33	2.32	2.15	2.27	2.36	2.34	1.97	2.76	2.61	1.01	1.75	0.91	0.96
(La/Yb)n	8.48	6.90	6.59	6.52	7.11	6.54	6.95	7.05	3.83	9.94	7.72	1.24	5.00	0.81	0.98
La/Nb	5.33	5.35	5.38	5.57	5.57	4.20	4.74	5.86	3.60	5.72	5.25	3.76	9.47	4.64	3.88

Table 6.1: Major (wt%) and trace element (ppm) analyses for the Selva Alegre and San Juan samples. -: not analysed.

Samples	t (Ma)	Sm	Nd	Rb	Sr	143Nd/144Nd	87Sr/86Sr	147Sm/144Nd	(143Nd/144Nd)i	εNd)i	87Rb/86Sr	(87Sr/86Sr)t	εSr)t	(206Pb/204Pb)i	(207Pb/204Pb)i	(208Pb/204Pb)i
980T4wr														18.94	15.60	38.51
980T5wr	90	4.77	22.86	110.8	557.1	0.512892	±6	0.704173 ±7	0.512818	5.77	0.575231	0.703437	-13.58	18.82	15.58	38.46
980T6wr	90	4.29	20.18	48.0	369.9	0.512890	±7	0.703936 ±6	0.512814	5.70	0.375225	0.703456	-13.32	18.86	15.59	38.41
980T7wr	90	3.99	18.72	54.5	317.7	0.512884	±5	0.704114 ±9	0.512808	5.58	0.496149	0.703480	-12.99	18.78	15.57	38.30
980T8wr	90	3.87	17.37	46.4	651.6	0.512870	±7	0.703720 ±7	0.134826	5.24	0.205946	0.703457	-13.31	18.95	15.59	38.68
980T10wr	90	4.81	23.31	33.0	743.5	0.512902	±5	0.703554 ±9	0.124685	5.98	0.128532	0.703390	-14.26	18.82	15.59	38.43
980T11wr														18.83	15.59	38.44
980T12wr	90	3.59	15.53	41.6	512.4	0.512925	±7	0.703710 ±9	0.139909	6.25	0.234616	0.703410	-13.97	18.79	15.58	38.32
980T13wr	90	5.22	26.49	57.9	629.5	0.512869	±6	0.703773 ±8	0.119170	5.40	0.266012	0.703433	-13.65	19.00	15.61	38.80
980T14wr	90	4.93	24.11	46.9	764.5	0.512862	±5	0.703736 ±7	0.123622	5.21	0.177424	0.703509	-12.57	19.08	15.59	38.81
980T5-cpx1	90	2.46	8.46			0.512946	±6	0.175807	0.512842	6.25						
980T5-cpx2	90	2.46	8.46			0.512922	±10	0.175806	0.512818	5.78						
980T8-cpx1	90	2.81	9.06			0.512922	±14	0.187520	0.512812	5.65						
980T8-cpx2	90	2.81	9.06			0.512905	±10	0.187519	0.512795	5.32						
980T13-cpx1	90	4.39	14.60	2.34	151.7	0.512902	±7	0.181901	0.512795	5.32						
980T13-cpx2	90	4.13	14.40			0.512920	±18	0.173403	0.512818	5.77				18.59	15.54	38.41

Table 6.2: Nd, Sr and Pb isotopic compositions for the Selva Alegre rocks and mineral separates. (i): recalculated initial ratios based on the Sm, Nd, U, Th and Pb contents determinated by ICP-MS (refer Table 6.1)

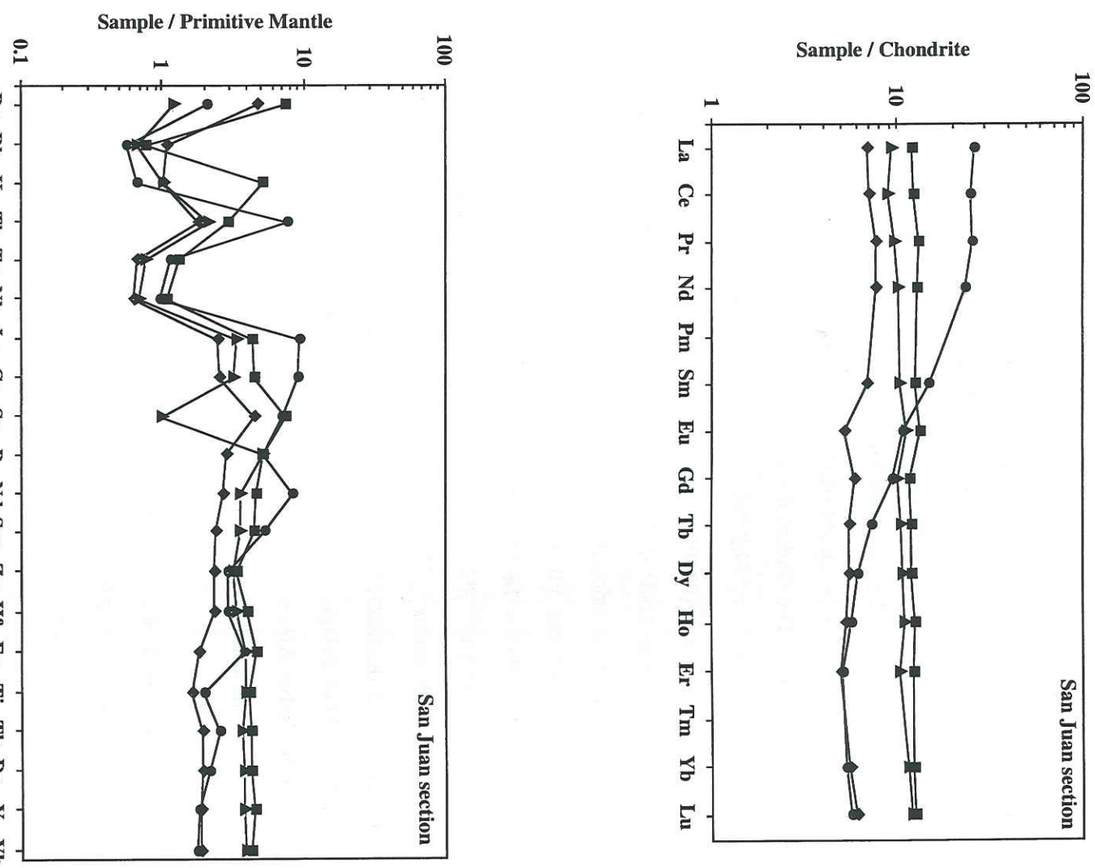

Fig. 6.4: Chondrite- and primitive mantle-normalized (Sun & McDonough, 1989) rare earth element patterns and multi-element diagrams for basalts of the San Juan section.

Trace element chemistry of the basalts and andesites is very homogeneous (Table 6.1; Fig 6.5). All the lavas are LREE-enriched (3.83 < (La/Yb)n < 9.94) and exhibit negative anomalies in Ta, Nb and Ti. These anomalies are characteristic of island arcs rocks. Clinopyroxene separates and whole rocks have similar trace element chemistry : similar LREE-enrichment, specially for the Pr, Sm and Nd and marked negative Ta and Nb anomalies (Table 6.2; Fig 6.6). Basalts and andesites from Selva Alegre differ from those of San Juan by higher LREE-enrichments and Th contents and thus, display calc-alkaline affinities.

Nd and Sr isotopic compositions of the whole rocks from Selva Alegre are extremely homogeneous (Table 6.3). The εNd of the clinopyroxene separates are very close to those of their host rock (Table 6.2). $(^{143}Nd/^{144}Nd)i$ ratios range between 0.512789 and 0.512843. Basalts, andesites and clinopyroxene separates cluster in the intra-oceanic arc field with εNd around +6 (Fig. 6.7). The εNd of the arc-tholeiitic basaltic dyke (98SJ5) is significantly higher (+8) than those of the calc-alkaline lavas.

The very homogeneous Pb initial isotopic compositions of the Selva Alegre basalts cluster around $(^{206}Pb/^{204}Pb)i$ = 18.7 to 19 (Table 3). Clinopyroxene separates differ from the whole rocks by lower $(^{206}Pb/^{204}Pb)i$ (< 18.7; Fig. 6.8). The two clinopyroxene-phyric andesites exhibit the highest Pb ratios [$(^{206}Pb/^{204}Pb)i$ > 19.00] than the basalts. In the $^{207}Pb/^{204}Pb$-$^{206}Pb/^{204}Pb$ correlation diagram, the Selva Alegre volcanic rocks plot above the NHRL line and close to the field of pelagic sediments. This suggests involvement of pelagic sediments in the genesis of the Selva Alegre calc-alkaline lavas. The Nd and Pb isotopic compositions of the Selva Alegre calc-alkaline volcanic rocks indicate that these rocks derived from an enriched source.

Thus, the San Juan arc-tholeiites and Selva Alegre calc-alkaline volcanic rocks represent the remnants of an intra-oceanic arc, dated by Boland et al. (2000) as Campanian-Maastrichtian (≈ 80-65 Ma).

N°Ech.	98OT5 Cpx	98OT8 Cpx	98OT13 Cpx
Ba	52.14	6.26	16.04
Rb	3.63	0.48	1.17
Sr	66.17	56.99	111.28
Ta	0.01	0.00	0.01
Th	0.14	0.06	0.19
Zr	18.74	16.33	26.43
Nb	0.23	0.07	0.17
Hf	0.80	0.80	1.15
U	0.06	0.02	0.16
La	4.33	3.03	4.25
Ce	10.48	8.71	13.96
Pr	1.62	1.55	2.51
Nd	8.66	9.06	14.45
Sm	2.46	2.81	4.13
Eu	0.80	0.91	1.24
Gd	2.78	3.12	4.29
Tb	0.40	0.44	0.59
Dy	2.51	2.69	3.59
Ho	0.47	0.49	0.66
Er	1.26	1.24	1.72
Tm	0.17	0.17	0.23
Yb	1.08	1.01	1.44
Lu	0.17	0.15	0.23
(Ce/Yb)n	2.51	2.24	2.50
(La/Sm)n	1.11	0.68	0.65
(La/Yb)n	2.70	2.03	1.99

Table 6.3: trace element (ppm) analyses for the Selva Alegre clinopyroxene

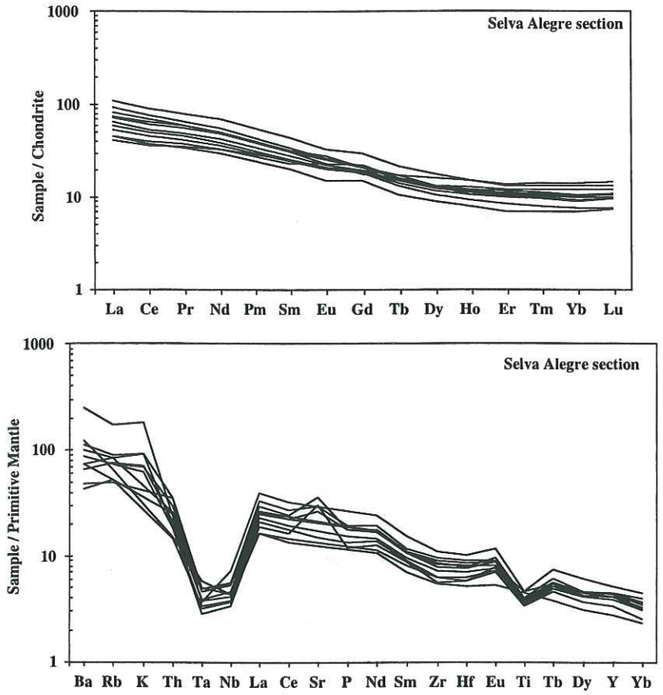

Fig. 6.5: Chondrite- and primitive mantle-normalized (Sun & McDonough, 1989) rare earth element patterns and multi-element diagrams for basalts and andesites of the Selva Alegre section.

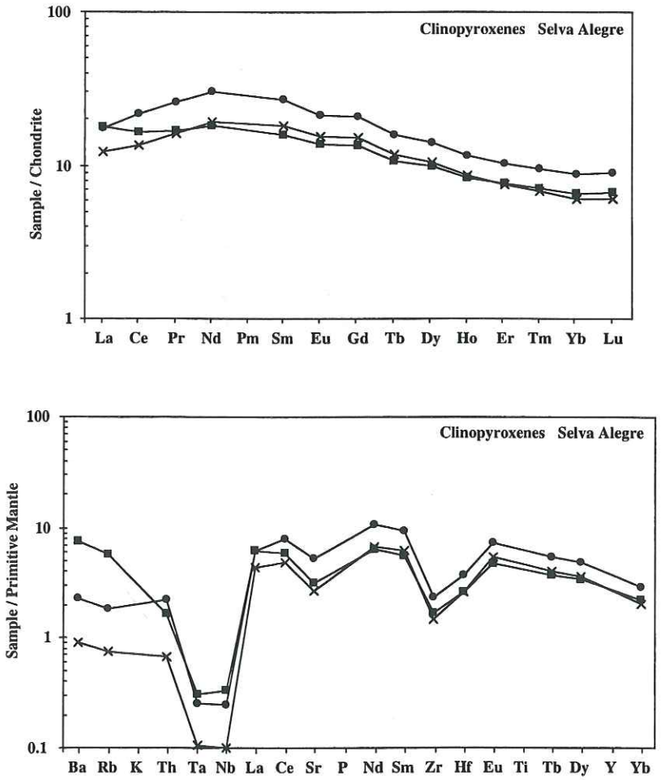

Fig. 6..6: Chondrite- and primitive mantle-normalized (Sun & McDonough, 1989) rare earth element patterns and multi-element diagrams for clinopyroxene of some lavas from Selva Alegre section.

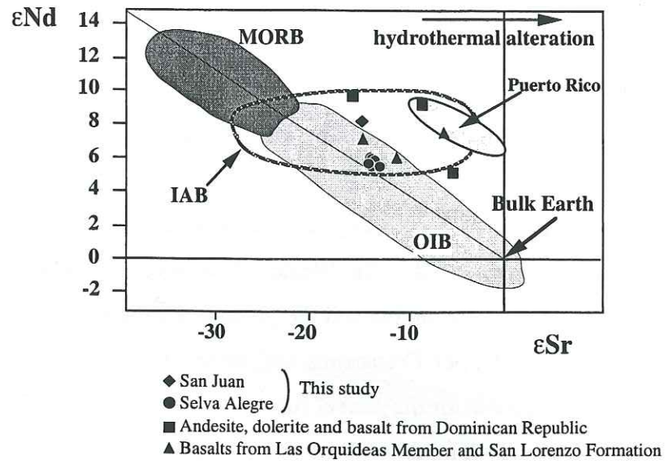

Fig. 6.7: Nd and Sr isotopic composition of the island arc rocks from Ecuador. Data from Dominican republic are reported after Dupuis (1999). Puerto Rico after Lebron and Perfit (1994). Data of basalts from Las Orquideas Member and San Lorenzo Formation after Reynaud et al. (1999).

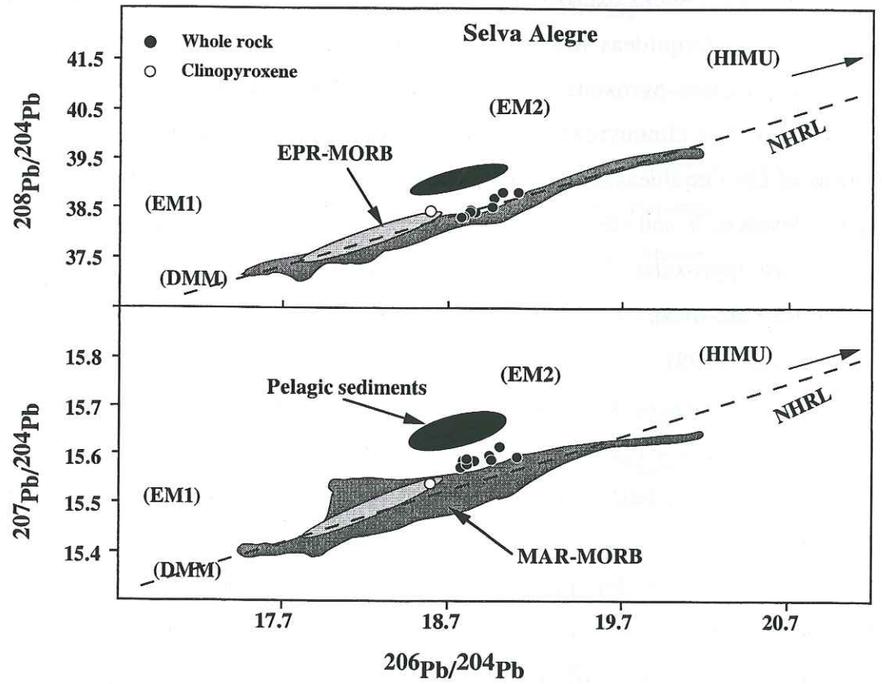

Fig. 6.8: $^{208}Pb/^{204}Pb$ vs $^{206}Pb/^{204}Pb$ and $^{207}Pb/^{204}Pb$ vs $^{206}Pb/^{204}Pb$ diagrams of some lavas from the Selva Alegre sequence. The "Northern Hemisphere Reference Line" (NHRL) and the field from some mantle reservoirs are reported after Zindler & Hart (1986). East Pacific ridge (EPR) MORB and Mid Atlantic Ridge (MAR) MORB data and Galapagos Islands field are from White et al. (1987). The pelagic sediment field is reported after Sun, 1980; White et Dupré, 1986; Ben Othman et al., 1989).

COMPARISON WITH THE CONTEMPORANEOUS ARC-ROCKS FROM COASTAL ECUADOR AND THE GREATER ANTILLES

This section is devoted to a petrological and geochemical comparison between the Upper Cretaceous arc-rocks accreted in the Western Cordillera and Coast of Ecuador, with those of similar age exposed in Colombia and the proto-Caribbean arc. This comparison will help to specify whether the Upper Cretaceous arc-tholeiites and calc-alkaline mafic lavas from Ecuador are correlatable with the coeval proto-Caribbean arc or with the arc-volcanic rocks from Costa Rica and the Colombian Western Cordillera.

Coastal Ecuador

In Ecuador, the arc-rocks exposed along the Pacific coast are mafic lavas and dolerites belonging to the Las Orquídeas Member and San Lorenzo Formation. The basalts and andesites are plagioclase-pyroxene phyric while the dolerites are formed of euhedral plagiocase and anhedral clinopyroxene. Both rocks display calc-alkaline affinities but the volcanic rocks of Las Orquídeas differ from rocks of the San Lorenzo Formation in that they have very low levels of Y and HREE (Reynaud et al., 1999). Basaltic fragments of the Cayo turbidites are orthopyroxene-clinopyroxene-plagioclase-phyric displaying calc-alkaline affinities. All these arc-rocks have high and homogeneous εNd ratios that range between +7 to +6 (Reynaud et al., 1999).

The volcanic rocks of Las Orquídeas show features of arc-tholeiites and are geochemically similar to the basaltic dykes (98SJ5) which intrude the 123 Ma hornblende-bearing gabbro, located at the top of the San Juan cumulate sequence. This geochemical similarity is shown in Figure 6.9.

The Campanian-Maastrichtian arc-rocks from the Western Cordillera (Rio Cala unit) are similar to those of the coeval island arc of the Manta area (San Lorenzo Formation). They exhibit tholeiitic and calc-alkaline affinities and likely developed in an intra-oceanic setting.

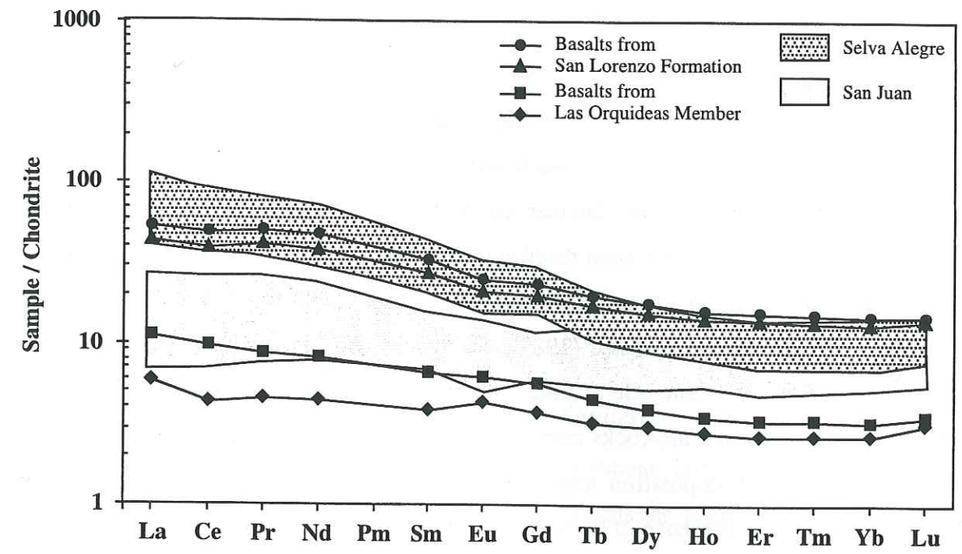

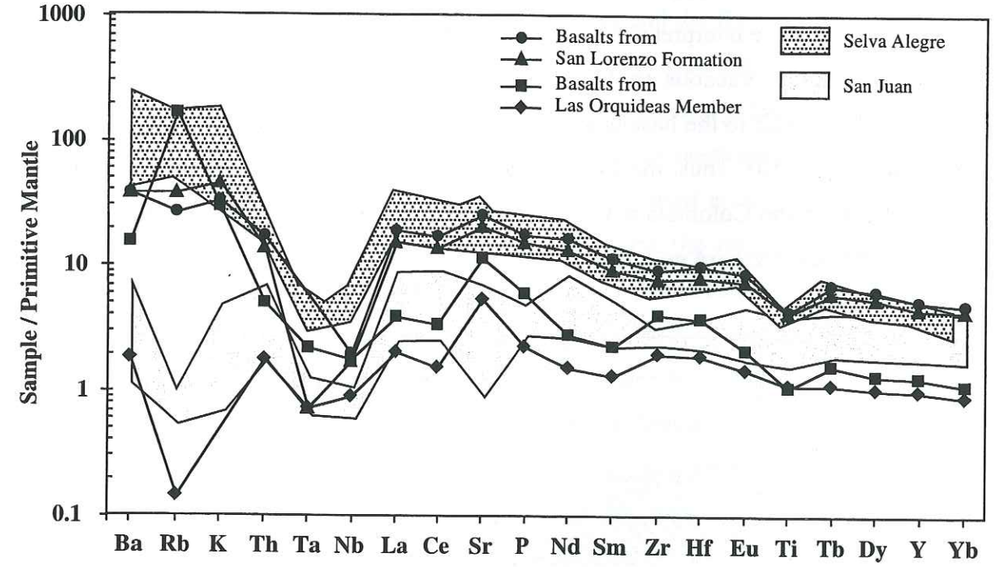

Fig. 6.9: Comparison of the chondrite- and primitive mantle-normalized (Sun & McDonough, 1989) rare earth element patterns and multi-element diagrams for island-arc basalts of Western Cordillera and Coast of Ecuador. Data of basalts from Las Orquideas Member and San Lorenzo Formation after Reynaud et al. (1999).

Western Cordillera of Colombia

The presence of Cretaceous arc-rocks tectonically imbricated with T-type MORB basalts (Diabase Group) from the Western and Coastal Cordilleras of Colombia have been recognized and characterized by Marriner and Millward (1984) and Millward et al. (1984). The T-type MORB basalts have been dated and identifed as oceanic plateau basalts belonging to the Late Cretaceous Caribbean-Colombian Plateau (Kerr et al., 1996). On the basis of geochemical investigations, Grösser (1989) and Spadea and Espinosa (1996) identified and characterized a thick volcanic pile of Late Cretaceous arc-rocks in the Western Cordillera of Colombia. These volcanic arc-rocks consist of submarine lavas, breccias, tuffs and dykes of basaltic to andesitic composition and minor shallow-level quartz-microdiorites. Grösser (1989) pointed out the presence of high-Mg basalts and andesites and calc-alkaline andesites. Spadea and Espinosa (1996) distinguished an older tholeiitic suite from a younger calc-alkaline suite represented by hornblende andesite. Based on the preserved igneous mineral chemistry and major and trace element compositions of the volcanic rocks, the tholeiitic and calc-alkaline suites are interpreted as developed in an intra-oceanic arc environment.

These Late Cretaceous tholeiitic and calc-alkaline arc-rocks from Colombia are geochemically similar to the basalts and andesites of the Selva Alegre and San Juan sections of Ecuador (Fig. 6.10). Thus, the Late Cretaceous arc-rocks from the Western Cordillera of northern Ecuador and Colombia may represent the remnants of the same intra-oceanic island arc, accreted to the northern margin of the South American plate.

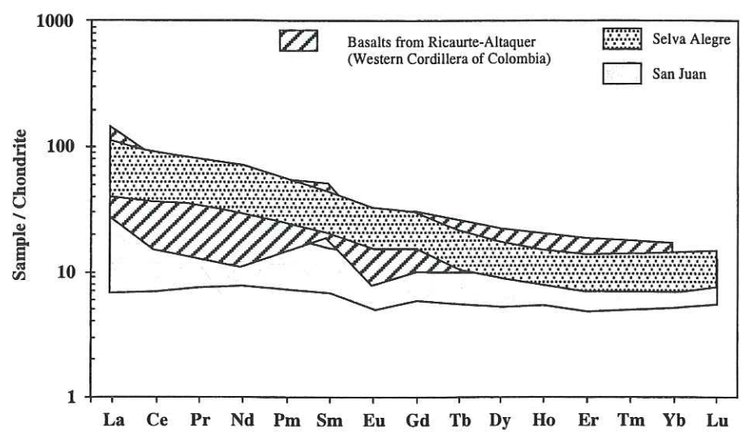

Fig. 6.10: Chondrite-normalized (Sun & McDonough, 1989) rare earth element diagrams for island-arc basalts from the Western Cordillera of Ecuador and Colombia. Data of basalts from the Colombia after Spadea & Espinosa (1996).

Central America

In Central America, Late Cretaceous calc-alkaline arc-magmatism is known throughout Honduras, Guatemala and Costa Rica. According to Gursky (1991), subduction of the Farallón plate occurred along the western margin of Costa Rica during the latest Cretaceous, leading to the development of an island arc, built on the southern edge of the Colombian-Caribbean oceanic plateau. Arc-volcanism ceased in the Eocene.

The proto-Caribbean arc in the Greater Antilles

During the Cretaceous, the so-called proto-Caribbean island arc resulted from the Southwest-ward subduction of the Atlantic ocean. It forms the present-day basement of the Greater Antilles.

Around 66 Ma (Late Maastrichtian) the proto-Caribbean arc of the Greater Antilles collided with the southernmost margin of North America and with the Bahamas carbonate platform, leading to the accretion of Cretaceous arc-rocks and the Caribbean oceanic plateau to the North American craton (Cuba, Hispaniola, Puerto Rico and the near by islands, Donnelly and Rogers, 1978, 1980; Donnelly et al., 1990). Similarly, the southern part of the proto-Caribbean arc and the Caribbean plateau accreted to the northwestern margin of South America during the Late Cretaceous or Early Tertiary (Millard et al., 1984; Berrangé and Thorpe, 1988; Burke, 1978). Remnants of this arc lie along the northern margin of South American from the Western Cordillera of Colombia, Venezuela to the West Indies (Aruba, Tobago and Bonaire).

The pre-Eocene island-arc assemblages in the Greater Antilles consist of a primitive island-arc suite (PIA of Donnelly and Rogers, 1978, 1980; Donnelly et al., 1990; Lebron and Perfit, 1993) of Late Jurassic to Early Cretaceous age, succeeded during the Late Cretaceous by arc-tholeiites and/or calc-alkaline silicic plutons and/or andesites (CA suite of Donnnely and Rogers, 1978, 1980; Donnelly et al., 1990) and shoshonitic suites.

In Puerto Rico and Virgin islands, the Upper Cretaceous arc-rocks consist of porphyritic andesitic flows, pyroclastic breccias and ignimbrites, intercalated with coarse-grained volcaniclastic sediments. Consanguinous calc-alkaline plutons intrude the volcanic and volcaniclastic rocks.

The island of Bonaire in the Netherlands Antilles consists of a 5 km thick succession of submarine basaltic to rhyolitic flows, sills and tuffs. These rocks are enriched in LREE and

incompatible trace elements and exhibit arc-tholeiitic affinities (Kerr et al., 1996). On the island of Aruba, a Late Cretaceous calc-alkaline batholith intrudes the Cretaceous Caribbean Colombian oceanic plateau and derives likely from the partial melting of the oceanic plateau (White et al., in press).

The Upper Cretaceous arc-rocks of the Dominican Central Cordillera are exposed on both sides of the Duarte Complex which forms the core of the Cordillera. The Upper Cretaceous unit (Tireo Formation) consists of a thick pile of basaltic to andesitic pillowed flows, overlain by felsic tuffs and volcaniclastic rocks (Lewis et al., 1991). Few available geochemical data indicate that the volcanic rocks exhibit calc-alkaline affinities and high εNd ratios (+5.3; Dupuis, 1999). The Las Lagunas Formation (tholeiitic basalts with Late Cretaceous age) consists of very few pillowed and massive basaltic flows overlain by thick volcaniclastic turbidites, the base of which is intruded by doleritic dykes. TiO_2-poor basalts and dolerites display arc-tholeiitic affinities with slightly depleted LREE patterns and high εNd ratios (+9; Dupuis, 1999; Fig. 6.11). The presence of a thick sequence of turbidites, the LREE depletion and high εNd ratios of the basalts suggest that the Las Lagunas Formation developed during the opening of a back-arc basin, east of the Tireo-arc.

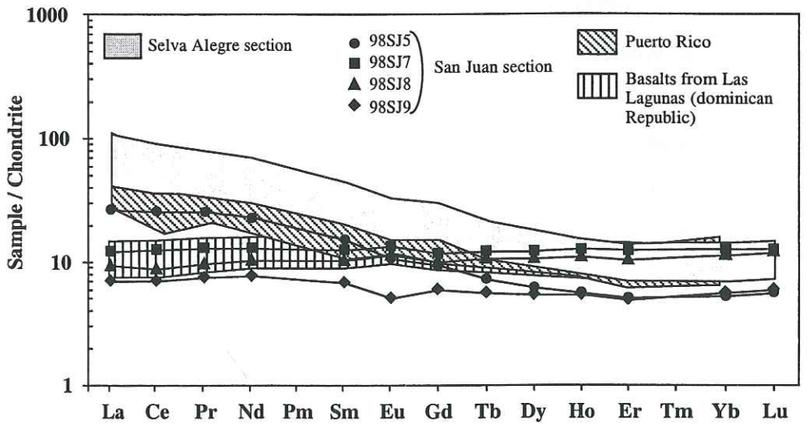

Fig. 6.11: Comparison of the chondrite-normalized (Sun & McDonough, 1989) rare earth element diagrams for island-arc basalts of Western Cordillera of Ecuador and peri-Caribbean area. Data of basalts from Dominican Republic and Puerto Rico after Dupuis (1999) and Freydier (1995) respectively.

In summary, the Late Cretaceous arc-rocks from Ecuador display tholeiitic or calc-alkaline affinities. Their high and homogneous εNd ratios fall in the range of intra-oceanic arcs and suggest derivation from a depleted mantle source which was slightly contaminated by subduction fluids. Field observations and mapping correlations bring evidence that these Late Cretaceous intra-oceanic arcs are coeval with those exposed in the Western Cordillera from Colombia. They could be also correlated with the arc-rocks from Costa Rica.

They differ from the contemporaneous proto-Caribbean arc because:

- felsic rocks are absent in Ecuador while they are volumetrically abundant in the Greater Antilles;

- the proto-Caribbean arc is related to the Southwest-ward subduction of the Atlantic ocean while the Ecuadorian-Colombian arcs of Campanian-Maastrichtian age are most probably due to the Northeast-ward subduction of the paleo-Pacific plate.

CONCLUSIONS AND GEODYNAMIC IMPLICATIONS

- The Campanian-Maastrichtian arc-rocks from the Western Cordillera and coastal Ecuador exhibit tholeiitic and calc-alkaline affinities and likely developed in an intra-oceanic setting.

- The Campanian-Maastrichtian (80-70 Ma) arc-rocks from the Western Cordillera of Ecuador and Colombia are geochemically similar and could belong to the same intra-oceanic arc. They could be coeval with the Upper Cretaceous arc of Costa Rica. This 80-70 Ma arc was probably built on the Late Cretaceous Caribbean Colombian oceanic plateau.

- In contrast, the 100-80 Ma intra-oceanic arcs from coastal Ecuador are built on the Early Cretaceous oceanic plateau. This implies, that at the end of the Cretaceous, the Early and Late Cretaceous plateaus were involved in the same subduction system.

- The geodynamic evolution of the Western Cordillera and coastal Ecuador during the Cretaceous and Early Tertiary is distinct from that of the proto-Caribbean arc from the Greater Antilles.

Chapter 7

PALINSPASTIC RECONSTITUTION OF THE GEODYNAMIC EVOLUTION OF THE WESTERN ECUADOR

CHAPTER 7: PALINSPASTIC RECONSTITUTION OF THE GEODYNAMIC EVOLUTION OF WESTERN ECUADOR

INTRODUCTION

In the previous chapters of this thesis, we have characterized the nature and tectonic setting of the oceanic crustal fragments, accreted to the northwestern margin of South America, and nowadays exposed in the Western Cordillera and the Coast of Ecuador. The data obtained during this work are based on field observations and petrological and geochemical investigations, including isotopic chemistry. In this last chapter, taking into account the crustal nature of these accreted fragments, i.e, oceanic plateau and/or intra-oceanic island arc, we will intent :

1 - to restore a cross section through the crust of the Early Cretaceous (123 Ma) oceanic plateau;

2 - to propose a palinspastic reconstitution of the geodynamic evolution of the northwestern margin of South America and neighbouring areas (Greater Antilles, Central America) from the Early Cretaceous (123 Ma, Barremian) up to Recent.

The data obtained during this work allowed us to charaterize the presence in the Western Cordillera of:

1- two distinct oceanic plateaus of Early and Late Cretaceous age, respectively.

2 - an intra-oceanic island arc of latest Cretaceous age (≈ 78-68 Ma; Boland et al., 2000) composed of arc-tholeiites and calc-alkaline basalts.

The Early Cretaceous (123 Ma) plateau (San Juan-Multitud Unit of the Western Cordillera) is composed of pillow basalts, dolerites and shallow level gabbroic plugs, and ultramafic to mafic cumulate rocks. The basalts, dolerites and isotropic gabbros are geochemically similar to oceanic plateau basalts (OPB), i.e., MgO = 7 %, flat REE, εNd = ~+7. Moreover, they have low Pb isotopic ratios. The cumulate rocks derive from the accumulation of olivine succeeded by clinopyroxene and plagioclase and are cogenetic with the basalts. The Piñón Formation exposed in coastal Ecuador is considered as part of the same Early Cretaceous plateau. The presence of some Piñón basalts with high εNd (+10) suggests that this Early Cretaceous plateau derived from a ridge-centered or near-ridge hotspot.

The igneous components of the Late Cretaceous plateau consist of sheeted picritic flows stratigraphically associated with Mg-rich basalts, ankaramites, basalts, dolerites and gabbroic

plugs. The picrites are LREE-depleted and characterized by high εNd values and low Pb isotopic ratios. This indicates that they derive from a depleted mantle source. The Mg-rich basalts and ankaramites are highly clinopyroxene-phyric and differ from the picrites by LREE-enriched patterns, lower εNd and high Pb ratios. The "normal" basalts (MgO = 6-7 %), dolerites and isotropic gabbros are geochemically similar to those of Early Cretaceous age but they differ in that they are highly radiogenic in Pb. These high Pb isotopic ratios of the MgO-rich basalts, ankaramites and normal basalts suggest the presence of a HIMU component in the source of the Late Cretaceous oceanic plateau basaltic melts. This is a feature common to all the basalts of the 92-86 Ma event of the Caribbean-Colombian Oceanic Plateau (CCOP), exposed in the Greater Antilles, Costa Rica and Colombia. In northwestern coastal Ecuador, in the vicinity of Pedernales and Esmeraldas, we have found exposures of hyaloclastites with basaltic and picritic fragments which are similar to those exposed in the Western Cordillera.

CROSS SECTION THROUGH THE EARLY CRETACEOUS OCEANIC PLATEAU

In chapter 3, we have shown that the San Juan ultramafic and mafic cumulate rocks and the basalts and dolerites of the Merced-Multitud Unit are cogenetic and represent different components of the same Early Cretaceous plateau. The San Juan ultramafic and mafic cumulate rocks can be considered as the plutonic part of the plateau and developed in a magma chamber which is not spatially connected with the basalts. Thus, we can try to restore a cross-section through the crust of this plateau. Even if the total thickness of this oceanic plateau crust is difficult to estimate, the dismembered San Juan and Merced-Multitud sections indicate that the Early Cretaceous plateau had a minimal total thickness ranging between 5 and 15 km.

Figure 7.1 illustrates a hypothetical cross-section through the Early Cretaceous Ecuadorian oceanic plateau. Several features can be pointed out.

First, we must notice that the uppermost levels of an oceanic plateau crust are always formed of pillow basalts, doleritic sheets and isotropic gabbroic plugs, regardless of the age and location of the plateau. Moreover, these rocks exhibit very homogeneous geochemical features (MgO = 6-7 %; flat REE patterns, εNd ~+7) which are those of most oceanic plateau basalts.

Second, we had the opportunity to study a cumulate sequence of oceanic plateau affinity. Cumulate plutonic rocks belonging to an oceanic plateau have been seldom

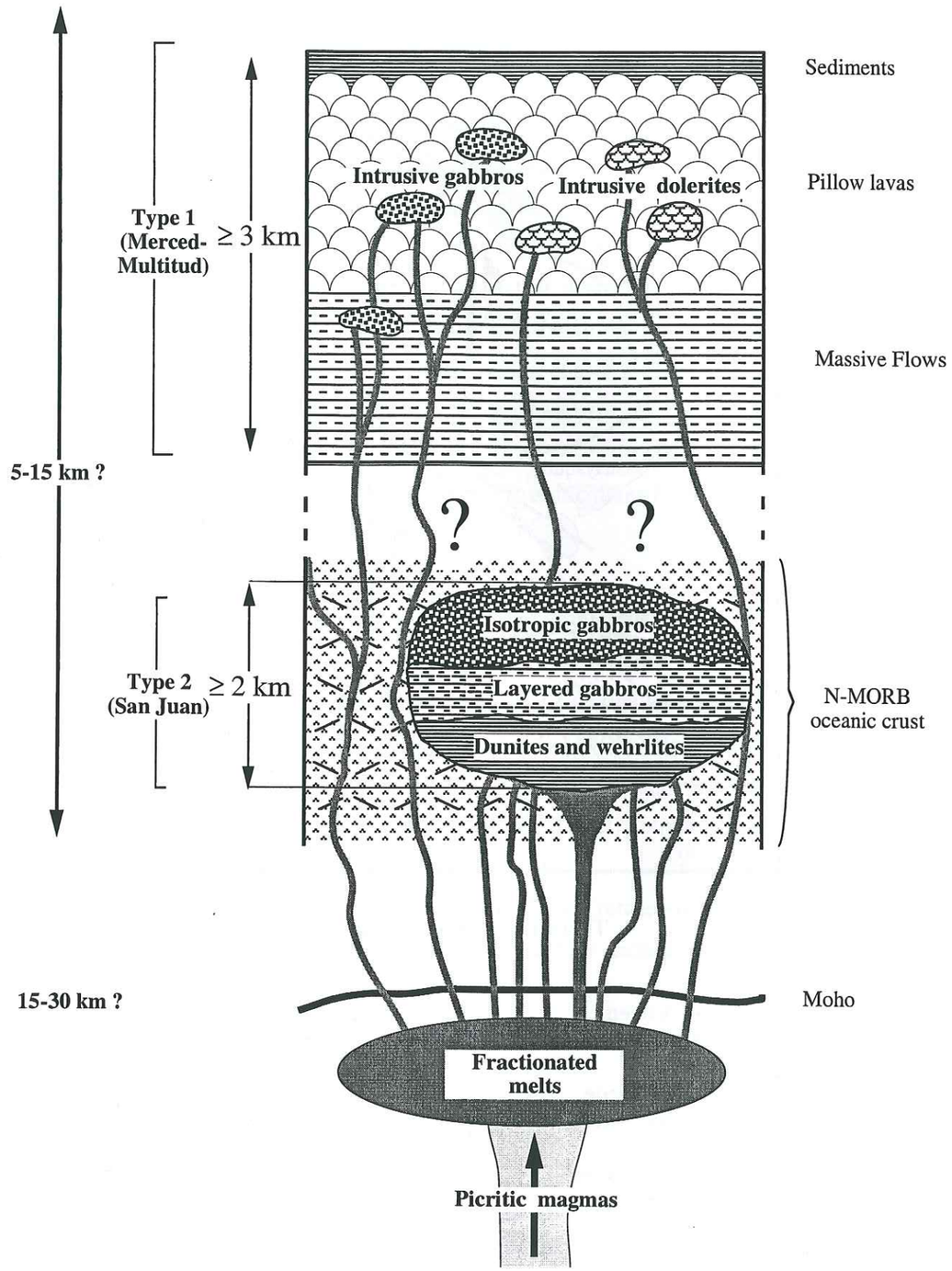

Fig. 7.1: Hypothetical cross section through the Early Cretaceous oceanic plateau.

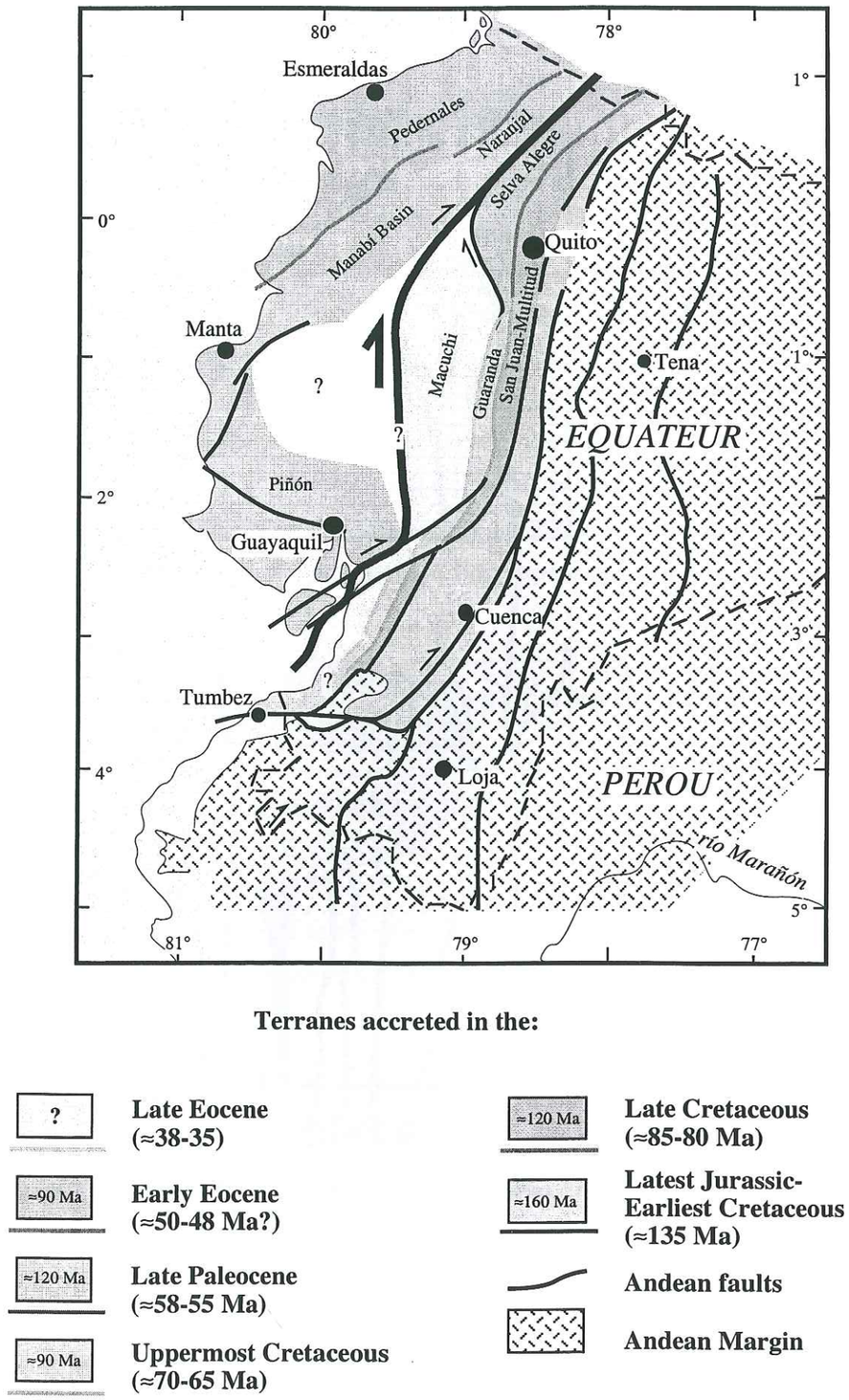

Fig. 7.2: Accretion sequences of oceanic terranes in Ecuador.

described. Among the very few examples that are thought to come from the interior of oceanic plateaus are the ultramafic and mafic cumulates associated with komatiites and picrites of the CCOP (Kerr et al., 1997; Spadea et al., 1987; Révillon et al., 2000), and cumulate gabbros and peridotites of the Solomon islands, inferred to represent acccreted fragments of the Ontong Java plateau (Parkinson et al., in press). It is difficult to assume at what depth the San Juan cumulate rocks crystallized. The igneous textures and mineral composition of the San Juan cumulates indicate that these rocks crystallized above the petrological and even the seismic Moho. Indeed, if the cumulate peridotites were located underneath the petrological Moho, as suggested by Kerr et al. (1997):

(1) they would have likely suffered locally high pressure and thermal deformations and recrystallizations,

(2) they would be intruded by doleritic and/or basaltic dikes feeding the extrusive rocks of the oceanic plateau.

This is not the case for the San Juan sequence.

The San Juan cumulates derived from the accumulation of olivine, succeeded by clinopyroxene and plagioclase of a basaltic liquid. This basaltic liquid is geochemically similar to the Merced-Multitud rocks. The mafic-ultramafic cumulates of the San Juan region correspond to intrusions at a deeper level. Because most of the oceanic plateau basalts are evolved melts, we suggest like Farnetani et al. (1996) that the high seismic velocities near Moho levels are due to the presence of crystal cumulates (chiefly olivine) that formed through large-scale fractionation of primary picritic magmas.

The absence of picrites and komatiites in the Early Cretaceous Ecuadorian plateau is probably due to the lack of exposures, or because they did not ascend to the surface.

TIMING OF ACCRETION OF THE TWO OCEANIC PLATEAUS AND INTRA-OCEANIC ISLAND ARCS

Recent maping and geological studies by Jaillard et al. (1995), Cosma et al. (1998), McCourt et al. (1998), Dunkley and Gaibor (1998), Reynaud et al. (1999), Hughes and Pilatasig (in press) and Boland et al. (2000) have precisely determined the ages of accretion of the oceanic terranes to the Ecuadorian margin (Table 7:1; Fig. 7.2).

Age	Location		Plateau	Arc	Accretion
123 Ma	Western Cordillera		San Juan-Multitud	Dykes-grauwackes	≈80-85 Ma
	Coast	Guayaquil	Piñón	Las Orquideas (~100 Ma) Cayo (~100-80 Ma)	≈58 Ma
		Manta	Piñón ?	San Lorenzo (~80-68 Ma)	≈58 Ma or ≈50 Ma
90 Ma	Western Cordillera		Guaranda	?	≈70-65 Ma
			Selva Alegre	Rio Cala (80-68 Ma)	≈50 Ma ?
	Coast		Esmeraldas-Pedernales	Naranjal (80-68 Ma)	≈50 Ma
	Western Cordillera		??	Macuchi (65-50 Ma)	≈38 Ma

Table 7.1: Characterisation of oceanic terranes accreted in Ecuador.

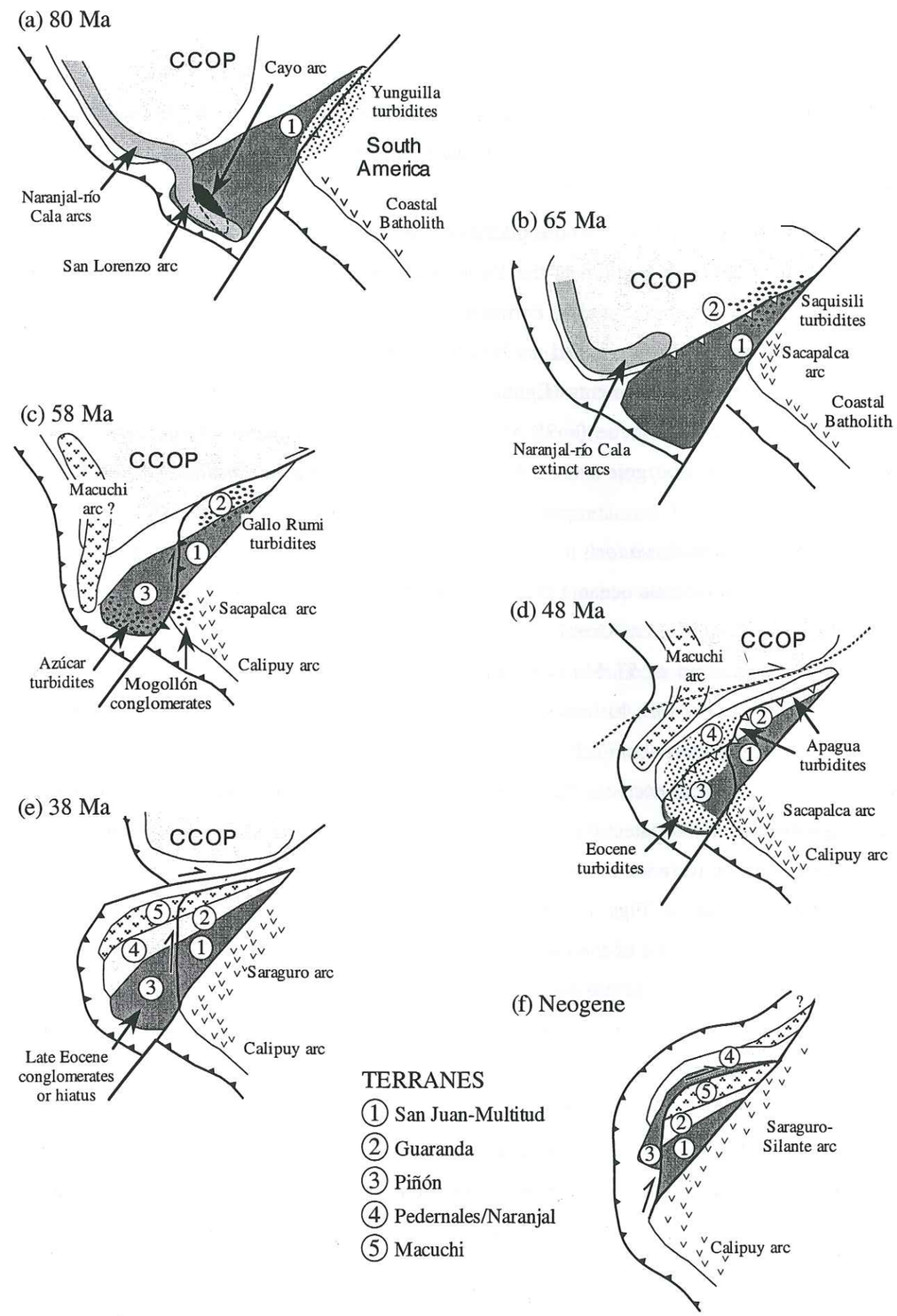

Fig. 7.3: Paleotectonic sketch of accretions in Ecuador.

Central Ecuador

In the Western Cordillera, the accretion of the Early Cretaceous plateau (San Juan-Multitud) is post-dated by the Late Campanian-Maastrichtian Yungilla Formation, and occurred therefore around 85-80 Ma (Reynaud et al. 1999, Hughes and Pilatasig, in press) (Fig. 7.3a).

Accretion of the Late Cretaceous plateau (Guaranda) occurred between 70-65 Ma, since it is subsequent to the deposition of the Yunguilla Formation, and is sealed by the Early to Mid- Paleocene, quartz-rich Saquisilí Formation (Hughes et al. 1999) (Table 7.1; Fig. 7.3b).

The Paleocene?-Eocene island arc (Macuchi) is associated with Early to Mid-Eocene oceanic -pre-accretion- sediments (Egüez, 1986), and its accretion is correlated with the deposition of the Late Eocene (≈ 38 Ma) Rumi Cruz conglomerates (Upper part of the Apagua Formation of Bourgois et al., 1990; Hughes and Pilatasig, in press) (Fig.7.3e).

Southern Coastal Ecuador

The Early Cretaceous oceanic plateau (Piñón) and Mid to Upper Cretaceous overlying island arcs (≈ 100-80 Ma, Las Orquídeas and Cayo; Fig. 7.3c), exposed in the Guayaquil area, accreted to the margin at 57 Ma (Late Paleocene) since deformations are sealed by the unconformable, quartz-rich turbiditic conglomerates of the Azúcar Group (Jaillard et al., 1995, 1997). Moreover, the Early Cretaceous oceanic plateau and related arcs probably collided farther south, in northern Peru, since clasts of island arc rocks have been identified in the conglomerates of the latest Paleocene-Early Eocene Mogollón Formation (Pécora et al., 1999). Later on, the terranes of the Guayaquil area migrated northwards by means of large transcurrent dextral faults (Figs. 7.3 and 7.3f).

The age of acccretion of the latest Cretaceous island arc (80-68 Ma, San Lorenzo) and underlying plateau (Manta) is still controversial (see below).

Northwestern Ecuador

Accretion history of the exotic oceanic terranes is still poorly constrained in northwestern Ecuador because the age of all the oceanic terranes is not determined. We shall distinguish the remnants of the Upper Cretaceous oceanic plateau (Selva Alegre and Pedernales-Esmeraldas Units) and related latest Cretaceous arcs (Naranjal arc), probably extending southwestwards to the Manta area

In the Western Cordillera, the age of accretion of the Late Cretaceous CCOP (Santonian Selva Alegre Unit) and overlying latest Cretaceous island arc (Río Cala arc, Boland et al., 2000) is not well constrained. The presence of quartz-bearing deposits of Campanian-Maastrichtian age (Mulaute, Pilatón and Natividad Fms, Hughes et al., 1999; Boland et al., 2000) suggests that accretion occurred in the Late Cretaceous.

On the basis of the transition from Late Paleocene cherts and sandstones (La Cubera Fm) to Eocene continental arc-suites (Tortugo Fm), Boland et al. (2000) proposed that accretion of the latest Cretaceous island arc (Naranjal arc; Boland et al., 2000) of the northwestern tip of the Western Cordillera occurred in the Early Eocene (≈ 55-50 Ma). However, the transition from oceanic cherts to massive sandstones mentioned by Boland et al. (2000) within the Late Paleocene (La Cubera Formation), would rather indicate a Late Paleocene accretion date (≈ 58 Ma). Southwest of the latest Cretaceous arc, the Manabí Basin (Fig. 7.2) recorded significant hiatuses and unconformities of latest Maastrichtian-Early Paleocene (≈ 68-60 Ma), and Late Paleocene-Early Eocene age (≈ 58-50 Ma), respectively (Deniaud, 2000), which may be consistent with both interpretations. However, the appearance of detrital quartz in the Mid- or Late Paleocene deposits of the Manabí Basin (Deniaud, 2000) would favour a Paleocene accretion date for this unit. Farther southwest (Manta area, Fig. 7.2), the accretion of the oceanic plateau and overlying latest Cretaceous San Lorenzo island arc, is postdated by Mid-Eocene quartz-rich sediments, only indicating that accretion occurred during the Late Maastrichtian - Early Eocene time span (≈ 65-50 Ma).

Finally, the Late Cretaceous (92-86 Ma) CCOP fragments (Pedernales-Esmeraldas unit), which are locally associated with island arc rocks of probable latest Cretaceous age, are unconformably overlain by Mid-Eocene quartz-rich sediments, indicating a comparable, Paleocene to Early Eocene accretion age (≈ 65-50 Ma).

The evolution and accretion of the oceanic terranes depend heavily on the motion of the Pacific plate during the Cretaceous-Paleogene. According to Pilger (1984) and Pardo-Casas and Molnar (1987), the Pacific plate moved towards the North during the latest Cretaceous. Then, the motion of the Pacific plate changed progressively from north- to east-ward during the Early Tertiary, with significant changes at ≈ 58-56, ≈ 42 and ≈ 26 Ma (Fig. 7.4). In the same way, dextral movements of the accreted terranes were controlled by the oblique component of convergence, which was especially pronounced between Late Cretaceous and Late Oligocene times (70-26 Ma, Fig. 7.4).

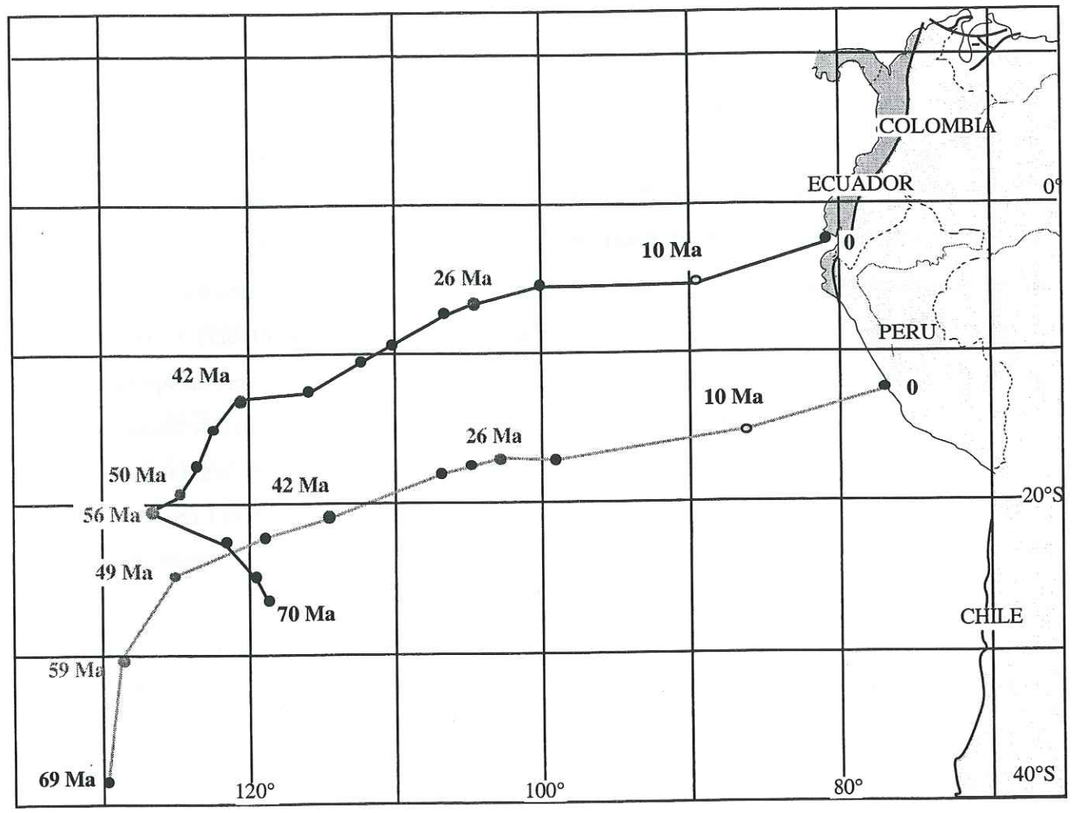

Fig. 7.4: Position and motion of one point on the Nazca plate, between anomalies 30-31 (69-70 Ma) and Present, with respect to south America (After Pardo-Casas & Molnar, 1987 (below); and Pilger, 1984 (above)).

RECONSTITUTION OF THE GEODYNAMIC EVOLUTION OF THE NORTHWESTERN SOUTH AMERICA AND NEIGHBOURING AREAS

Location of the hotspots linked to the Early and Late Cretaceous (CCOP) oceanic plateaus

The Early Cretaceous oceanic plateau probably derived from a near-ridge hotspot, located far southwest of Ecuador, somewhere in the southeastern Pacific (Reynaud et al., 1999; Lapierre et al., 2000).

The identification of the hotspot responsible for the 92-86 Ma komatiites, picrites and basalts of the CCOP is still a matter of debate. Two types of models have been proposed for the genesis of the CCOP.

In the first type, the Caribbean plateau was formed in the Pacific (Duncan & Hargraves, 1984; Pindell and Barret, 1990), and accreted to the Greater Antilles arc and the margin of South America in the Late Cretaceous (80 to 70 Ma) because of the eastward component of displacement of the Farallón Plate. In this model, the major Early Late Cretaceous magmatic event of the CCOP (≈ 92-86 Ma) would be linked to the incipient activity of the Galápagos hotspot (Duncan & Hargraves, 1984; Donnelly et al., 1990; Pindell and Barret, 1990; Mauffret and Leroy, 1997; Hauff et al., 2000). Other authors proposed that the CCOP has been originated at the Sala y Gómez hotspot (at least for the 90 Ma event; Kerr et al., 1998; Révillon et al., 2000).

In the second type of models, the Caribbean plateau was formed in the Eastern Pacific at Equatorial latitudes, much closer to South America than the Galápagos hotspot. Then, the Caribbean plate remained grossly fixed, while the opening of the Atlantic Ocean triggered the westward motion of the North and South American plates, leading to the pinching of the Caribbean plateau between North and South America (Meschede et al., 1998; Dupuis, 1999).

Preliminary remarks

Before to present an attempt of geodynamic evolution of the Caribbean plateau and northwestern South America, we must first recall recently published data relevant for this reconstitution.

- The oceanic crust which represents most likely the basement of the CCOP is exposed in the Duarte complex of Dominican Republic. This oceanic crust consists of slices of pillow basalts stratigraphically associated with Late Jurassic radiolarian fauna documenting a Pacific origin (Montgomery et al., 1994), and doleritic dykes cross cutting serpentinized foliated harburgites. Basalts and dolerites show N-MORB affinities but the Nd isotopic compositions of the basalts suggest that this oceanic crust was formed near a hotspot (Lapierre et al., 1999).

- Remnants of the 92-86 Ma CCOP are known in Ecuador, Colombia (Kerr et al., 1997), Costa Rica (e.g. Hauff et al., 2000), Curaçao (Kerr et al., 1997), Dominican Republic (Lapierre et al., 1999), Haiti (Sen et al. 1988) and perhaps in Venezuela, i.e., mainly in the southern part of the peri-Caribbean domain.

- The proto-Caribbean arc, which forms the basement of the present-day Greater Antilles arc, comprises the Early Cretaceous Guerrero terrane of southwestern Mexico (Tardy et al., 1994, Freydier et al., 1997), the Early to Late Cretaceous arc-terranes of the Greater Antilles (Puerto Rico, Virgin islands, Hispaniola and probably Cuba, Donelly et al., 1990). The proto-Caribbean arc and the northern margin of the late Cretaceous CCOP collided with and accreted to the southern margin of North America during the Maastrichtian (70 Ma).

- Around 80 Ma (Mid-Campanian), subsequently to the first Late Cretaceous accretion episode in Ecuador, subduction began beneath the southern margin of the CCOP leading to the development of the intra-oceanic arc of western Costa Rica, and to the latest Cretaceous island arcs of northwestern Ecuador (San Lorenzo, Río Cala, Naranjal arcs).

- The accretion in Ecuador of part of the CCOP before Mid-Eocene times (≈ 50 Ma) implies that either the CCOP was still in a southern position at that time, or that it was more elongated than suggested by its present-day shape.

- Eocene island arc rocks are known in Ecuador (Macuchi), Colombia (Kerr et al., 1997) and in southern Central America (Pindell and Barrett, 1990; Astorga, 1997), and suggest that oceanic subduction occurred beneath the southwestern edge of the Caribbean plate until the Eocene. Late Eocene times are then marked by the end of thrusting of Cuba onto the Bahamas platform, and by the beginning of arc-magmatism in the Lesser Antilles (Donnelly et al. 1990).

Geodynamic evolution of northwestern South America and the peri-Caribbean area.

On the basis of the plate-tectonic models of the peri-Caribbean areas proposed by Stéphan et al. (1990) and Dupuis (1999), and the data acquired during this work and those published recently by several authors which worked in the peri-Caribbean and northwestern South America, we propose a palinspastic reconstitution of the north-western margin of South America and neighbouring areas. This reconstitution depicts several stages. Following the chronological order, these stages are: Early Cretaceous (Barremian, 120 Ma), Coniacian (87.5 Ma), Mid-Campanian (≈ 80 Ma), Mid-Maastrichtian (≈ 70 Ma), Late Paleocene (60-55), Early to Mid Eocene (48 Ma) and Recent (0 Ma). These different stages represent major magmatic or tectonic events in the geology of northwestern South America, central America and the peri-Caribbean area.

During the **Barremian** (≈ 120 Ma), the development of the near-ridge Early Cretaceous plateau (Piñón, San Juan-Multitud unit) began on the Farallón oceanic plate, far southwest of Ecuador (Reynaud et al., 1999) (Fig. 7.5a). North- to northeast-ward subduction of the Farallón plate led to the development of the intra-oceanic proto-Caribbean arc (present-day Greater Antilles) between the western margins of North and South America, and to continent-based arcs in Central America and central South America (Peru, Chile). Farther north, in western Mexico, the oceanic crust of the Arperos basin was subducting southwestwards under the Farallón plate leading to the development of the Guerrero island arc. Soon after, the Early Cretaceous oceanic plateau (Piñón Fm. San Juan-Multitud Unit) shifted passively toward the North or NNE.

During the Early and Mid-Cretaceous, subduction-related volcanism continued in the proto-Caribbean arc and on the western margins of South and North America. Arc-volcanism related to the northeast dipping subduction of the Farallón plate may have already began at the southern margin of the Early Cretaceous plateau leading to the development of the pre-Turonian island arc known in southern coastal Ecuador (Las Orquídeas). The Early Cretaceous oceanic plateau and related arcs are moving north- to northeast-ward towards the western margin of northern South America. In Mexico, the closure of the Arperos basin brought to an end the activity of the Guerrero arc, which collided with the Mexican margin during the Abian-Cenomanian. Before Albian times, opening of the Central Atlantic led to the westward migration of North America and to the opening of a proto-Caribbean oceanic arm,

whereas from Albian onwards, active accretion in the southern Atlantic Ocean triggered the westward drift of South America (Emery and Uchupi, 1984).

Barremian (≈ 120 Ma)

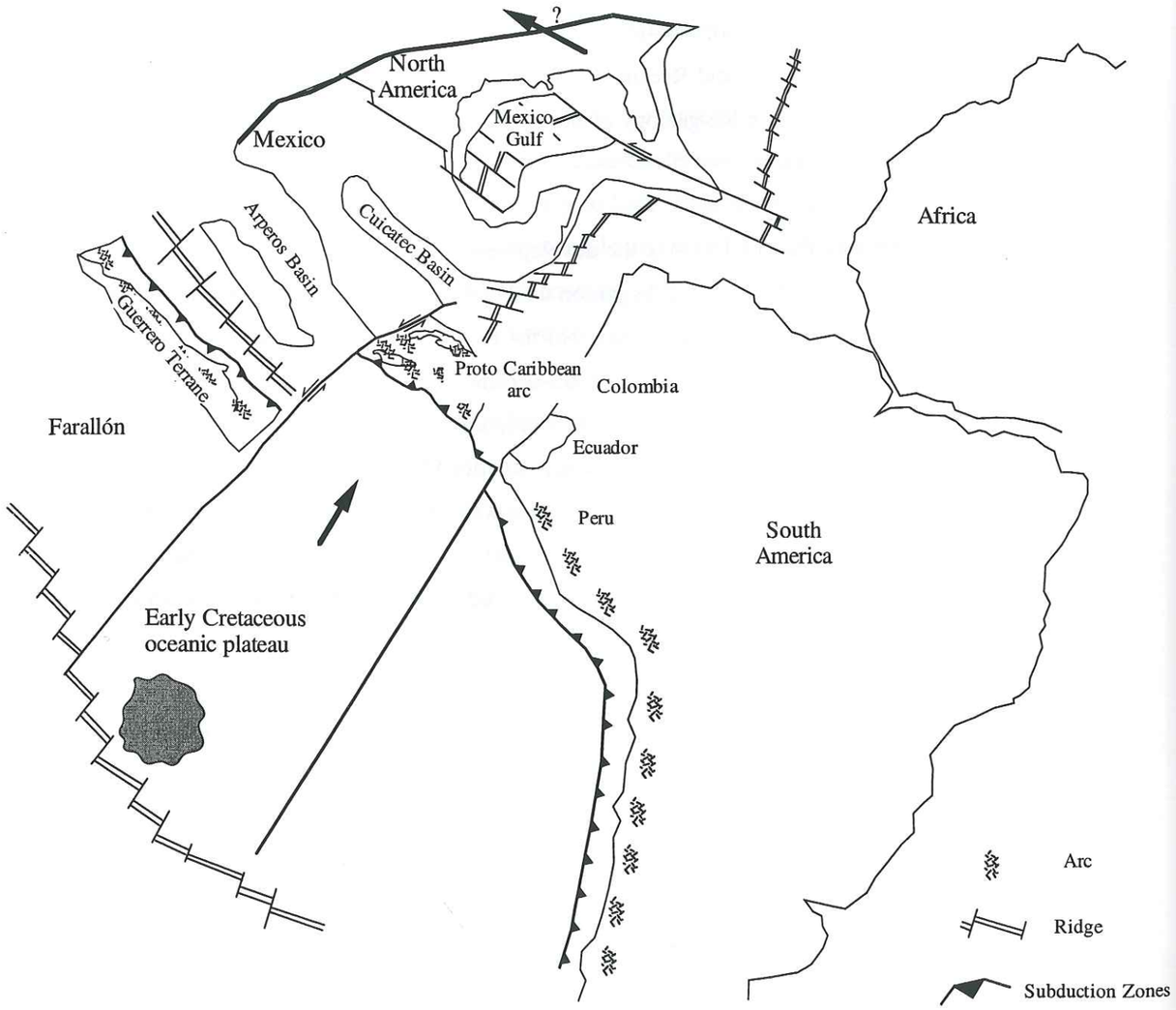

Fig. 7.5a

Santonian-Early Campanian (≈ 85-80 Ma) represents a key-period in the evolution of northern South America and the Caribbean.

In the Santonian, development of the Late Cretaceous CCOP on the Farallón plate was coming to an end (Fig. 7.5b). The hotspot linked to the development of this oceanic plateau was located somewhere in the Equatorial Pacific. Convergence of the Farallón plate was still toward the north or northeast, leading to an Andean-type magmatism on the western margins of both southern North America (Mexico) and South America. Because of the ongoing opening of the Atlantic Ocean, both the North and South American plates moved westwards. The Early Cretaceous oceanic plateau and its related 100-80 Ma island arc (Cayo arc, which succeeded the Las Orquídeas arc in the Guayaquil area) were already probably close to the margin of northern Peru, but were still located off shore.

As soon as the CCOP was formed, it seems to have collided with the Greater Antilles island arc, metamorphosing CCOP basalts into amphibolite facies around 85 Ma in Hispaniola (Lapierre et al., 1999). This must have provoked the end of the former northeastward subduction of the Farallón Plate, which will imply two consequences (see below).

Mid-Campanian times (≈ 80 Ma) are marked by regional unconformities in northwestern South America, Central America and the Caribbean (Astorga, 1994; 1997; Iturralde-Vinent et al., 2000; Jaillard et al., 2000), usually interpreted as the result of incipient tectonic interactions (docking, transpressional movements, ...) between the Caribbean plate and continental blocks or continent (Pindell and Barrett, 1990; Fourcade et al., 1993; Astorga, 1994; Di Marco, 1994; Stanek et al., 2000). We favour the interpretation of a collision of the CCOP with the continental margins of the Chortis or Maya blocks (Pindell and Barrett, 1990), rather than the northern American margin (Mercier de Lépinay, 1987). As a matter of fact, since parts of the CCOP accreted to Ecuador in the latest Paleocene (≈ 58 Ma, Jaillard et al., 1997) or even in the Early Eocene (≈ 50 Ma, Boland et al., 2000, see below), the CCOP must have remained in a southerly location until that time.

Part of the Early Cretaceous oceanic plateau accreted to the north Peruvian or Ecuadorian margin. The newly accreted fragments of this plateau (San Juan-Multitud unit) are stratigraphically associated with continent-derived, quartz-bearing turbidites of Mid-Campanian to Maastrichtian age (Yunguilla Fm). This accretionary event and the subsequent reorganization of the subduction zones brought to an end the Cayo arc activity, and led to the beginning of latest Cretaceous island arcs (e.g. San Lorenzo), some of them being built on the southern edge of the CCOP (Río Cala, Naranjal).

Therefore, as mentioned above, this upheaval had important geodynamic consequences.

Extension of the Ecuadorian island arc system of Campanian-Maastrichtian age to the north or NW is suggested by latest Cretaceous island arc rocks identified in Colombia (Grösser, 1987; Pindell and Barrett, 1990), Costa Rica (Hauff et al., 2000) and by volcanic intercalations in Campanian-Maastrichtian sediments of southern Central America (Donelly et al., 1990; Pindell and Barrett, 1990; Astorga, 1994; 1997). On the other hand, arc-related volcanism was no longer active along the northern or northeastern margin of the CCOP, where the late Cretaceous island arc rocks are often overlain by unconformable shelf limestones (Iturralde-Vinent et al., 2000), but seems to have gone on farther south in the island arc system of the Aves Ridge (Pindell and Barrett, 1990).

This leads to the hypothesis that accomodation of convergence has been transferred from the northeastern active margin to the southwestern subduction zone at that time (≈ 80 Ma; Astorga, 1994). From then on, the proto-Caribbean (and/or Atlantic) oceanic crust subducted westward beneath the Aves Ridge (Duncan and Hargraves, 1984; Lapierre et al., 1999). Convergence of the Farallón oceanic plate was accomodated by northeast-ward subduction beneath the southwestern edge of the CCOP, leading to the development of latest Cretaceous island arcs of Campanian-Maastrichtian age, at least partly built on the CCOP (Pindell and Berrett, 1990; Astorga, 1997). Being bounded by active margins at its eastern and southwestern edges, the CCOP may have remained grossly fixed. Relative motions between the Caribbean, and the North and South American plates were accomodated by transform faults.

Santonian-Early Campanian (85-80 Ma)

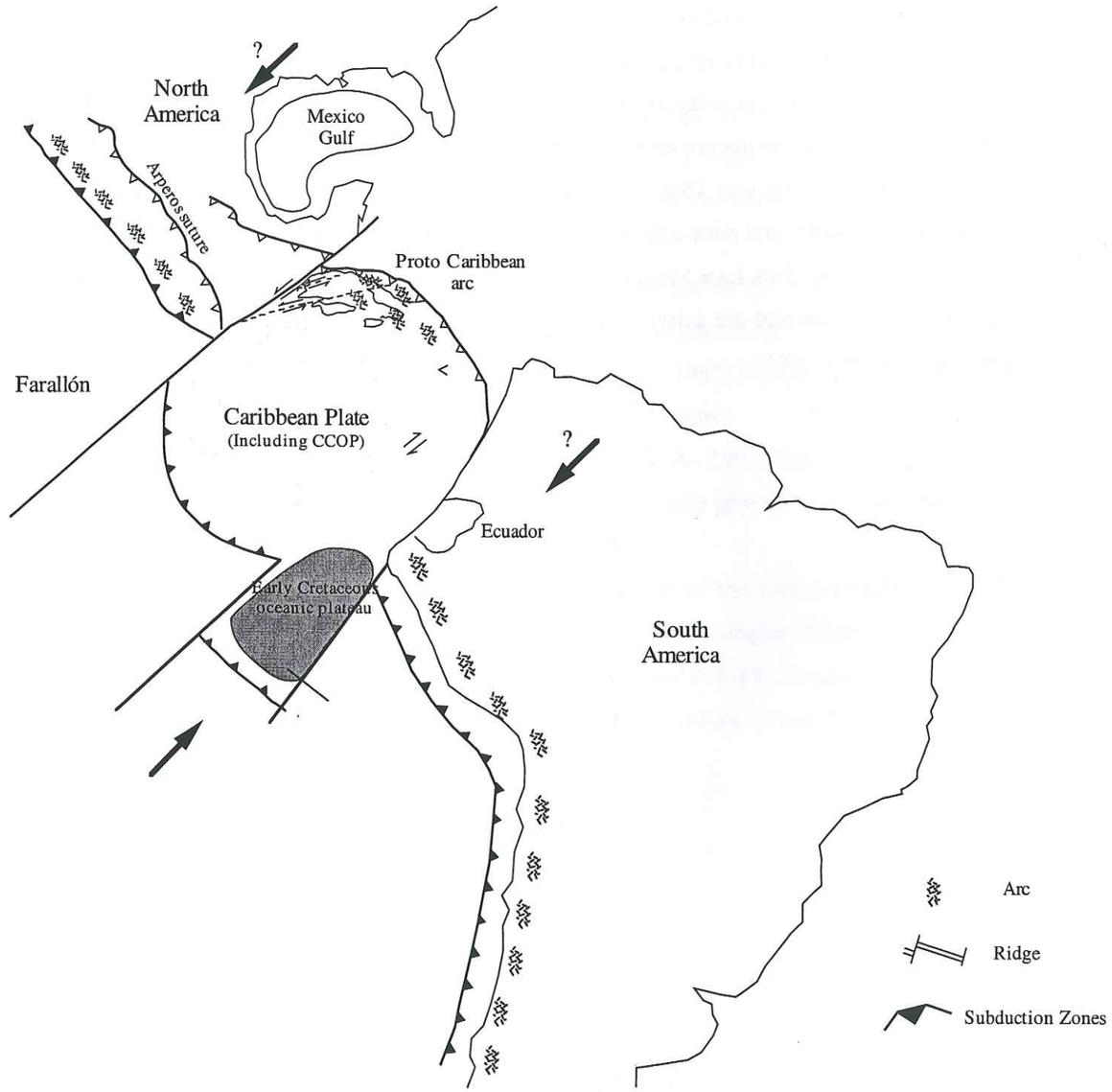

Fig. 7.5b

During the **Mid to Late Maastrichtian** (≈ 68 Ma), a significant tectonic event occurred in Colombia (Cheilletz et al., 1997) and in Central America (Donelly et al., 1990; Astorga, 1997) (Fig. 7.5c). In Central America, "ophiolite" obducted on the Maya Block. In Hispaniola, a Mid-Maastrichtian unconformity has been interpreted as the result of the collision and accretion of the proto-Caribbean arc and part of the northeastern margin of CCOP to the southern margin of North America (Mercier de Lépinay, 1987), but many authors assume that this occurred later (Late Paleocene-Eocene).

Part of the CCOP, presently exposed in the Western Cordillera of Ecuador (Guaranda unit), was accreted to the margin of South America. This accretion triggered the end of the latest Cretaceous island arcs (San Lorenzo, Río Cala, Naranjal) and the deposition of unconformable, quartz- and mica-rich turbidites of Early to Mid Paleocene age (Saquisilí Fm, Hughes et al., 1999). This Late Maastrichtian event seems to have triggered the temporary resumption of continental arc activity in southern Ecuador (Sacapalca Fm, Jaillard et al., 1996; Hungerbühler, 1997).

Mid to Late Maastrichtian (68 Ma)

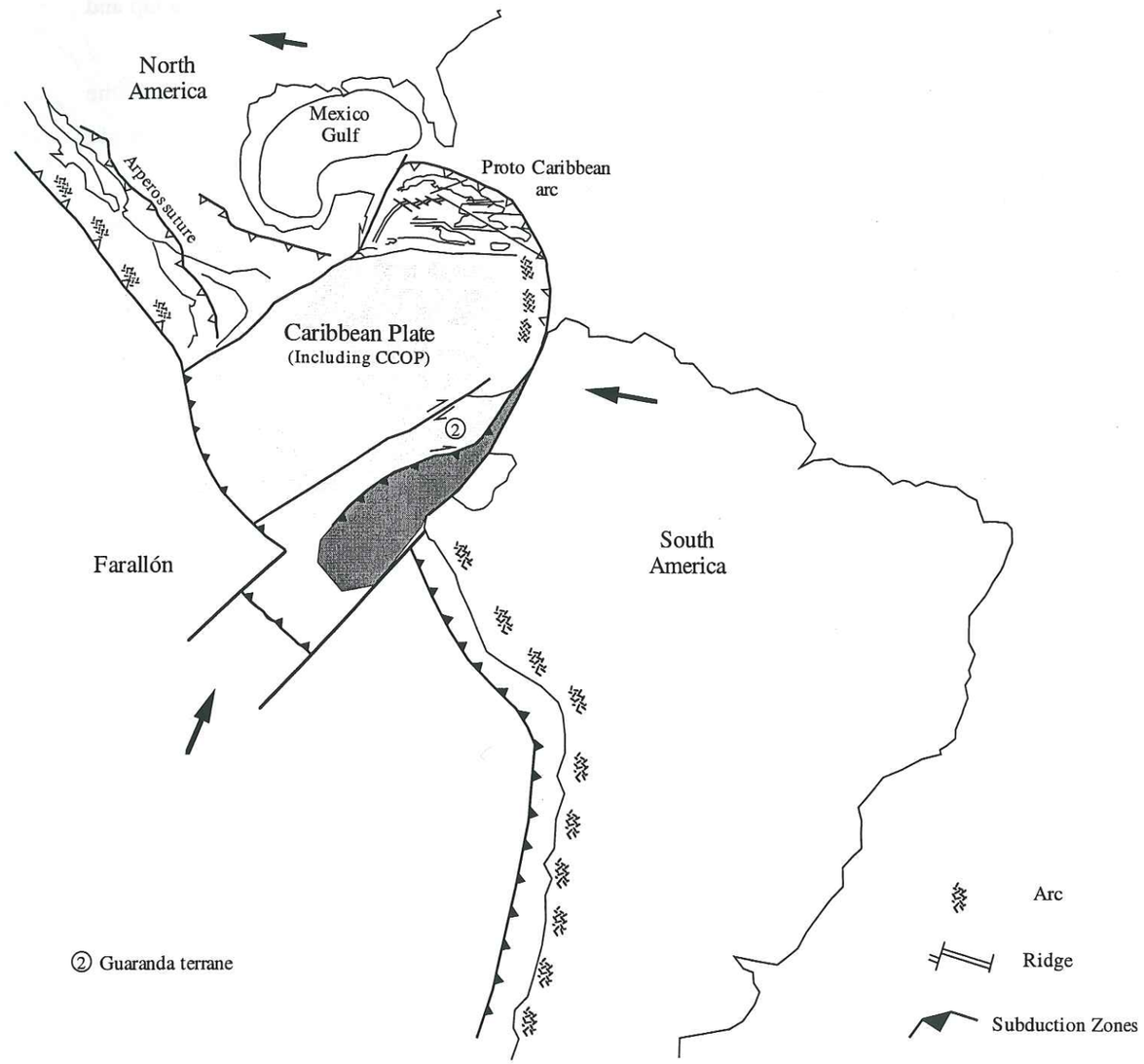

Fig. 7.5c

During the **Late Paleocene** (≈ 58 Ma), a drastic change occurred in the motion of the paleo-Pacific plate, which turned from North- to NE-ward (Fig. 7.5d; Pardo-Casas and Molnar, 1987). This change may have provoked the dislocation of the Early Cretaceous plateau, fragments of which (present-day Guayaquil area) collided the South American margin in northern Peru (Pécora et al., 1999), leading to the deposition of unconformable quartz-rich conglomerates in northern Peru (Mogollón Fm) and in Ecuador (Azúcar Gp and Rumi Cruz Fm).

This new reorganization of subduction zones west of Ecuador may have triggered the development of the Macuchi island arc of Paleocene(?)-Mid-Eocene age (Hughes et al., 1999), of which the nature of the basement is still not precisely known.

In the Caribbean, the proto-Caribbean arc began to collide with, and to be thrust onto, the North American margin; this collision is slightly diachronous and lasted until Early to Late Eocene times (Brallower and Iturralde-Vinent, 1997; Stanek et al., 2000). This accretion episode is also recorded in Costa Rica (Di Marco, 1994). The Granada Basin opened by means of a N-S trending accretion rodge (Pindell and Barrett, 1990).

Late Paleocene (58 Ma)

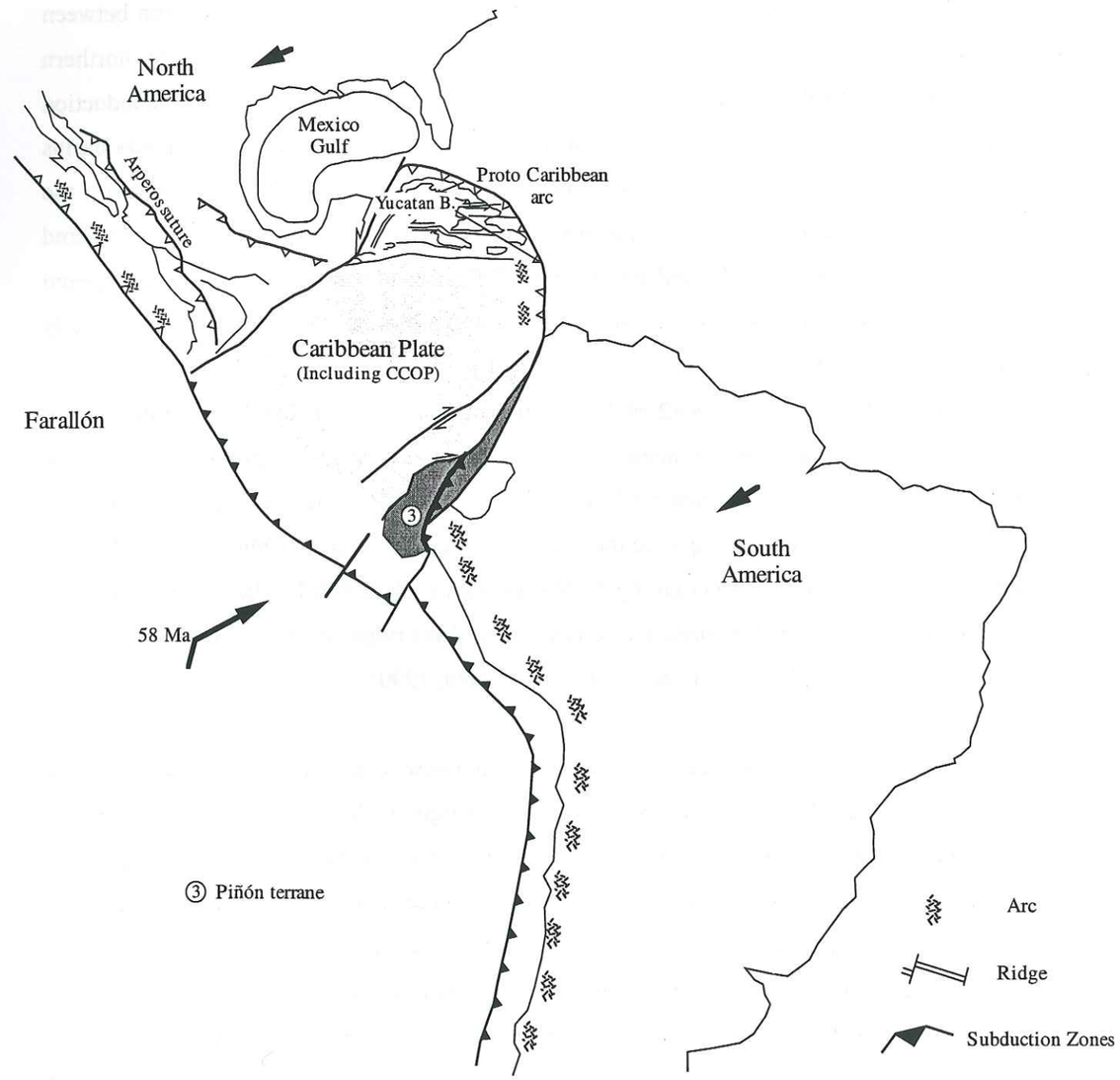

Fig. 7.5d

During the **Mid-Eocene**, several important kinematic changes occur (Fig. 7.5e).

Near the Early-Mid Eocene boundary (≈ 50-49 Ma), the motion of the paleo-Pacific plate turned from NE- to ENE-ward, and the motion of the North and South American plates changed from SW- to west-ward. Because of this new E-W convergence direction between the American and Caribbean plates, sinistral transcurrent faults formed on the northern margin of the CCOP. This led to the rapid displacement of the Lesser Antilles subduction zone toward the east. The Cayman pull-apart trough, and the Yucatan and Granada basins opened (Donelly et al. 1990). In the south, Caribbean nappes began to emplace on the continental margin of Venezuela, and metamorphic events of Early Eocene age occurred mainly in Central America (Pindell and Barrett, 1990). This reoganization may have triggered the accretion of the Late Cretaceous arc (Naranjal arc) of northwestern Ecuador in the Early Eocene (Boland et al., 2000).

In the late Mid-Eocene (≈ 42 Ma), a significant change in the global plate convergence directions occurred ("Hawaii-Emperor elbow"), which seems to have provoked the paleo-Pacific plate to change again from a NE- to a ENE-ward motion (Pilger 1984). This new plate kinematic change may have triggered the accretion of the Paleocene(?)-Mid Eocene Macuchi island arc to the Ecuadorian margin by 38 Ma (Hughes et al., 1999; Hughes and Pilatasig, in press). In the Caribbean, the island arc acrivity of the Aves ridge ceased and is relayed by the Lesser Antilles (Donelly et al., 1990; Pindell and Barrett, 1990).

Accretions in Ecuador are now achieved, and a new, continent-based volcanic arc of Late Eocene age developed on the Ecuadorian margin (Silante oand/or Saraguro Fm, Steinmann, 1997; Dunkley and Gaibor, 1998; Boland et al., 2000; Hughes and Pilatasig, in press). Subsequently, ongoing dextral movements continued to tear apart the accreted oceanic fragments, leading to the displacement and eventual stacking along the Ecuadorian margin of slices of the Early and Late Cretaceous plateaus and associated island arcs. Especially, formerly accreted oceanic terranes of coastal Ecuador accreted in Late Paleocene-Early Eocene times (Piñón, Manta-Naranjal and Pedernales areas) will be shifted west of the Macuchi island arc, the accretion of which is assumed to have occurred in the Late Eocene (Hughes and Pilatasig, in press). This situation implies a minimum dextral displacement of ≈ 400 km of the western terranes with respect to the Macuchi arc since the Late Eocene (≈ 40 Ma), which means about 10 km / Ma or 1 cm / year (Fig. 7.2 and 7.3f).

The accretion history of the CCOP in the Andean realm will come to an end in Miocene times, with the accretion of the Serranía de Baudó terrane in northwestern Colombia (Mégard, 1989), but interraction between the CCOP and northern South America goes on in Venezuela (Pindell and Barrett, 1990).

Mid-Eocene (40-49 Ma)

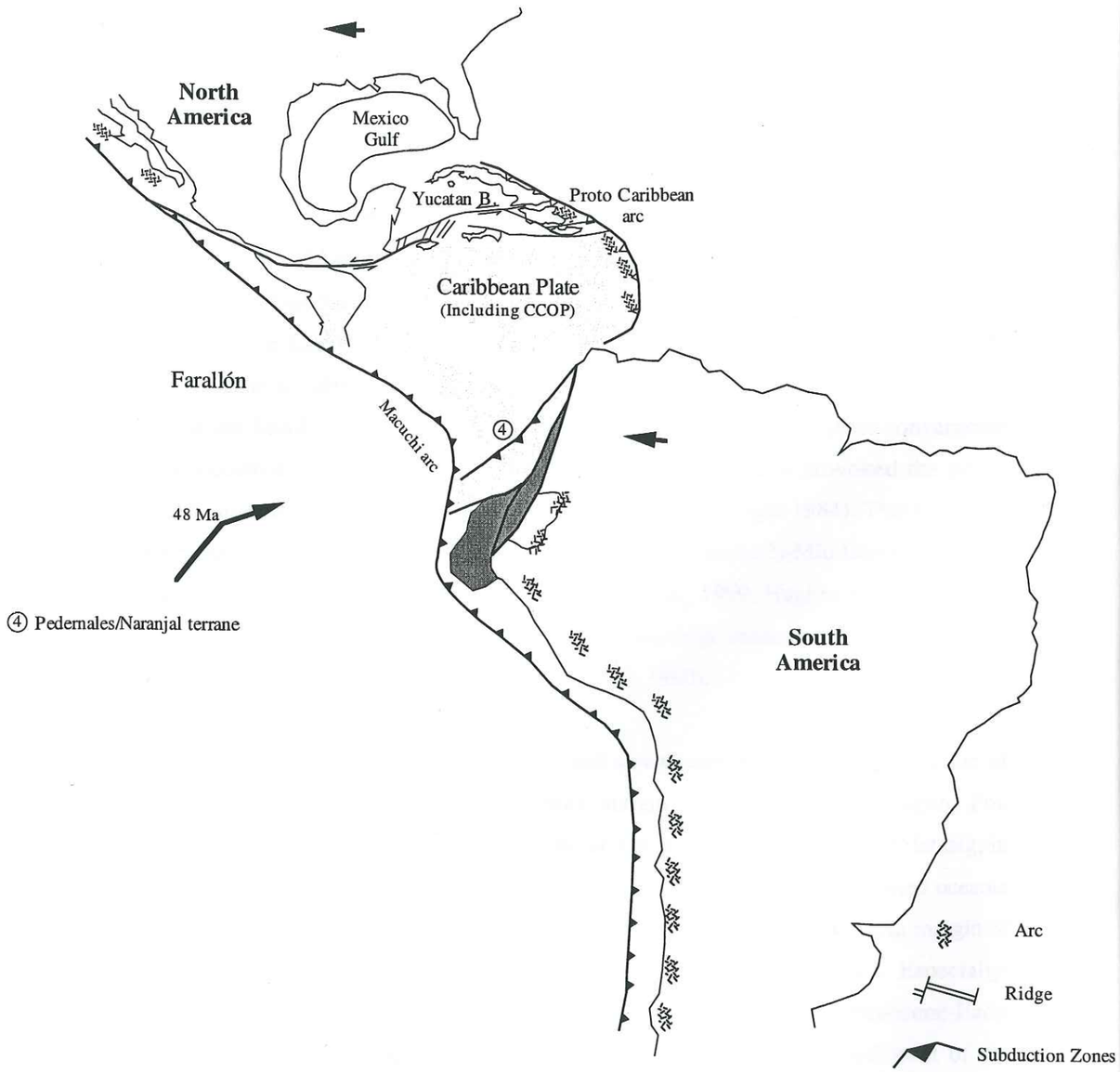

Fig. 7.5e

Presently, the lateral displacements along the northern margin of the Caribbean plate are still continuous (Fig. 7.5f). South of the island of Hispaniola, the South Haiti peninsula represents an emerged fragment of the Late Cretaceous Caribbean plateau. Coastal Ecuador is affected by large transcurrent faults. Andean-type magmatism occurs along the western margins of North and South America.

Presently

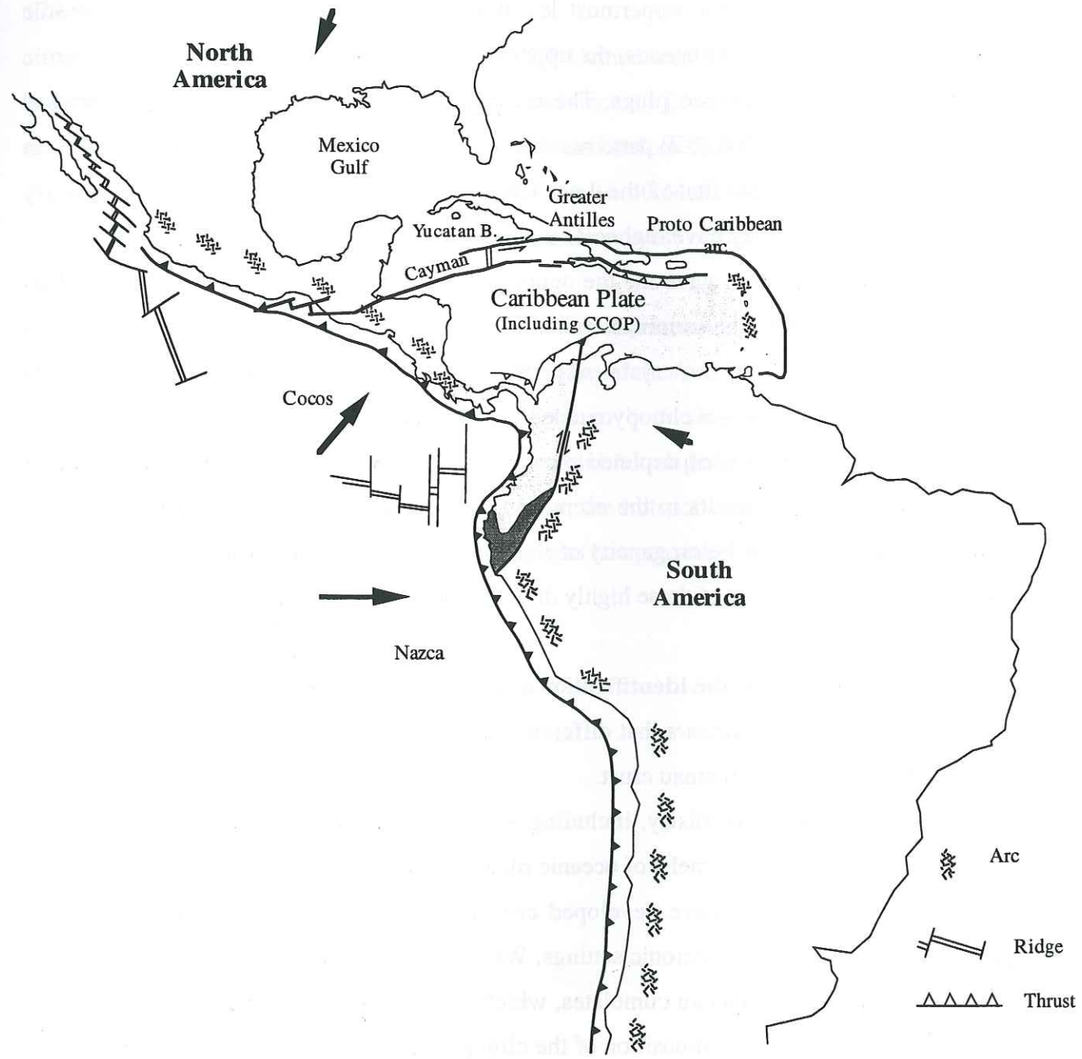

Fig. 7.5f

GENERAL CONCLUSIONS

The results acquired during the last three years of investigations, here in presented in this thesis, can be subdivided in three main topics.

1. Petrological and geochemical features of the different components of an oceanic plateau crust.

The components of the uppermost levels of the Early and Late Cretaceous oceanic plateau are similar. In both plateaus, the uppermost levels consist of pillow basalts, doleritic sheets and subdoleritic gabbro plugs. These rocks exhibit very homogeneous geochemical features (MgO = 6-7 %; flat REE patterns, εNd ~+7), which are those of most oceanic plateau basalts. However, the basalts of the Late Cretaceous plateau differ from those of Early Cretaceous age in that they have higher Pb isotopic ratios.

The San Juan section gave me the opportunity to study the plutonic components of an oceanic plateau. There, the cumulate rocks are essentially formed of clinopyroxene with olivine or plagioclase, and the crystal sequence of these cumulates resembles that of intra-plate magmas, i.e., olivine --> clinopyroxene --> plagiocase.

Finally, the presence of depleted picrites associated with LREE-enriched MgO-rich basalts and MgO-poor basalts in the accreted fragments of the Late Cretaceous CCOP has allowed us to confirm the heterogeneity of mantle plume sources and proposed a multi-stage model for the emplacement of these highly diversed picritic or basalts.

2. Criteria allowing the identification of crustal fragments of an oceanic plateau.

From this study, it appears that different tools can be used to characterize the different components of an oceanic plateau crust.

Petrology and geochemistry, including Pb and/or Nd isotopic chemistry are the best tools to characterize basaltic melts of oceanic plateaus. To establish that plutonic rocks belong to an oceanic plateau, we have developed criteria that discriminate intrusions of oceanic plateaus from those of other tectonic settings. We specified the mineralogy and crystallization sequence of the oceanic plateau cumulates, which are similar to intra-plate magmas. Finally, we used the trace-element composition of the clinopyroxene separates to demonstrate that the melts in equilibrium with the clinopyroxene were tholeiitic basalts similar to those of the oceanic plateau basalts.

3. Late Cretaceous-Paleogene evolution of northwestern South America.

The characterization in Ecuador of fragments of two accreted oceanic plateaus allowed us to specify the geodynamic evolution of northwestern South America.

We refined the structure and geodynamic evolution of the Western Cordillera of Ecuador. Its eastern part is made of an Early Cretaceous plateau (125-120 Ma) accreted in the Late Santonian-Early Campanian (85-80 Ma), while the high parts of the Western Cordillera is made of part of the Late Cretaceous CCOP (90-85 Ma) accreted in the Late Maastrichtian (70-65 Ma).

The identification of remnants of the CCOP located west of the Macuchi arc, strongly suggests that major dextral displacements occurred since the Late Eocene. As a matter of fact, the CCOP terranes of the Coastal zone were accreted before Mid Eocene times (≥ 50 Ma), while the Macuchi arc accreted in the Late Eocene (≈ 40 Ma). This situation can be only explained by the shift of the formerly accreted terranes west of the newly accreted one, by means of major transurrent dextral faults.

The presence of accreted fragments of the Late Cretaceous CCOP in the Ecuadorian Western Cordillera sets the problem of the relationship of the Late Cretaceous CCOP with the Galápagos hotpsot. The presence of island arcs on both sides of the CCOP in latest Cretaceous times allows to assume that the latter did not migrate significantly between its formation and accretion dates. As a consequence, the hotspot that formed the CCOP was probably closer to South America than the Galápagos hotspot was ≈ 85 Ma ago.

REFERENCES

REFERENCES

Aitken, B. G., 1983, Compositional variation in clinopyroxene from komatiites, Gorgona Island, Colombia: Terra Cognita, v. 3.

Aitken, B. G., and Echeverria, L. M., 1984, Petrology and geochemistry of komatiites from Gorgona island Colombia: Contrib. Mineral. Petrol., v. 86, p. 94-105.

Alvarado, G. E., Denyer, P., and Sinton, C. W., 1997, The 89 Ma Tortugal komatiitic suite, Costa Rica: Implications for a common geological origin of the Caribbean and Eastern Pacific region from a mantle plume: Geology, v. 25, p. 439-442.

Anderson, D. L., 1994, Komatiites and picrites: evidence that the "plume" source is depleted: Earth Planet. Sci. Lett., v. 128, p. 303-311.

Arndt, N. T., 1994, Archean Komatiites, *in* Evolution, A. C., ed., Elsevier, Amsterdam, K.C. Condie.

Arndt, N. T., Kerr, A. C., and Tarney, J., 1997, Dynamic melting in plume heads; the formation of Gorgona komatiites and basalts: Earth Planet. Sci. Lett., v. 146, p. 289-301.

Aspden, J. A., Bonilla, W., and Duque, P., 1995, The El Oro metamorphic complex, Ecuador: geology and economic mineral deposit: Oversas Geol. Miner. Res., v. 37, 63p., 1 map. BGS publi., Nottingham.

Aspden, J. A., Harrison, S. H., and Rundle, C. C., 1992, New geological control for the tectono-magmatic evolution of the metamorphic basement: J. South Am. Earth Sci., v. 6 (1/2), p. 77-96.

Aspden, J. A., and Litherland, M., 1992, The geology and Mesozoic collisional history of the Cordillera Real, Ecuador: Tectonophysics, v. 205, p. 187-204.

Aspden, J. A., Mc Court, W. J., and Brook, M., 1987, Geometrical control of subduction-related magmatism: the Mesozoic and Cenozoic plutonic history of Western Colombia: J. geol. Soc. London, v. 144, p. 893-905.

Aspden, J. A., and McCourt, W. J., 1986, Mesozoic oceanic terrane in the Central Andes of Colombia: Geology, v. 14, p. 415-418.

Astorga, A., 1997, El Puente istmo de América Central, y la evolución de la placa Caribe (con énfasis en el Mesozoico): Profil, 12, p. 1-201, Stuttgart.

Astroga, A., 1994, El Mesozoico del Sur de América Central: consecuancias para el origen y evolución de la Placa Caribe: Profil, 7, p. 171-233, Stuttgart.

Baldock, J. W., 1982, Geologia del Ecuador: Boletin de Explicación del Mapa geológico de la República del Ecuador. Ministerio de Resursos Naturales y Energéticos, Dir. Gen. de Geologica y Minas, Quito-Ecuador, 54p.

Bard, J. P., 1983, Metamorphism of an obducted island arc; example of the Kohistan Sequence (Pakistan) in the Himalayan collided range: Earth Planet. Sci. Lett., v. 65, p. 133-144.

Barley, M. E., and Bickle, M. J., 1982, Komatiites in the Pilbara block, Western Australia, *in* Komatiites, ed., Allen & Unwin London, N.T. Arndt & E.G. Nisbet.

Barrat, J.-A., Keller, F., Amossé, J., Taylor, R. N., Nesbitt, R. W., and Hirata, T., 1996, Determination of rare earth elements in sixteen silicate reference samples by ICP-MS using a Tm addition and an ion-exchange chromatography procedure: Geostand. Newsl., v. 20, p. 133-139.

Ben Avraham, Z., Nur, A., Jones, D., and Cox, A., 1981, Continental accretion; from oceanic plateaus to allochthonous terranes: Science, v. 213, p. 47-54.

Ben Othman, D., White, W. M., and Patchett, J., 1994, The geochemistry of marine sediments, island arc, magma genesis, and crust-mantle recycling: Earth Planet. Sci. Lett., v. 94, p. 1-21.

Benítez, S., 1995, Evolution géodynamique de la province côtière sud-équatorienne au Crétacé supérieur - Tertiaire: Géol. Alp., v. 71, p. 3-163.

Benoit, M., 1997, Caractérisation Géochimique (traces, isotopes) d'un système de drainage magmatique fossile dans l'ophiolite d'Oman: Unpub. Doctorat en Géochimie thesis, Université Paul Sabatier.

Benoit, M., Polvé, M., and Ceuleneer, G., 1996, Trace element and isotopic characterization of mafic cumulates in a fossil mantle diapir (Oman ophiolite): Chem. Geol., v. 134, p. 199-214.

Boland, M. P., McCourt, W. J., and Beate, B., 2000, Mapa geológico de la cordillera occidental del Ecuador entre 0° - 1° N, escala 1/200.000: CODIGEM-Min. Energ. Min.-BGS publs., Quito.

Bosch, D., Gabriele, P., Lapierre, H., Malfere, J.-L., and Jaillard, 2001, Geodynamic significance of the Raspas Metamorphic Complex (SW Ecuador) : geochemical and isotopic constraints: Tectonophysics, p. in press.

Bourgois, J., Egüez, A., Butterlin, J., and De Wewer, P., 1990, Evolution géodynamique de la Cordillère Occidentale des Andes d'Equateur : la découverte de la formation éocène d'Apagua: C. R. Acad. Sci. Paris, v. 311, p. 173-180.

Bourgois, J., Toussaint, J. F., Gonzales, H., Azema, J., Calle, B., Desmet, A., Murcia, L. A., Acevedo, A. P., Parra, E., and Tournon, J., 1987, Geological history of the Cretaceous ophiolitic complexes of thenorthwestern South America (Colombia Andes): Tectonophysics, v. 143, p. 307-327.

Bowin, C., 1966, Geology of the Central Dominican Republic (case history part of an island arc): in Caribbean Geological Studies, edited by H.H. Hess, Geol. Soc. Am. Mem., v. 98, p. 11-84.

Bowin, C. O., 1975, The Geology of Hispaniola: in The Ocean Basins and Margins, p. 501-552.

Bralower, T. J., and Iturralde-Vinent, M. A., 1997, Micropaleontological dating of the collision between the North American plate and the Greater Antilles Arc in western Cuba: Palaios, v. 12, p. 133-150.

Bristow, C. R., and Hoffstetter, R., 1977, Lexique Stratigraphique International, V, 5a2, *in* publ., C., ed., Paris, p. 410.

Brunet, D., and Yuen, D. A., 2000, Mantle plumes pinched in the transition zone: Earth Planet. Sci. Lett., v. 178, p. 13-27.

Burke, K., Fox, P. J., and Sengor, A. M. C., 1978, Buoyant ocean floor and the evolution of the Caribbean: J. Geophy. Res., A, Space Physics, v. 83, p. 3949-3954.

Campbell, I. H., and Griffiths, R. W., 1992, The changing nature of mantle hotspots through time; implications for the chemical evolution of the mantle: J. Geol., v. 100, p. 497-523.

Cannat, M., Karson, J. A., Miller, D. J., and et al., 1995, Site 923: Ocean Drilling Program, v. 153, p. 217-258.

Casey, J. F., 1997, Comparison of major- and trace-element geochemistry of abyssal peridotites and mafic plutonic rocks with basalts from the MARK region of the Mid-Atlantic ridge: Ocean Drilling Program, v. 153, p. 181-241.

Castillo, P., Batiza, R., and Stern, R. J., 1986, petrology and geochemistry of Nauru basin igneous complex: large volume, off-ridge eruptions of MORB-like basalt during the Cretaceous: Init. Rep., v. 89, p. 555-576.

Cheilletz, A., Giuliani, G., Branquet, Y., Laumonier, B., Sanchez, A. J., Féraud, G., and Arhan, T., 1997, Datation K-Ar et 40Ar/39Ar à 65 ± 3 Ma des gisements d'émeraude du district de Chivor-Macanal : argument en faveur d'une déformation précoce dans la Cordillère orientale de Colombie: C. R. Acad. Sci. Paris, v. 324, IIa, p. 369-377.

Christophoul, F., Baby, P., Rivadeneira, M., and Dávila, C., 2001, Stratigraphic response to a major tectonic event in a foreland basin : the Ecuadorian Oriente Basin from Eocene to Oligocene times: Tectonophysics, p. in press.

Clague, D. A., 1987, Hawaiian xenolith populations, magma supply rates, and development of magma chambers: Bull. Volcanol, v. 49, p. 577-587.

Clague, D. A., and Chen, C.-H., 1986, Ocean crust xenoliths from Hualalai, Hawaii: Geol. Soc. America, Absrtact with programs 18, v. 6, p. 565.

Cloos, M., 1993, Lithospheric buoyancy and collisional orogenesis; subduction of oceanic plateaus, continental margins, island arcs, spreading ridges, and seamounts: Geol. Soc. America Bull., v. 105, p. 715-737.

Coffin, M. F., and Eldholm, O., 1993, Scratching the surface; estimating dimensions of large igneous provinces: Geology, v. 21, p. 515-518.

Collins, A. S., Khan, M. A., Stern, R. J., Gribble, R. F., and Windley, B. F., 1998, Geochemical and isotopic constraints on subduction polarity, magma sources and palaeogeography of the Kohistan Arc, northern Pakistan; discussion and reply: J. Geol. Soc. London, v. 155, p. 893-895.

Coney, P. J., Jones, D. L., and Monger, J. W. H., 1980, Cordilleran suspect terranes: Nature (London), v. 288, p. 329-333.

Cosma, L., Lapierre, H., Jaillard, E., Laubacher, G., Bosch, D., Desmet, A., Mamberti, M., and Gabriele, P., 1998, Pétrographie et géochimie des unités magmatiques de la Cordillère occidentale d'Equateur (0° 30'); implications tectoniques: Bull. Soc. Geol. France, v. 169, p. 739-751.

Daly, M. C., 1989, Correlations between Nazca/Farallón plate kinematics and Forearc basin evolution in Ecuador: Tectonics, v. 8, p. 769-790.

Dávila Alcocer, A. V. M., and Martínez Reyes, J., 1987, Una edad cretácica para las rocas basales de la Sierra de Guanajuato, paper presented at Simposio sobre la Geología de la Sierra de Guanajuato, Inst. Geol., Univ. Nac. Auto. de Mexico.

Deniaud, Y., 2000, Enregistrement sédimentaire et structural de l'évolution géodynamique des Andes équatoriennes au cours du Néogène : étude des bassins d'avant-arc et bilans de masse: Unpub. Sciences de la terre thesis, Univ. J. Fourier, Grenoble.

Desmet, A., 1994, Ophiolites et séries basaltiques crétacées des régions caraïbes et norandines: bassins marginaux, dorsales ou plateaux océaniques?: Unpub. Doctorat science thesis, Université de Nancy 1.

Di Marco, G., 1994, Les terrains accrétés du Sud du Costa Rica. Évolution tectono-stratigraphique de la marge occidentale de la plaque Caraïbe: Mém. Géol., Lausanne, v. 20, 184pp.

Dick, H. J. B., Meyer, P. S., Bloomer, S., Kirby, S., Stakes, D., and Mawer, C., 1991, Lithostratigraphic evolution of an in situ section of oceanic layer 3: in Von Herzen R.P., Robinson, P.T. et al., Proc. ODP Sci. Results, 118, College Station, p. 439-537.

Donaldson, C. H., 1975, Calculated diffusion coefficients and the growth rate of olivine in a basalt magma: Lithos, v. 8, p. 163-174.

Donaldson, H. C., 1976, An Experimental investigation of Olivine morphology: Contrib. Mineral. Petrol., v. 57, p. 187-213.

Donnelly, T., Melson, W., Kay, R., and Rogers, J. J. W., 1973, basalts and dolerites of Late Cretaceous age from the Central Caribbean: Initial Rep. Deep Sea Drill. Proj., v. 15, p. 989-1012.

Donnelly, T. W., and al., e., 1990, History and tectonic setting of Caribbean magmatism, *in* Case, G. D. a. J. E., ed., The Geology of North America, of Am.Geol. Soc., p. 339-374.

Donnelly, T. W., and Rogers, J. J. W., 1978, The distribution of igneous rocks throughoutthe Caribbean: Geol. Mijnbouw., v. 57, p. 151-162.

Donnelly, T. W., and Rogers, J. J. W., 1980, Igneous series in island arcs: the northeastern Caribbean compared with worldwide island-arc assemblages: Bull. Volcanol., v. 43-2, p. 347-382.

Draper, G., and Lewis, J. F., 1991, Metamorphic belts in central Hispaniola: in Geologic and Tectonic Development of the North America-Caribbean Plateau Boundary in Hispaniola, Geol. Soc. Am., v. 262, p. 29-45.

Duncan, R. A., and Hargraves, R. B., 1984, Plate tectonic evolution of the Caribbean region in the mantle reference: In: W. E. Bonini, R. B. Hargraves and R. Shagam (Editors), The Caribbean-South American Plate Boundary and Regional Tectonics. Geological Society of America Memoir, Boulder, p. 81-84.

Dunkley, P. N., and Gaibor, A., 1998, Mapa geológico de la Cordillera Occidental del Ecuador entre 2° - 3° S., escala 1/200.000: CODIGEM-Min. Energ. Min.-BGS publs., Quito.

Dupré, B., and Echeverria, L. M., 1984, Pb isotopes of Gorgona Isaland (Colombian): Isotopic variation correlated with magma type: Earth Planet. Sci. Lett., v. 67, p. 186-190.

Dupuis, V., 1999, Origine et mise en place des témoins accrétés du plateau océanique caraïbe en République Dominicaine (Grandes Antilles): Unpub. Doctorat en Sciences de la Terre thesis, Université de Nice-Sophia Antipolis, 303pp.

Echeverria, L. M., 1980, Tertiary or Mesozoic komatiites from Gorgona Island, Colombia; field relations and geochemistry: Contrib. Mineral. Petrol., v. 73, p. 253-266.

Egüez, A., 1986, Evolution Cénozoïque de la Cordillère Occidentale Septentrionale d'Equateur (0°15'S-1°10'S) : les minéralisations associées: Unpublished thesis University Paris VI, 116 p., Paris.

Emery, K. O., and Uchupi, E., 1984, The geology of the Atlantic Ocean: Springer Verlag, New York, 1050 pp.

Farnetani, C. G., Richards, M. A., and Ghiorso, M. S., 1996, Petrological models of magma evolution and deep crustal structure beneath hotspots and flood basalt provinces: Earth Planet. Sci. Lett., v. 143, p. 81-94.

Faucher, B., Vernet, R., Bizon, G., Bizon, J. J., Grekoff, N., Lys, M., and Sigal, J., 1971, Sedimentary Formations in Ecuador. A stratigraphic and micropaleontological survey, *in* Bureau Études Indust. Coop. Inst. Franç. Pétrole (BEICIP), ed., p. 220.

Feininger, T., and Bristow, C. R., 1980, Cretaceous and Paleogene geologic history of coastal Ecuador: Geol. Rundsch., v. 3, p. 849-874.

Fourcade, E., Méndez, J., Azéma, J., Cros, P., De Wever, P., Duthou, J.-L., Romero, J. E., and Michaud, F., 1994, pré-santonien-campanien de l'obduction des ophiolites du Guatemala: C. R. Acad. Sci., Paris, v. 318, (II), p. 527-533.

Francheteau, J., Armijo, R., Cheminee, J. L., Hekinian, R., Lonsdale, P. F., and Blum, N., 1990, 1 Ma East Pacific Rise oceanic crust and uppermost mantle exposed by rifting in Hess Deep (equatorial Pacific Ocean): Earth Planet. Sci. Lett., v. 101, p. 281-295.

Francheteau, J., Armijo, R., Cheminée, J. L., Hekinian, R., Lonsdale, P. F., and Blum, N., 1992, Dyke complex of the East Pacific Rise exposed in the walls of Hess Deep and the structure of the upper oceanic crust: Earth Planet. Sci. Lett., v. 111, p. 109-121.

Francis, D., Ludden, J., Johnstone, R., and Davis, W., 1997, Picrite evidence for more Fe in Archean mantle reservoirs, *in* Anonymous, ed., AGU 1997 fall meeting: Eos, Transactions, Am. Geophy. Union, Washington, DC, United States, p. 819.

Freydier, C., 1995, L'arc du "Guerrero terrane" et le bassin d'Arperos (Cordillères mexicaines): Caractérisation pétro-géochimique et évolution géodynamique: Unpub. Sciences de la terre thesis, Université Joseph Fourier - Grenoble I.

Freydier, C., Martínez, R., Lapierre, H., Tardy, M., and Coulon, C., 1996, The Early Cretaceous Arperos oceanic basin (western Mexico): Geochemical evidence for an aseismic ridge formed near a speading center: Tectonophysics, v. 259, p. 343-367.

Freydier, F., Lapierre, H., Briqueu, L., Tardy, M., Coulon, C., and Martinez-Reyes, J., 1997, Volcaniclastic sequences with continental affinities with the Late Jurassic-Early Cretaceous Guerrero intra-oceanic arc terrane: J. Geol., v. 105, p. 483-502.

Freymuller, J. T., Kellogg, J. N., and Vega, V., 1993, Plate motions in the North Andean region: J. Geophys. Res., v. 98, p. 21853-21863.

Gabriele, P., Ballevre, M., Jaillard, E., and Hernandez, J., 1999, Decompression at decreasing temperatures in Eclogite-facies metapellites (El Oro metamorphic complex, SW-Ecuador): a record of fast exhumation rates: Fourth ISAG, Goettingen, Germany.

Gansser, A., 1954, The Guiana Shield (S. America). Geological observations: Ecl. Geol. Helvetiae, v. 47, p. 77-112.

Gansser, A., 1973, Facts and theories on the Andes: J. Geol. Soc. London, v. 129, p. 93-131.

Gansser, A., Dietrich, V. J., and Cameron, W. E., 1979, Paleogene komatiites from Gorgona Island: Nature, v. 278, p. 545-546.

Gillis, K. M., 1996, Rare earth element constraints on the origin of amphibole in gabbroic rocks from site 894, Hess Deep: Ocean Drilling Program, v. 147, p. 59-75.

Giret, A., and Beaux, F., 1984, Le pluton du Val Gabbro (îles Kerguelen), un complexe tholéiitique, témoin de l'activité de la paléo ride Est-Indienne: C. R. Acad. Sci. Paris, v. 299, n° 14, p. 965-970.

Goossens, P. J., and Rose, W. I., 1973, Chemical Composition and Age Determination of Tholeiitic Rocks in the Basic igneous Complex, Ecuador: Geol. Soc.America Bull., v. 84, p. 1043-1051.

Goossens, P. J., Rose, W. I., and Flores, D., 1977, Geochemistry of tholeiites of the Basic Igneous Complex of northwestern South America: Geol. Soc. America Bull., v. 88, p. 1711-1720.

Gordon, R. G., and Jurdy, D. M., 1986, Cenozoic global plate motions: J.Geophys. Res., v. 91, p. 12389-12406.

Gradstein, F. M., agterberg, F. P., Ogg, J. G., Hardenbol, J., Van Veen, P., Thierry, J., and Huang, Z., 1994, A Mesozoic scale: J.Geophys. Res., v. 99, p. 24051-24074.

Grégoire, M., Cottin, J.-Y., Giret, A., Mattielli, N., and Weis, D., 1998, The meta-igneous rocks granulite xenoliths from Kerguelen Archipelago: evidence of a continent nucleation in an oceanic setting: Contrib. Mineral. Petrol., v. 133, p. 259-283.

Grösser, J.R., 1989, Geotectonic evolution of the Western Cordillera of Colombia: New aspect from geochemical data on volcanic rocks: J. South Am. Earth Sci., v. 2, p. 359-369.

Gurenko, A. A., and Chaussidon, M., 1995, Enriched and depleted primitive melts included in olivine from Icelandic tholeiites; origin by continuous melting of a single mantle column: Geoch. Cosmo. Acta, v. 59, p. 2905-2917.

Gursky, M. M., 1991, Tectonics of the Nicoya Peninsula, Costa Rica and implications for the geodynamic histtory of the Caribbean: Zentralbl. Geol. Paläontol., v. I (6), p. 1557-1570.

Hancock, J. M., and Kaufmann, E. G., 1979, The great transgression of the late Cretaceous: J. Geol. Soc. London, v. 136, p. 175-186.

Haq, B., Hardenbol, J., and Vail, P., 1987, Chronology of fluctuating Sea levels since the Triassic: Science, v. 235, p. 1156-1167.

Hart, S. R., and Dunn, T., 1993, Experimental cpx / melt partitioning of 24 trace elements: Contrib. Mineral. Petrol., v. 113, p. 1-8.

Hauff, F., Hoernle, K., Schminke, U., and Werner, R. A., 1997, Mid-Cretaceous origin for the Galápagos hotspot: volcanological, petrological and geochemical evidence from Costa Rica oceanic crustal fragments: Geol. Rundsch., v. 86, p. 141-155.

Hauff, F., Hoernle, K., Van den Bogaard, P., Alvarado, G., and Garbe-Schönberg, D., 2000, Age and geochemistry of basaltic complexes in western Costa Rica: Contributions to the geotectonic evolution of Central America: Geoch. Geophys. Geo., v. 1.

Henderson, W., 1979, Cretaceous to Eocene volcanic arc activity in the Andes of Northern Ecuador: J. Geol. Soc. London, v. 136, p. 367-378.

Henderson, W., 1981, The volcanic Macuchi Formation, Andes of Northern Ecuador: Gebrüder Borntraeger. Eds., Newsl. Stratigr., v. 9 (3), p. 157-168.

Hofmann, A. W., 1988, Chemical differentiation of the Earth; the relationship between mantle, continental crust, and oceanic crust, *in* Welin, E., ed., Isotope geochemistry; the Crafoord symposium: Earth and Planetary Science Letters, Amsterdam, Netherlands, Elsevier, p. 297-314.

Hofmann, A. W., Jochum, K. P., Seufert, M., and White, W. M., 1986, Nb and Pb in oceanic basalts: new constraints on mantle evolution: Earth Planet. Sci. Lett., v. 79, p. 33-45.

Hughes, R. A., Bermúdez, R., and Espinel, G., 1999, Mapa geológico de la Cordillera Occidental del Ecuador entre 0° - 1° S, escala 1:200.000: CODIGEM-Min. Energ. Min.-BGS publs., Quito.

Hughes, R. A., and Pilatasig, L. F., in press, Cretaceous and Tertiary terrane accretion in the Cordillera Occidental of the Andes of Ecuador: Tectonophysics.

Humphris, S. E., 1984, The mobility of rare earth elements in the crust, *in* Henderson, P., ed., Rare Earth Element Geochemistry, Elsevier, p. 317-342.

Hungerbühler, D., 1997, Neogene basins in the Andes of southern Ecuador: evolution, deformation and regional tectonic implications: Unpub. n°12371,182 p., 1 map thesis, ETH Zurich.

Hungerbühler, D., Steinmann, M., Winkler, W., Seward, D., Egüez, A., Heller, F., and Ford, M., 1995, An integrated study of fill and deformation in the Adean intermontane basin of Nabón (Late Miocene), southern Ecuador: Sedim. Geol., v. 96, p. 257-279.

Iturralde-Vinent, M., Stanek, K.-P., Wolf, D., Thieke, H. U., and Müller, H., 2000, Geology of the Camagüey region, Central Cuba : Evolution of a collisional margin in the northern Caribbean. in Miller, H. & Hervé, F., eds., Geoscientific Cooperation with Latin America. Zeitschr. Angewandte Geol. SH1, 267-273, Hannover: .

Jaillard, Hérail, G., Monfret, T., Díaz-Martínez, E., Baby, P., Lavenu, A., and Dumont, J.-F., 2000, Tectonic evolution of the Andes of Ecuador, Peru, Bolivia and northernmost Chile. in: *Tectonic evolution of South America*, Cordani, U.G., Milani, E.J., Thomaz F., A., Campos, D.A., Eds., 481-559, Publ. 31st Int. Geol. Cong., Rio de Janeiro: .

Jaillard, E., 1997, Síntesis estratigráfica y sedimentológica del Cretáceo y Paleógenode la cuenca oriental del Ecuador, Orstom-Petroproducción publ., Quito, p. 164.

Jaillard, E., Benitez, S., and Mascle, G. H., 1997, Les déformations paléogènes de la zone d'avant-arc sud-équatorienne en relation avec l'évolution géodynamique: Bull. Soc. Géol. France, v. 168, p. 403-412.

Jaillard, E., Laubacher, G., Bengtson, P., Dhondt, A., and Bulot, L., 1999, Stratigraphy and evolution of the Cretaceous forearc "Celica-Lancones Basin" of Southwestern Ecuador: J. South Am. Earth Sci., v. 12, p. 51-68.

Jaillard, E., Laubacher, G., Bengtson, P., dhondt, A., Philip, J., Bulot, L. G., and Robert, E., 1998, Revisión estratigráfica del Cretáceo superior del Noroeste peruao y Suroeste ecuatoriano. Datos preliminares y consecuencias tectónicas: Bol. Soc. geol. Perú, v. 88, p. 101-115.

Jaillard, E., Ordoñez, M., Bengtson, P., Berrones, G., Bonhomme, M., Jiménez, N., and Zambrano, I., 1996, Sedimentary and tectonic evolution of the arc zone of southwestern Ecuador during Late Cretaceous and Early Tertiary times: J. South Am. Earth Sci., v. 9, p. 131-140.

Jaillard, E., Ordoñez, M., Benitez, S., Berrones, G., Jimenez, N., Montenegro, G., and Zambrano, I., 1995, Basin development in an accretionary, oceanic-floored fore-arc setting; southern coastal Ecuador during Late Cretaceous-late Eocene time: AAPG Memoir, v. 62, p. 615-631.

Juteau, T., Mégard, F., Raharison, L., and Whitechurch, H., 1977, Les assemblages ophiolitiques de l'occident équatorien: nature pétrographique et position structurale: Bull. Soc. Géol. France, v. 5, p. 1127-1132.

Kausar, A. B., 1998, L'Arc Sud Kohistan: Evolution Pétrologique et Distribution des Eléments et Minéraux du Groupe du Platine: Unpub. Doctorat en Sciences de la Terre thesis, Université Joseph Fourier.

Kehrer, W., and Van der Kaaden, G., 1979, Notes on the geology of Ecuador with special reference to the Western Cordillera: geol. Jahrbuch, v. B53, p. 5-57.

Kempton, P. D., and Hunter, A., 1997, A Sr-, Nd-, Pb-, O-isotope study of plutonic rocks from MARK, Leg 153: implications for mantle heterogeneity and magma chamber processes: in J. A. Karson, M Cannat, D. J. Miller et al. (EDS), Proc. Sci.Res., v. Ocean Drilling Program Leg 153, p. 305-320.

Kerr, A., Tarney, J., Saunders, A., Marriner, G., and Arndt, N., 1994, Komatiites, basalts and ultramafic tuffs from the heterogeneous Gorgona plume: Eos, Transactions, Am. Geophys. Union, v. 75, p. 726.

Kerr, A. C., Marriner, G. F., Arndt, N. T., Tarney, J., Nivia, A., Saunders, A. D., and Duncan, R. A., 1996a, The petrogenesis of Gorgona komatiites, picrites and basalts: new field, petrographic and geochemical constraints: Lithos, v. 37, p. 245-260.

Kerr, A. C., Marriner, G. F., Tarney, J., Nivia, A., Saunders, A. D., Thirlwall, M. F., and Sinton, C. W., 1997a, Cretaceous basaltic terranes in western Colombia; elemental, chronological and Sr-Nd isotopic constraints on petrogenesis: J. Petrol., v. 38, p. 677-702.

Kerr, A. C., Tarney, J., Marriner, G. F., Nivia, A., Klaver, G. T., and Saunders, A. D., 1996b, The geochemistry and tectonic setting of Late Cretaceous Caribbean and Colombian volcanism: J. South Am. Earth Sci., v. 9, p. 111-120.

Kerr, A. C., Tarney, J., Marriner, G. F., Nivia, A., and Saunders, A. D., 1997b, The Caribbean-Colombian Cretaceous igneous province; the internal anatomy of an oceanic plateau: Geophys. Monog., v. 100, p. 123-144.

Kerr, A. C., Tarney, J., Nivia, A., Marriner, G. F., and Saunders, A. D., 1998, The internal structure of oceanic plateaus; inferences from obducted Cretaceous terranes in western Colombia and the Caribbean: Tectonophysics, v. 292, p. 173-188.

Kesler, S. E., Lewis, J. F., Jones, L. M., and Walker, R. L., 1977, Early island arc intrusive acttivity, Cordillera Central, Dominican Republic: Contrib. Mineral. Petrol., v. 65, p. 91-99.

Khan, M. A., Jan, M. Q., and Weaver, B. L., 1993, Evolution of the lower arc crust in Kohistan, N. Pakistan; temporal arc magmatism through early, mature and intra-arc rift stages, *in* Treloar, P. J., and Searle, M. P., eds., Himalayan tectonics.: Geological Society Special Publications, London, United Kingdom, Geological Society of London, p. 123-138.

Khan, M. A., Jan, M. Q., Windley, B. F., Tarney, J., and Thirlwall, M. F., 1989, The Chilas mafic-ultramafic igneous complex; the root of the Kohistan island arc in the Himalaya of northern Pakistan, *in* Malinconico, L. L. J., and Lillie, R. J., eds., Tectonics of the western Himalayas.: Special Paper - Geological Society of America, Boulder, CO, United States, GSA, p. 75-94.

Lagabrielle, Y., and Cannat, M., 1990, Alpine Jurassic ophiolites resemble to modern central Atlantic basement: Geology, v. 18, p. 319-322.

Lapierre, H., Bosch, D., Dupuis, V., Polvé, M., Maury, R. C., Hernandez, J., Monié, P., Yeghicheyan, D., Jaillard, E., Tardy, M., Mercier de Lépinay, B., Mamberti, M., Desmet, A., Keller, F., and Sénebier, F., 2000, Multiple plume events in the genesis of the peri-Caribbean Cretaceous oceanic plateau province: J. Geophys. Res., v. 105, p. 8403-8421.

Lapierre, H., Dupuis, V., Mercier de Lepinay, B., Tardy, M., Ruiz, J., Maury, R. C., Hernandez, J., and Loubet, M., 1997, Is the lower Duarte igneous complex (Hispaniola) a remnant of the Caribbean plume-generated oceanic plateau?: J. Geol., v. 105, p. 111-120.

Larson, R. L., 1991, Latest pulse of Earth: Evidence for a mid-Cretaceous superplume: Geology, v. 19, p. 547-550.

Lavenu, A., Noblet, C., Bonhomme, M. G., Egueez, A., Dugas, F., and Vivier, G., 1992, New K-Ar age dates of Neogene and Quaternary volcanic rocks from the Ecuadorian Andes; implications for the relationship between sedimentation, volcanism and tectonics: J. South Am. Earth Sci., v. 5, p. 309-320.

Leake, B. E., Wooley Alan, R., Arps, C. E. S., Birch, W. D., Gilbert, M. C., Grice, J. D., Hawthorne, F. C., Kato, A., Kisch, H. J., Krivovichec, V. G., Linthout, K., Laird, J., Mandarino, J., Maresch, W. V., Nickel, E. H., Rock, N. M., Schumacher, J. C., Smith, D. C., Stephenson, N. C. N., Ungaretti, L., Whittaker, E. J. W., and Youzhi, G., 1997, Nomenclature of amphiboles; report of the Subcommittee on Amphiboles of the International Mineralogical Association Commission on New Minerals and Mineral Names: European J. Mineral., v. 9, p. 623-651.

LeBas, M. J., 2000, IUGS Reclassification of the High-Mg and Picritic Volcanic Rocks: J. Petrol., v. 41, p. 1467-1470.

Lebrat, M., Megard, F., Dupuy, C., and Dostal, J., 1987, Geochemistry and tectonic setting of pre-collision Cretaceous and Paleogene volcanic rocks of Ecuador; with Suppl. Data 87-23: Geol. Soc.Am. Bull., v. 99, p. 569-578.

Lebrat, M., Mégard, F., Juteau, T., and Calle, J., 1985, Pre-orogenic assemblages and structure in the Western Cordillera of Ecuador between 1°40'S and 2°20'S: Geol. Rundsch., v. 74, p. 343-351.

Lebron, M. C., and Perfit, M. R., 1993, Stratigraphic and petrochemical data support subduction polarity reversal of the Cretaceous Caribbean island arc: J. Geol., v. 101, p. 389-396.

Lewis, J. F., Amarante, A., Boise, G., Jimenez, J. G., and Dominguez, H. D., 1991, Lithology and stratigraphy of upper Cretaceous volcanic and volcanoclastic rocks of the Tireo Group, Dominican Republic, and correlations with the massif du nord in Haiti, in Mann, P., Draper, G., and Lewis, J.F., eds., Geologic and Tectonic development of the North America-Caribbean plateau boundary, in Hispaniola: America. soc. Special. Paper 262, pp143-163: .

Lewis, J. F., and Jimémez, J. G., 1991, The Duarte Complex in the La Vega-Jarabacoa-Janico area, central Hispaniola: in Geologic and Tectonic Development of the North America-Caribbean Plateau Boundary in Hispaniola, Geol. Soc. Am., v. 262, p. 115-141.

Li, J. P., O'Neil, H. S. C., and Seifert, F., 1995, Subsolidus phase relations in the system MgO-SiO (sub 2) -Cr-O in equilibrium with metallic Cr, and their significance for the petrochemistry of chromium: J. Petrol., v. 36, p. 107-132.

Liang, Y., and Elthon, D., 1990, Evidence from chromium abundances in mantle rocks for extraction of picrite and komatiite melts: Nature (London), v. 343, p. 551-553.

Lister, J. R., Campbell, I. H., and Kerr, R. C., 1991, The eruption of komatiites and picrites in preference to primitive basalts: Earth Planet. Sci. Lett., v. 105, p. 343-352.

Litherland, M., Aspden, J. A., and Jemielita, R. A., 1994, The metamorphic belts of Ecuador: British Geol. Surv., Overseas Memoir, v. 11, p. 147.

Maaloe, S., 1982, Geochemical aspects of permeability controlled partial melting and fractional crystallization: Geoch. Cosmo. Acta, v. 46, p. 43-57.

Mahoney, J. J., 1987, An isotopic survey of Pacific oceanic plateaus; implications for their nature and origin: Geophys. Monog., v. 43, p. 207-220.

Mahoney, J. J., Neal, C. R., Petterson, M. G., McGrail, B. A., Saunders, A. D., and Babbs, T. L., 1993, Formation of an oceanic plateau; speculations from field and geophysical observations of the Ontong Java Plateau: Eos, Transactions, Am. Geophys. Union, v. 74, p. 552.

Mahoney, J. J., Storey, M., Duncan, R. A., Spencer, K. J., and Pringle, M., 1993, Geochemistry and age of the Ontong Java Plateau: Geophys. Monog., v. 77, p. 233-261.

Malone, P., Fantin, F., Rossello, E., and Miller, M., 1999, Stratigraphic characterization of the Ancón Group from seismic data (Santa Elena Peninsula, Ecuador): 4th Int. Symp. And. Geodyn.-ISAG, v. Göttingen, p. 467-471.

Mamberti, M., Lapierre, H., Bosch, D., Jaillard, E., Ethien, R., Hernandez, J., and Polvé, M., submit, Accreted fragments of the Late Creatceous Caribbean-Colombian Plateau in Ecuador: J. Geol.

Mamberti, M., Lapierre, H., Bosch, D., Jaillard, E., Hernandez, J., and Polvé, M., submit, The Early Cretaceous San Juan Plutonic Suite, Ecuador: a Magma Chamber in an Oceanic Plateau: J. Petrol.

Mamberti, M., Walker, R. J., Eggins, S., Lapierre, H., Hernandez, J., Bosch, D., Jaillard, E., and Polvé, M., In prep, Ultra-depleted picrite in Ecuador: remnant of the CCOP plume head: Earth Planet. Sci. Lett.

Mancini, F., 1993, Skeletal olivine in the Saaksjarvi Sill; evidences for a picritic origin: Geology, v. 45, p. 99-103.

Manhès, G., Allègre, C. J., Dupré, B., and Hamelin, B., 1978, Lead-lead systematics, the age and chemical evolution of the Earth in a new representation space: Open File Report U. S. Geological Survey., p. 275-276.

Marriner, G. F., and Millward, D., 1984, The Petrology and geochemistry of Cretaceous to Recent volvanism in Colombia: the magmatic history of an accretionary plate margin: J. Geol. Soc. London, v. 141, p. 473-486.

Mattielli, N., 1996, Magmatisme et métasomatisme associés au panache des Kerguelen: Contribution de la géochimie des enclaves basiques et ultrabasiques: Thèse d'Université Libre de Bruxelles, 232 pp.

Mauffret, J. J., and Leroy, S., 1997, Intraplate deformation in the Caribbean region: J. Geodynamics, v. 21 (1), p. 113-122.

McCourt, W. J., Aspden, J. A., and Brook, M., 1984, New geological and geochronological data from the Colombian Andes: Continental growth by multiple accretion: J. Geol. Soc., London, v. 141, p. 831-845.

McCourt, W. J., Duque, P., Pilatasig, L. F., and Villagómez, R., 1998, Mapa geológico de la Cordillera Occidental del Ecuador entre 1° - 2° S., escala 1/200.000: CODIGEM-Min. Energ. Min.-BGS publs.

Mégard, F., Roperch, P., Lebrat, M., Laj, C., Mourier, T., and Noblet, C., 1987, L'Occident Equatorien: un terrain océanique pacifique accolé au continent sud-américain: Bull. Inst. Fr. Et. Andines, v. 1-2, p. 39-54.

Mercier de Lépinay, B., 1987, L'évolution géologique de la bordure nord-caraïbe: L'exemple de la transversale de l'île d'Hispaniola (Grandes Antilles): Thèse d'état, Univ. Pierre et Marie Curie, 336pp, Paris.

Meschede, M., 1998, The impossible Galápagos connection : geometric constraints for a near-American origin of the Caribbean plate: Geol. Rundsch., v. 87, p. 200-205.

Millward, D., Marriner, G. F., and Saunders, A. D., 1984, Cretaceous tholeiitic volcanic rocks from the Western Cordillera of Colombia: J. geol. Soc. London, v. 141, p. 847-860.

Montgomery, H., Pessagno, E. A., Jr., and Pindell, J. L., 1994, A 195 Ma terrane in a 165 Ma sea; Pacific origin of the Caribbean Plate: GSA Today, v. 4, p. 1, 3-6.

Morimoto, M., 1988, Nomenclature of pyroxenes: Miner. Mag., v. 52, p. 535-550.

Neal, C. R., Mahoney, J. J., Kroenke, L. W., Duncan, R. A., and Petterson, M. G., 1997, The Ontong Java Plateau: Geophys. Monog., v. 100, p. 183-216.

Nisbet, E. G., 1982, The tectonic setting and petrogenesis of komatiites, *in* Komatiites, ed., Allen & Unwin, London, N.T. Arndt & E.G. Nisbet.

Nivia, A., 1996, The Bolivar mafic-ultramafic complex, SW Colombia; the base of an obducted oceanic plateau: J. South Am. Earth Sci., v. 9, p. 59-68.

Noble, S. R., Aspden, J. A., and Jemielita, R., 1997, Northern Andean crustal evolution : New U-Pb geochronological constraints from Ecuador: Geol. Soc. Am. Bull., v. 109, p. 789-798.

Nur, A., and Ben Avraham, Z., 1982, Oceanic plateaus, the fragmentation of continents, and mountain building: J. Geophys. Res., v. 87, p. 3644-3661.

Ordoñez, M., 1996, Aplicaciones del estudio de microfósiles en la industria petrolera ecuatoriana: Actas VII Cong. Ecuat. Geol. Min. Petrol, p. 38-52.

Palmer, H., 1979, Geology of the Moncion-Jarabacao area, Dominican Republic, Hispaniola: in Tectonic Focal Point of the Northern Caribbean, edited by B. Lidz and F. Nagle, p. 29-68.

Pardo-Casas, F., and Molnar, P., 1987, Relative motion of the Nazca (Farallón) and South America plates since late Cretaceous times: Tectonics, v. 6, p. 233-248.

Parkinson, I. J., Arculus, R. J., Duncan, R. A., and Stanton, R. L., Island arc-oceanic plateau collision; Santa Isabel, Solomon Islands: in press.

Pécora, L., Jaillard, E., and Lapierre, H., 1999, Accrétion paléogène et décrochement dextre d'un terrain océanique dans le Nord du Pérou: C. R. Acad. Sci.Terre et des Planètes, v. 329, p. 389-396.

Pedersen, R. B., Malpas, J., and Fallon, T., 1996, Petrology and geochemistry of gabbroic and related rocks from site 894, Hess Deep: Ocean Drilling Program, v. 147, p. 3-19.

Pichler, H., and Aly, S., 1983, Neue K-Ar Alter plutonischer Gesteine in Ecuador: Zeitblatt der deutschen geologische Gesellschaft, v. 134, p. 495-506.

Pilger, R. H., 1984, Cenozoic plate kinematics, subduction and magmatism: J. geol. Soc. London, v. 141, p. 793-802.

Pilger, R. H., and Handschumacher, D. W., 1981, The fixed hotspot hypothesis and origin of the Easter-Sala y Gomez-Nezca trace: Bull. geol. Soc. Am., v. 92, p. 437-446.

Pindel, J. L., and Barret, S. F., 1990, Geological evolution of the Caribbean region; a plate tectonic perspective: In Dengo, G. and Case, J. E. (Editors). The Caribbean Region. Geological Society of America, v. H, p. 405-432.

Pratt, W. T., Figueroa, J. F., and Flores, B. G., 1998, Mapa geológico de la Cordillera Occidental del Ecuador entre 3°- 4° S, escala 1/200.000: CODIGEM-Min. Energ. Min.-BGS publs., Quito.

Qasim, J. M., and Howie, R. A., 1980, Ortho- and clinopyroxenes from the pyroxene granulites of Swat Kohistan, northern Pakistan: Mineral. Mag., v. 43, p. 715-726.

Révillon, S., 1999, Origine and composition du Plateau Océanique Caraïbe: Unpub. Sciences de la terre, thesis, Université de Rennes 1, 337 pp.

Révillon, S., Arndt, N. T., Chauvel, C., and Hallot, E., 2000, Geochemical study of ultamafic sills, Gorgona island, Colombia: Plumbing system of an oceanic plateau: J. Petrol., v. 41, p. 1127-1153.

Révillon, S., Arndt, N. T., Hallot, E., Kerr, A. C., and Tarney, J., 1999, Petrogenesis of picrites from the Caribbean Plateau and the North Atlantic magmatic province: Lithos, v. 49, p. 1-21.

Révillon, S., Hallot, E., Arndt, N. T., Chauvel, C., and Duncan, R. A., 2000, A complex history for the Caribbean Plateau: petrology, geochemistry and geochronology of the Beata Ridge, South Hispaniola: J. Geol., v. 108, p. 641-661.

Reynaud, C., Jaillard, E., Lapierre, H., Mamberti, M., and G.H., M., 1999, Oceanic plateau and island arcs of southwestern Ecuador; their place in the geodynamic evolution of northwestern South America: Tectonophysics, v. 307, p. 235-254.

Rœder, P. L., and Emslie, R. F., 1970, Olivine-liquid equilibrium: Contrib. Mineral. Petrol., v. 29, p. 275-289.

Roperch, P., Mégard, F., Kaj, C., T., M., Clube, T., and Noblet, C., 1987, Rotated oceanic blocks in western Ecuador: Geophys. Res. Lett., v. 14, p. 558-561.

Saunders, A. D., Tarney, J., Kerr, A. C., and Kent, R. W., 1996, The formation and fate of large oceanic igneous provinces: Lithos, v. 37, p. 81-95.

Scott, D. J., and Hegner, E., 1990, Two mantle sources for the two-billion year-old Purtuniq ophiolite, Cape Smith Belt, northern Quebec: Geol. Ass. Canada Prog. with Abstract, v. 15, p. A118.

Scott, D. J., Helmstdaedt, H., and Bickle, M. J., 1992, Purtuniq ophiolite, Cape Smith Belt, northern Quebec, Canada: A reconstructed section of Early Proterozoic oceanic crust: Geology, v. 20, p. 173-176.

Sen, G., Hickey-Vargas, R., Waggoner, D. G., and Maurrasse, F., 1988, Gechemistry of basalts from the Dumisseau Formation, southern Haiti: implications for the origin of the Caribbean sea crust: Earth Planet. Sci. Lett., v. 87.

Shimizu, H., Sangen, K., and Masuda, A., 1982, Experimental study on rare earth-element partitioning in minerals formed at 20 and 20 kbar for basaltic systems: Geochem. J., v. 16.

Sigal, J., 1969, Quelques acquisitions récentes concernant la chrono-stratigraphie des formations sédimentaires de l'Équateur: Rev. Espagn. Micropal, v. 1, p. 205-236.

Sigurdsson, H. e. a., 1997, caribbean ocean history and the Cretaceous-tertiary boundary event: Proc. Ocean Drill. Program Initial Rep., v. 165, p. 377-400.

Sincalir, J. H., and Berkey, C. P., 1924, geology of Guayaquil, Ecuador, South America: Am. J. Science, v. 7 (42), p. 491-497.

Sinton, C. W., and Duncan, R. A., 1997, Nicoya Peninsula, Costa Rica: A single suite of Caribbean oceanic plateau magmas: J. Geophys. Res., v. 102, p. 15507-15520.

Sinton, C. W., Duncan, R. A., Storey, M., Lewis, J., and Estrada, J. J., 1998, An oceanic flood basalt province within the Caraibbean plate: Earth Planet. Sci. Lett., v. 155, p. 221-235.

Sobolev, A. V., and Shimizu, N., 1993, Ultra-depleted primary melt included in an olivine from Mid-Atlantic Ridge: Nature, v. 363, p. 151-154.

Spadea, P., Delaloye, M., Espinosa, A., Orrego, A., and Wagner, J. J., 1987, Ophiolite Complex from La Tetilla, southwestern Colombia, South America: J. Geol., v. 95, p. 377-395.

Spadea, P., and Espinosa, A., 1996, Petrology and chemistry of late Cretaceous volcanic rocks from the southernmost segment of the Western Cordillera of Colombia (south America): J. South Am. Earth Sci., v. 9, p. 79-90.

Spadea, P., Espinosa, A., and Orrego, A., 1989, High-Mg extrusive rocks from the Romeral Zone ophiolites in the southwestern Colombian Andes, *in* Beccaluva, L., ed., Ophiolites and lithosphere of marginal seas: Chemical Geology, Amsterdam, Netherlands, Elsevier, p. 303-321.

Stanek, K.-P., Cobiella-Reguera, J. L., Maresch, W. V., Trujillo, G. M., Graffe, F., and Grevel, C., 2000, Geological development of Cuba. in Miller, H. & Hervé, F., eds., Geoscientific Cooperation with Latin America. Zeitschr. Angewandte Geol. SH1, 259-265, Hannover.: .

Steinmann, M., 1997, The Cuenca Basin of southern Ecuador: tectono-sedimentary history and the Tertiary Andean evolution: Unpub. PhD. Thesis thesis, ETH Zurich, n° 12297, 176pp.

Steinmann, M., Hungerbühler, D., Seward, D., and Winkler, W., 1999, Neogene tectonic evolution and exhumation of the outhern Ecuadorian Andes: a combined stratigraphy and fission-track approach: Tectonophysics, v. 307, p. 255-276.

Stéphan, J.-F., Mercier de Lépinay, B., Calais, E., Tardy, M., Beck, C., Carfantan, J.-C., Olivet, J.-L., Vila, J.-M., Bouysse, P., Mauffret, A., Bourgeois, J., Théry, J.-M., Tournon, J., Blanchet, R., and Dercourt, J., 1990, Paleodynamic maps of the Caribbean: 14 steps from Lias to Present: Bull. Soc. géol. France, v. 8, VI, 6, p. 915-919.

Storey, M., Mahoney, J. J., Kroenke, L. W., and Saunders, A. D., 1991, Are oceanic plateaus sites of komatiite formation?: Geology, v. 19, p. 376-379.

Sun, S. S., and McDonough, W. F., 1989, Chemical and isotopic systematics of oceanic basalts; implications for mantle composition and processes: Geol. Soc. Special Publications, v. 42, p. 313-345.

Tardy, M., Carfantan, J.-C., and Rangin, C., 1986, Essai de synthèse sur la structure du Mexique: Bull. Soc. Géol. Fr., ser. II, v. 6, p. 1025-1031.

Tardy, M., Lapierre, H., Freydier, C., Coulon, C., Bill, J.-B., Mercier de Lepinay, B., Stein, G., Bourdier, J.-L., and Yta, M., 1994, The Guerrero suspect terrane (western Mexico) and coeval arc terranes (the Greater Antilles and Western Cordillera of Colombia): a late Mesozoic intra-oceanic arc accreted to cratonal America during the Cretaceous: Tectonophysics, v. 230, p. 49-73.

Tejada, M. L. G., Mahoney, J. J., Duncan, R. A., and Hawkins, M. P., 1996, Age and geochemistry of basement and alkalic rocks of Malaita and Santa Isabel, Solomon Islands, southern margin of Ontong Java Plateau: J. Petrol., v. 37, p. 361-394.

Thalmann, H. E., 1946, Micropaleontology of Upper Cretaceous and Paleocene in Western Ecuador: Am. Ass.Petrol. Geol. Bull., v. 30, p. 337-347.

Thompson, R. N., and Gibson, S. A., 2000, Transient high temperatures in mantle plume heads inferred from magnesian olivines in Phanerozoic picrites: Nature, v. 407, p. 502-505.

Toussaint, J.-F., and Restrepo, J. J., 1994, The Colombian Andes during Cretaceous times: Cretaceous Tectonics in the Andes, edited by J. A. Salfity, p. 61-100.

Ulmer, P., 1989, Partitioning of high field strengh elements among olivine, pyroxenes, garnet and calcalkaline picrobasalt: Experimental results and an application: Annu. Rep. Dir. geophys. Lab., v. 1988/89, p. 42-47.

Van Thournout, F., Quevedo, L., and Pasteels, P., 1992, Edades radiométricas de rocas igneas en el Noroccidente Ecuatoriano: Bol. Geol. Ecuatoriano, v. 1, p. 3-10.

Vance, D., Stone, J. O. H., and O'Nions, R. K., 1989, He, Sr and Nd isotopes in xenoliths from Hawaii and other oceanic islands: Earth Planet. Sci. Lett., v. 96, p. 147-160.

Viljoen, R. P., and Viljoen, M. J., 1982, Komatiites - an historitical review, *in* Komatiites, ed., Allen & Unwin, London, N.T. Arndt & E.G. Nisbet.

Walker, D., Kirkpatrick, R. J., Longhi, J., and Hays, J. F., 1976, Cristallization history of lunar picritic basalt sample 12002: Phase-equilibria and cooling rate stuidies: Geol. Soc. Am.Bull., v. 87, p. 646-656.

Walker, R. J., Echeverria, L. M., Shirey, S. B., and Horan, M. F., 1991, Re-Os isotopic constraints on the origin of volcanic rocks, Gorgona Island, Colombia; Os isotopic evidence for ancient heterogeneities in the mantle: Contrib. Mineral. Petrol., v. 107, p. 150-162.

Walker, R. J., Storey, M., Kerr, A. C., Tarney, J., and Arndt, N. T., 2000, Implications of ^{187}Os heterogeneities in a mantle plume: Evidence from Gorgona Island and Curaçao: Geoch. Cosmoch. Acta, v. 63, p. 713-728.

Wallrabe-Adams, H. J., 1990, Petrology and geotectonic development of the western Ecuadorian Andes: the Basic Igneous Complex: Tectonophysics, v. 185, p. 163-182.

Wasserburg, G. J., Jacobsen, s. B., DePaolo, D. J., McCulloch, M. T., and Wen, T., 1981, Precise determination in Sm/Nd ratios, Sm and Nd isotopic abundance in standard solutions: Geoch. Cosmoch. Acta, v. 45, p. 2311-2323.

White, R., and McKenzie, D., 1989, Magmatism at rift zones: The generation of Volcanic Continental Margins and Flood Basalts: J. Geophys. Res., v. 94, p. 7685-7729.

White, W. M., Hofmann, A. W., and Puchelt, H., 1987, Isotope geochemistry of Pacific mid-ocean ridge basalt: J. Geophys. Res., v. 92, p. 4881-4893.

White, W. M., McBirney, A. R., and Duncan, R. A., 1993, Petrology and geochemistry of the Galápagos island: portrait of the pathological mantle plume: J. Geophys. Res., v. 98, p. 19533-19563.

Winsemann, J., 1994, Origin and tectonic history of the western Caribbean region: in Geology of an evolving arc. The isthmus of southern Nicaragua, Costa Rica, and western Panamá, H. Seyfried and W. Hellmann, eds., Profil, band 7, 1-15, Stuttgart.

Zindler, A., and Hart, S., 1986, Chemical geodynamics: *Annu. Rev.* Earth Planet. Sci. Lett., v. 14, p. 493-571.